THE ELECTRON MICROSCOPY PROTEOMIC ORGANELLAR PREPARATION ROBOT

Raymond Waterbury

Department of Biomedical Engineering
McGill University, Montréal
Canada

June 2006

A thesis submitted to McGill University in partial fulfillment of the requirements of the degree of Doctor of Philosophy

Your file Votre référence
ISBN: 978-0-494-27856-7
Our file Notre référence
ISBN: 978-0-494-27856-7

Abstract

An Electron Microscopy Proteomic Organellar Preparation (EMPOP) robot was developed as a tool for high-throughput preparation of subcellular fraction samples for electron microscopic identification. It will provide a means for validation of subcellular sample purity and confirmation of protein localization needed for organellar proteomics.

The device automates all chemical and mechanical manipulations required to prepare organelles for electron microscopic examination. It has a modular, integrated design that supports automated filtration, chemical processing, delivery and embedding of up to 96 subcellular fraction samples in parallel. Subcellular fraction specimens are extremely fragile. Consequently, the system was designed as a single unit to minimize mechanical stress on the samples by integrating a core mechanism, composed of four modular plates, and seven support subsystems for: (1) cooling, (2-3) fluid handling, (4-7) positioning. Furthermore, control software was developed specifically for the system to provide standardized, reproducible sample processing while maintaining flexibility for adjustment and recall of operational parameters.

Development of the automated process progressed from initial validation experiments and process screening to define operational parameters for preservation of sample integrity and establish a basic starting point for successful sample preparation. A series of successive modifications to seal the local environment of the samples and minimize the effect of fluidic perturbations further increased process performance. Subsequent testing of the robot's full sample preparation capacity used these refinements

to generate 96 samples in approximately 16 hours; reducing the time and labor requirement of equivalent manual preparation by up to 1,000 fold.

These results provide a basis for a structured approach toward process optimization and subsequent utilization the device for massive, parallel preparation of subcellular fraction samples for electron microscopic screening and quantitative analysis of subcellular and protein targets necessary for high-throughput proteomics.

Résumé

Un robot Préparateur d'Organites pour Microscopie Électronique en Protéomique (EMPOP) fut développé comme outil pour la préparation à haut débit d'échantillons de fractions sub-cellulaires pour des fins d'identification au microscope à transmission électronique. Il servira à valider la pureté d'échantillons sub-cellulaires et à confirmer la présence de protéines essentielles dans l'approche par organites cellulaires en protéomique.

L'appareil automatise toutes les manipulations chimiques et mécaniques nécessaires à la préparation d'organites à des fins de microscopie électronique. Sa conception, modulaire et intégrée, automatise la filtration, le procédé chimique, la livraison et l'enrobage de 96 échantillons de fractions sub-cellulaires en parallèle. Les spécimens de fractions sub-cellulaires sont extrêmement fragiles. Conséquemment, le système a été conçu en une seule unité afin de minimiser le stress mécanique imposé aux échantillons en intégrant un mécanisme central, composé de quatre plaques modulaires et sept sous-systèmes de support de : (1) refroidissement, (2-3) transport des liquides, (4-7) positionnement. De plus, un programme de contrôle fut développé spécifiquement pour le système, ce qui permet la standardisation d'un procédé d'échantillonnage de fractions sub-cellulaires reproductible, tout en conservant une flexibilité pour des ajustements et en mémorisant les paramètres opérationnels.

Le développement du procédé automatisé a progressé grâce aux expériences préliminaires de validation ainsi qu'à un criblage de procédé qui a défini les paramètres

opérationnels pour la préservation de l'intégrité des échantillons, établissant ainsi le point de départ pour la préparation réussie d'échantillons. Une succession de modifications afin d'étanchéifier l'environnement local des échantillons et de minimiser l'effet des perturbations fluidiques a amélioré grandement la performance du procédé. Subséquemment, le robot fut testé à pleine capacité de préparation d'échantillons, en utilisant les améliorations déterminées auparavant, et fut en mesure de générer 96 échantillons en 16 heures approximativement, réduisant ainsi le temps et le travail nécessaires jusqu'à 1000 fois, comparé à la préparation manuelle.

Ces résultats offrent une base pour une approche structurée d'optimisation de procédé et une éventuelle utilisation de l'appareil pour la préparation massive d'échantillons de fractions sub-cellulaires, en parallèle, pour criblage au microscope électronique et analyse quantitative de cibles sub-cellulaires ou protéiniques nécessaires à la protéomique à haut débit.

Acknowledgments

I would like to acknowledge the financial support of the Natural Science and Engineering Research Council of Canada (NSERC), Canadian Institutes of Health Research (CIHR), Genome Quebec (GQ), and Genome Canada (GC).

I would like to thank my supervisor, Dr. Robert E. Kearney, for his guidance, patience, and wisdom, and my Co-supervisor, Dr. John J.M. Bergeron, for his support and unbounded enthusiasm for science. I also owe a debt of gratitude to my thesis co-advisors, Dr. Frank Ferrie and Dr. Henriatta Galiana, for their kindness and guidance over the last eight years.

I would also like to thank all those who offered their technical support for this work. Karishma Punwani did all programming for the robot and without her help, the project may have been impossible to complete. Dr. Ali Fazel offered his experience, insight and extensive biological support. Eric Johnstone was my electronics guru and Daniel Seliskar developed a sensor device that may see a future generation of this robot.

For Shantal,
My life's delight,
To whom I owe endless love and appreciation

For Danaë Tulipe and Lorian Cyr,
My life's joy,
Who give me my greatest inspiration just by being

For Ruth,
My mother,
And God's gift to me

Contents

1 Introduction 1

1.1 Thesis Overview 7

2 Background 10

2.1 Overview 10

2.2 Proteomics Methodologies 10

2.3 Transmission Electron Microscopy 19

2.3.1 Transmission Electron Microscope Operation 19

2.3.2 TEM for Organellar Proteomics 21

2.4 TEM Sample Preparation 26

2.4.1 TEM Sample Preparation Criteria 26

2.4.2 Manual TEM Sample Preparation Protocol 27

2.4.3 Limitations of the Manual TEM Sample Preparation Method 37

2.5 Development of Laboratory Automation 39

2.5.1 Development of Proteomics Laboratory Automation 40

2.5.2 Limitations of Lab Automation for Organelle Sample Preparation 41

2.6 Thesis Objective: Development of the EMPOP Robot 44

3 Overview of Design and Operation of the EMPOP Robot 46

3.1 Overview..... 46

3.2 Design Objectives..... 46

3.3 Design Overview..... 47

3.4 Process Description..... 51

3.5 Core Mechanism..... 55

3.5.1 Plate Descriptions..... 56

3.5.2 Plate Configurations..... 59

3.6 Support Subsystems..... 62

3.6.1 Cooling Support Subsystem..... 63

3.6.2 Fluid Handling Support Subsystems..... 64

3.6.2.1 Reagent Handling Support Subsystem..... 64

3.6.2.2 Pneumatic Support Subsystem..... 68

3.6.2.3 Cleaning and Waste Management Support Subsystem..... 68

3.6.3 Positioning Support Subsystems..... 70

3.6.3.1 Motion Control Support Subsystem..... 70

3.6.3.2 Electromagnetic Transfer Arm Support Subsystem..... 72

3.6.3.3 Transfer Platform Support Subsystem..... 73

4 Mechanical Design of the EMPOP Robot..... 75

4.1 Overview..... 75

4.2 Core Mechanism..... 78

4.2.1 Core Mechanism Design Features and Concepts..... 78

4.2.2 Filter Plate..... 87

4.2.3 Fluid Transfer Plate..... 89

4.2.4 Vacuum-pressure Plate..... 89

4.2.5 Retainer Plate..... 92

4.2.6 Inter-plate Positioning..... 94

4.3 Cooling Subsystem..... 95

4.3.1 Thermoelectric Cooling..... 104

4.4 Fluid Handling Support Subsystems..... 109

4.4.1 Processing Reagent Handling Subsystem..... 110

4.4.1.1 Operation of the Processing Reagent Handling Subsystem..... 121

4.4.2 Pneumatic Subsystem..... 121

4.4.2.1 Operation of the Pneumatic Subsystem..... 125

4.4.3 Cleaning and Waste Management Subsystem..... 127

4.4.3.1 Operation of the Cleaning and Waste Management Subsystem.. 133

4.5 Positioning Support Subsystems..... 135

4.5.1 Motion Control Subsystem..... 137

4.5.2 Electromagnetic Transfer Arm Subsystem..... 142

4.5.3 Transfer Platform Subsystem..... 143

5 EMPOP Robot Electronics..... 153

5.1 Overview..... 153

5.2 Overview of the EMPOP Robot Electronics..... 153

5.2.1 Automation Control Electronics System..... 154

5.2.2 Power Supply Subsystem..... 166

5.2.3 Robot controller and extended I/O..... 171

5.3 Core mechanism..... 173

5.4 Cooling subsystem..... 179

5.5 Fluid Handling Subsystems..... 184

5.5.1 Processing Reagent Handling Subsystem..... 184

5.5.2 Pneumatic Subsystem..... 185

5.5.3 Cleaning and Waste Management Subsystem..... 187

5.6 Positioning Subsystems..... 188

5.6.1 Motion Control Subsystem..... 188

5.6.2 Electromagnetic Transfer Arm Subsystem..... 192

5.6.3 Transfer Platform Subsystem..... 195

6 Operation and Control of the EMPOP Robot..... 197

6.1 Overview..... 197

6.2 Automated Operation of the EMPOP Robot..... 197

6.3 Automation Control..... 212

6.3.1 Automation Control Software..... 212

6.3.2 Operator Tier..... 213

6.3.2.1 Interaction with the Operator Tier..... 221

6.3.3 Control Tier..... 224

6.3.3.1 Independent Control Tier Routines..... 225

6.3.3.2 Dependent Control Tier Routines..... 229

7 Experimental Results..... 235

7.1 Overview..... 235

7.2 Experiment I: Process Feasibility..... 235

7.2.1 Test Device..... 236

7.2.2 Experimental Methods..... 238

7.2.3 Results of the Process Feasibility Experiment..... 239

7.3 Experiment II: Process Screening..... 240

7.3.1 Process Validation Experiments..... 240

7.3.2 Experimental Methods..... 240

7.3.3 Results of Initial Process Validation Experiments..... 241

7.4 Conditions for Process Refinement..... 242

7.5 Process Screening..... 244

7.5.1 Process Screening Experimental Results..... 253

7.5.2 Summary..... 260

7.6 Experiment III: Optimization of Robotic Processing..... 260

7.6.1 Experiment IIIa: Filter Screen Sealing..... 262

7.6.2 Experiment IIIb: Adjustable Reagent Dispensing Velocity..... 265

7.6.3 Experiment IIIc: Pre-delivery Epon Incubation..... 268

7.6.4 Experiment IIId: Continuous Reagent Aspiration..... 270

7.6.5 Summary..... 272

7.7 Experiment IV: Full Sample Preparation Capacity..... 273

7.7.1 Experiment IVa: Implementation of Process Improvements..... 273

7.7.2 Experiment IVb: Implementation of Process Improvements..... 277

7.8 Summary..... 280

8 Discussion..... 281

8.1 Sample Preparation..... 281

8.2 Original Contributions..... 282

8.3 Future Work..... 283

8.3.1: Process Optimization and Application..... 284

8.3.2: Improvements to the Current Prototype..... 284

8.3.3 The Application to Cells in Culture..... 287

8.3.4 Second Generation EMPOP Robot..... 287

Bibliography..... 288

List of Figures

1.1	Major organelles of eukaryotic cell.....	5
2.1	Two MS-based strategies for the large-scale proteomics.....	12
2.2	Two-dimensional gel electrophoresis.....	13
2.3	Parts of a mass spectrometer.....	14
2.4	MALDI-TOF MS principles and instrumentation.....	15
2.5	LC-MS/MS principles and instrumentation.....	16
2.6	Resulting mass spectra and analyses for protein identification.....	18
2.7	Light and the transmission electron microscopes.....	20
2.8	Organellar proteomic strategy including TEM.....	22
2.9	Transmission electron micrograph to evaluate sample purity.....	23
2.10	Transmission electron micrographs illustrating immunolocalization...	25
2.11	Subcellular fraction filtration device.....	31
2.12	Centrifugation artifacts left in EM subcellular fraction preparations...	33
2.13	Pressure filtration and minimization of distribution heterogeneity.....	34
2.14	Filtered subcellular fraction samples.....	36
3.1A	Front view of the EMPOP robot.....	49
3.1B	Rear view of the EMPOP robot	50
3.2	Flowchart of the two manual preparation protocols.....	52
3.3	Channel of the core mechanism during automated preparation.....	53

3.4	Top view of the fluid transfer plate.....	56
3.5	Top view of the filter plate.....	57
3.6	Top view of the vacuum-pressure plate.....	58
3.7	Top view of the retainer plate.....	59
3.8	Top view of the core mechanism processing configuration.....	60
3.9	Top view of the core mechanism embedding configuration.....	61
3.10	Top view of the core mechanism delivery configuration.....	62
3.11	Top view of the cooling platform.....	63
3.12	The reagent handling panel and the reagent reservoir bank.....	65
3.13	Front view of the dispensing needle manifolds.....	66
3.14	Front view of the vacuum-pressure manifold.....	67
3.15	The pneumatic subsystem in-line valves.....	68
3.16	Top view of the clean station.....	69
3.17	The waste removal manifold and ball valve components.....	69
3.18	The EMPOP robot motion control subsystem.....	71
3.19	The electromagnetic transfer arm interacting with configuration.....	72
3.20	Front view of the transfer platform.....	73
4.1A	A front perspective rendering of the EMPOP robot.....	76
4.1B	A rear perspective rendering of the EMPOP robot.....	77
4.2	Core mechanism plate design features and standard plate components	79
4.3	Te core mechanism fluid transfer plate.....	84
4.4	The core mechanism interaction mechanisms.....	85

4.5 The filter plate assembly of components..... 88

4.6 The vacuum-pressure plate components..... 90

4.7 The vacuum-pressure plate stopper plate mechanism components..... 91

4.8 The retainer plate components..... 93

4.9 The processing configuration method of plate assembly..... 94

4.10 A rendering of the EMPOP robot showing the cooling platform..... 95

4.11 The spatial arrangement of the cooling platform subsections..... 96

4.12 The cooling platform modules..... 98

4.13 The cooling platform side platform components..... 99

4.14 A cooling platform side platform cooling block..... 101

4.15 The cooling platform central base components..... 102

4.16 The cooling platform central base cooling block..... 103

4.17 The cooling platform during plate decoupling..... 104

4.18 The arrangement of TEC/cooling block modules..... 105

4.19 The cooling water recycling flow path..... 107

4.20 The EMPOP robot fluids handling subsystems layout..... 109

4.21 The processing reagent handling system reagent bank..... 112

4.22 The reagent handling subsystem reagent handling panel..... 113

4.23 The arrangement of liquid handling components..... 114

4.24 The pump operations for reagent aspiration and dispensing..... 115

4.25 The mixer and the two mixing stages..... 117

4.26 The reagent dispensing needle manifold components..... 118

4.27 The dispensing needle manifold components..... 119

4.28 The reagent dispensing flow paths for single and mixed reagents..... 120

4.29 The spatial arrangement of the pneumatic subsystem..... 122

4.30 The vacuum-pressure manifold..... 124

4.31 The pneumatic subsystem flow paths..... 126

4.32 The arrangement of the cleaning and waste management subsystem... 128

4.33 The clean station components..... 129

4.34 Needle manifold interaction and operation of the clean station..... 130

4.35 Method for removal of vacuum reservoir accumulated liquid waste... 131

4.36 The cleaning and waste management subsystem flow paths..... 134

4.37 The positioning subsystems layout of the EMPOP robot..... 136

4.38 The six axis, servo motion control subsystem..... 138

4.39 The range of motion of the motion control subsystem axes..... 139

4.40 The positioning required for inversion of the core mechanism..... 140

4.41 The electromagnetic transfer arm..... 142

4.42 The transfer platform subsystem components..... 145

4.43 The range of motion transfer platform subsystem..... 146

4.44 Transfer platform stabilizing and positioning components..... 147

4.45 The transfer platform rotational actuator..... 148

4.46 The transfer platform vertical actuator..... 149

4.47 The transfer platform plate stabilizer..... 150

4.48 Operation of the transfer platform repositioning during inversion..... 151

5.1 Generalized arrangement of the EMPOP robot electronics system..... 154

5.2 The arrangement of the automation control electronics system..... 155

5.3 The component groups of the automation control electronics system.. 156

5.4 The motion control power group..... 158

5.5 The robot control group..... 159

5.6 The subcomponent control and interfacing group..... 160

5.7 The card cage sub-rack..... 161

5.8 The rail mounted relays and interface manifolds..... 162

5.9 Organization of the automation control enclosure rear surface..... 163

5.10 The 110 VAC automation control enclosure interface panel..... 164

5.11 The DC automation control enclosure interface panel..... 165

5.12 The arrangement of components of the power subsystem..... 167

5.13 The power supply organization in the power subsystem..... 168

5.14 Organization of the power subsystem enclosure rear surface..... 169

5.15 The power subsystem enclosure output panel..... 170

5.16 The robot controller connections to the robot control group..... 172

5.17 The magnetic proximity sensing method..... 175

5.18 The RTD/temperature transmitter component arrangement..... 176

5.19 The plate electromagnet decoupling circuit..... 177

5.20 The 60 VDC plate decoupling controller, unregulated power supply... 178

5.21 TEC power supply..... 181

5.22 The TEC controller arrangement..... 182

5.23	The cooling subsystem power distribution.....	183
5.24	The interconnection of motion control components to the controller...	189
5.25	The electromagnetic arm controller circuit and method.....	194
5.26	The transfer platform linear actuator control circuit.....	196
6.1	The manual processing steps in a core mechanism channel.....	198
6.2	Manual steps of a sample preparation run.....	199
6.3	A single channel during filtration, reagent dispensing/ aspiration.....	200
6.4	Direction of air flow in the processing configuration during filtration.	200
6.5	The cycle of events for the chemical processing stage.....	201
6.6	A single channel during the reconfiguration and inversion stage.....	203
6.7	Plate interchange steps for assembly of the delivery configuration.....	204
6.8	The plate inversion step of the core mechanism.....	205
6.9	Vertical positioning with the transfer platform.....	206
6.10	Repositioning of the core mechanism.....	207
6.11	Solvent washing and infiltration steps in the embedding stage.....	208
6.12	The sequence of events during for the delivery and embedding stage..	209
6.13	The delivery sequence.....	210
6.14	Direction of air flow in the delivery configuration.....	211
6.15	The embedding configuration is decoupled, leaving the retainer plate on the cooling platform, to complete the automated sample preparation run.	211
6.16	Logical diagram of the two-tier PC-based automation control system.	212
6.17	The EMPOP robot HMI Ethernet Connection GUI.....	214

6.18 The EMPOP robot HMI Motion Calibration GUI..... 215

6.19 The EMPOP robot HMI System Setup GUI..... 217

6.20 The EMPOP robot HMI Reagent Setup GUI..... 218

6.21 The EMPOP robot HMI Process Control GUI..... 219

6.22 The Process Monitoring GUI..... 220

6.23 Block diagram of the top-down organization of control routines..... 226

6.24 State diagram of the control-tier PLC program..... 228

6.25 Flow chart for the *Plate Cooling* routine first-order control algorithm. 230

6.26 The *Sample Filtration* routine first-order control algorithm..... 231

6.27 The *Sample Delivery* routine first-order control program..... 232

6.28 The *Reagent Handling* routine first-order control algorithm..... 233

6.29 The *Plate Manipulation* routine first-order control program..... 234

7.1 Two configurations of the processing channel test device..... 237

7.2 Retainer plate microfuge tube of the processing channel test device... 239

7.3 The filter/filter screen/delivered samples from an initial run..... 241

7.4 Renderings of the single processing channel arrangements..... 245

7.5 The screening platform..... 246

7.6 A single processing channel during a sample preparation protocol..... 248

7.7 The filters/filter screens/artifacts from screening experiments..... 257

7.8 delivery configuration of a single processing channel..... 258

7.9 A time-course illustration of Teflon filter screen deflection..... 259

7.10 Results of the sealed filter screen experiment..... 263

7.11 Close view of results of the sealed filter screen experiment..... 264

7.12 Modification for an adjustable aspiration needle manifold residence time and adjustment of reagent dispensing velocities..... 266

7.13 Results of the adjustable reagent dispensing experiment..... 267

7.14 Results of the pre-delivery Epon incubation experiment..... 269

7.15 Results of the aspiration needle residence time experiment..... 271

7.16 Results of the of the first full capacity experiment..... 275

7.17 Embedded samples of the of the first full capacity experiment..... 276

7.18 Results of the of the second full capacity experiment..... 278

7.19 Embedded samples of the of the first full capacity experiment..... 279

List of Tables

1.1	Principle function and morphology of major organelles.....	6
2.1	Manual preparation protocol for TEM morphometic analysis.....	28
2.2	Manual preparation protocol for TEM immunolocalization analysis...	29
7.1	modified protocol for single channel optimization experiments.....	249
7.2	Tested conditions for process screening experiments.	255
7.3	Parameters and materials for process development experiments.....	261
7.4	Parameters and materials for the full capacity experiments.....	274

1 Introduction

Biology has experienced great successes in the last several decades – most notably the recent completion of the global effort to sequence the human genome [1, 2]. While genome sequencing results have been spectacular, it is clear that the detailed record of genes is not sufficient to understand the intricacy of the cell. It is accepted that the genome represents only the first level of complexity and that genomic analysis presents limited information at the tissue, cellular and subcellular levels, in which proteins, not genes, direct function. For example, aspects of mature proteins such as splice variants and post-translational modifications (PTMs) (e.g., phosphorylation, glycosylation, ubiquitination, and methylation), determine protein function and represent an extraordinary level of complexity [3]. Moreover, although quantitative high-throughput biological tools, such as DNA microarrays, offer immense potential for understanding the molecular changes that occur during biological processes, they do not capture mechanisms of regulation such as changes in cellular localization, sequestration by interaction partners, proteolysis, and recycling [4]. Biological function is not carried out by the static genome but by changes in global protein expression or the dynamic population of proteins determined by the interplay of gene and protein regulation with extracellular influences.

Methods have been developed to quantify important classes of biological molecules and efforts are being made to examine their interactions. Systems biology,

through an integrated perspective, aims to interpret the mechanisms behind the complex phenomena whereby all components of a biological system interact functionally over time [4-6]. Although the field is in its infancy, this approach is required to understand the full scope of the complex interrelationships among all elements (rather than studying them one at a time) of the cell. Genomics and other systems disciplines, which have become possible with the advent of high-throughput tools and technologies to analyze and process enormous amounts of data, provide the infrastructure to expedite traditional biological research into the functions of single genes and the mechanisms of particular cellular processes. Eventually, large-scale methods of studying biology will revolutionize the field by providing systems-level information and patterns that traditional research approaches could ever generate.

The genome sequences of many species are available [1, 2, 5] and the focus now is shifting to large-scale experiments enabled by this data. Following in the footsteps of genomics, there is increasing interest in the global study of all the proteins in organs, tissues, or individual cell types - the field of proteomics.

The term proteome was originally defined as the complete protein complement expressed by a genome ("PROTeins expressed by the genOME") [7]. However, the definition has been extended to recognize that the proteome is highly dynamic and will change with cellular state and the extracellular environment; a more extensive definition is the protein complement of a given cell at a specified time, including the set of all protein isoforms and protein modifications [8-18].

The appeal of proteomics lies in its ability to acquire data on selected populations of proteins in specific circumstances, offering direct insight into their function. While the

information resulting from proteomics research is valuable, there are three properties of proteins that make them particularly challenging for global analyses: (1) the enormous dynamic range of abundance (1 to 10^6 copies per cell), (2) the dynamic patterns of expression, and (3) protein identity. Although great progress has been made in developing instrumentation, experimental strategies, and bioinformatics methods for proteomics, there is a continuing need to develop more innovative instrumentation and high-throughput platforms to deal with these protein complexities.

Proteomics depends on a rapidly emerging set of key technologies that make it possible to identify large numbers of proteins in a mixture, to map their cellular locations, and analyze their biological roles and behavior [5]. Mass-spectrometry (MS) has evolved into a flexible tool that, when coupled with various separation methods, is capable of examining the simultaneous expression of more than 1000 proteins as well as identifying and mapping their PTMs [18, 20-31]. High-throughput array methods have enabled large-scale characterization of protein localization, protein-protein interactions, and biochemical analysis of protein function [18, 32, 33]. Finally, the vast amount of data generated in recent years has led to the development of approaches for their integration to increase understanding of both individual protein function and complicated biological processes [15].

Although promising, the information gathered from proteomics efforts also indicates that the complexity of the cell poses a significant challenge in determining the proteome. Thus, the complexity of eukaryotic cells is such that a single-step characterization of the complete proteome is too complex for existing technology [34].

Present estimates are that >10,000 genes are expressed in a single cell type [34]; the number of proteins is much larger due to alternative splicing. In addition, posttranslational modifications occur [3, 10, 18] that alter enzymatic activity, binding ability, active life, and other properties of proteins. Thus, the size of the human proteome is much larger than the number genes expressed [18]. Furthermore, the range of expression for different proteins in a cell or tissue offers further complexity because high abundance proteins will mask those in low abundance. Consequently, proteomic studies of whole cells or tissues will be incomplete. The challenge is to combine high-throughput screening with a sample preparation that permits the detection of low copy number proteins. There is no amplification method for proteins, such as the polymerase chain reaction method for amplifying DNA. Therefore, proteomics is still restricted by the lack of an analogous amplification method for proteins and/or an alternative method to analyze and identify focused subsections of the proteome in a quantitative manner.

One approach to mapping proteomes has been to concentrate on protein subsets. Affinity fractionation is a method that isolates groups of proteins having similar features and concentrates proteins in low abundance [35]. This approach permits low abundance proteins to be identified, but offers no information about the cellular location.

Another approach to the analysis of the cellular proteome is to focus on organellar or subcellular proteomes [34-46], to link proteomic data with the components of the cell. Figures 1.1A and B and Table 1.1 shows that eukaryotic cells are organized into subcellular compartments and macromolecular structures having specialized roles - the organelles. Organelles can provide subsets of proteins for analysis because they can be fractionated from a cell or tissue homogenate [35, 41, 43, 47-50], essentially dividing a

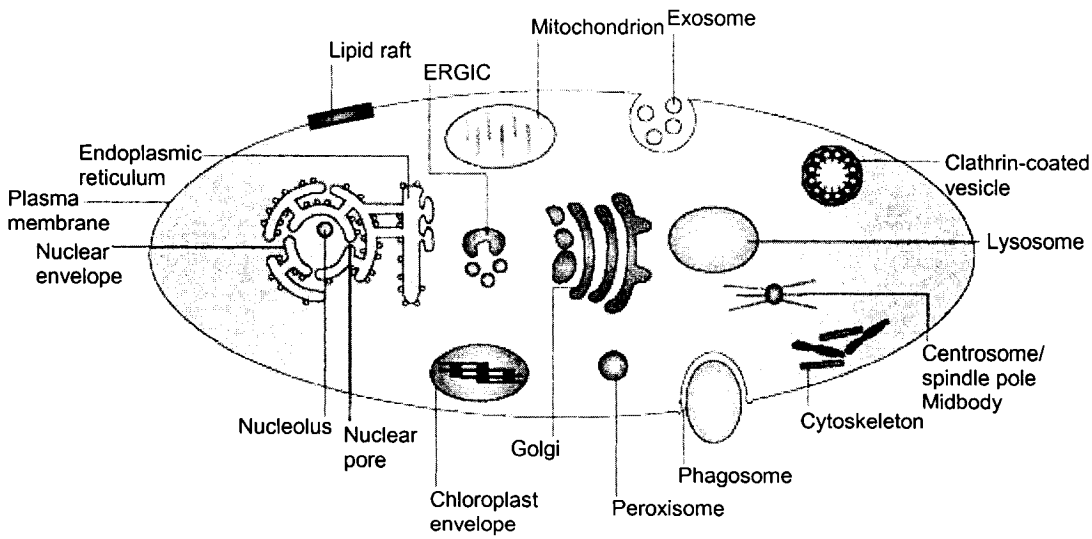

Figure 1.1: A schematic of a eukaryotic cell showing major organelles and large subcellular structures [46].

proteomics strategy into analysis of sub-proteomes. Furthermore, different organelles contain specific sets of proteins that support their processes (e.g. protein synthesis and degradation, provision of energy-rich metabolites, protein glycosylation, DNA replication, etc.). Therefore, the organellar approach to proteomics, in which focused subsets of proteins are identified at the subcellular level (according to the inherent organization of cells), represents a good method for mapping the proteome and understanding cellular function.

Transmission electron microscopy (TEM) [51-58] is a technique that combines sensitive immunological protein detection with detailed morphological information for subcellular substructure. This combined information gives TEM a central position in organellar proteomics to: (1) screen the homogeneity of subcellular fraction samples, (2) define intracellular protein distribution patterns, and (3) identify the location of novel

Table1.1: Major organelles and large subcellular structures [46].

Exosomes	Vesicles discharged into the extracellular environment when multivesicular endosomes fuse with the plasma membrane.
Phagosomes	Subcellular compartments resulting from invagination of the plasma membrane for internalization and degradation of a large macromolecular complex or pathogen.
Clathrin-coated vesicles	Mediate sorting and selective transport of membrane-bound proteins for several pathways of intracellular membrane traffic. They are responsible for receptor-mediated endocytosis at the plasma membrane and sorting of proteins at the trans-Golgi network during the biogenesis of lysosomes and secretory granules.
Mitochondria	Function in oxidative phosphorylation and ATP production in all cells.
Peroxisomes	Specialized for oxidative reactions that produce hydrogen peroxide and linked to numerous functions including fatty acid metabolism and plasmalogen synthesis.
Endoplasmic reticulum (ER)	Principle site of protein and lipid synthesis, and protein glycosylation. The rough ER is studded with ribosomes where the mRNAs of transmembrane and secretory proteins are translated. The newly synthesized proteins subsequently enter the protein-folding 'factory' of the ER lumen. The smooth ER lacks ribosomes and is the principle site for fatty acid and phospholipid synthesis.
Endoplasmic-reticulum-Golgi-intermediate-compartment (ERGIC)	Intermediate compartment composed of tubular–vesicular structures that mediate transport in the exocytic pathway from the ER to the Golgi.
Golgi complex	The central organelle of the exocytic pathway that is responsible for many of the post-translational modifications of newly synthesized proteins and lipids, as well as for the sorting of these molecules to their site of function.
Chloroplast envelope	Two membranes (inner and outer) that surround the chloroplasts of plants and algae.
Lysosomes	Main degradative compartment of the cell. Representative of the end point of the endocytic pathway, they contain many different hydrolytic enzymes that degrade cellular macromolecules.
Nucleus	Contains the main genome and is the site for DNA and RNA synthesis.
Nuclear pore	The nuclear pore complex bridges the inner and outer membranes of the nuclear envelope. The "hole" in the center (the nuclear pore) is an aqueous channel through which water-soluble molecules shuttle between the nucleus and the cytoplasm.
Nucleolus	Ribosome-generating region of the nucleus where transcription is coordinated with processing of ribosomal RNA and ribosome biogenesis.
Nuclear envelope	Composed of two concentric membranes that are continuous with the endoplasmic reticulum. It encloses the DNA and defines the nuclear compartment.
Plasma membrane	Selectively permeable membrane composed of a thin and structured bilayer of phospholipid and protein molecules that envelopes the cell. It maintains the essential differences between cell contents and often contains receptor proteins, cell adhesion proteins as well as other proteins important for the regulation of cell behavior and the organization of cells in tissues.
Membrane domains and lipid rafts	Subdomains of the plasma membrane that contain high concentrations of cholesterol and glycosphingolipids. They may constitute a relatively large fraction of the plasma membrane and, while having a distinctive protein and lipid composition, they do not appear to be identical in terms of either the proteins or the lipids that they contain. A variety of proteins, especially those involved in cell signaling, have been shown to partition into lipid rafts. As a result, extremely dynamic functional domains are thought to be involved in the regulation of signal transduction.
Cytoskeleton	A dynamic three-dimensional structure that fills the cytoplasm and acts as both muscle and skeleton, for movement and stability. The long fibers of the cytoskeleton are polymers of subunits. The primary types of fibers comprising the cytoskeleton are microfilaments, microtubules, and intermediate filaments.
Centrosome	Composed of a pair of centrioles that are each made up of a ring of nine groups of microtubules (three per group). During cell division, the centrosome divides and the centrioles replicate, resulting in two centrosomes. The centrosomes move to opposite ends of the nucleus, and microtubules grow from each into a "spindle", which is responsible for separating replicated chromosomes into the two daughter cells.
Mitotic spindle	A network of microtubules formed during prophase. Some microtubules attach to the centromeres of the chromosomes and help draw the chromosomes apart during anaphase.
Midbody	During cytokinesis, when membrane cleavage is almost complete, the plasma membrane of the cleavage furrow tapers to form the midbody. It is derived from the central spindle and persists as an attachment between the two daughter cells before final separation.

proteins in isolated organelles. Although TEM is powerful, sample preparation is an important bottleneck at present.

The current, manual, method requires a first filtration step to deposit and localize the sample onto a charged filtration membrane; ensuring random sampling of the preparation [59]. This is followed by a complex chemical processing protocol to prepare the samples as specimens for TEM. The manual method takes several days for an experienced scientist or technician to complete and reproducibility is difficult or impossible to attain. Thus, TEM analyses of multiple, subcellular fraction samples are impractical for large-scale proteomics.

In response to the need for a high-throughput sample preparation method for proteomics research, we have developed the Electron Microscopy Proteomic Organellar Preparation (EMPOP) robot [60-62]. The EMPOP robot is a high-throughput tool to prepare samples for electron microscopic characterization. Its autonomous, integrated design allows it to prepare up to 96 subcellular fraction samples within the period of a day; enabling quantitative analysis and reducing the time and labor requirement up to 1,000 fold.

1.1 Thesis Overview

Chapter Two presents a general introduction to MS-based organellar proteomics, subcellular fractionation, TEM for organellar proteomics and its limitations. A discussion of the development of laboratory automation for proteomic research is offered and then the limitations of the use of commercially available laboratory automation to

process subcellular fraction samples for electron microscopy are discussed. The chapter ends with a statement of the thesis objective: development of the EMPOP robot.

Chapter Three introduces the operational concepts of the automated process and acquaints the reader with the robot design by describing the robot's sample processing "center", the core mechanism, and each of its seven support subsystems. The next two chapters are organized similarly.

Chapter Four describes the mechanical design of the robot and the methods used to integrate the core mechanism and support subsystems. Based upon the fragility of the samples and the complexity of the preparation process, the rationale was design of an autonomous system to minimize mechanical perturbations and maximize chemical, biological, and mechanical parameters.

Chapter Five describes the electrical and electronic components of the robot. It starts with an overview of the control and power components and progresses to a detailed description of the electrical system, from the robot controller through each of the components.

Chapter Six describes operation and control. It is comprised of two sections dealing with: (1) operation of all system components through an automated sample preparation run, and (2) the operator interface and programming for system control.

Chapter Seven describes a progression of four experiments carried out during the development and validation of the EMPOP robot. The first experiment investigates the feasibility of automatic processing and demonstrated the need to define essential process parameters and determine optimal operating conditions. A second set of experiments was undertaken to meet this need by screening a wide range of operation parameters. The

third experiment used these results to demonstrate that the EMPOP robot could generate samples successfully using a limited number of samples. The fourth experiment tested the full capacity of the robot to prepare 96 parallel samples.

Chapter Eight summarizes the contributions made in this thesis, and offers suggestions for further developments and improvements.

2 Background

2.1 Overview

This chapter reviews the principles of organellar proteomics using MS-based analysis strategies to introduce the need for TEM. We argue that the current manual sample preparation method is not adequate for large-scale proteomics and that an automated approach is required. This provides the motivation for the thesis objective: the development of an Electron Microscopy Proteomic Organellar Preparation robot.

2.2 Proteomics Methodologies

Although some proteomics experiments require only well established laboratory procedures to be scaled and/or automated, large-scale proteomics experiments require specialized tools designed to fit the particular experimental design. There is currently no tool or method to identify and quantify the components of a complex protein sample in a single-step. The complexity of the proteome and the current level of sophistication of analytical instrumentation requires the combined application of individual tools for separating, identifying, and quantifying proteins as well as integrating and analyzing data.

Eukaryotic cells segregate and organize molecules that carry out specific functions in organelles. In the organellar approach to proteomics, organelles are isolated *via* subcellular fractionation techniques to reduce sample complexity [35, 41, 43, 47-50].

This well established method separates organelles based on their physical properties (largely size and density), and consists of two principle steps: (1) disruption of cellular organization (homogenization), and (2) fractionation of the homogenate *via* a combination of centrifugation approaches to separate the different populations of organelles [35, 41, 43]. Generally, fractionation is repeated several times to enrich the target organelle(s).

A typical organellar specimen will still contain thousands of different proteins; the application of additional fractionation technologies can further enrich organelle proteins and improve the ability to detect low abundance proteins. Examples of these techniques include protein and peptide affinity purification of samples, chromatographic protein prefractionation, zoom gels of narrow pH ranges for 2DE and preparative isoelectric focusing, or multidimensional peptide separations [35].

Combining these methods with the tools of large-scale proteomics research provides a strategy for the functional characterization of organelles; permitting the identification of protein subsets, characterization of protein localization, and tracking their transport among different compartments. Moreover, promising approaches are being developed to identify and characterize integral membrane proteins, previously difficult to analyze, to provide more thoroughly representative proteomic analysis [63-65].

A typical, large-scale proteomics analysis of organellar protein mixtures involves three stages: (1) protein separation, (2) protein digestion/peptide extraction, and (3) mass spectrometric analysis. Figure 2.1 shows generalized schemes for two commonly used MS-based strategies.

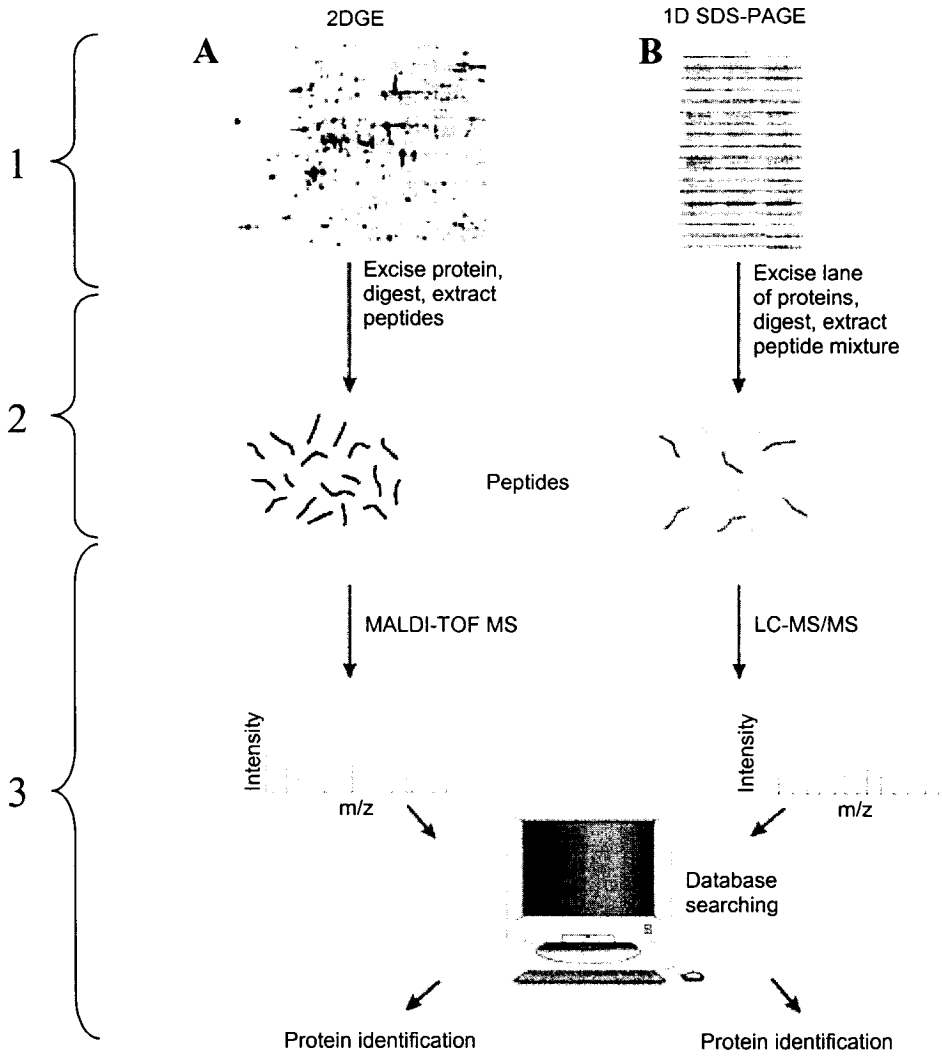

Figure 2.1: Generalized schemes of two commonly used MS-based strategies for the large-scale proteomics analysis of organellar protein mixtures. (A) 2DGE and MALDI-TOF MS and (B) 1D-SDS-PAGE with LC-MS/MS, progress through three stages for: (1) protein separation, (2) protein digestion/peptide extraction, and (3) mass spectrometric analysis [46].

Part A of Figure 2.1 shows a scheme that uses a two-dimensional electrophoresis (2DGE) separation method for soluble proteins [66-70]. Figure 2.2 shows how separation *via* 2DGE begins with isoelectric focusing of proteins on an immobilized pH gradient strip. Proteins migrate across the pH gradient until they reach the pH that renders their charge neutral, the isoelectric point (pI). In the second dimension of 2DGE,

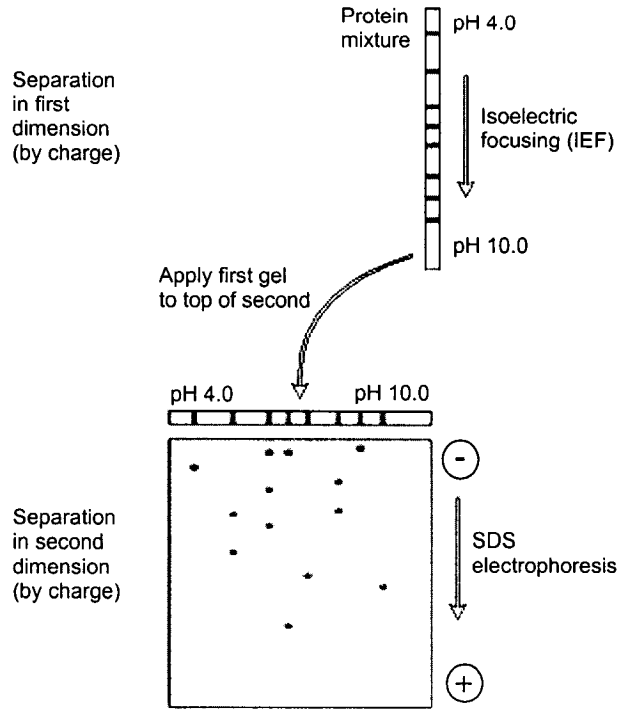

Figure 2.2: In two-dimensional gel electrophoresis (2DGE) proteins are separated based on their charge by isoelectric focusing (IEF) in the first dimension and then their mass by sodium dodecyl sulfate polyacrylamide gel electrophoresis (SDS-PAGE) in the second dimension [67].

Differences in proteins isoelectric points (pI) are the basis of separation by isoelectric focusing (IEF). The pI is the pH at which a protein will not migrate in an electric field and is determined by the charged groups in the protein. Proteins can carry positive, negative or zero charge depending on their local pH, and for every protein there is a specific pH at which its net charge is zero; the pI. If the protein diffuses to a region outside its pI it will pick up a charge and migrate back to the position where it is neutral. This ensures that proteins are condensed, or focused, into sharp bands.

SDS binds to most proteins in a constant manner (~1.4 g/g, SDS/protein) and masks the charge of proteins by forming large anionic complexes. SDS also disrupts any hydrogen bonds, blocks many hydrophobic interactions and partially unfolds the protein molecules minimizing differences based on secondary or tertiary structure. To ensure separation based on molecular weight, a reducing agent such as beta-mercapthoethanol or dithiothreitol is often included to unfold proteins and separate subunits.

When electrical current is applied, the detergent saturated proteins are then sieved through the polyacrylamide gel (toward the cathode) based of their molecular weight. The rate of migration is inversely proportional to molecular weight, larger proteins exhibit more resistance and migrate slowly down the gel.

proteins with similar isoelectric points are separated further according to their molecular weight *via* sodium dodecyl sulfate polyacrylamide gel electrophoresis (SDS-PAGE). The detergent, SDS, coats all proteins in a mass ratio of ~1.4:1 to generate a uniform charge density and thereby permit protein separation on the basis of molecular weight. The gel is stained to visualize the protein pattern (silver, Coomassie blue or fluorescent staining) [71] and spots containing proteins of interest are excised from the gel. Because MS analysis of whole proteins is less sensitive than peptide MS, the proteins are enzymatically digested (typically with trypsin) to peptides of ~20 amino acids. The peptides are analyzed *via* MS techniques (see Figure 2.3), such as matrix-assisted laser

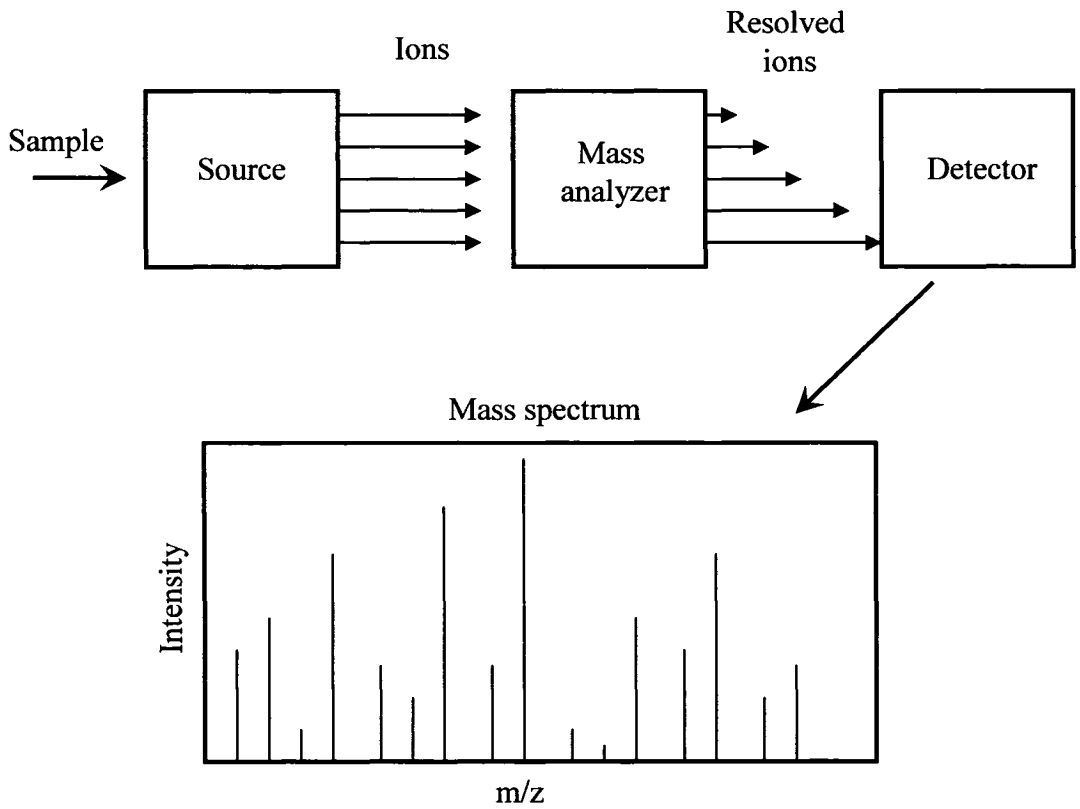

Figure 2.3: A mass spectrometer consists of three principle parts: (1) an ion source to volatize or ionize the proteins or peptides, (2) a mass analyzer that measures the charge to mass ratio (m/z) of the ionized analytes, and (3) a detector that registers the number of ions at each m/z value to produce the mass spectrum for a mixture of peptides [74].

desorption/ionization-time-of-flight (MALDI-TOF) [20, 50, 72-79]. As Figure 2.4 shows, MALDI sublimates and ionizes the peptide samples out of a dry, crystalline matrix *via* laser pulses. Peptide ions are passed through a TOF mass analyzer to the detector resulting in a mass spectrum; a recording of the ion signal intensity across the mass-to-charge (m/z) scale. Data analysis for peptide mass fingerprinting proceeds by comparing the resulting peptide mass spectra against protein sequence databases (see Figure 2.6) [52, 80-88]. The result is the identity of the peptides and therefore the proteins making up the protein population of the organelle.

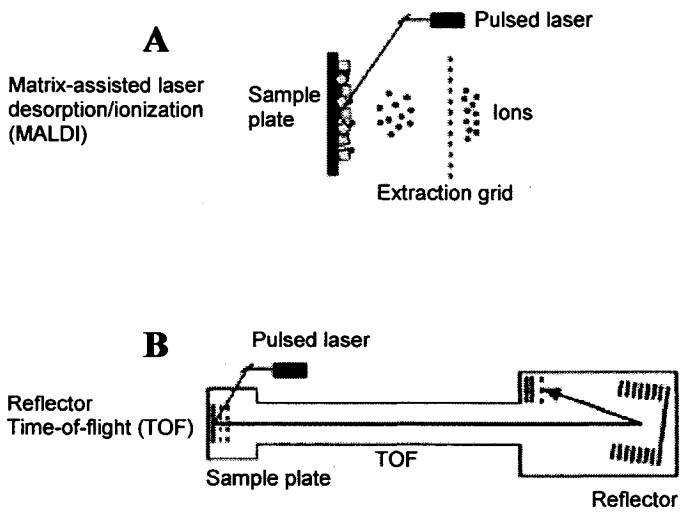

Figure 2.4: MALDI-TOF MS principles and instrumentation [20]. (A) For MALDI, the analyte is mixed with a large excess of an ultraviolet (UV) absorbing chemical matrix; typically a small organic molecule with a chromophore (normally a low molecular weight aromatic compound) that absorbs a specific wavelength of light. The mixture is spotted onto a small plate and allowed to evaporate, causing crystallization of the mixture. Irradiation of this crystallized target with a focused laser beam causes electronic excitement by the UV absorbing matrix. The excess energy is transferred to the peptides (as heat) causing them to sublimate. Gas-phase ion-molecule collisions in the sublimating plume forms highly protonated analyte ions, which are accelerated by electric potentials into the TOF mass analyzer. (B) In TOF mass analyzers, m/z ratios are determined by measurement of the time it takes for ions to pass through a field free region. With a constant acceleration voltage, the flight time to the detector is related to the m/z ratio of an ion. Introduction of a reflector to the TOF mass analyzer corrects for small kinetic energy differences among ions with similar m/z ratios; minimizing differences in flight times and increasing resolution.

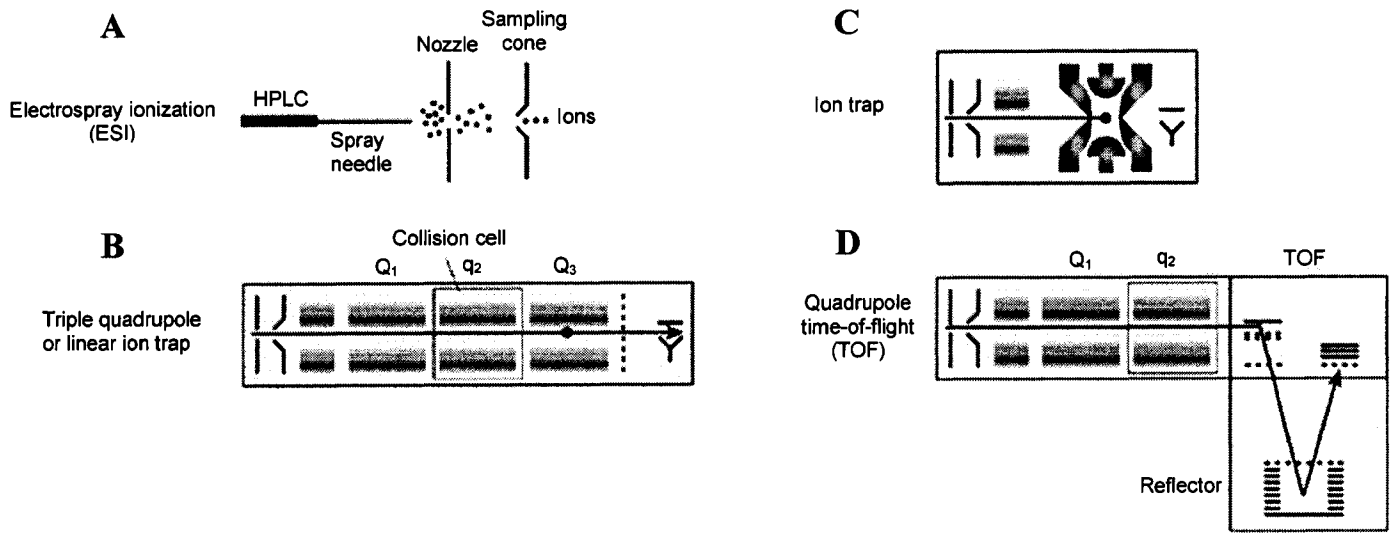

Figure 2.5: LC-MS/MS principles and instrumentation [20]. (A) Peptide mixtures are fed to an electrospray ionization source (ESI) by way of HPLC; to separate the peptides as well as to remove buffers, salts and detergents that may interfere with the mass spectrometric analysis. The eluted peptide samples enter the ESI source through a stainless steel needle that is held at a high electrical potential (several kV). The potential difference relative to the mass spectrometer entrance causes electrostatic dispersion of the flow steam; spraying out as a fine mist. Desolvation of the ions (removal of the HPLC mobile phase) *via* application of heat or dry gas, precedes introduction the ions to the mass analyzer.

Three types of tandem mass analyzers are commonly used to resolve m/z ratios of peptides: the triple quadrupole (triple quad), the ion trap, and the quadrupole-time-of-flight (Q-TOF). Quadrupole mass spectrometers select peptide ions by a combination of DC and radiofrequency (RF) voltages applied to four parallel metal rods. (B) The triple quad is composed of three quadrupoles (Q_1, q_2 and Q_3). To acquire tandem mass data, Q_1 is used as a mass filter, where adjustment of the DC to RF ratio creates stable trajectories for ions with selected m/z ratios, permitting passage to the next quadrupole. In the quadrupole collision cell, q_2, selected ions collide with argon gas atoms to fragment. Repeated scanning over a designated mass range, by Q_3, permits detection and analysis of the fragmented ions on the basis of their m/z ratio. (C) Tandem mass analysis in ion traps occurs by capture of the ions from the source followed by quick excitement by increasing voltages in the trap. Fragments are formed by collisions with helium gas atoms, which are then scanned out according to their m/z ratios. In the linear ion trap (see Figure B), where ions are captured in a quadrupole section (designated by the dot in Q_3). (D) In the Q-TOF, a TOF mass analyzer replaces Q_3, when m/z ratios are determined by the time it takes for ions to pass through a field-free region.

Methods employing electrophoresis and liquid chromatographic pre-separation steps are rapidly displacing this 2D strategy described above. Part B of Figure 2.1 shows the current standard for MS-based proteomics analyses; a combination of one-dimensional (1D) SDS-PAGE and liquid-chromatography-tandem MS (LC-MS/MS) [20, 46, 50, 63, 76, 89, 90]. SDS-PAGE [67] (see Figure 2.2) is an effective method to separate complex protein mixtures containing membrane proteins; the detergent (SDS) solubilizes membrane proteins. After electrophoretic separation, a lane of the stained gel is excised, cut into bands, and the proteins are digested for MS analysis.

Figure 2.5 show the principles of LC-MS/MS, where the peptide are introduced to the mass spectrometer by way of a high performance liquid chromatography (HPLC) column [20, 52]; this provides an additional dimension for separation after SDS-PAGE. An organic solvent gradient elutes the peptides from the column to the tandem mass spectrometer, which determines the amino acid sequence of peptides. In tandem MS, peptide masses are determined in the first mass analyzer. Further fragmentation at peptide bonds generates a nested set of peptides that differ in size by single amino acids. Their masses are determined in a second stage, and it is possible to deduce the amino acid sequence by considering the mass difference between neighboring peaks in a series. As Figure 2.6 shows, a partial amino acid sequence of the original protein is determined by repeated application of the procedure. Similar to the previous MS-based scheme, database searching is then used to determine the identity of the protein(s) [80-84, 90-94].

Several algorithms permit matching of tandem mass spectra to peptide sequences [90], and a typical sequence of events proceeds as follows:

(1) Match tandem mass spectra to calculated peptide mass or fragment ion mass values.

(2) Apply appropriate protease cleavage rules, to matched theoretical peptide masses to the protein database.

(3) Score probability of corresponding mass values to determine the identity of the peptide or protein that best matches the data (closest sequence homology) [10, 90, 91].

(4) Take into account PTMs *via* mass spectrometric peptide sequencing combined with other analytical technologies [20-31, 90, 91].

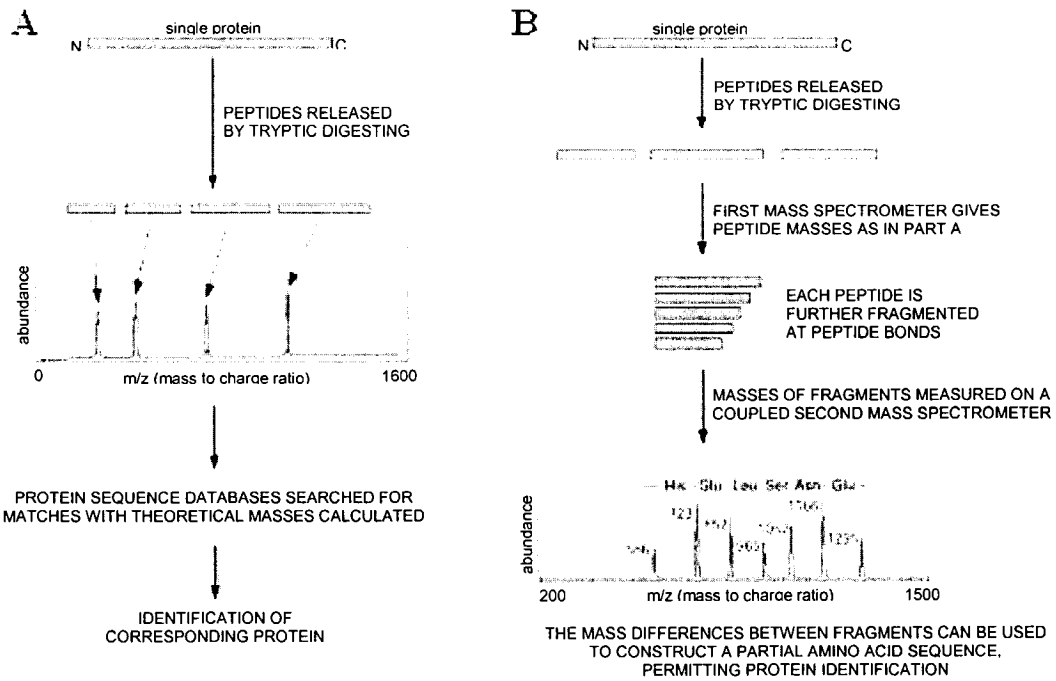

Figure 2.6: Analysis schemes showing protein digestion, resulting mass spectra and analyses for protein identification *via* (A) MS-based peptide mass fingerprinting and (B) MS/MS-based peptide sequence analysis [52].

Although MS-based strategies generate robust and impressive analyses, technological innovations not just in mass spectrometry, bioinformatics and data analysis will advance proteomics. Efforts are also underway to develop antibody based technology to provide the high sensitivity, specificity and reproducibility required for analysis and visualization for large-scale proteomics [95, 96].

Epitope tagging and antibody screening of cells *via* high throughput analytical light microscopy (LM) is a current initiative [97-102]. However, organelles are beyond the resolution of LM and the fine details of protein localization must be determined at the EM level [103]. EM methods at present are arduous and highly specific to each laboratory. Hence, to apply EM to proteomics, standard and reproducible methods are required.

2.3 Transmission Electron Microscopy

The current analytical methods for organellar proteomics are powerful, but methods are still needed to provide direct proof of organelle sample homogeneity and that the proteins identified by mass spectrometric analysis are actually present within that organelle. TEM can provide both [51-58].

2.3.1 Transmission Electron Microscope Operation

TEM is a high-resolution imaging technique that can image specimen details with a resolution at or approaching the Ångstrom level (10^{-10} m). Figure 2.7 shows that the transmission electron microscope in a manner analogous to the operation of a light

microscope, applies a focused, high-voltage, beam of electrons to a specimen to magnify features up to 500,000 times [52, 104].

A transmission electron microscope consists of four principle components: (1) an electron source, (2) a specimen holder, (3) electromagnetic coils and (4) a viewing screen. Electrons travel down a column (wavelength ~0.002 nm) where electromagnetic coils, located along the axis of the column, focus the particles into a thin beam. To prevent random scattering of electrons by air molecules, air is pumped out of the column to create a vacuum.

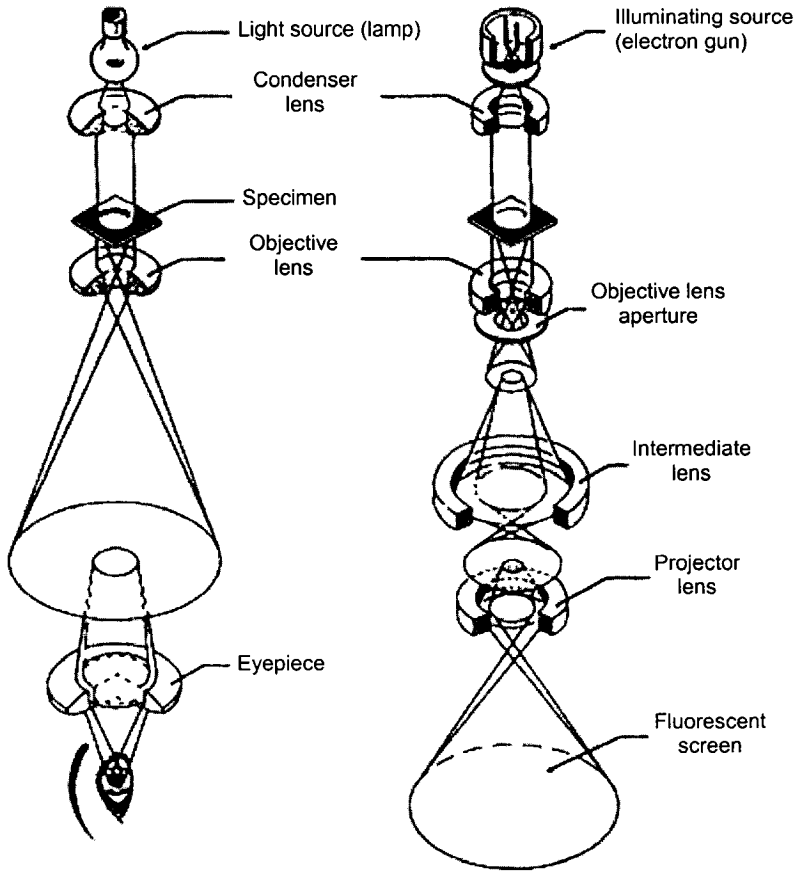

Figure 2.7: A comparison of schematics illustrating the analogous components and methods of operation of light and the transmission electron microscopes [51].

When the electron beam meets the specimen, some of the electrons penetrate and others reflect or scatter away. The degree of scattering is directly dependent on the local density of the specimen. Therefore, only electrons that permeate the specimen arrive at the phosphorescent screen, to produce a "shadow image" of the specimen. This density-based image, where dark regions represent specimen areas of high density, is the product of the transmission electron microscope [51, 52].

2.3.2 TEM for Organellar Proteomics

Since the mid 1950s, transmission electron microscopy has been used to visualize organelles. Since then, the power of the device has increased with the development of fixing, staining, embedding and sectioning techniques as well as the instruments themselves [104, 105]. In parallel, fractionation [47] and centrifugation [106] techniques have also improved. High resolution pictures of mitochondria [109], the Golgi complex [110], the endoplasmic reticulum [111], lysosomes [112], and peroxisomes [113] are now available. Consequently, biologists have a wealth of knowledge concerning cellular ultrastructure [114, 115] and the molecular details of organelle composition, structure, function, and biogenesis.

Regardless of advances made in other imaging tools, TEM remains the only technique that can provide detailed information about intracellular structures with specific, sensitive detection methods to define intracellular protein location and distribution patterns. This makes TEM a very valuable analytical tool for organellar proteomics [34]. In this regard, Figure 2.8 shows how TEM analysis is required at the beginning and end of a large-scale organellar based approach to proteomics to:

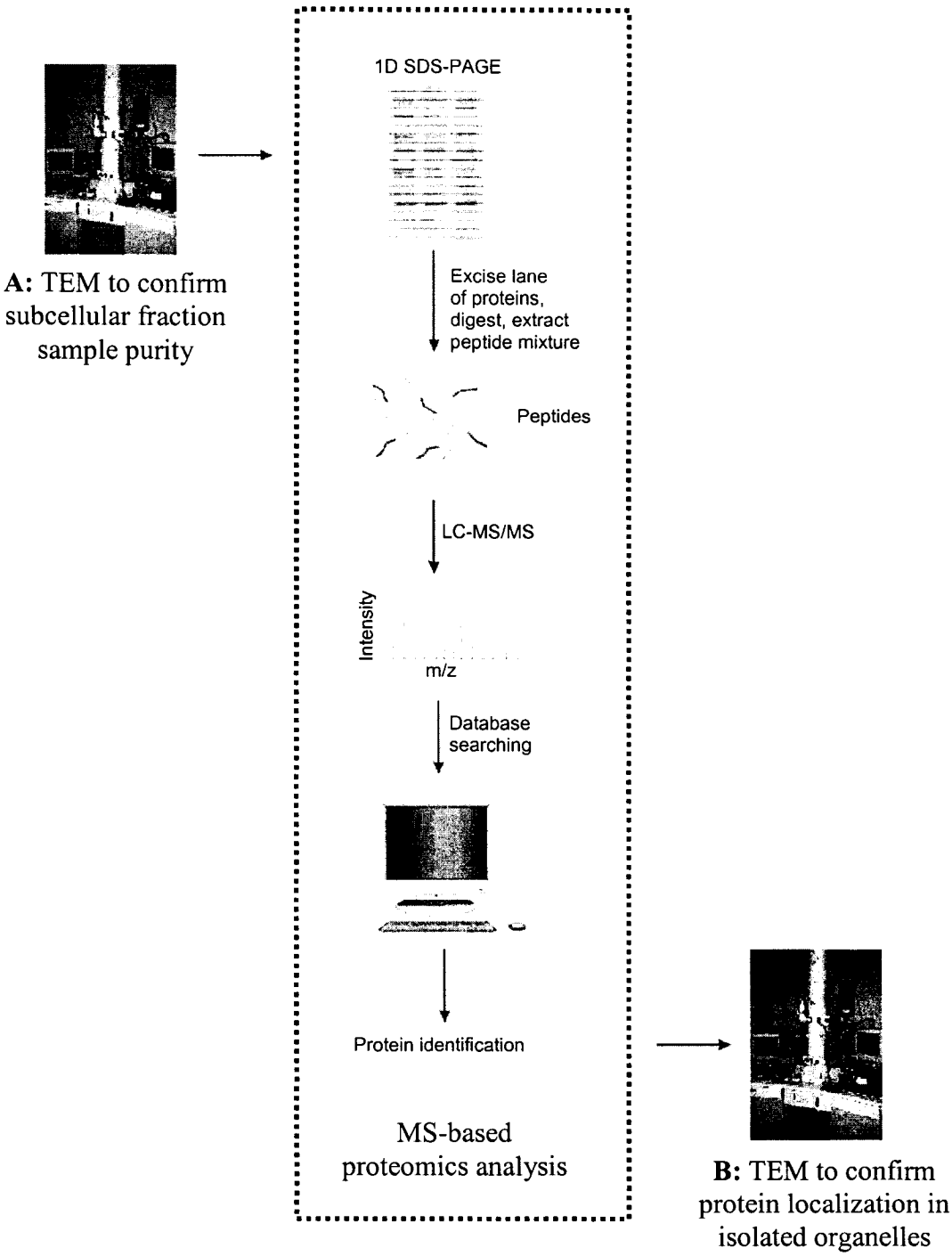

Figure 2.8: Organellar proteomic strategy including TEM in the initial and final phases for confirmation of (A) subcellular fraction sample purity and (B) protein localization in isolated organelles [46].

(1) confirm the sample purity by morphometry of subcellular fraction preparations and (2) to confirm protein localization in isolated organelles.

(1) Sample purity. Often contaminating cell debris and other relatively heavy cellular membranes (ER, plasma membrane, cytoskeltal elements, and large cytoplasmic protein complexes) are carried through all the steps of a purification procedure. TEM provides a means to screen or monitor the efficiency of the fractionation

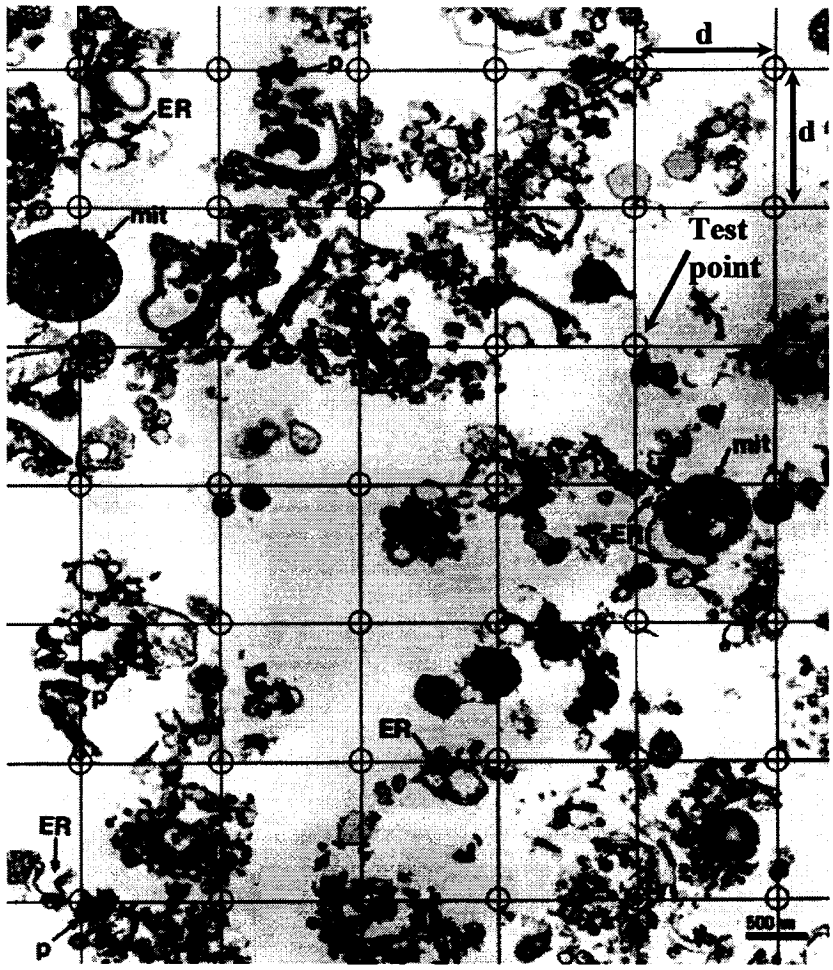

Figure 2.9: Transmission electron micrograph with superimposed regular point lattice illustrating the point hit stereological test method used for statistical evaluation of organelle sample purity. The test points are spaced by a distance, d, such that no more than one point can land on the same organelle [129, 130]. Organelles are indicated as ER (endoplasmic reticulum), mit (mitochondria), and p (perioxisome) [117].

steps and to compare the enrichment and purity of different preparations [34, 116-128]. Figure 2.9 illustrates the point hit stereological test method [129, 130] used to determine organelle sample purity. A regular point lattice is superimposed on micrographs of the randomly dispersed organelles to permit a statistical evaluation of organelle density (mean, median, standard deviation, etc.). Each point constitutes an independent sample, and the points are spaced (by a distance, d) such that no more than one point can land on the same organelle. In using the method, magnification of electron micrographs must be optimized to allow unambiguous localization of test points within organelles (adequately high magnification) while ensuring that a large enough section area is included in the micrograph (adequately low magnification).

(2) Protein localization. Validation of proteomic data must be performed once a list of high-confidence protein identifications is obtained from an MS/bioinformatics approach. Organellar proteomic studies have illustrated the power of TEM immunolocalization methods [117, 120, 123, 127] to provide direct evidence, as well as further insight, for target protein subcellular localization and distribution. An example of resultant images from such studies are shown in Figure 2.10. Indirect immunocytochemical use of colloid gold-labeled secondary antibodies against target protein-specific primary antibodies permits visualization of the protein location [52, 55]. The electron dense colloid gold spheres permit visualization indirectly, by appearing as small black dots in an electron micrograph. The density and frequency of target proteins are quantified using methods similar to those used to evaluate organelle purity.

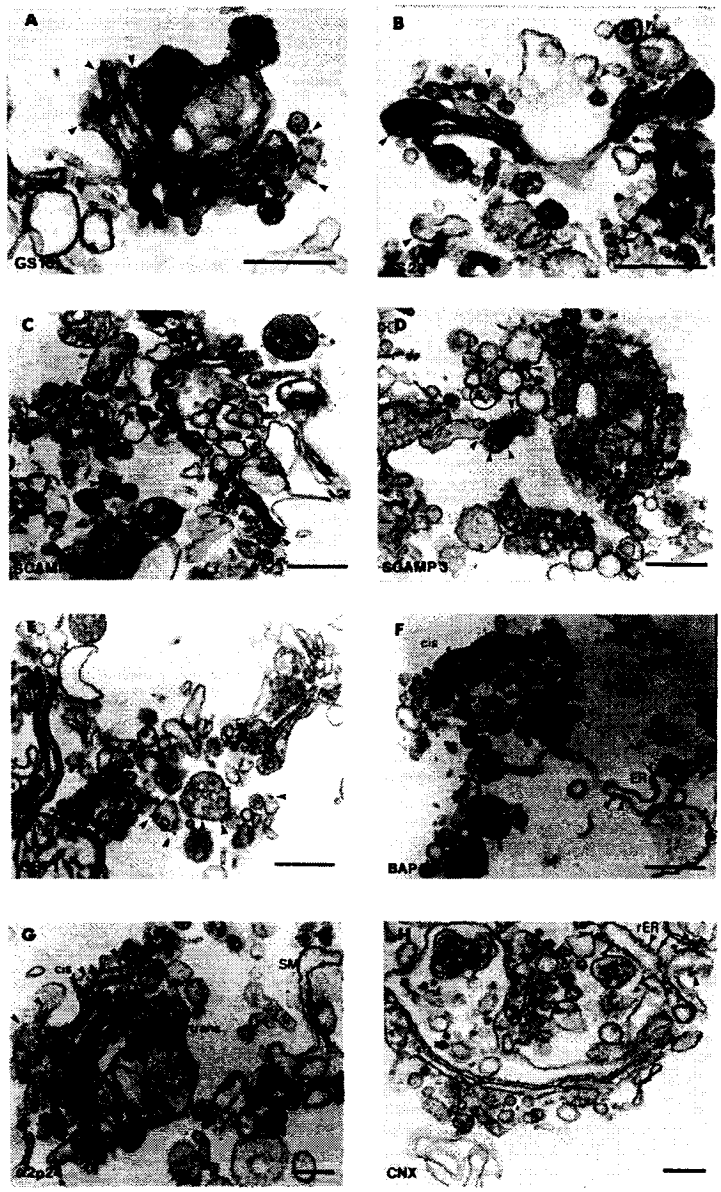

Figure 2.10: Transmission electron micrographs illustrating immunolocalization of hepatic Golgi apparatus to validate the presence of eight membrane associated proteins: (A) GS15, (B) GS28, (C) SCAMP1, (D) SCAMP3, (E) GBF1, (F) BAP31, (G) α_2p24, and (H) CNX. The arrowheads identify gold particles indicating the antigenic sites of the target proteins. Figures F and G show cis and trans orientation of the stacked Golgi cisternae; mitochondria (mit) contaminants are indicated in E. Smooth membranes (SM) are indicated in G. ER and rough ER (rER) contaminants are indicated in F and H, respectively. The arrow in H identifies ribosomes on a rough ER contaminant. The bars correspond to 500 nm [117].

2.4 TEM Sample Preparation

Extensive chemical processing must be applied to biological samples for TEM analysis. Chemical preparation is necessary to improve the sample contrast and support them within the severe environment of a transmission electron microscope.

2.4.1 TEM Sample Preparation Criteria

In general, a TEM sample must meet five technical criteria for successful imaging. It must (1) be anhydrous and void of volatile solvents, (2) be able to maintain its structural integrity under high vacuum conditions, (3) remain stable under the thermal and physical stress of an electron beam, (4) contain areas of electron opacity and transparency; (5) be of suitable size for the TEM (1-10 μm thick) [130-134]. Subcellular fraction samples meet none of these criteria in their native state. Cells have a high water content and, furthermore, aqueous buffer solutions are used throughout fractionation procedures. Moreover, subcellular fraction samples are fragile, have relatively uniform electron density (therefore, poor contrast), and are too thick for TEM.

In preparing these samples for TEM analysis, three general criteria must be followed. Thus, the preparations must:

(1) Preserve as many features of the specimen as possible. Faulty preservation will result in incorrect data interpretation.

(2) Avoid inclusion of artifacts that could obscure or influence interpretation of the specimen.

(3) Render the specimen stable for TEM examination.

2.4.2 Manual TEM Sample Preparation Protocol

Depending upon the organelle's physical characteristics (size, structure, etc.) and features of the specimen to be resolved (morphology, protein distribution, etc.), there are a number of methods and protocols available for TEM sample preparation. Tables 2.1 and 2.2 show standard organelle preparation protocols for morphometric and immunolocalization TEM analysis, respectively. The protocol in Table 2.1 is typical and consists of seven stages: (1) fixation, (2) filtration, (3) post-fixation/staining, (4) dehydration, (5) dehydration/membrane dissolution, and (6) infiltration, and (7) embedding [130-134].

(1) Fixation. Fixation rapidly arrests organellar processes and cross-links structures, preserving their ultrastructural details and chemical composition.

Glutaraldehyde is the typical fixative reagent used to cross-link all proteins of organelles. It has two aldehyde groups [173] that cross- link compounds and act as a molecular bridge between macromolecules. Furthermore, glutaraldehyde reacts so efficiently that it is often reduced to a minimal concentration when immunocytochemistry is performed. In these cases, formaldehyde (a smaller molecule with one aldehyde group [173]) is often used in conjunction with glutaraldehyde to preserve the antigenicity of organellar proteins while sacrificing some ultrastructural details for the sake of preservation. In general, aldehydes do not react well with most lipids and do not impart any electron opacity to the sample because they have no heavy metal atoms associated

Table 2.1: Manual subcellular fraction sample preparation protocol for TEM morphometic analysis [130-135].

Fixation:

1. Add equal volume of fixative (5% glutaraldehyde, 0.1% $CaCl_2$, 100 mM cacodylate buffer, pH 7.4) to 2 ml of 100 μg/ml protein and leave in cold overnight.

Filtration:

2. Filter on Millipore™ filter type HA 0.45 μm or 0.8 μm.
3. Wash the filter with bound sample in 100 mM cacodylate buffer, pH 7.4 three times and leave in buffer overnight.

Post fixation/staining:

A. Incubate the samples in 2% reduced osmium tetroxide, 1.5% potassium ferrocyanide in 100 mM cacodylate buffer, pH 7.4 for 1 hour at 4°C.
B. Wash 3 times with 100 mM cacodylate buffer, pH 7.4 for 10 minutes each and leave overnight.
C. Wash in 100 mM maleate buffer, pH 5.7 for 10 minutes at 4°C.
D. Incubate in 5% uranyl acetate in 100 mM maleate buffer, pH 5.7 for 2 hours at 4°C.
E. Wash 2 times with 100 mM maleate buffer, pH 5.7 for 10 minutes each at 4°C.
F. Wash in 100 mM cacodylate buffer, pH 7.4 for 10 minutes at 4°C.

Dehydration:

4. Incubate in 50% ethanol for 10 minutes at 4°C.
5. Incubate in 70% ethanol for 10 minutes at 4°C.
6. Incubate in 90% ethanol for 10 minutes at 4°C.
7. Incubate in 95% ethanol for 10 minutes at 4°C.
8. Incubate in 100% ethanol 3 times for 10 minutes each at 4°C.

Dehydration/membrane dissolution:

9. Incubate in propylene oxide for 1 hour at 4°C.
10. Transfer to Epon pre-embed block.

Infiltration:

11. Incubate in 1:3 Epon 812:propylene oxide for 1 hour at room temperature.
12. Incubate in 1:1 Epon 812:propylene oxide for 1 hour at room temperature.
13. Incubate in 100% Epon 812 for 1 hour at room temperature.

Embedding:

14. Polymerize at 65°C for 24 hours.

Table 2.2: Manual subcellular fraction sample preparation protocol for TEM immunolocalization analysis [130-135].

Light Fixation:

1. Add equal volume of fixative (0.05% glutaraldehyde, 0.1% $CaCl_2$, 100 mM cacodylate buffer, pH 7.4) to 100 μg protein (after incubation with primary antibody), mix gently and leave at 4°C for 30 minutes.

Filtration:

2. Filter on Millipore™ filter type HA 0.45 μm with saline solution (10 mM TRIS, 0.9% NaCl, pH7.4).
3. Wash the filter with bound sample in saline solution three times for 15 minutes each at 4°C.

Pre-incubation:

4. Wash the filter with bound sample with 3% BSA in saline solution three times for 15 minutes each at room temperature.

Gold-complex incubation:

5. Add the gold-complexes (0.5 nm) to the samples and incubate for 1 hour at room temperature.
6. Wash the filter with bound sample in large amounts of saline solution three times for 15 minutes each at room temperature

Post fixation/staining:

A. Incubate the samples in 2.5 % glutaraldehyde, 100 mM cacodylate buffer, pH 7.4 and leave overnight at 4°C
B. Wash 3 times with 100 mM cacodylate buffer, pH 7.4 for 15 minutes each at 4°C.
C. Incubate the samples in 2% reduced osmium tetroxide, 1.5% potassium ferrocyanide in 100 mM cacodylate buffer, pH 7.4 for 1 hour at 4°C.
D. Wash in 3 times in 100 mM maleate buffer, pH 6.0 for 15 minutes at 4°C.
E. Incubate in 5% uranyl acetate in 50 mM maleate buffer, pH 4.2 for 1 hour at 4°C.
F. Wash 3 times with 100 mM maleate buffer, pH 6.0 for 15 minutes each at 4°C.

Dehydration:

7. Incubate in 75% ethanol for 10 minutes at 4°C.
8. Incubate in 95% ethanol for 10 minutes at 4°C.
9. Incubate in 100% ethanol 3 times for 10 minutes each at 4°C.

Dehydration/membrane dissolution:

10. Incubate in propylene oxide for 1 to 2 hours at room temperature.
11. Transfer to Epon pre-embed block.

Infiltration:

12. Incubate in 1:1 Epon 812:propylene oxide for 2 hours at room temperature
13. Incubate in 100% Epon 812 for 1 hour at room temperature

Embedding:

15. Polymerize at 65°C for 24 hours.

with them. Post-fixation steps minimize these problems, by using osmium tetroxide as a secondary fixative (see below).

Fixatives are typically prepared in a solution with cacodylate buffer (effective in the 6.4-7.4 pH range). To avoid deforming the organelles and keep the proteins electrically neutral, the solution is isotonic and adjusted to physiological (isoelectric) pH. Furthermore, the fixative is washed from the sample with cacodylate buffer, which has the same concentration and pH as that used for the fixative solution (similar washes are done in the following stages).

(2) Filtration. A random filtration technique is used to deposit and localize the fixed sample suspension onto a charged filter membrane [59]. Using a specialized filtration device (see Figure 2.11), the method immobilizes a thin layer of organelles (pellicle) on a filter disk, which can be moved between baths of processing reagents using forceps (as is done for the next stage of the protocol).

Filtration begins when pressurized nitrogen is introduced to the top of the chamber that is filled with the subcellular fraction sample suspension. The pressurized flow deposits the subcellular fraction sample onto the filter membrane and the filtrate passes into the collection vial. Filtration continues until the suspension solution passes below the conductivity probes. The process stops when loss of continuity between the probes triggers the 3-way solenoid valve to close the path to the pressurized nitrogen and open the path to atmosphere.

The filtration method eliminates the inherent error in electron microscopic examination of subcellular fractions collected by centrifugation, in which the

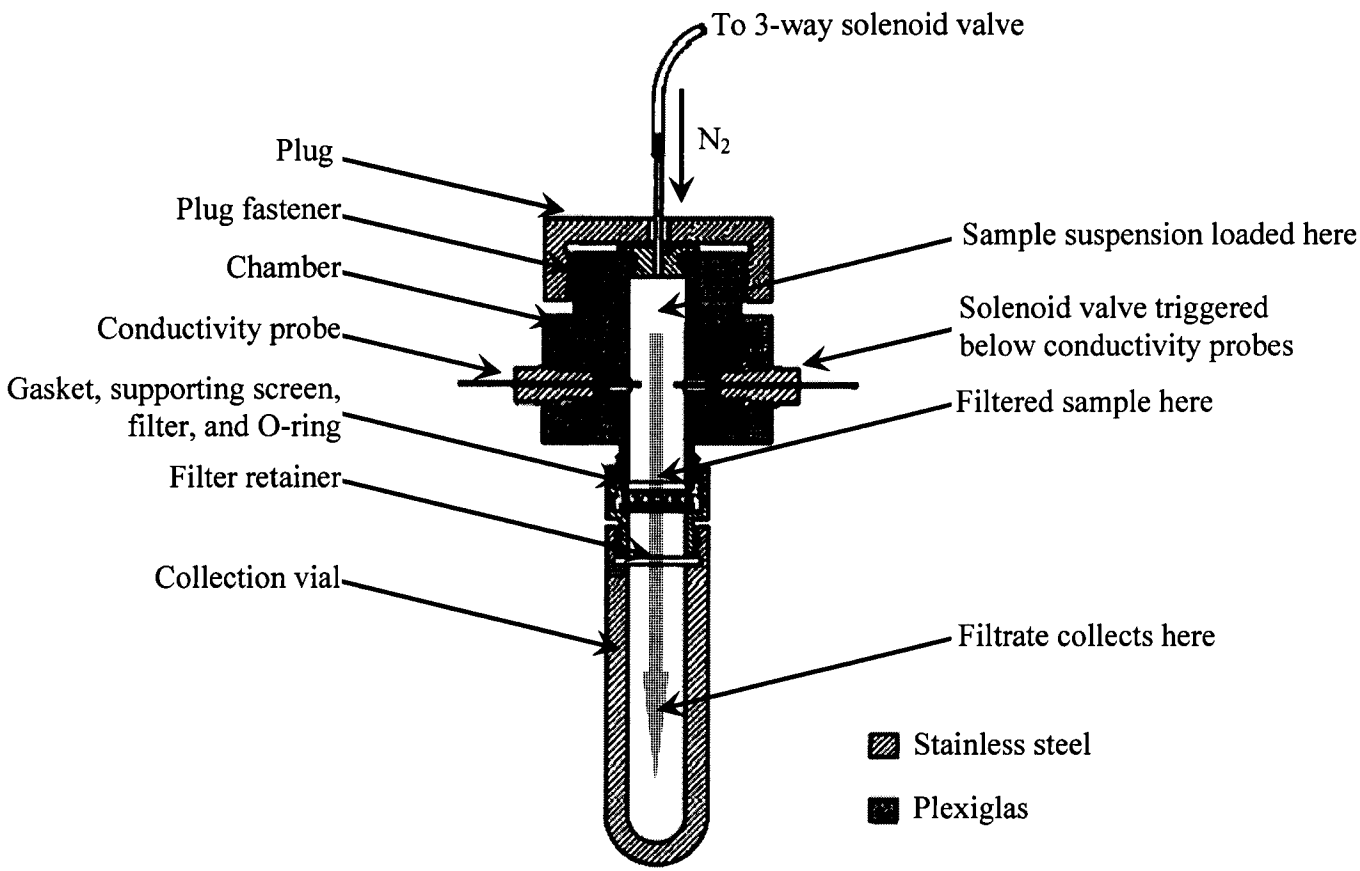

Figure 2.11: Cross sectional illustration of the subcellular fraction filtration device [59]. The stainless steel plug connects to a 3-way solenoid valve (to pressurized gas) and screws onto the chamber. The Plexiglas chamber holds the subcellular fraction suspension and is equipped with the conductivity probes. An assembly of a Teflon gasket, a supporting screen, a charged filter membrane, and a Teflon O-ring is secured to the bottom of the chamber with the treaded filter retainer. A collection vial screws onto the other end of the filter retainer to collect the filtrate and complete the air-tight assembly of the filtration device. The grey shaded arrow indicates the direction of flow.

pellet is processed and sectioned for examination. As Figure 2.12 shows, the distribution of particles (with differing sedimentation coefficients or densities) in the pellet is not homogeneous. Particles are not randomly scattered, but follow a gradient; heterogeneity arises in the direction of the centrifugal field as well as along the surface of the pellet. This causes particles of different types to occur with differing frequencies in the center and the periphery of the preparation.

Unlike centrifugation, the filtration technique minimizes the impact of particle density and structure on the resulting distribution. Under the force of pressurized nitrogen, as the suspending liquid is displaced, it carries and deposits the particles to the charged membrane, where they adhere. Therefore, when an aliquot of subcellular fraction suspension (a random sample) is filtered with this technique, Figure 2.13 shows how heterogeneity is restricted to a single direction. Thus, for TEM analysis, each section of the processed sample may be considered truly representative of the whole subcellular fraction preparation and can be used for direct comparison between biochemical and morphological data [59, 107, 108, 130].

(3) Post-fixation. Post-fixation procedures stabilize organellar membranes and impart contrast to the samples using a combination of heavy-metal compounds.

The first compound applied in the sequence is typically osmium tetroxide, which is used as a secondary fixative that binds to and stabilizes lipid bilayers. Osmium tetroxide is an excellent fixative because each oxygen atom of the molecule is a potential reaction site. However, it has a relatively slow rate of

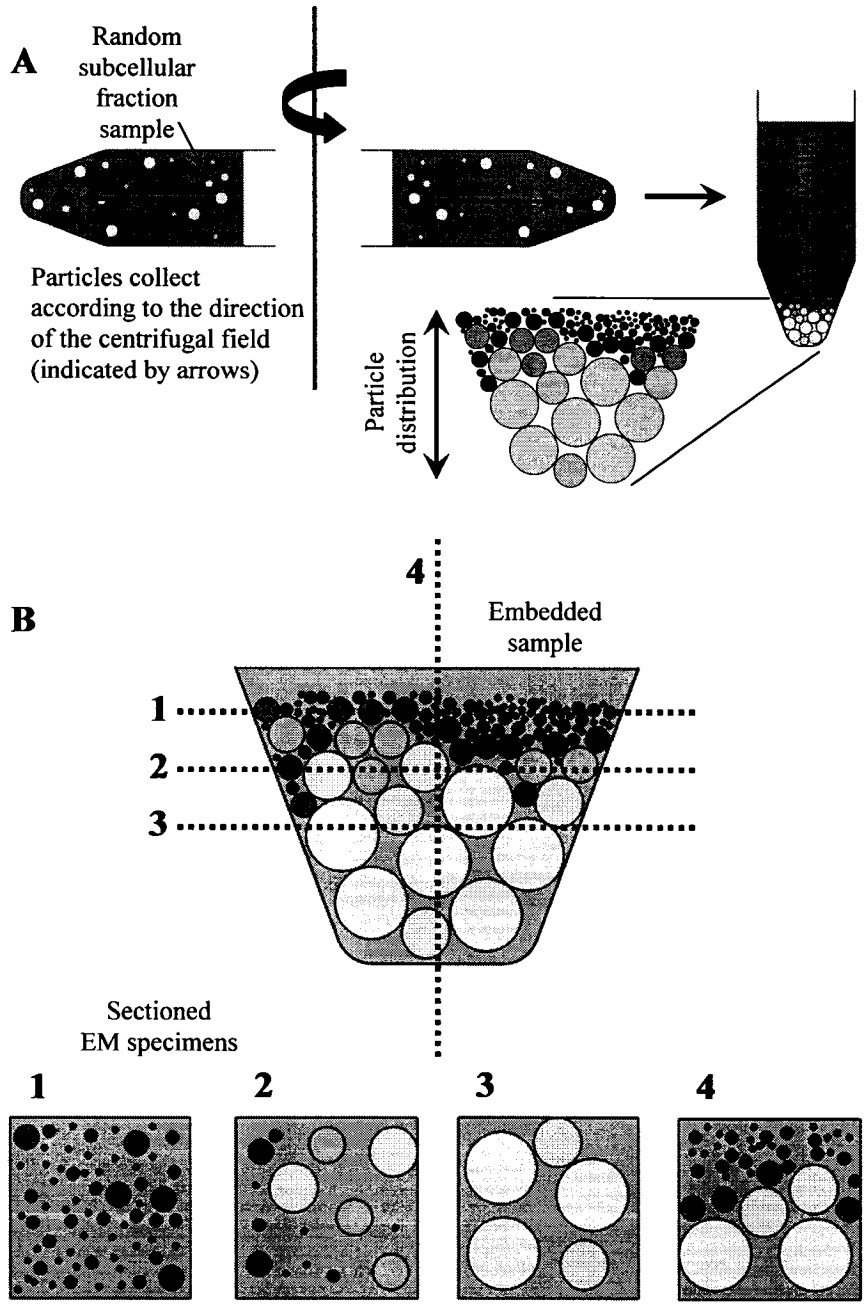

Figure 2.12: Schematic illustration of centrifugation artifacts left in EM subcellular fraction preparations. A swinging bucket rotor model simplifies the direction of the centrifugal field and spherical particles represent organelles with differing densities and sedimentation coefficients; the largest particles are the quickest to settle. (A) The resulting distribution of largest to smallest particles in the pellet is heterogeneous and follows the direction of the centrifugal field. (B) Sectioning of the embedded sample in any plane reveals the centrifugation artifacts and demonstrates the inherent error in the technique. The pellet is cut along the four indicated lines and representations of the resulting sections appear below. Sections 1, 2 and 3 illustrate specimens taken along the distribution and section 4 illustrates a specimen taken from a perpendicular cut through the distribution [59, 130].

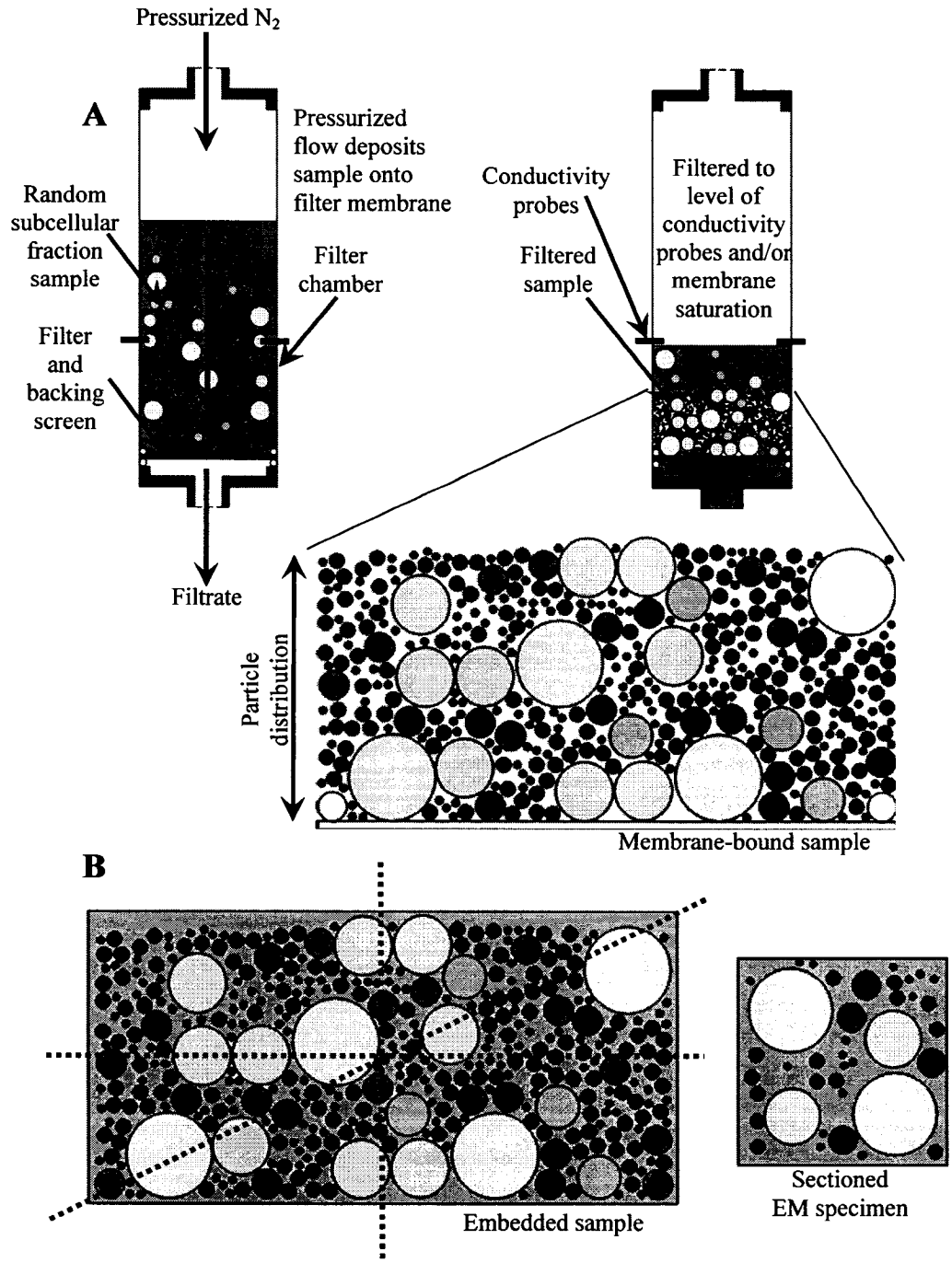

Figure 2.13: Schematic illustration of the pressure filtration method and minimization of particle distribution heterogeneity. A cylindrical model of the pressure filtration unit simplifies illustration of pressurized flow and spherical particles represent organelles with differing densities and sedimentation coefficients. (A) Particle distribution heterogeneity in the filtered pellet is restricted to the direction of pressurized flow and minimized by the dimension of the pellet in this direction. All particles are quickly carried and deposited (independently of their densities and/or sedimentation coefficients) as a thin layer (accumulated on the membrane surface) by a liquid that is displaced across the filter membrane. (B) Sectioning the embedded sample on any plane produces specimens for EM with homogeneous particle distributions that are representative of the random sample applied to the device [59, 130].

membrane penetration, which justifies its use as a secondary post fixative rather than as a primary fixative. Regardless, lipids cross-link and stain darkly with the heavy metal, osmium (see Figure 2.14A). Osmium adds contrast to the organelle and reveals the locations of organelle membranes. After this step, unused osmium tetroxide is removed by multiple cacodylate washes to avoid introduction of artifacts in prepared EM samples.

After treatment with osmium tetroxide, *en bloc* staining with uranyl acetate maximizes contrast for viewing ultrastructure by impregnating organelles with the electron dense heavy metal, uranium. The compound also acts as a sequential fixative for further stabilization of the organellar membranes. Preceding this step, organelles are washed several times with maleate buffer to avoid co-precipitation of uranyl salts with cacodylate. Post-staining, the organelles are washed again with maleate buffer to remove unused uranyl acetate and prepare them for dehydration.

(4) Dehydration. The dehydration process involves the exchange of water in the sample with an organic solvent. Although shrinkage of organelles often accompanies dehydration steps with sudden and pronounced changes in solvent concentration, it is a necessary part of the process. Ultimately, the organelle samples are embedded in a hard supporting medium, which is typically a resin polymer that is not miscible with water. Consequently, the removal of all water is critical.

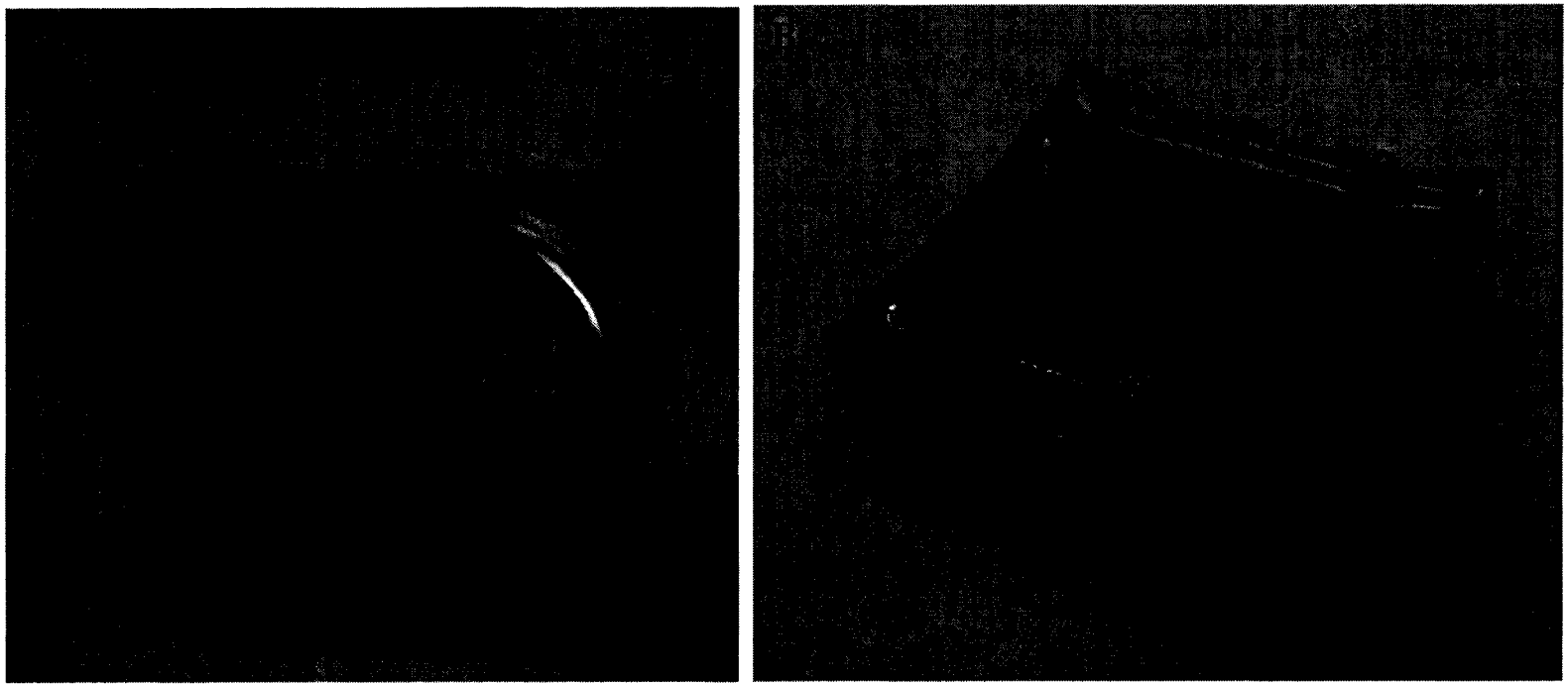

Figure 2.14: Illustrations of filtered subcellular fraction samples. (A) A filter-bound sample after the post-fixation stage of a preparation protocol, where the originally clear sample is darkly stained. (B) A processed sample embedded in Epon 812.

An ethanol step-gradient is normally used for solvent dehydration of the fixed and stained samples, where a number of short exposures are used with slowly increasing concentrations of ethanol.

(5) Dehydration/membrane dissolution. The samples are repeatedly incubated with a pure organic solvent (e.g., propylene oxide or acetone) to complete dehydration of the sample, dissolve the filter membrane, and free the sample.

(6) Infiltration. This stage saturates the samples with an epoxy resin support medium (e.g., Epon 812) that is eventually polymerized to permit cutting of specimens for EM. During infiltration, the unpolymerized, liquid form of the medium is introduced by way of a step-gradient to replace the dehydration solvent in the organelle samples. The process is similar to the dehydration stage, however, due to the high viscosity of the resin incubations can last many hours.

(7) Embedding. In this stage, the epoxy resin support medium is hardened. After complete infiltration by the pure epoxy resin, the sample is placed in a mold and the resin is polymerized (see Figure 2.14B). Afterward, the hardened sample is presented to an ultramicrotome, where it is cut into sections thin enough (~100 nm) for full resolution in the electron microscope.

2.4.3 Limitations of the Manual TEM Sample Preparation Method

The manual method for organelle sample preparation has proven to be a very useful tool in cell biology. However, it has a number of limitations for large-scale applications:

(1) The method is time intensive. The sample preparation protocol takes approximately four days to complete.

(2) The method is labor intensive. At least 25 steps must be executed to complete the protocol.

(3) The method cannot be scaled. Due to the number of manipulations required; no more than four samples can be prepared in parallel. Also, the reagents used for sample preparation are highly toxic and the protocol must be completed in the restricted space of a fume hood or vented enclosure.

(4) The method is difficult to standardize. Materials and preparation protocols are often adjusted for the application or an individual's technical skills.

(5) The method is difficult to reproduce. It requires a very high level of technical skill to obtain reproducible results.

To employ the method for routine use in proteomics, an automated device is necessary to provide standardized, reproducible, subcellular fraction sample processing in a parallel, high-throughput manner. A laboratory automation instrument implementing this task would remove the labor and "art". Moreover, it would enable routine organelle sample screening and validation of target protein localization and distribution in organelles. Also, as is necessary in a large-scale proteomics effort, controlled automation would reduce the technical skill required for routine operation and improve intra- and inter-laboratory repeatability.

2.5 Development of Laboratory Automation

Commercially available laboratory robots were introduced in the 1980s. They were not designed to be powerful or robust, but to replace humans to perform routine, repetitive tasks with small objects such as test tubes. Because of the quantity and quality of work that could be done using automation, interest grew rapidly in biological, chemical and clinical laboratories [136-140]. This era found laboratory automation implemented within the pharmaceutical industry. In fact, the history of laboratory automation parallels the development of modern drug discovery.

By the end of the 1990s, drug discovery projects involving screening of less than 100,000 drug-like compounds against a disease target were considered small. The high volume compound screening on drug target (immunoassays, enzyme reactions, cell-based assays, etc.) motivated the establishment of automated platforms or facilities to interface with either end of the process: combinatorial chemistry platforms [141-147], automated storage and retrieval systems, and quality control laboratories. The resulting approach to automated drug discovery is known as high-throughput screening (HTS) [148-157]. Because the economic cost of developing a new drug from laboratory to market is high, HTS found wide acceptance among pharmaceutical companies.

Central to these high-throughput developments was the multi-well microplate, which is more convenient to manipulate than individual test tubes. Based on the microplate format, a multitude of workstations were developed to execute tasks in a uniform, parallel, and high-throughput manner. To maximize efficiency, workstations were integrated with articulated arms to create simple, flexible and powerful workcells; establishing fully automated laboratory automation systems. Presently, the automation

approach for drug discovery utilizes entire high-throughput facilities, where most aspects of the high-volume process (preparation, screening, storage and retrieval, etc.) is managed with robots.

Simultaneously, automation was developed to sequence the human genome [158-162]. Today, there is a tremendous variety of instruments that automate nearly every step of a large-scale sequencing process.

2.5.1 Development of Proteomics Laboratory Automation

Although there has been tremendous influence from the technology developed for pharmaceutical HTS and genomics, the same "first-approach" development scenario experienced in these fields is witnessed in the current state of proteomics research. While future development of sophisticated methods are anticipated, during the last several years, the priority has been to first establish high-throughput laboratory automation to streamline and standardize processes for sample preparation, experimentation and data analysis [163-170].

As proteomic research strategies develop, so do the requirements to expand, compliment or replace the current methods by novel automated devices with improved throughput. At first, modular robots were developed to address immediately identifiable stages of the process such as gel staining, image analysis, gel spot excision, protein digestion and mass spectrometry. Later, employing the important lessons taught by pharmaceutical HTS and large-scale genomics, instruments were developed to integrate these operations and improve accuracy, flexibility, speed, and connectivity.

The task of deciphering a proteome is considered orders of magnitude larger in scope than a genome. Therefore, to attain the level of success seen in genomics, there must be innovations for automated, parallel processing and analysis of proteins. These challenges lie not only in eliminating rate-limiting steps by integrated systems of established high-throughput sub-processes, but more importantly, in the development of new methods and technologies for preparation, experimentation and analysis.

2.5.2 Limitations of Laboratory Automation for Organelle Sample Preparation

There is currently no commercial, automated device for organelle sample preparation. Current sample preparation devices are restricted to liquid handling and so, are not appropriate for organelle preparation. Common laboratory automation systems perform many sophisticated tasks in multi-well microplates and are typically used to assay or isolate macromolecules [170]. Furthermore, automatic EM specimen processors normally operate by immersing samples into successive reagent vials and are used to mainly prepare tissue samples, which are much more durable than filtered pellicles of subcellular fractions. The manipulations required to process subcellular fraction samples for TEM go beyond liquid handling or moving of multi-well microplates from one station to another.

Typical laboratory automation platforms are designed for high-throughput, mass-parallel experimentation that requires extensive liquid handling. Viewing all of the current commercially available laboratory automation platforms from a composite perspective, they have the following attributes:

(1) Ready ability for repeated execution of complex liquid handling protocols.

(2) Modules for vacuum filtration in a manifold configuration.

(3) Temperature control modules for heating or cooling microplates.

(4) Devices for liquid level sensing in individual microplate wells.

(5) Expandable and capable of integration with other instrumentation and/or analytical devices.

(6) Positioning systems that provide Cartesian motion, pick-and-place manipulation and single-plane rotational motion with a gripper arm.

Although these devices are flexible and robust, they are not designed specifically to automate processing of organelles as specimens for electron microscopy.

These samples, generated by the deposition and immobilization of material onto charged filter membrane, consist of thin and fragile pellicles that must be processed through an entire protocol of fixation, staining, dehydration, filter membrane dissolution, and infiltration/embedding with an epoxy resin. Executing these steps *via* the manual sample preparation method requires very gentle handling to avoid fragmentation or disruption of the sample. The fragile nature of these samples prohibits preparation methods that shuffle them through a series of devices and automated instruments. To minimize damaging the sample structure by repeated manipulation in different devices (for successive steps of the preparation protocol) and/or losing the sample within the many necessary liquid handling steps, an automated preparation device must be implemented as a single platform that executes all manipulations and treatments to the

samples in one place. The design of such a device requires novel mechanisms. The challenge is even greater when the simultaneous, parallel, automated processing of multiple organelle samples is considered.

A successful device design must support all processing steps in one automated platform and provide mechanisms to support all of the following manipulations or conditions:

(1) The samples must be filtered by way of a vacuum or pressure source.

(2) The samples must be immobilized in sealed localizations.

(3) There must be adequate volume within the sample processing space for iterated incubations with all processing reagents.

(4) The filter membrane support must permit efficient solvent penetration for dissolution of the filter membrane.

(5) The membrane-released samples must be transferred to and captured by a subsection that supports the embedding of stage of sample processing.

(6) The membrane-released samples must be trapped during the embedding of stage of sample processing.

(7) Undissolved filter membrane must be removed before the samples are embedded.

(8) The processed samples must be retrieved.

This task requires a sophisticated level of automation and mechanical control that cannot be obtained using a series of automated preparation instruments or by modifying instruments intended for a completely different task. Therefore, in addition to liquid

handling and positioning capabilities, an automated device for preparing sub-cellular fraction samples for electron microscopy requires an integrated, modular and multifunctional platform for: (1) gentle handling of organelles, (2) quantitative control over sample filtration and transfer, and (3) capture and isolation of processing samples for embedding and retrieval.

2.6 Thesis Objective: Development of the EMPOP Robot

The objective of this thesis was to develop the Electron Microscopy Proteomic Organellar Preparation (EMPOP) robot to remove the sample preparation bottleneck that limits the use of TEM for large-scale organellar proteomics research, by preparing up to 96 subcellular fraction samples automatically. It is intended to reduce the time and labor requirements of sample preparation by approximately 1,000 fold and, provide a standardized protocol to improve reproducibility for quantitative analyses.

By developing a specific platform, the shortcomings of typical laboratory automation platforms will be overcome by the following aspects of the robots design:

(1) The robot will have an integrated, autonomous design that will accomplish all tasks in one location and impose minimal mechanical perturbations on the samples.

(2) All work on the samples will be completed within the core mechanism of the robot, a modular and multi-configurable processing platform.

(3) All sample processing channels within the core mechanism will be sealed to isolate processing samples and permit processing of up to 96 samples in parallel.

(4) System components will be reusable and chemically compatible with reagents used for processing subcellular fractions.

(5) There will be quantitative control over temperature, vacuum filtration, pressurized sample delivery, reagent delivery (flow, volume and mixing), and reagent aspiration.

(6) A five degree-of-freedom motion control and electromagnetic pick-and-place sub-systems will provide a wide range of motion, permitting system reconfiguration to execute alternative automated methods or protocols.

(7) The automated system will have a closed-loop design for documentation of automation parameters and performance and to ensure reproducibility of the sample preparation protocol.

3 Overview of Design and Operation of the EMPOP Robot

3.1 Overview

This chapter provides and overview of the operational concepts of the automated process and the robot design by describing the robot's sample processing "center", the core mechanism, and each of its seven support subsystems, which control temperature, fluid handling and positioning.

3.2 Design Objectives

The primary focus of the design was to produce an automated, high-throughput device to prepare subcellular fractions as well as other samples. A design objective was to ensure gentle treatment of the samples to prevent damage to the morphology of organelles and/or loss of samples during processing. Organelles are often between 50 to 250 nm on their principle dimension and held together only by a thin membrane between 5-10 nm in thickness. Any damage leads to the breakdown of morphology.

The design selected was an integrated, stand-alone unit that would minimize mechanical perturbations and maximize compatibility of chemical, biological, and mechanical parameters. Moreover, quantitative control over all steps was required to

provide standardized and reproducible processing of parallel samples. Consequently, the robot was designed to incorporate multiple feedback parameters to minimize the effects of disturbances.

3.3 Design Overview

The EMPOP robot, shown in Figures 3.1, is comprised of subsections that permit coordinated execution of the process. Automated sample processing is centered around the core mechanism; a system of stackable processing plates. The plates accommodate all aspects of the preparation process as a modular, automated device that operates in multiple configurations. Moreover, the core mechanism was designed to interact with the robot's seven support subsystems for gentle treatment of subcellular fraction samples throughout processing; preserving their structural and morphological integrity. The subsystems include:

(1) The cooling subsystem maintains the core mechanism temperature at 4°C. The central assembly of the subsystem, the cooling platform, integrates with the core mechanism to support localized cooling and plate positioning during reconfiguration.

Sample processing relies on fluid handling for reagent dispensing and aspiration, sample filtration and delivery as well as cleaning and waste removal. To coordinate and control these tasks, the robot uses three fluid handling support subsystems.

(2) The processing reagent handling subsystem is a network of miniature liquid handling components that pumps, mixes and dispenses of all reagents to the processing channels of the core mechanism.

(3) The pneumatic subsystem controls pressurized air and vacuum levels in one localized manifold, to distribute and regulate flow to the core mechanism and the cleaning and waste management subsystem.

(4) The cleaning and waste management subsystem operates with dedicated liquid handling component and the pneumatic subsystem to clean surfaces and move excess processing reagents to waste.

The sample preparation process requires coordinated automated positioning to support core mechanism reconfiguration as well as reagent dispensing, reagent aspiration and cleaning steps. Three integrated support subsystems fulfill the positioning requirements:

(5) The motion control subsystem carries tools for plate manipulation and liquid handling for positioning within the robot's workspace.

(6) The electromagnetic transfer arm is a magnetic gripper that interacts with the core mechanism for automated positioning of core mechanism plates and configurations.

(7) The transfer platform augments the vertical positioning capabilities of the robot to support core mechanism inversion in the sample delivery stage.

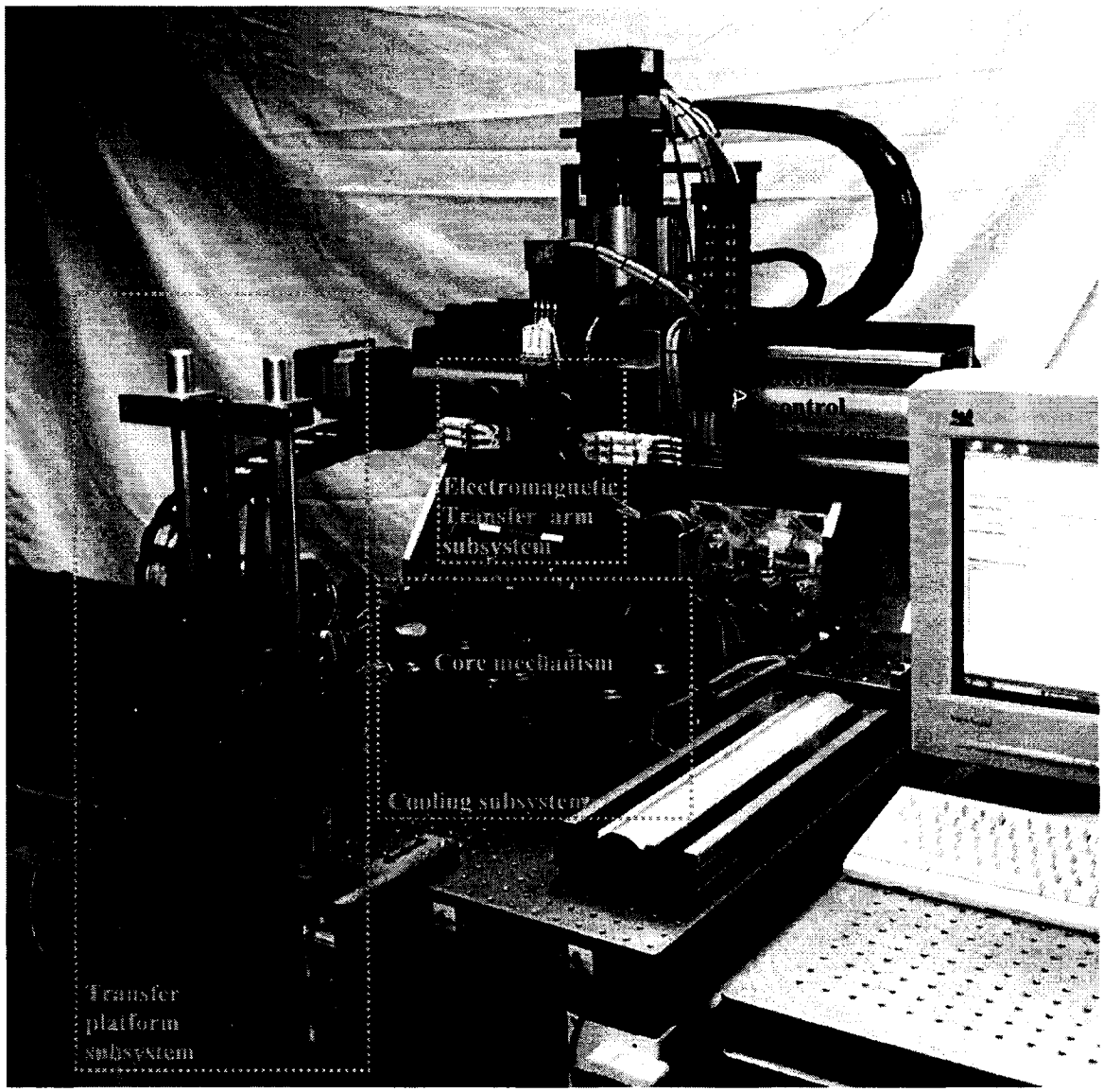

Figure 3.1A: Front view of the EMPOP robot. Subcellular fraction samples are processed in the system of stacking, multifunctional plates that make up the core mechanism. Cooling, positioning and fluid handling are provided by an integrated support subsystems located around the central core mechanism.

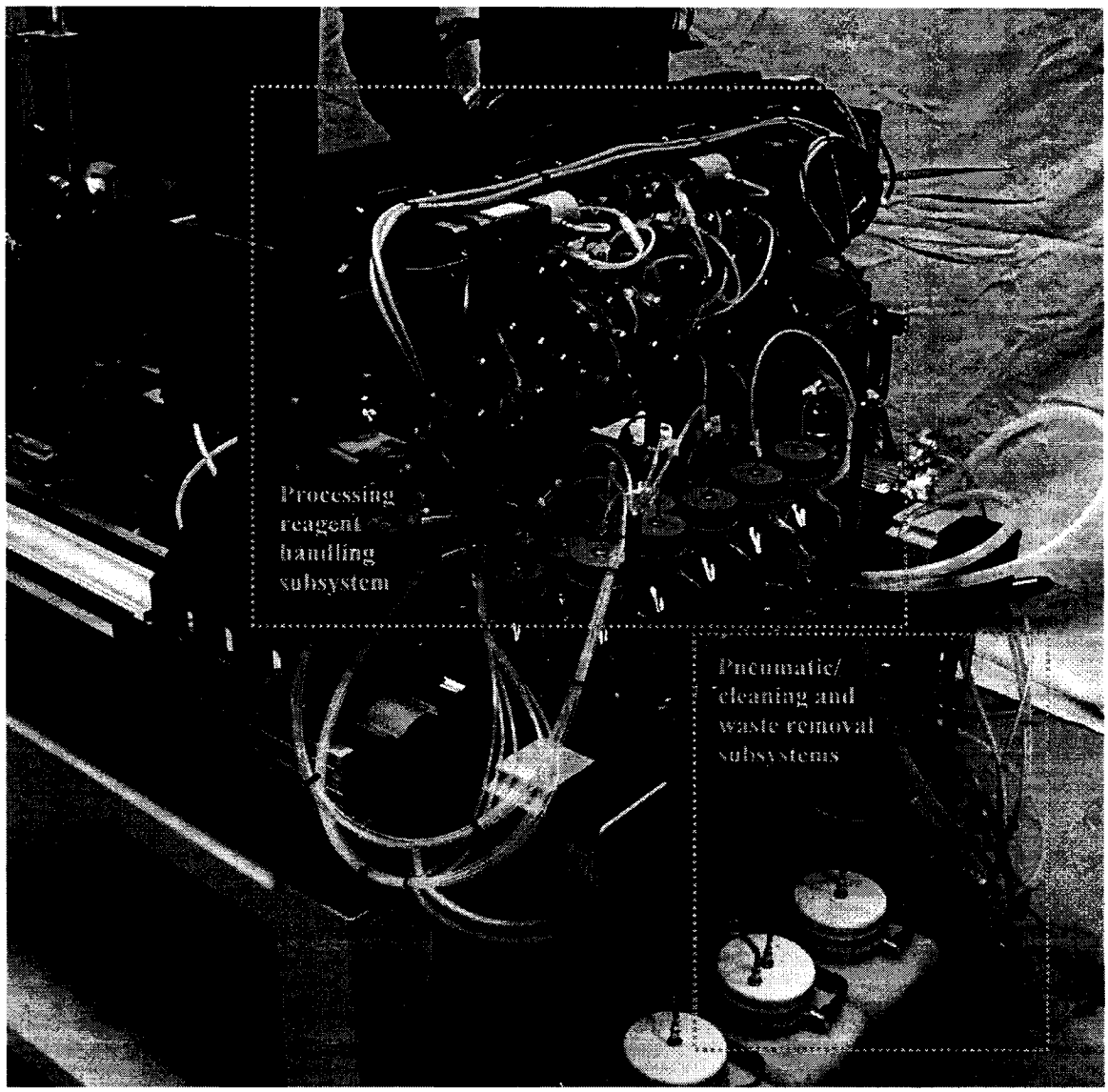

Figure 3.1B: Rear view of the EMPOP robot showing principle components of the fluid handling support subsystems.

3.4 Process Description

The EMPOP robot automates all of the physical and chemical steps of the two standard manual protocols [130-135] for subcellular fraction sample preparation shown in Figure 3.2. Parallel sample processing is centered at the robot's core mechanism, a reconfigurable system of four stacking plates that forms 96 internal processing channels arranged in the standard microplate geometry (see Section 3.4). The overall process carried out by the EMPOP robot is demonstrated in a series of cross–sectional schematics shown in Figure 3.3, which shows an individual channel of the core mechanism at the different steps that make up the three stages of sub-cellular fraction sample preparation: processing, delivery and embedding.

Processing stage

(1) The first two steps (Figures 3.3A and B) are manual. First, the plates are magnetically coupled to form the processing configuration used in the first stage of the procedure. Secondly, subcellular fraction samples are loaded into the individual processing channels. All subsequent manipulations in the sample processing protocol are automated

(2) Vacuum filtration of the subcellular fraction deposits samples onto a charged filter membrane (Figure 3.3C).

(3) Reagents are dispensed and aspirated to and from the 96 individual processing channels (Figures 3.3D and E). The cycle of dispensing chemicals, incubating,

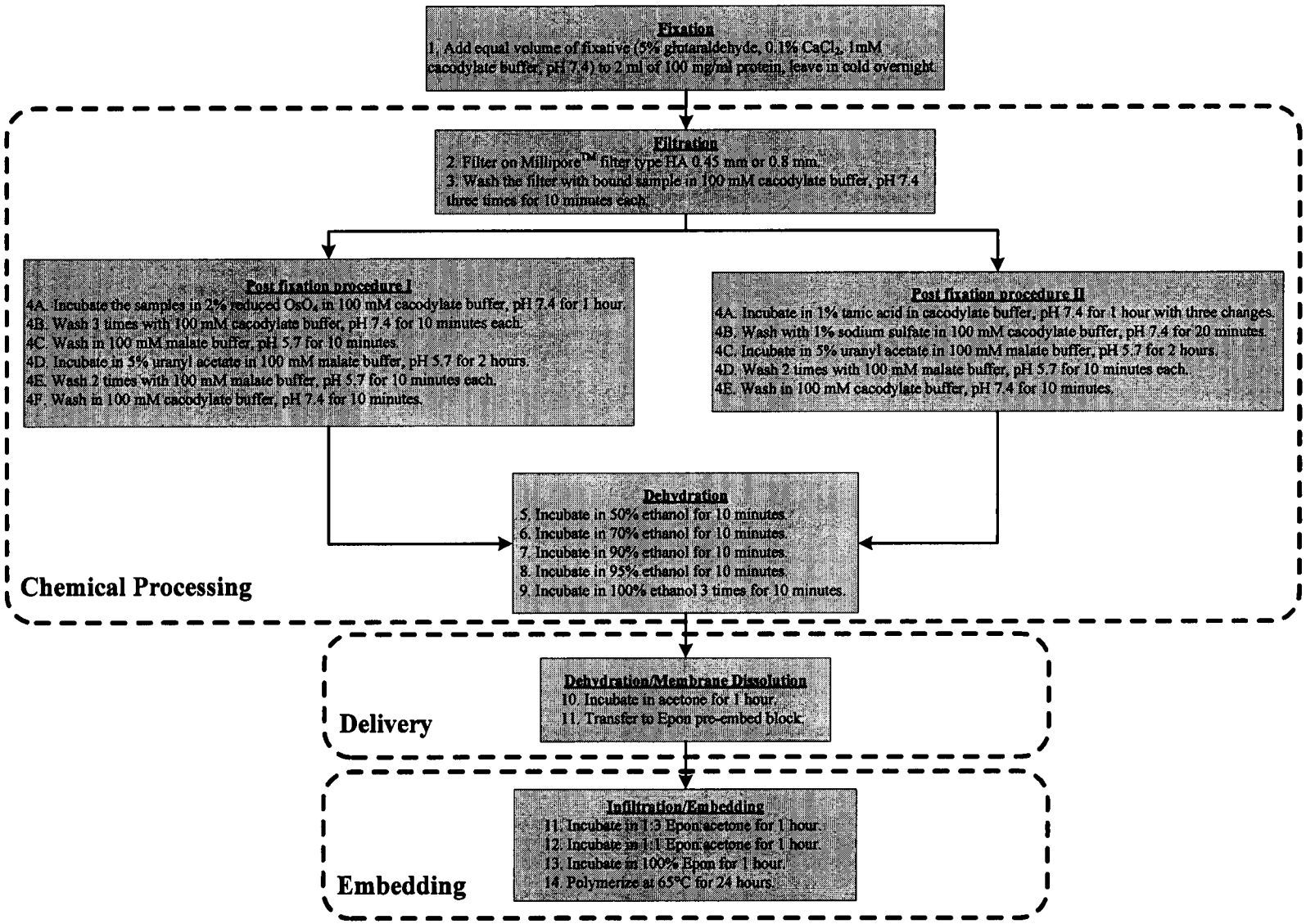

Figure 3.2: Flowchart showing generalized representations of the two manual subcellular fraction sample preparation protocols automated by the EMPOP robot. The dashed-line boxes indicate the corresponding stages of the automated processing.

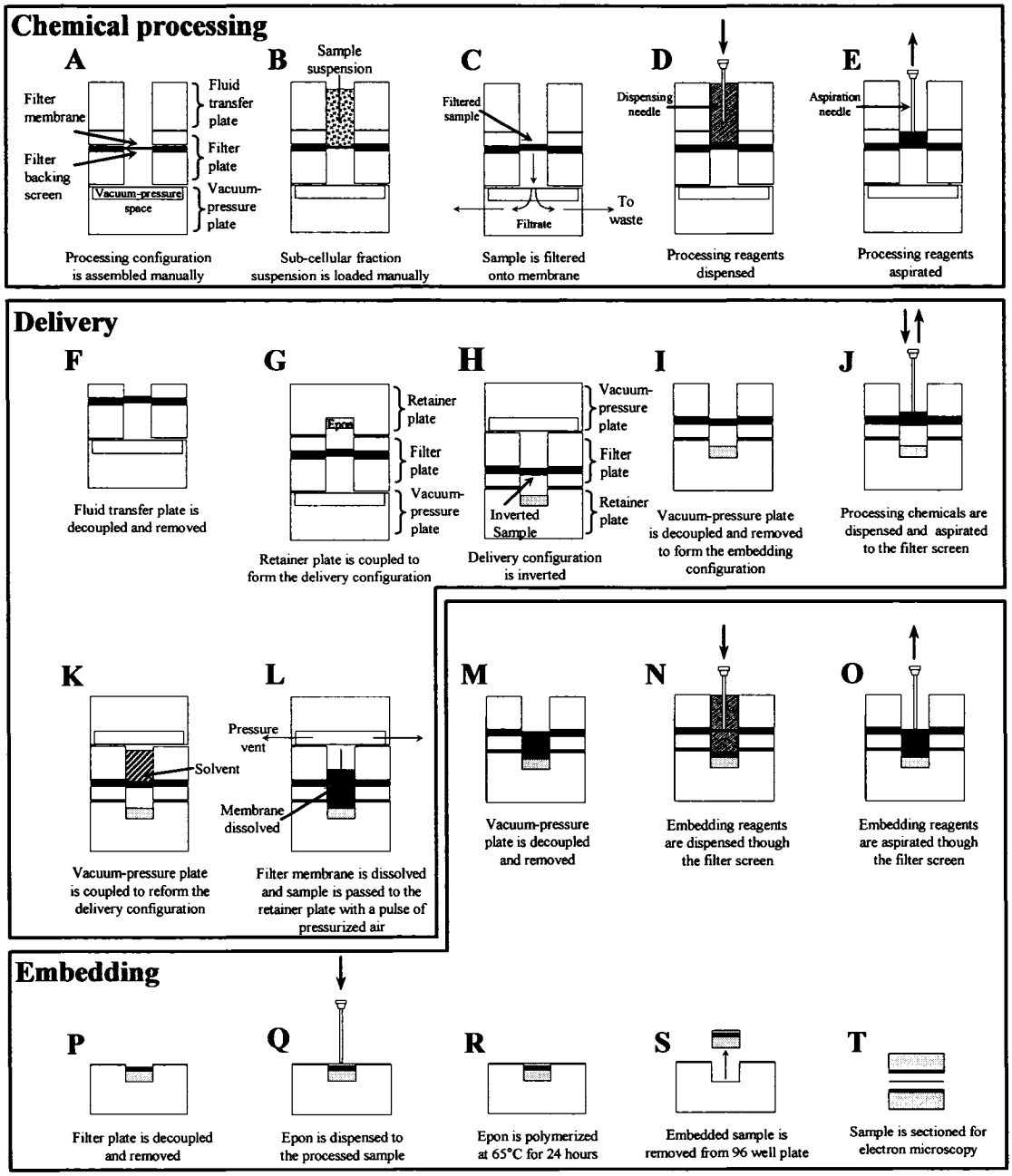

Figure 3.3: Cross sectional illustrations of an individual channel of the EMPOP robot core mechanism during the three stages of automated subcellular fraction sample preparation. Chemical processing: (A-B) manual steps of processing configuration assembly and sample loading, (C) sample filtration, and (D-E) reagent dispensing and aspiration for chemical processing; Delivery: (F-G) formation of the delivery configuration, (H-J) formation of the embedding configuration and chemical processing samples to dissolve the filter membrane, and (K-L) sample delivery; Embedding: (M-O) plate de-coupling to form the embedding configuration, reagent dispensing and aspiration through and embedding sequence, and (P) plate de-coupling to leave retainer plate with processed samples, and (Q-T) processed samples are embedded and gathered, presented to a microtome, and sectioned for EM analysis.

and aspirating chemicals is repeated as many times and with as many repeats as is necessary to complete the chemical processing stage of the protocol.

Delivery stage

(4) The fluid transfer plate is de-coupled from the processing plate configuration and is replaced with the retainer plate, to form the delivery plate configuration (Figures 3.3F and G).

(5) This configuration is inverted and the vacuum-pressure plate is temporarily removed (to form the embedding plate configuration) for further chemical processing that dissolves the filter membrane, and frees the sample (Figures 3.2H, I and J).

(6) The processed samples are transferred to a 96 well microplate (in the retainer plate) loaded with polymerized embedding solution (Epon) by a pulse of pressurized air from the replaced vacuum-pressure plate (Figures 3.2K and L).

Embedding stage

(7) The vacuum-pressure plate is decoupled and the embedding sequence takes place in a manner similar to the chemical processing sequence (Figures 3.3M, N and O).

(8) The plates are de-coupled leaving the retainer plate holding the processed samples (Figure 3.3P).

(9) Figure 3.3Q to T illustrate the subsequent manual steps required to prepare the samples for EM analysis. The processed subcellular fraction samples are gathered

for final embedding in 100% Epon, which is then polymerized at 65°C. Finally, samples are removed for sectioning on a microtome, and EM analysis.

To introduce the operational concepts of the EMPOP robot, the description of these steps focused on a single processing channel of the core mechanism. In practice, operation proceeds as described above, but with numerous coordinated and controlled mechanisms for automatic preparation of up to 96 samples on a single platform. In addition to a core mechanism, designed to accommodate multiple parallel samples, support subsystems for cooling, fluids handling and positioning are needed for automated execution of the process. The remainder of this chapter will show how the robot was designed to meet the requirements of the processing steps outlined above.

3.5 Core Mechanism

As the previous section showed, all operations performed by the EMPOP robot are centered about the core mechanism. Stacking the plates into different configurations provides the flexibility needed to automate complex chemical protocols. Furthermore, the core mechanism incorporates mechanical components that integrate with the positioning support subsystems.

Each plate is a subsection of an array of O-ring sealed sample processing channels, organized in a standard 96 well microplate geometry. All plates have the same dimensions and are equipped with mechanisms for alignment, position sensing, magnetic coupling and decoupling, inter- and intra-plate sealing, and interfacing electrically to the digital and analog input/output (I/O) of the robot controller.

3.5.1 Plate Descriptions

The *fluid transfer plate*, shown in Figure 3.4, plate provides individual reservoirs for the 96 samples. This plate couples to the top face of the filter plate (*see below*) and holds the reagents used in the different chemical processing steps of the protocol.

The *filter plate*, shown in Figure 3.5, holds the membrane-bound samples and couples to other plates of the core mechanism during the different stages of sample processing. It consists of a screw-fastened cap, a filter-backing screen, and plate body,

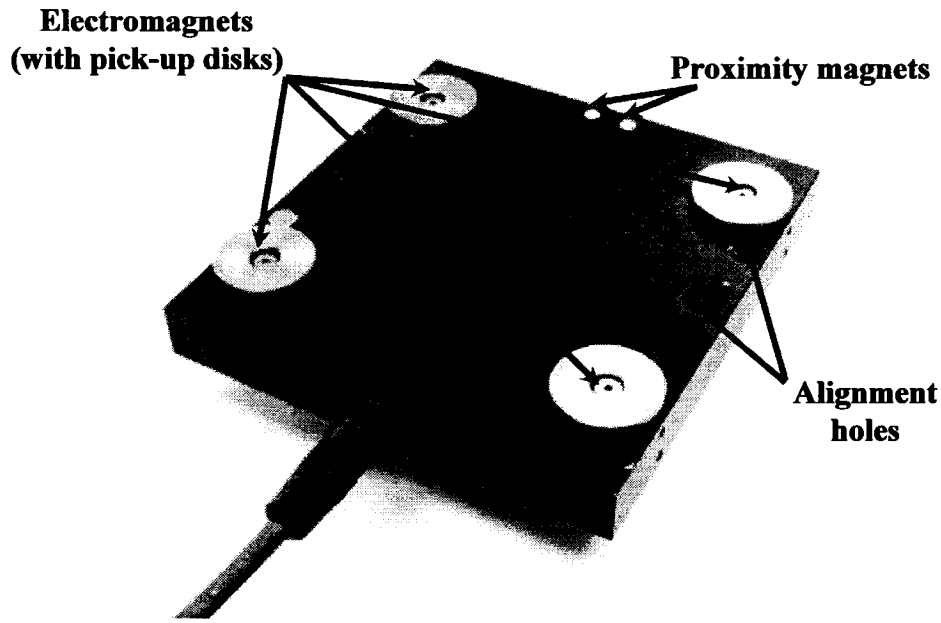

Figure 3.4: Top view of the fluid transfer plate showing the 96 passages that serve as reagent reservoirs. The photograph shows all design aspects for plate-to-plate and arm-to-plate coupling and positioning as well as the cable interface to the control electronics.

that allows individual, samples to be approached from either the top or bottom. The charged filter membrane is sealed within the plate during the filtration, staining and

dehydration steps. When rotated by 180°, the plate design accommodates the processing steps of membrane dissolution, sample delivery, capture and embedding.

The *vacuum-pressure plate*, shown in Figure 3.6, serves three purposes: (1) it provides a vacuum source for sample filtration, (2) it provides a pressure source for sample delivery, and (3) acts as an array of "false-bottoms" to retain reagents within the sample processing channels. The plate is an assembly having two ports for vacuum and

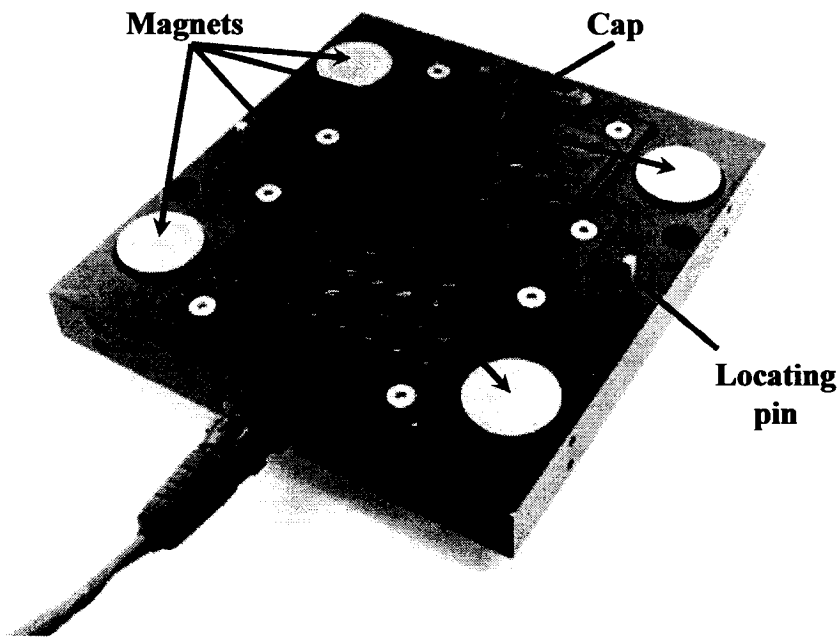

Figure 3.5: Top view of the filter plate showing the filter cap sealing the 96 sample processing channel locations across a filter membrane. The photograph shows the permanent magnets and locating pins for plate coupling and alignment as well as the cabled interface for proximity sensors to control electronics.

pressurized air sources, a screw-fastened sealing cap, the plate body, and an internal sealing mechanism that is normally held closed by spring-loaded for compression but can be electromagnetically retracted. It couples to the bottom face of the filter plate. When vacuum or pressurized air sources are required, the internal sealing mechanism is

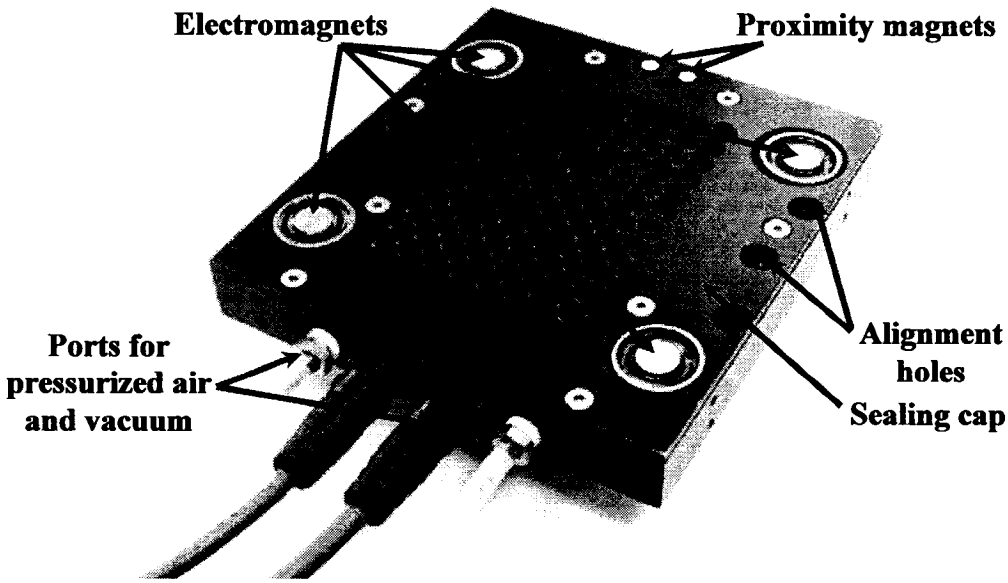

Figure 3.6: Top view of the vacuum-pressure plate showing the 96 sealed locations that simultaneously open for passage of pressurized air for sample filtration and delivery. The photograph shows all design aspects for plate-to-plate and arm-to-plate coupling and positioning, tubing interfaces to the pneumatic subsystem as well as the cabled interface to the control electronics.

retracted to connect it to the array of 96 processing channels. Otherwise, the internal sealing mechanism closes the bottom opening of the sample processing channels, creating 96 isolated cylinders for delivery and aspiration of reagents to the processing samples.

The *retainer plate*, shown in Figure 3.7, holds a 96 well microplate loaded with polymerized Epon. It collects the samples when they are delivered and contains them during the sample embedding steps at the end of the protocol. The plate is an assembly of a screw-fastened sealing cap and the plate body; it couples to the bottom face of the filter plate.

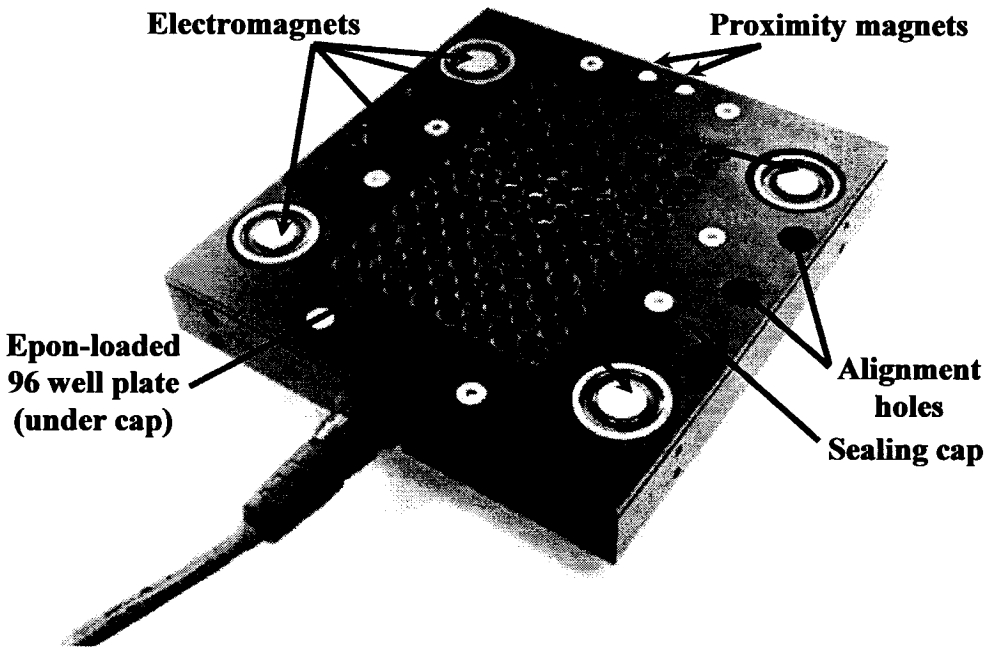

Figure 3.7: Top view of the retainer plate showing the sealed channels to an Epon-loaded 96 well plate where captured samples are embedded after the delivery stage. The photograph also shows all aspects for plate-to-plate and arm-to-plate coupling and positioning as well as the cable interface to the control electronics.

3.5.2 Plate Configurations

Three plate configurations are used throughout the automated sample processing protocol: processing, delivery and embedding. The filter plate is part of all three configurations; located at the center or top. It is attached to other plates firmly for plate-to-plate and channel-to-channel sealing by eight high-power permanent magnets built into the filter plate. The other plates use electromagnets to permit automated de-coupling. Locating pins and corresponding holes are used to align the plates. Miniature

magnets and magnetic proximity sensors embedded in the plates transduce plate alignment to the robot motion controller.

The *processing configuration* of the core mechanism, shown in Figure 3.8, is composed of the fluid transfer, filter, and vacuum-pressure plates. In this configuration, samples are loaded into the core mechanism through channel openings on the surface of the fluid transfer plate. Samples are filtered onto the charged filter membrane by applying vacuum to the vacuum-pressure plate. Once samples are deposited and bound to the filter membrane, reagents can be delivered/aspirated as needed for the chemical processing steps, through the holes in the fluid transfer plate.

The *embedding configuration*, shown in Figure 3.9, is comprised of the inverted

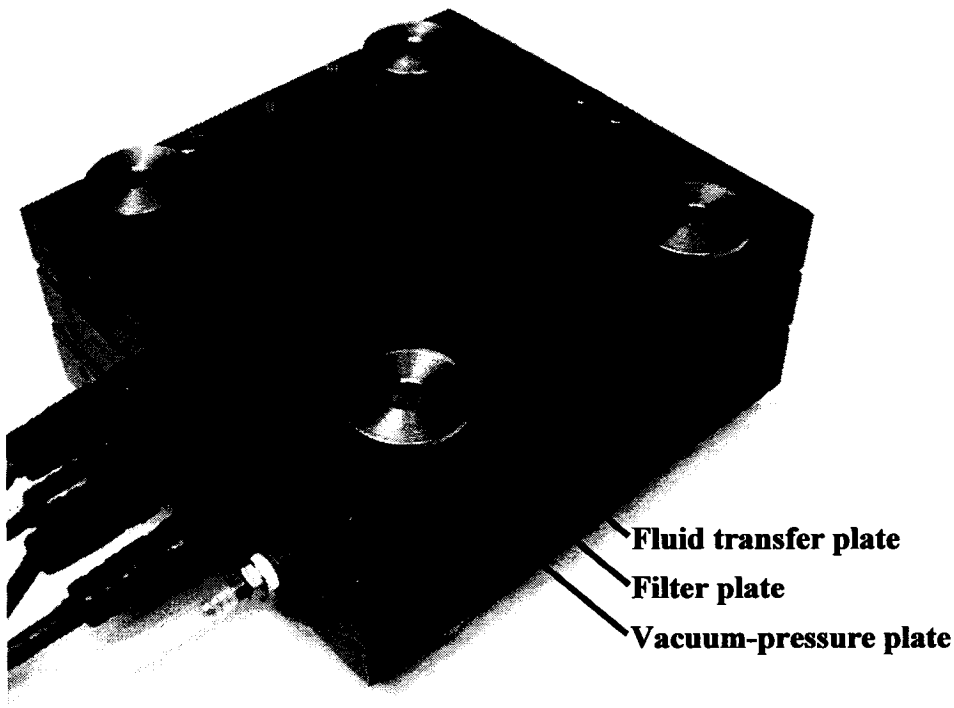

Figure 3.8: Top view of the core mechanism processing configuration illustrating the plate stacking method used to create parallel channels for vacuum filtration and chemical processing of up to 96 samples.

filter plate and the retainer plate. This configuration allows the filter membrane to be dissolved by delivery of an organic solvent through the bottom face of the filter-backing screen. The filter-backing screen also isolates and retains the samples during the embedding steps of the protocol.

The *delivery configuration*, shown in Figure 3.10, is composed of the filter and vacuum pressure plates inverted and coupled to the retainer plate. This configuration is used to deliver the membrane-freed samples to the Epon loaded wells in the retainer plate.

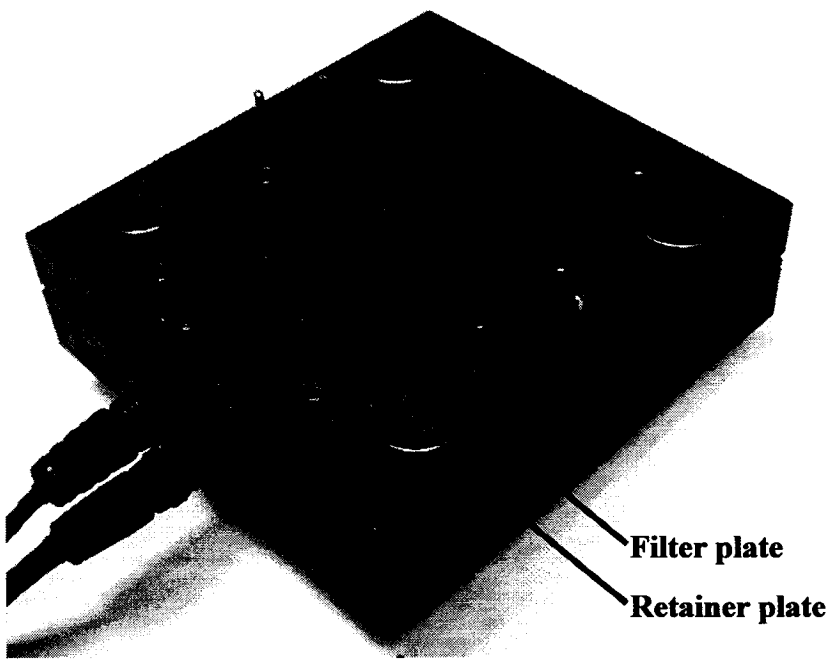

Figure 3.9: Top view of the core mechanism embedding configuration showing the inverted filter plate and the stacking method used to capture, trap and embed up to 96 parallel samples in the retainer plate.

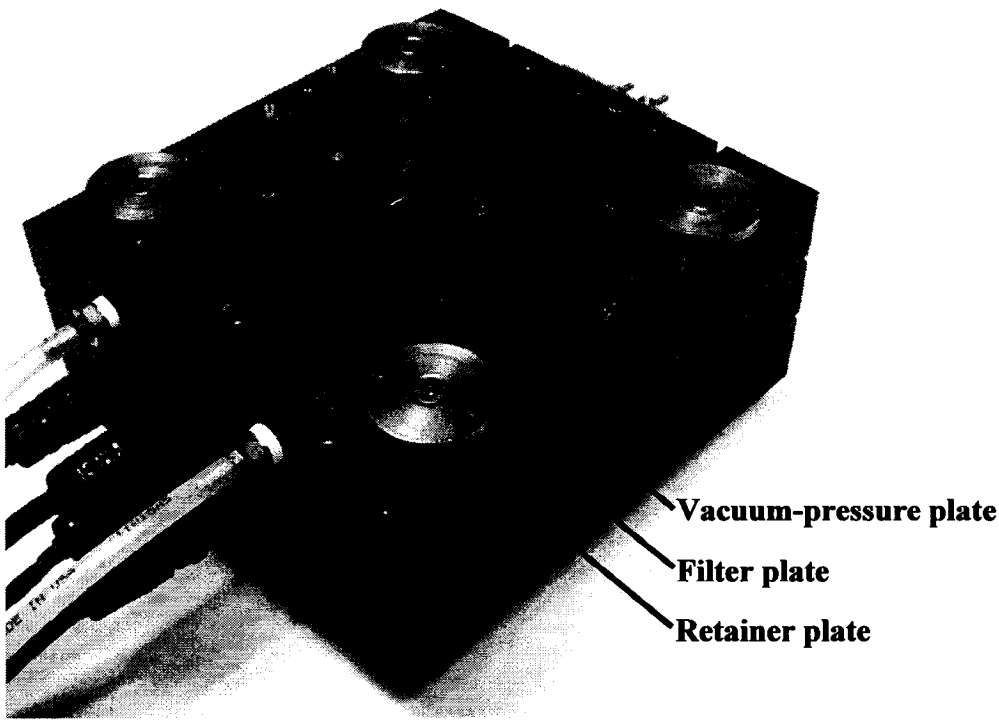

Figure 3.10: Top view of the core mechanism delivery configuration showing the inverted filter and vacuum-pressure plates as well as the plate stacking method used to deliver all processing samples from the filter plate to the Epon-loaded wells of the 96 well plate.

3.6 Support Subsystems

Operations on the core mechanism of the EMPOP robot are carried out by support subsystems for cooling, fluid handling, and positioning. These subsystems are modular and have geometries and mechanisms for positioning, alignment and stabilization that match those of the core mechanism. The subsystems impose minimal mechanical perturbations on the processing samples due to (1) close integration with the core mechanism and (2) the extensive use of sensor feedback for closed-loop control.

3.6.1 Cooling Support Subsystem

The cooling subsystem is centered around the cooling platform shown in Figure 3.11. It is an assembly of two side platform modules and a central base that serves two purposes: (1) it maintains the temperature of the core mechanism at a constant 4°C and (2) it stabilizes and aligns the individual plates and configurations of the core mechanism during different processing steps.

The side modules and the central base each contain a bank of thermoelectric coolers within the surfaces facing the core mechanism configuration, which is located on

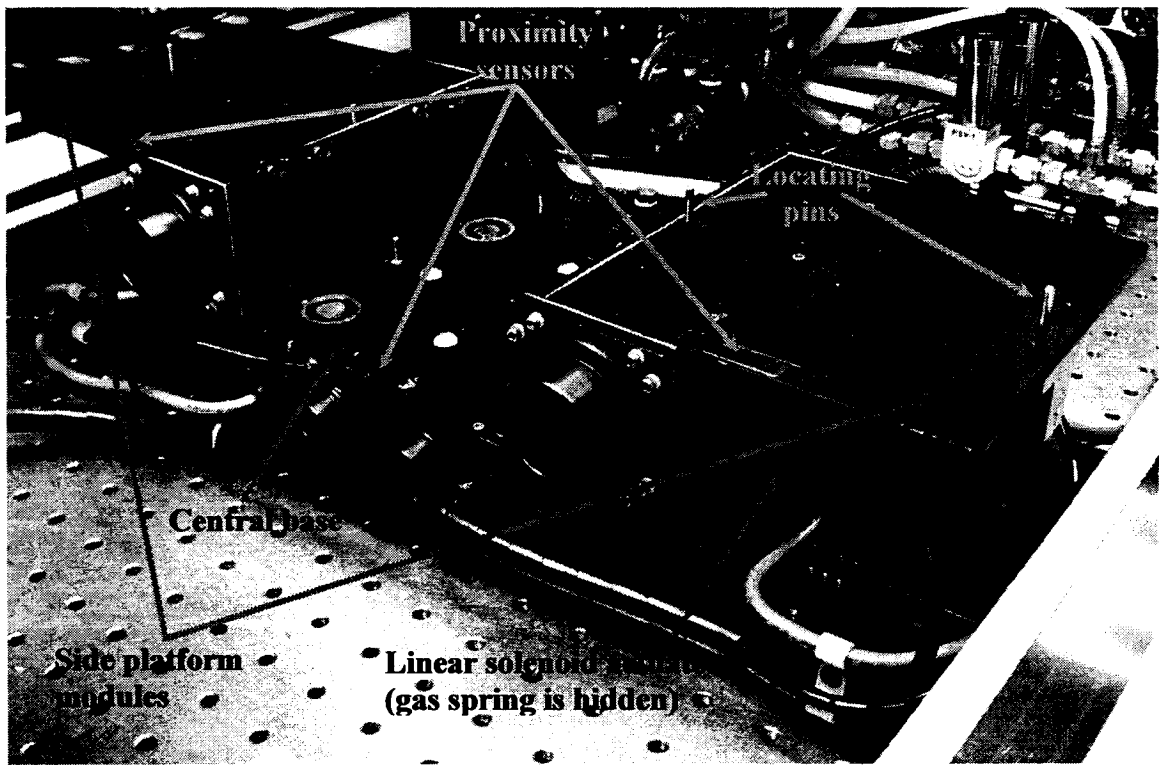

Figure 3.11: Top view of the cooling platform showing the surfaces for core mechanism cooling and positioning on the three subsections. The photograph also shows locating pins and proximity sensors for plate stabilization and detection as well as linear solenoid actuators side platform positioning.

the central base. The top surfaces of the two side platforms and the central base have locating pins to stabilize and align plates when they are stowed during processing or reconfiguration of the core mechanism. Miniature magnets embedded in the plates and magnetic proximity sensors sense the location of plates on the cooling platform. Linear solenoid actuators retract the walls of the two side platforms to provide clearance during configuration. At other times, the gas springs compress the walls against the core mechanism to ensure efficient cooling.

3.6.2 Fluid Handling Support Subsystems

Processing of subcellular fraction samples with the EMPOP robot requires automated, quantitative, fluid handling to filter the samples onto a charged membrane, dispense reagents to the samples, aspirate spent reagents to waste, clean the surfaces of dispensing and aspiration needles, and deliver samples with pressurized air. There are three fluid handling support subsystems: (1) processing reagents handling, (2) pressurized air handling, and (3) cleaning and waste management.

3.6.2.1 Reagent Handling Support Subsystem

Processing reagents are dispensed with microliter-range precision and mixed by a panel of miniaturized, automated liquid handling components mounted on the back of the Y-axis of the motion control subsystem (see Figure 3.12). Directional control of processing reagent dispensing is achieved by four banks of miniature 2 and 3-way solenoid valves interfaced to directional manifolds. Pumping and mixing of reagents is achieved by two variable-volume stepper pumps coordinated with the solenoid valves to deliver

processing reagents to the core mechanism *via* two multi-channel dispensing needle manifolds located on the θ-axis of the robot (see Figure 3.13). Delivery of reagents is controlled to the microliter-range *via* the stepper pumps (2.5 μl/step).

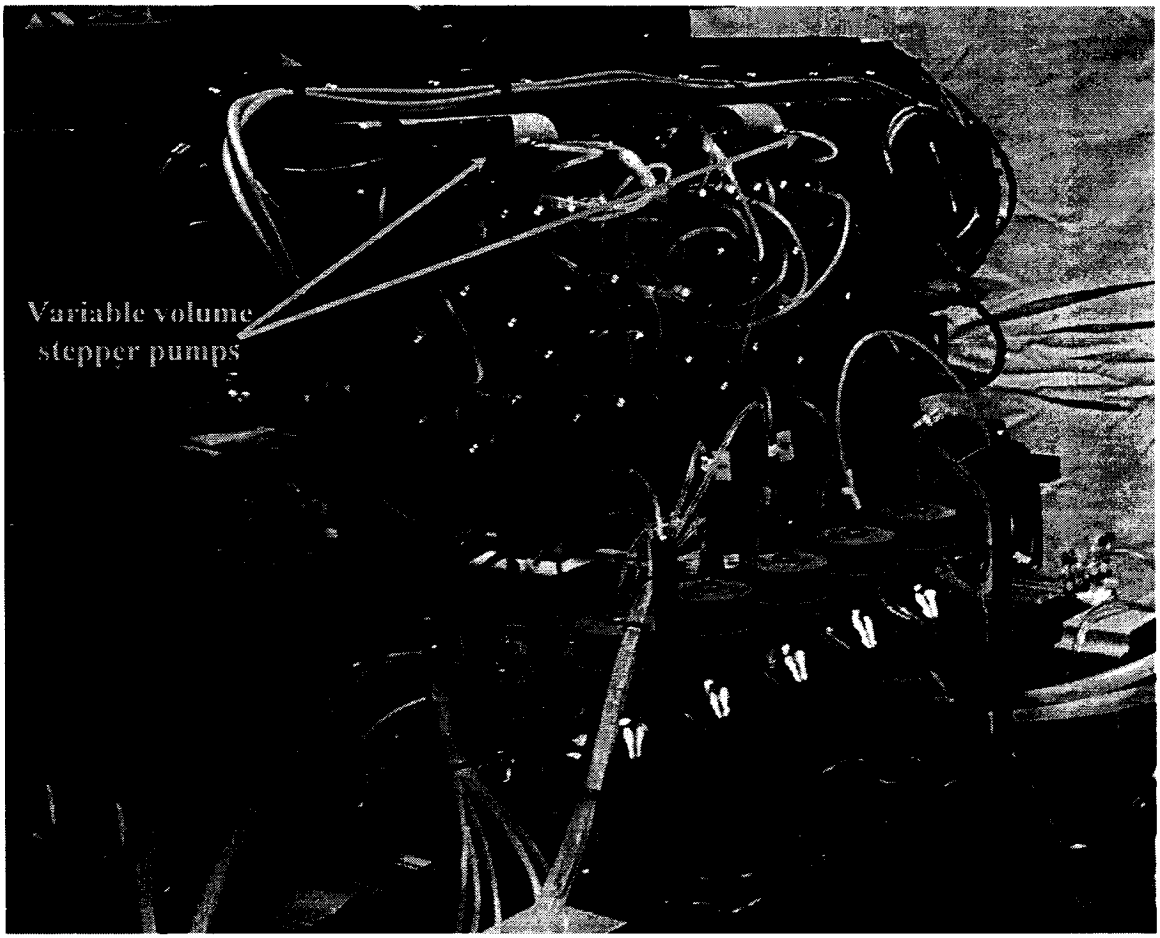

Figure 3.12: Photograph of the reagent handling panel and the reagent reservoir bank. All tubing from the reservoirs leads to directional manifolds of miniature solenoid valves, which permit individualized dispensing and/or mixing of reagents by way of two variable volume stepper pumps.

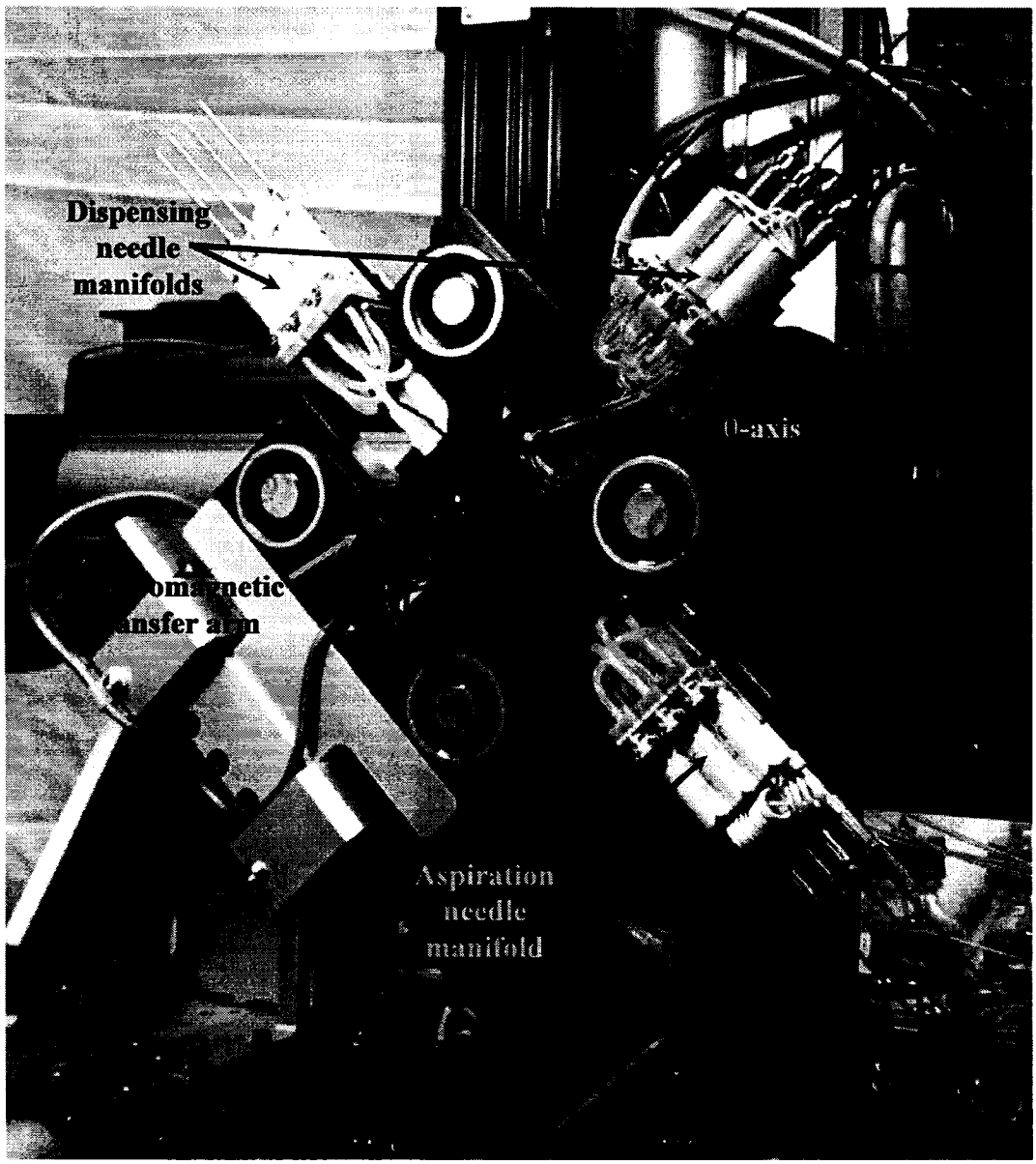

Figure 3.13: Front view of the dispensing needle manifolds with all other fluid handling and plate positioning components located on the θ-axis of the motion control subsystem.

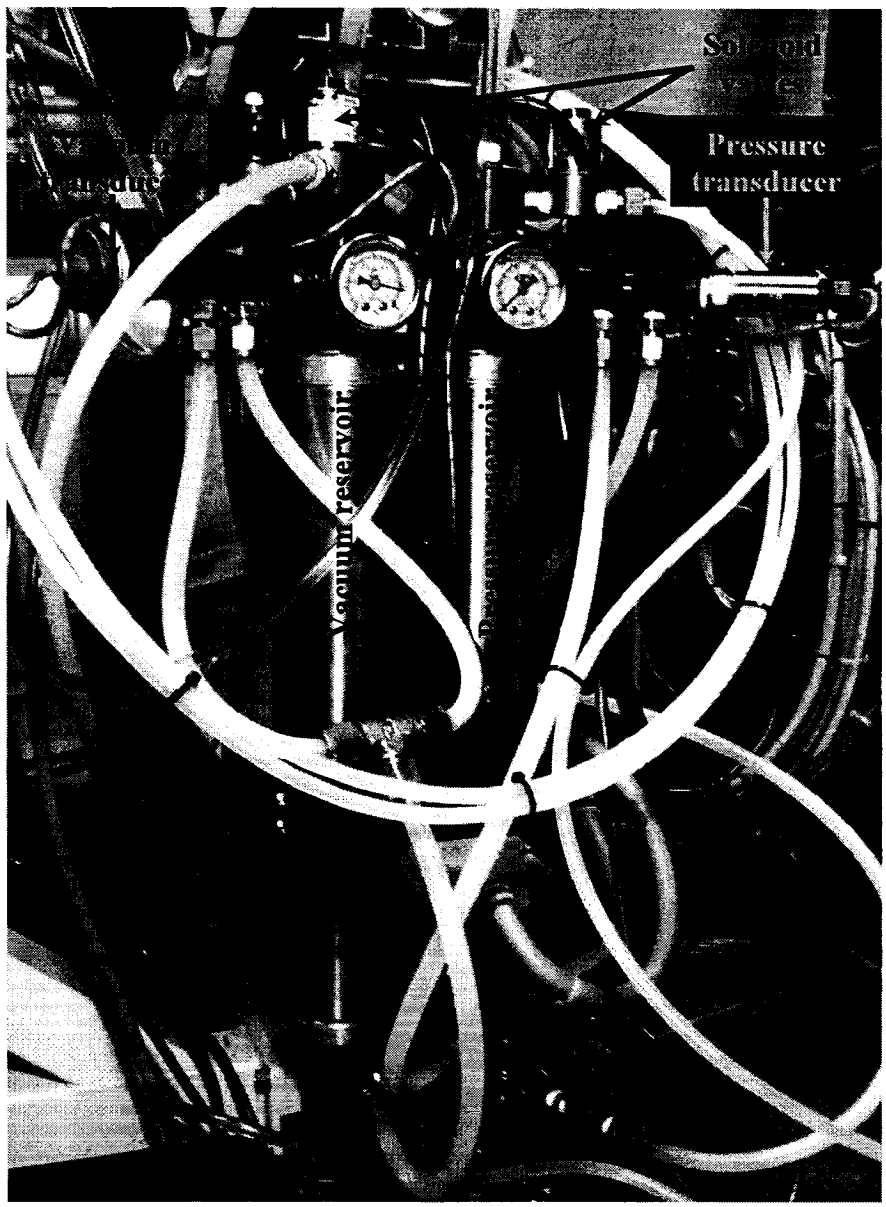

Figure 3.14: Front view of the vacuum-pressure manifold showing the valves that link it to the other components of the pneumatic and cleaning and waste management subsystems. The transducers for feedback control of vacuum and pressure levels as well as the interface and cable connection to the control electronics are shown.

3.6.2.2 Pneumatic Support Subsystem

Pressurized air and vacuum sources are used for sample filtration and delivery and waste removal operations. Figure 3.14 shows the manifold for pressurized air and vacuum mounted to the back of the antivibrational table where two air reservoirs are charged by an air compressor. Manifolds of solenoid valves (direct acting and proportional) and pressure transducers, mounted in-line with the reservoirs, provide directional, quantitative control of vacuum and pressurized air (see Figure 3.15).

Figure 3.15: Photograph of the pneumatic subsystem in-line valves that permit control of vacuum and pressurized air to the core mechanism and the cleaning and waste management subsystem.

3.6.2.3 Cleaning and Waste Management Support Subsystem

The robot's clean station, shown in Figure 3.16, is composed of two sections that successively wash and dry the outer surfaces of the aspiration and dispense needles. Needles are washed in a stream of distilled water that is passed through the wash section

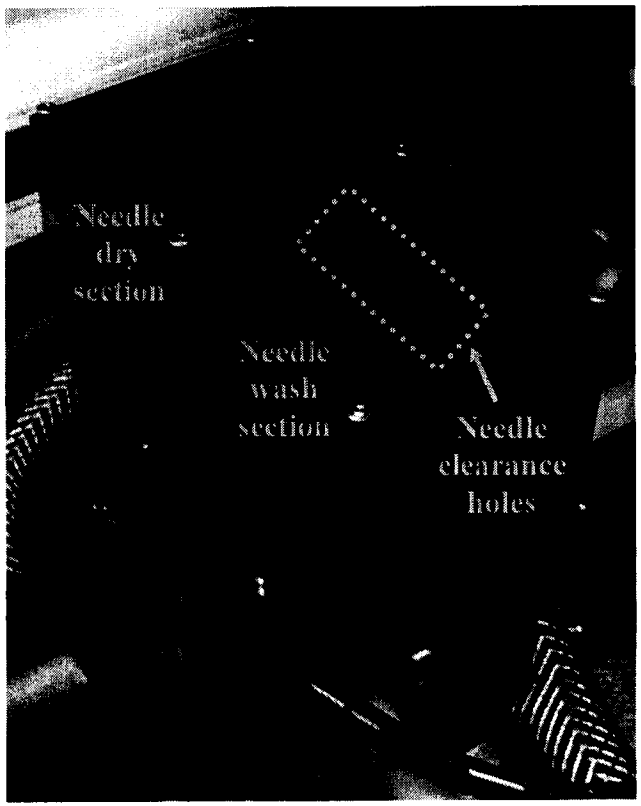

Figure 3.16: Top view of the clean station showing the two sections for needle washing and drying as well as the clearance holes for passage of a manifold of four needles.

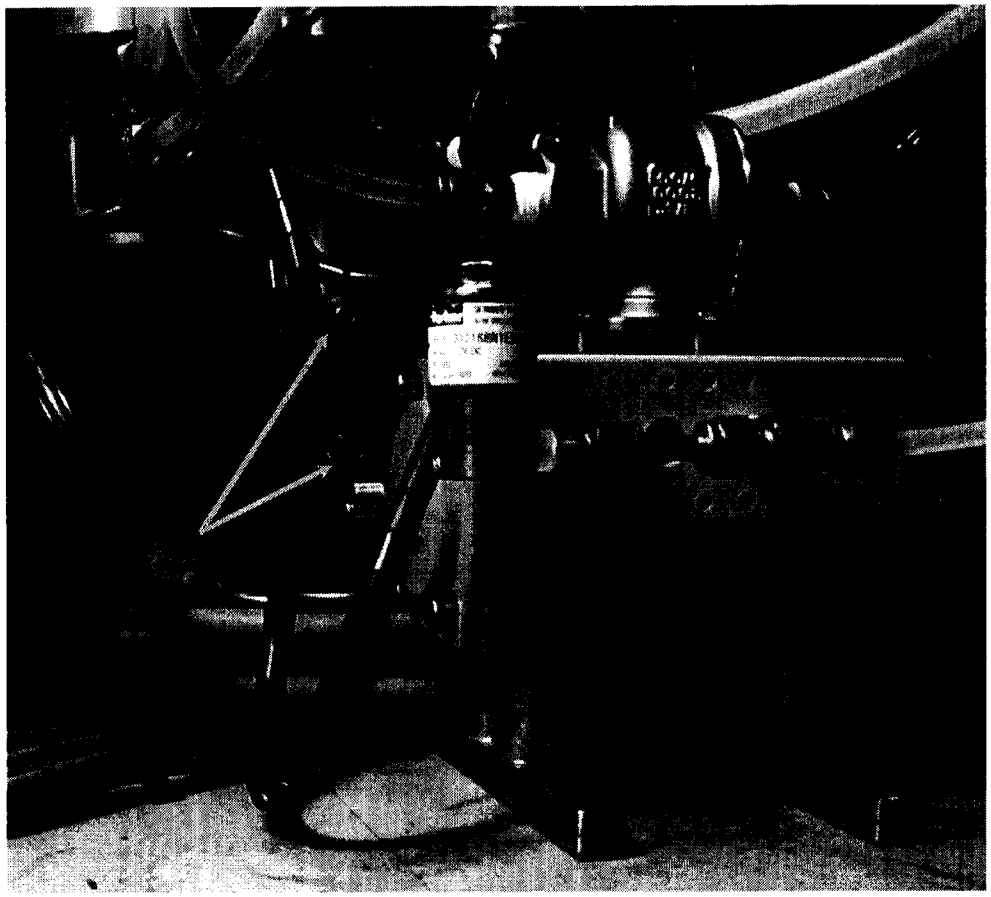

Figure 3.17: Photograph of the waste removal manifold and ball valve components that that provide automatic delivery of system waste to three reservoirs.

by two simultaneously acting miniature pumps. Subsequently, the application of vacuum in the needle dry section removes residual moisture from the needle surfaces.

The waste removal system also utilizes vacuum to aspirate spent processing reagents from the sample processing channels of the core mechanism *via* the aspiration needle manifold located on the θ-axis of the robot (see Figure 3.13).

As shown in Figure 3.17, waste that accumulates within the vacuum reservoir is removed by way of a ball valve connected to a miniature pump and two three-way solenoid valves. The arrangement directs waste to one of three reservoirs; one for low-toxicity material (such as water, buffers, ethanol, etc.), or two other reservoirs that are reserved to separate waste that is highly toxic.

3.6.3 Positioning Support Subsystems

The EMPOP robot relies upon three coordinated support subsystems for automated plate interchange, positioning of the core mechanism, and placement of fluid handling tools: (1) an electromagnetic arm, (2) a transfer platform and (3) a motion control system.

3.6.3.1 Motion Control Support Subsystem

Figure 3.18 shows the motion control subsystem. It positions the three needle manifolds and the electromagnetic transfer arm using five serially coupled, linear and rotational servo controlled axes. It provides closed-loop positioning for liquid handling in the core mechanism and for the coordinated motion needed to transfer core mechanism plates or configurations.

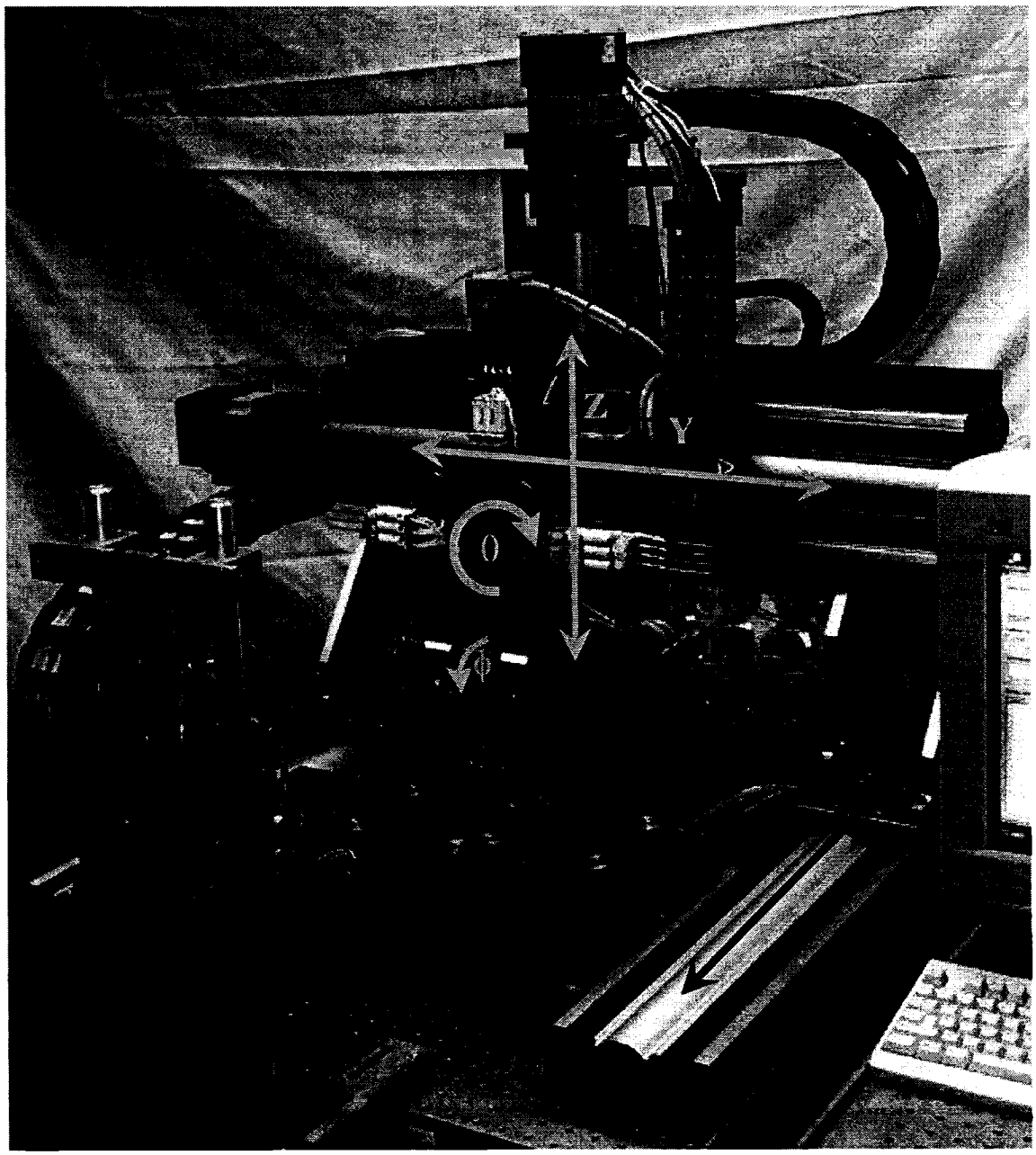

Figure 3.18: Photograph of the EMPOP robot showing the motion control subsystem and positioning capabilities for all axes. The serially coupled, 5-axis, servo-controlled system permits linear travel along the X-, Y- and Z-axes. The θ-axis carries all reagent dispensing and aspiration needle manifolds as well as the ϕ-axis, which holds the electromagnetic arm. The θ-axis has a 270° range of motion and the ϕ-axis has a range of motion greater than 90°.

3.6.3.2 Electromagnetic Transfer Arm Support Subsystem

The electromagnetic transfer arm is located on the ϕ-axis of the motion control system, as shown in Figures 3.13 and 3.19; is it used for plate positioning. It retrieves, places, and rotates the plate configurations to and from the cooling platform and transfer platform. Four high-power electromagnets per face grip the plates during operation. Locating pins align and stabilize the core mechanism while magnetic proximity sensors monitor arm-to-plate interaction. It has more than 90° of a servo-controlled range of motion, which permits flexible arm-to-plate positioning, and retraction of the arm into a stowed position when not in use.

Figure 3.19: Photograph of the electromagnetic transfer arm interacting with the processing configuration located on the cooling platform. Proximity sensors on all components permit controlled positioning of the core mechanism and its plates.

3.6.3.3 Transfer Platform Support Subsystem

The transfer platform, shown in Figure 3.20, is used during inversion of the core mechanism. Its geometry matches that of the electromagnetic transfer arm and provides

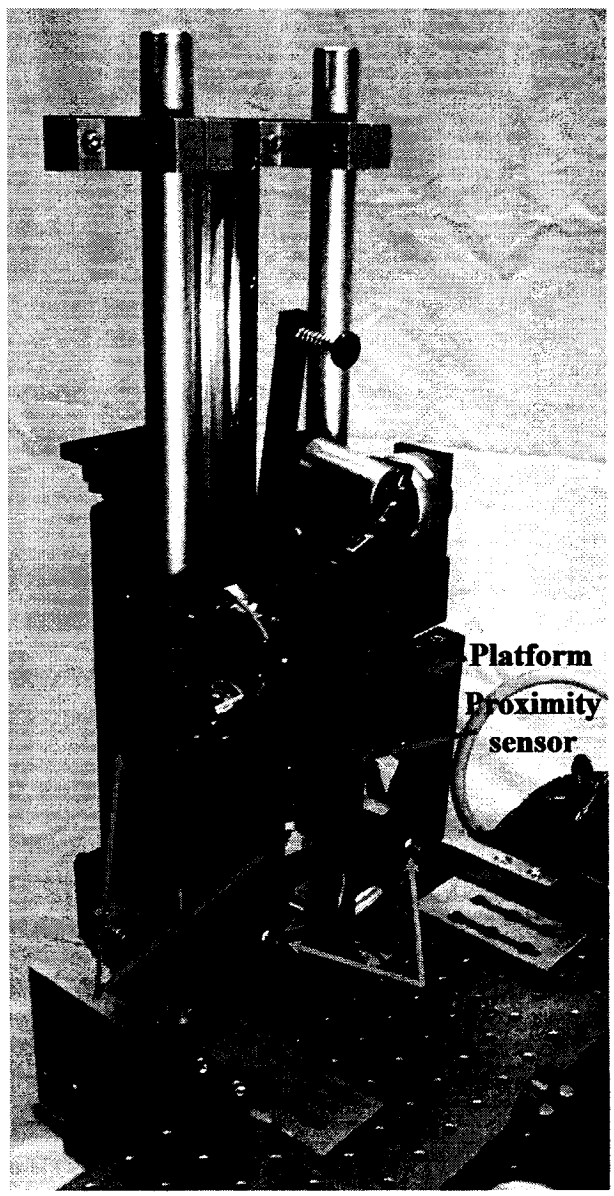

Figure 3.20: Front view of the transfer platform showing the platform geometry that permits stabilization of the core mechanism and passage of the electromagnetic transfer arm. The photograph also shows all actuators for platform positioning and core mechanism stabilization.

additional vertical positioning needed to invert and retrieve the core mechanism. The transfer platform geometry allows the electromagnetic arm to pass through it once the core mechanism is decoupled. The transfer platform locating pins align and stabilize the core mechanism. It also has magnetic proximity sensors that signal its location to the robot's controller. Two linear actuators position the platform vertically to permit retrieval of the core mechanism and to retract the platform into a stowed position when not in use.

4 Mechanical Design of the EMPOP Robot

4.1 Overview

This chapter describes the mechanical design of the EMPOP robot and the methods used to integrate the core mechanism and support subsystems. As a first generation prototype, the robot consists of robust, modularized subsections that facilitate component troubleshooting or modification, provide reliable operation, and retain enough flexibility to accommodate for changes in development of the automated process. Moreover, the objective of the integrated, autonomous design was to minimize mechanical perturbations and maximize control of chemical, biological and mechanical parameters to ensure successful automated subcellular fraction sample preparation.

Figures 4.1A and B illustrate the complete mechanical design and assembly of the robot, in which an antivibrational table supports the core mechanism and seven integrated subsystems for: (1) cooling, (2-4) fluids handling and (5-7) positioning. The manual for the EMPOP robot [171] gives specific details of the mechanical design and construction and the associated Master's thesis, "Automated Control of the Electron Microscopy Proteomic Organellar Preparation Robot" [172] describes subsystem performance.

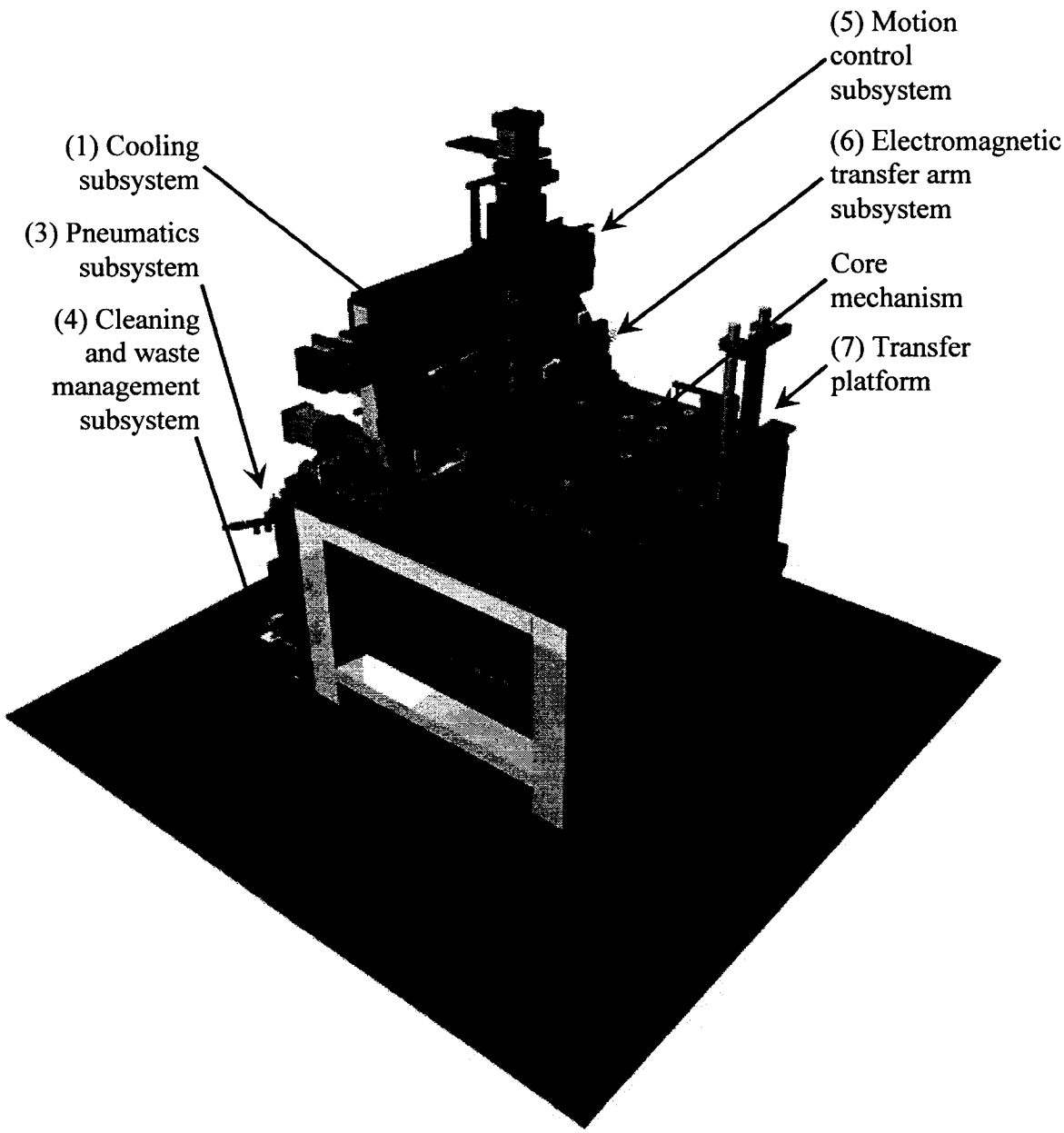

Figure 4.1A: A front perspective rendering of the EMPOP robot illustrating all mechanical components assembled on a 900 mm x 900 mm antivibrational table. The arrows indicate the core mechanism and subsystems visible from the front of the robot.

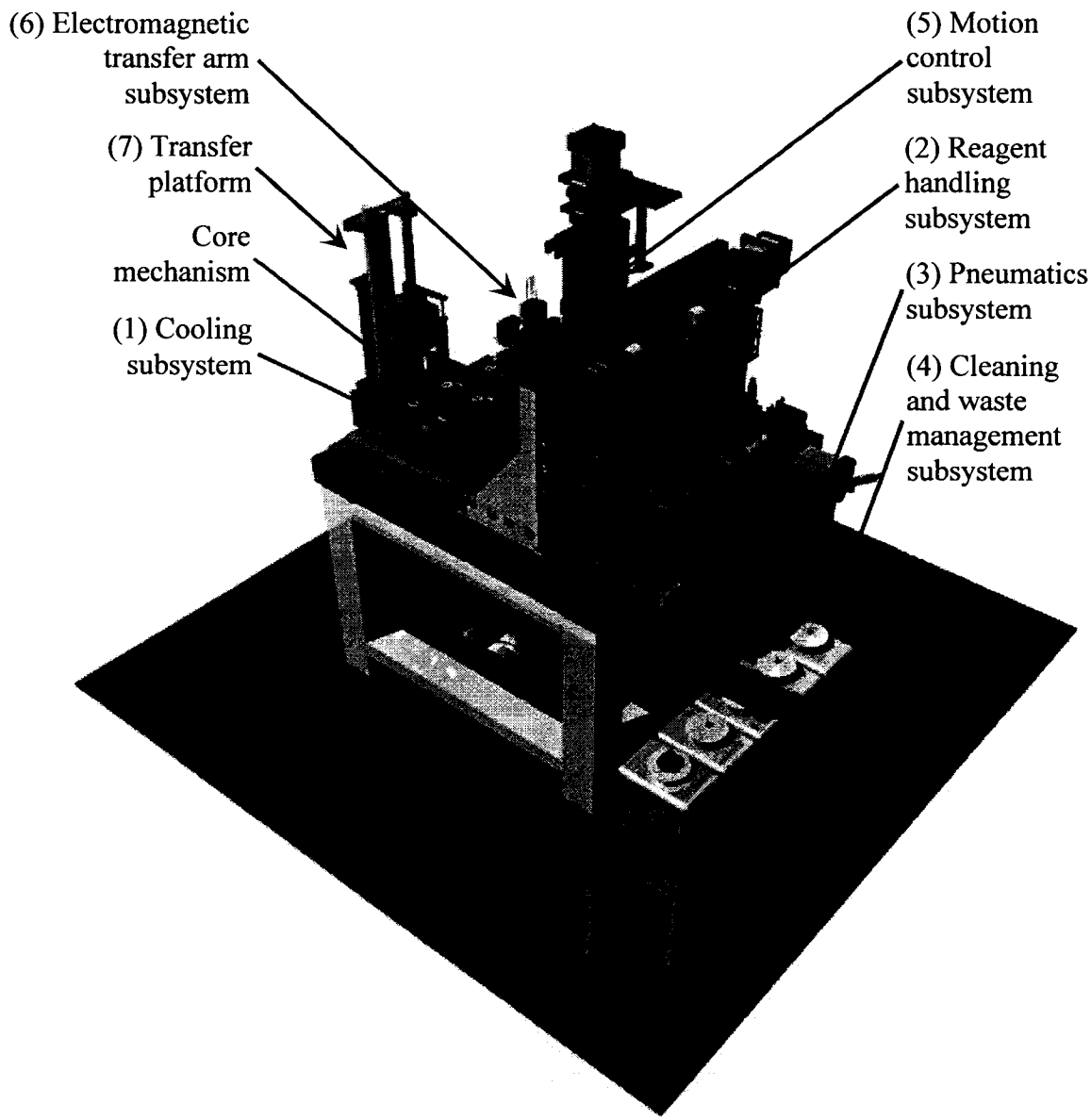

Figure 4.1B: A rear perspective rendering of the EMPOP robot illustrating all mechanical assemblies. The arrows indicate the core mechanism and subsystems visible from the rear of the robot.

4.2 Core Mechanism

All work done by the EMPOP robot centers around the system of stackable and reconfigurable processing plates that form the core mechanism. All processes occur within the core mechanism to impose minimal mechanical perturbations on subcellular fraction samples and to preserve their morphological integrity. Moreover, the designs of core mechanism plates accommodate all static and dynamic aspects of the preparation process as a modular, automated device that operates in multiple configurations. Although each plate has a particular purpose, a set of design features and concepts unify the plates. Furthermore, they provide the flexibility needed for execution of an automated protocol by extending the robot's operations for cooling, fluid handling and positioning to the locality of the processing samples.

4.2.1 Core Mechanism Design Features and Concepts

To ensure inter-plate compatibility as well as integration with the cooling, fluidic and positioning subsystems of the EMPOP robot, a set of nine design features were standard. As illustrated for the filter plate in Figure 4.2A, each plate had:

(1) Three basic plate body features.

(i) An aluminum body for its high thermally conductivity ($k_{Al\ Alloy\ 6061,\ 20°C}$ ~170 W/(m°C)) [173-175], which permits efficient cooling to 4°C.

(ii) Anodized body surfaces for electrical neutrality, chemical compatibility and resistance to corrosion [174-177].

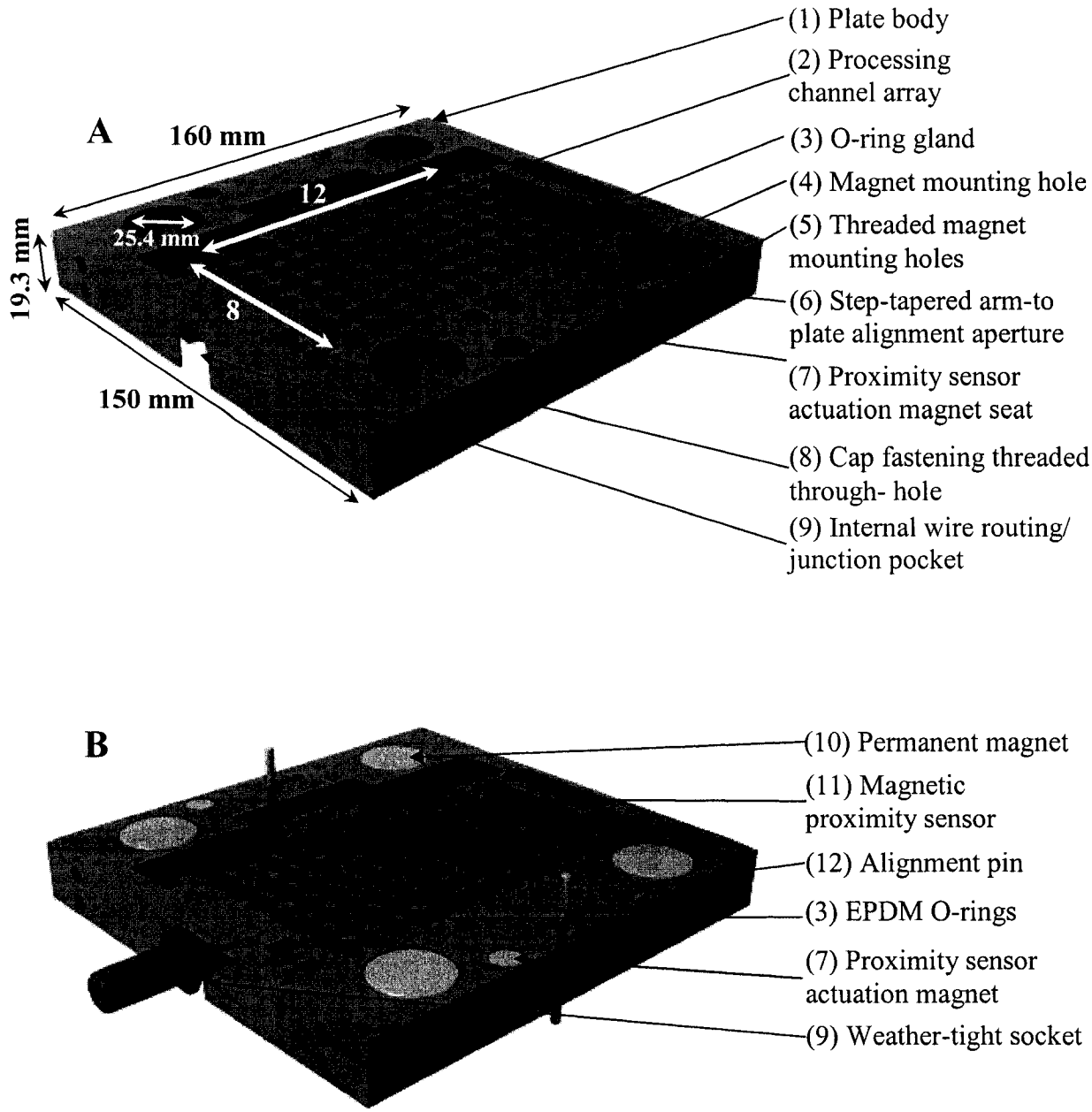

Figure 4.2: (A) Common core mechanism plate design features and (B) standard plate components and filter plate components required for automated interaction of core mechanism plates.

(iii) A compact body geometry of 160 mm x 150 mm x 19.3 mm that accommodates all components for sealing, coupling, alignment and proximity sensing within a structure that can interact easily with the robot subsystems.

(2) A plate-centered 8 x 12 array of processing channels, with standard microplate 9 mm center-to-center spacing [178], which provides isolated, parallel sample processing.

(3) Individual processing channel O-ring glands fitted with ethylene-propylene-diene-monomer (EPDM) rubber, size 009 Shore A, 40 durometer O-rings, which provide:

(i) Chemical compatibility with all sample preparation process reagents [179].

(ii) Maximized sealed area for each processing channel.

(iii) High deformability (i.e. low durometer [179-182]) to ensure channel-to channel and plate-to-plate static sealing under the compressive force of permanent magnet.

(4) A symmetric array of four, 25.4 mm diameter mounting holes for permanent magnets or electromagnets; located to provide direct interaction and equal distribution of force for coupling and decoupling across the top and bottom surfaces of all plates.

(5) Sets of two threaded holes at locations corresponding to the centers of the 25.4 mm diameter mounting holes to fasten all permanent magnets or electromagnets.

(6) A set of two arm-to-plate surface alignment apertures [183, 184] with a step-tapered geometry to compensate for small misalignment (~ 1 mm) of the arm alignment pins; guiding them into the apertures (i.e. remote centers of compliance for effector-to-object interaction) (see Figure 4.4A) under the force of the arm electromagnets [184].

(7) Two seats in the top and bottom surfaces to accommodate miniature nickel-plated neodymium-iron-boron ($Nd_2Fe_{14}B$) magnets [185-191] for arm-to-plate magnetic proximity sensing. The stable and high magnetic strength of $Nd_2Fe_{14}B$ magnets permits non-contact proximity sensing [175, 184, 188] of arm-to-plate interaction. The level arrangement of the seated magnet and the plate surfaces permits close contact between the surfaces of the arm and plates.

(8) Eight threaded though-holes for sealing cap fastening and compression (see below).

(9) Internal routing passages for electromagnet and sensor wires leading to a junction pocket, where a multi-pin, miniature, moisture-tight socket consolidates all conductors.

All stages of the sample preparation process use the filter plate, which is always located in the center of any plate configuration. Consequently, it holds the components that direct and monitor plate interaction. Figure 4.2B shows the three symmetrically located components in the top and bottom faces of filter plate that provide compression and alignment across the coordinately staged system of plates:

(10) An array of four 25 mm diameter x 10 mm height, rare-earth, samarium-cobalt ($SmCo_5$) encased, permanent magnets. The following characteristics make these magnets suitable for this application where high compressive force for static fluid sealing is essential and high repulsive magnetic fields are directly applied for magnetic plate decoupling:

(i) Permanent magnets produce no heat load in the core mechanism.

(ii) High magnetic strength (i.e. high energy product of induction (B) with applied field (H), $(BH)_{max}$ ~160 kJm^{-3})) [186, 190, 191]; each magnet provides 90 N holding force (on a clean, ground, mild steel surface) for a total of 360 N holding power on each surface of the filter plate.

(iii) They are essentially insensitive to demagnetization by external magnetic fields (i.e. high intrinsic coercivity (H_{ci} ~2000 kAm^{-1})) [186, 190, 191], which makes them ideal for magnetic repulsion applications.

(iv) $SmCo_5$ is resistant to oxidation [186, 189, 191]; avoiding the corrosive effects of aqueous processing reagents, condensate build up or repeated plate cleaning for reuse. Because surface treatment is unnecessary, direct contact with the corresponding electromagnets of other plates is possible; eliminating a loss in flux density from gaps between magnetic surfaces [187-189, 191].

(v) The encased permanent magnet design concentrates the magnetic flux from both poles to one face of the magnet (all other sides are non-magnetic). One magnetic pole dominates the center of the surface that is directly in-line with the electromagnet poles of other plates. The non-

magnetic surfaces and the geometry of the magnets permit back-to-back stacking of magnet pairs to coordinate magnetic faces with the top and bottom surfaces of the filter plate as well as directing any magnetic fields away from the processing samples.

(11) A magnetic proximity sensor to monitor plate-to-plate coupling. The filter plate is always located in the center of any configuration. Therefore, coupling and alignment of interfacing plates is monitored in a non-contact manner [175, 184, 188] that is reliable and effective regardless of any moisture or debris that may accumulate on the plates during sample processing.

(12) A set of two miniature stainless steel dowel pins that serve as locating devices for interaction with plate alignment apertures (see Figure 4.4A) [183, 184]. The pins line up of all processing channels across plate surfaces as well as restrict positioning to the direction normal to the surface of the plate during plate positioning events.

The plates of the core mechanism function as a single, integrated unit. The fluid transfer plate, in Figure 4.3, exemplifies the four aspects for structural design and component conservation among the three other plates. The following features

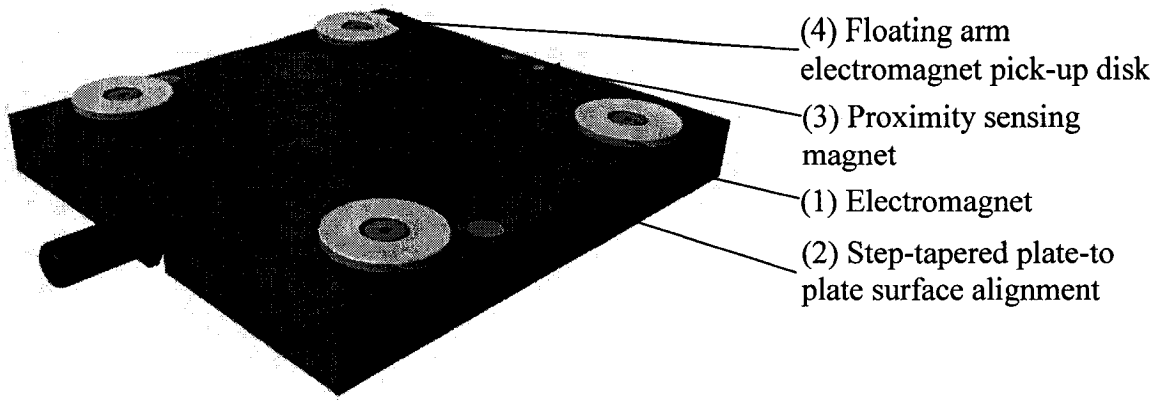

Figure 4.3: Illustration of the core mechanism fluid transfer plate showing structure and components used for all plates that interface with the filter plate.

compliment the alignment, coupling and stabilization mechanisms of the filter plate as well as standardize automated function of the core mechanism:

(1) An array of four 25.4 mm diameter x 19.1 mm height, surface-contact, round electromagnets. The geometry of the electromagnets is suitable for the dimensions of the plates and corresponds directly to that of the permanent magnets. They serve two functional roles within the core mechanism:

(i) The electromagnet cores (mild steel) are in-line with the central flux line of the permanent magnet's center poles and serve as the mating magnetic surfaces for plate coupling.

(ii) The electromagnets provide the repulsive force [188, 192-197, 199] against the permanent magnets for plate decoupling. A high power DC pulse energizes the electromagnet coils (see Section 5.3) to generate a magnetic field of the same polarity as that of the permanent magnets and normal to their surfaces. As Figure 4.4B shows, the result is an axial thrust that disengages

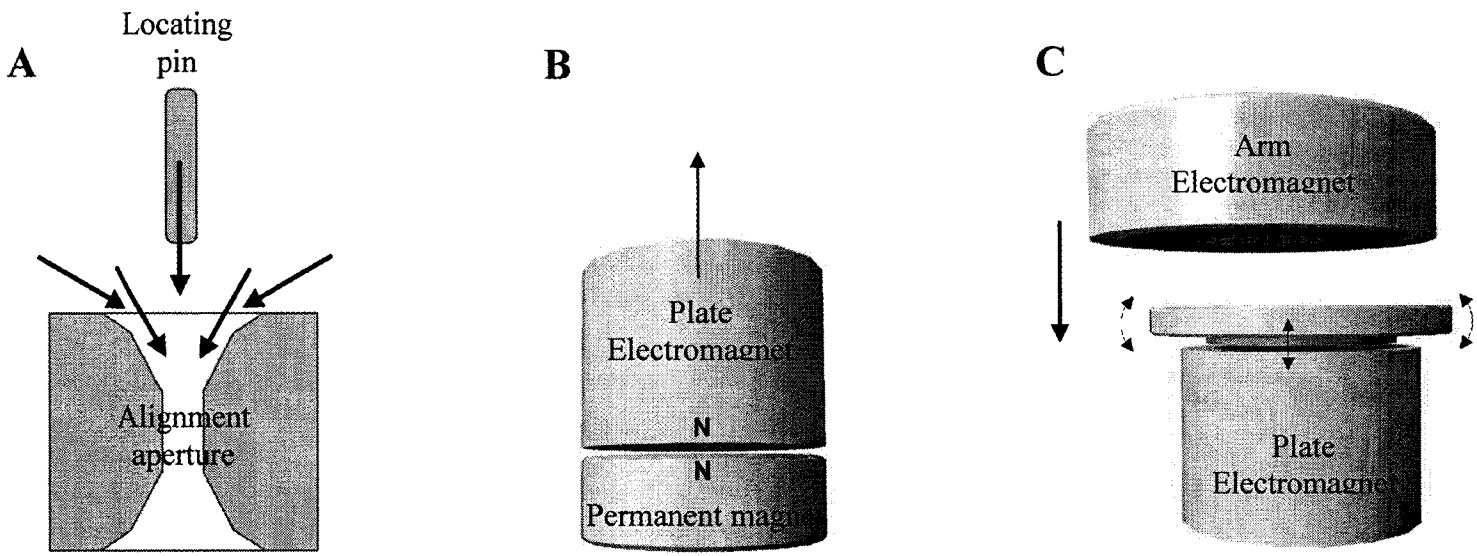

Figure 4.4 : Schematic illustrations of core mechanism interaction mechanisms (arrows indicate the directions of motion). (A) Locating pin/alignment aperture mechanism for plate-to-plate and arm-to-plate alignment and stabilization [183, 184]. The step-tapered design of the aperture guides the alignment pin to the center. (B) Electromagnet/permanent magnet repulsion [186, 188, 190-197, 199] for plate decoupling. Both magnetic fields have identical polarity (indicated by "N" (north pole) on each magnet) on their interfacing surfaces and similar field strengths. The resulting repulsive force produces an air gap between each of the four pairs per plate. (C) Arm electromagnet coupling with plate pick-up disks. Wobble and vertical movement from the spring loaded plate pick-up disks compensate for any arm electromagnet misalignment and ensure correct arm-to-plate interaction.

the four coupled permanent/electromagnet pairs; levitating the plate and producing an air gap between all electromagnet/permanent magnet pairs [192-197]. As the plates separate, the flux density (Φ) (from permanent magnets) decreases rapidly across an increasing air gap (following an inverse square proportionality with the distance (d) between the magnets faces ($\Phi \propto 1/d^2$) [187, 188, 191]) (see Figure 4.4B), permitting plate decoupling by the simultaneous upward motion of the electromagnetic arm coupled to the plate (see Figure 4.17).

(2) A set of two step-tapered, plate-to-plate, surface alignment apertures. Similar to the arm-to-plate apertures described above, they permit plates to descend into the correct coupled position ensuring alignment of all processing channels (see Figure 4.4A).

(3) A set of two mounting locations in each surface of the plate that accommodate miniature $Nd_2Fe_{14}B$ magnets for non-contact, plate-to-plate proximity sensing. The arrangement allows the surfaces of the magnets and the plates to be level and permits close contact between the plate surfaces of the arm and plates. The $Nd_2Fe_{14}B$ magnets are sufficiently powerful [186, 188-190] to monitor arm-to-plate interaction *via* a magnetic proximity sensor regardless of the presence of moisture or debris.

(4) Four assemblies of stainless steel floating arm electromagnet pick-up disks with top and bottom interface disc springs that are fastened to the electromagnets. Figure 4.4C shows how the disks provide magnetic surface area [187] for interaction with the corresponding electromagnets of the electromagnetic transfer

arm. The disc springs permit flexible surface alignment to ensure proper interaction of all arm electromagnets.

Sealing caps for three of the four plates provide a uniform, reliable method for inter- and intra-plate fluid sealing. Although the details of individual caps varied with the plates, three structural aspects were conserved in all plates:

(1) A sealing cap thickness of 3.2 mm; a minimal thickness to maintain the cap rigidity with the array of 96 processing channels.
(2) Eight countersunk clearance holes for installation of sealing cap fasteners level with the cap surface
(3) Clearance for surface alignment holes, permanent magnets, electromagnets and O-ring glands.

4.2.2 Filter Plate

Figure 4.5 shows the filter plate, an assembly of the plate body and the sealing cap, that secures a stacked arrangement of a filter membrane and a filter screen. The filter plate holds the membrane bound subcellular fraction samples and so is the focus of all core mechanism processing configurations. Furthermore, the body incorporated a recess to hold the samples internally for chemical processing; where the samples can be approached with needle manifolds from either surface. For intra-plate sealing, the body and sealing cap are equipped with standard O-rings on the surfaces facing the filter membrane/filter screen.

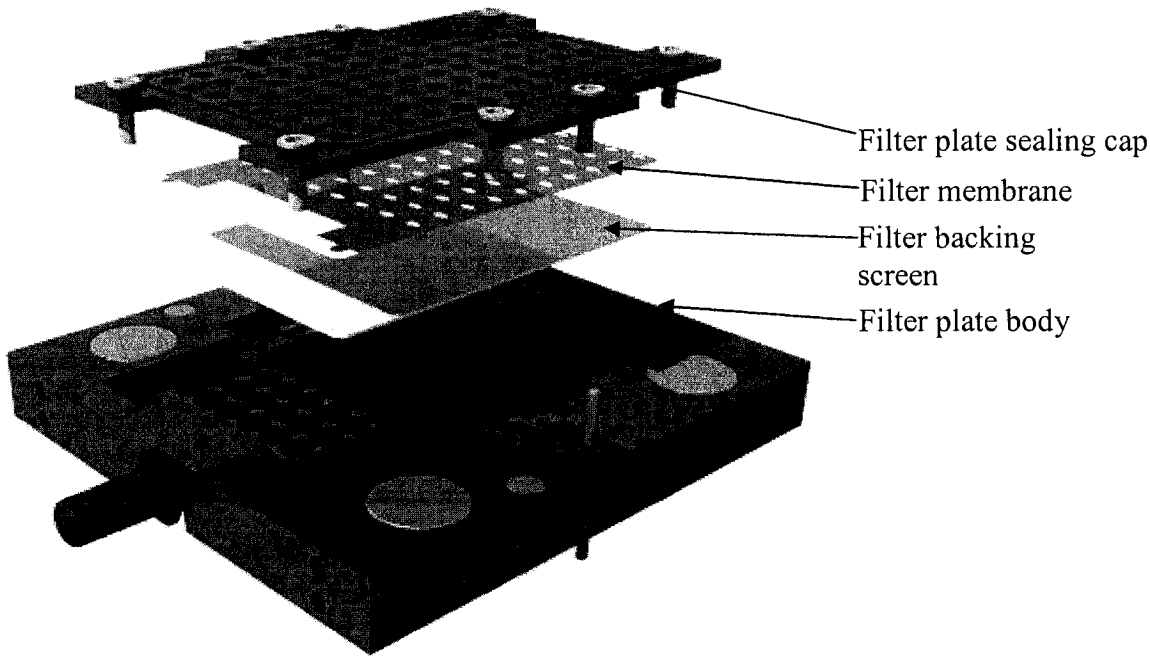

Figure 4.5: Illustration of the filter plate assembly of components. All other plates interface with the top and bottom of the filter plate *via* the permanent magnets and the alignment pins. The filter membrane is sealed within the filter cap recess, where is approachable for processing from either surface of the plate.

The design of the recess and sealing cap places the samples close to the top surface of the filter plate to: (1) restrict the processing channel volume required for application of any processing reagents to the channels of the fluid transfer plate and (2) minimize the travel distance for sample delivery to the retainer plate.

The bottom face interfaces to the vacuum-pressure plate for sample filtration and delivery as well as for static fluid sealing during the course of an automated sample processing run. It also accommodates dispensing and aspiration of processing reagents to and from the 96 channels.

As the focus of all processing configurations, the filter plate holds all components that direct or monitor inter-plate alignment and coupling. Furthermore, because the

samples are located in the filter plate during most of the process, the temperature of this plate is what must be controlled. Consequently, it has an embedded, miniature platinum resistance temperature detector (RTD) [202-205, 263-265] that reports the core mechanism temperature to the robot controller (see Section 5.3).

4.2.3 Fluid Transfer Plate

The fluid transfer plate, illustrated in Figure 4.3, is a removable array of reservoirs to hold sample suspensions for filtration and reagents for chemical processing of the membrane-bound samples. The 96 identical reservoirs are 6 mm diameter through holes with the standard inter-plate sealing O-rings located on the bottom surface of the plate. Otherwise, the plate is composed of the standard components for automated function of the core mechanism.

4.2.4 Vacuum-pressure Plate

The vacuum-pressure plate operates as a simultaneously acting array of normally closed valves that seal the bottom surface of each processing channel or, when actuated, permit passage of fluids under vacuum or pressure. Figure 4.6 shows that the vacuum-pressure plate is an assembly of three components:

(1) Vacuum-pressure plate body. A recess holds the stopper mechanism and provides passage for the flow of pressurized air and sample filtrate. To support stopper mechanism retraction, two holes pass through the front end of the plate and into the sides of the recess to serve as mounting locations for surface-contact, round

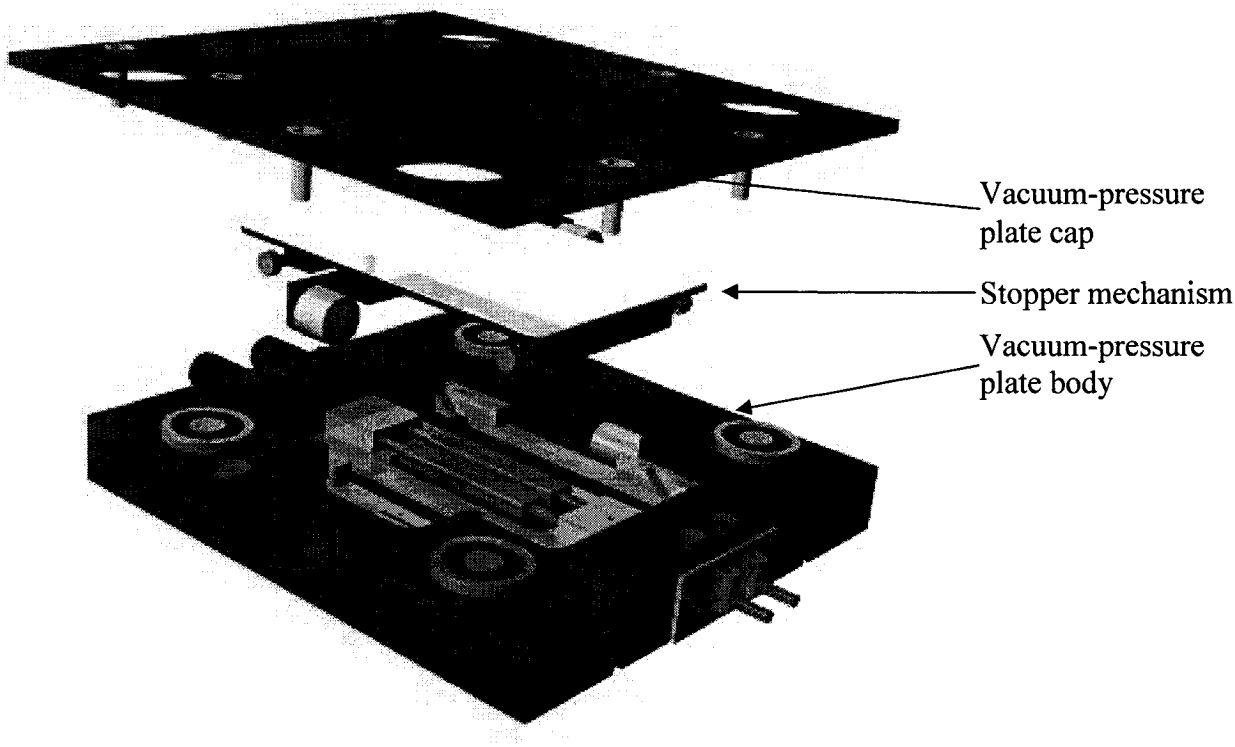

Figure 4.6: Illustration of the vacuum-pressure plate components. A recess holds all components for automated fluid handling with interfacing plates. A perimeter O-ring seals the recess against the interfacing vacuum-pressure cap, which has an array of O-rings on each surface for inter- and intra-plate sealing.

electromagnets. Otherwise, the plate body is composed of the standard core mechanism components.

For plate-to-cap sealing, an O-ring gland fitted with 1.6 mm diameter EPDM O-ring material surrounds the perimeter of the recess. Vacuum and pressurized air sources interface with the plate *via* two fluid line channels located in the wall of the recess terminated by miniature barbed fittings.

(2) Vacuum -pressure cap. A 96 processing channel array of 2 mm diameter through holes with corresponding inter- and intra-plate seals controls fluid flow between interfacing plates. The 2 mm diameter holes present a small cross-sectional area

to manage fluid movement and sealing with small, low surface area, O-rings that interface to the stopper mechanism. The O-ring glands located in the bottom surface face of the cap are fitted with size 004 EPDM O-rings. Standard O-rings are in corresponding locations on the top surface of the cap for inter-plate sealing against the channels of the filter plate.

(3) Stopper mechanism. Figure 4.7 illustrates the mechanism that controls fluid flow in the core mechanism. When actuated, the stopper mechanism operates as a valve for the 96 parallel processing channel; permitting the passage of fluid *via*

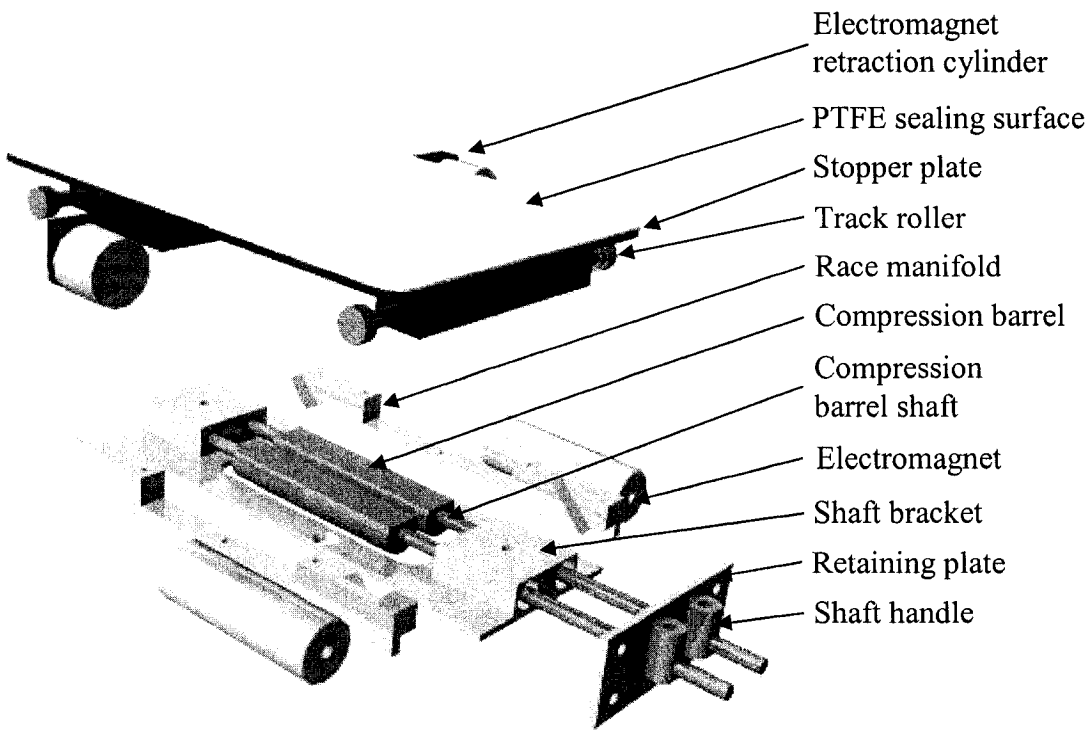

Figure 4.7: Illustration of the vacuum-pressure plate stopper plate mechanism components. Track rollers allow the stopper plate to ride on 45° races with equal vertical (compression) and horizontal (retraction) motion; to seal against the vacuum-pressure cap or permit the free passage of pressurized air. Two electromagnets act on the stopper plate retraction cylinders to provide the force for retraction. Two compression springs (not shown) force the stopper plate to move vertically on the races and seal against the vacuum-pressure cap. Manual rotation of the compression barrels produces the same sealing result.

vacuum or pressurized air. Otherwise, when not actuated, the mechanism seals against the bottom surface O-rings of the vacuum-pressure cap to create an array of independently sealed, parallel processing channels.

Two brackets hold miniature radial load track rollers that ride on a set of 45° linear races; that permit vertical motion for compression and horizontal motion for retraction. Another bracket holds two stainless steel cylinders that serve as the soft magnetic material [185, 187, 188] for electromagnetic retraction of the stopper plate along the races, which frees the flow of fluids through the vacuum-pressure plate cap. Otherwise, two stainless steel compression springs mounted on the bottom surface of the recess of the plate body supply the compressive force for sealing the 96 processing channels.

The compression lock provides an additional, manually operated, compressive sealing force for the stopper plate. Two independent compression barrels, with one flat side for clearance, fasten to miniature shafts. When rotated, using miniature brass handles, the round surfaces compress the stopper plate to seal it against the vacuum-pressure plate cap.

4.2.5 Retainer Plate

The retainer plate holds a 96 well microplate for capture and embedding of subcellular fraction samples. Figure 4.8 shows that it is an assembly of the retainer plate body and the retainer cap.

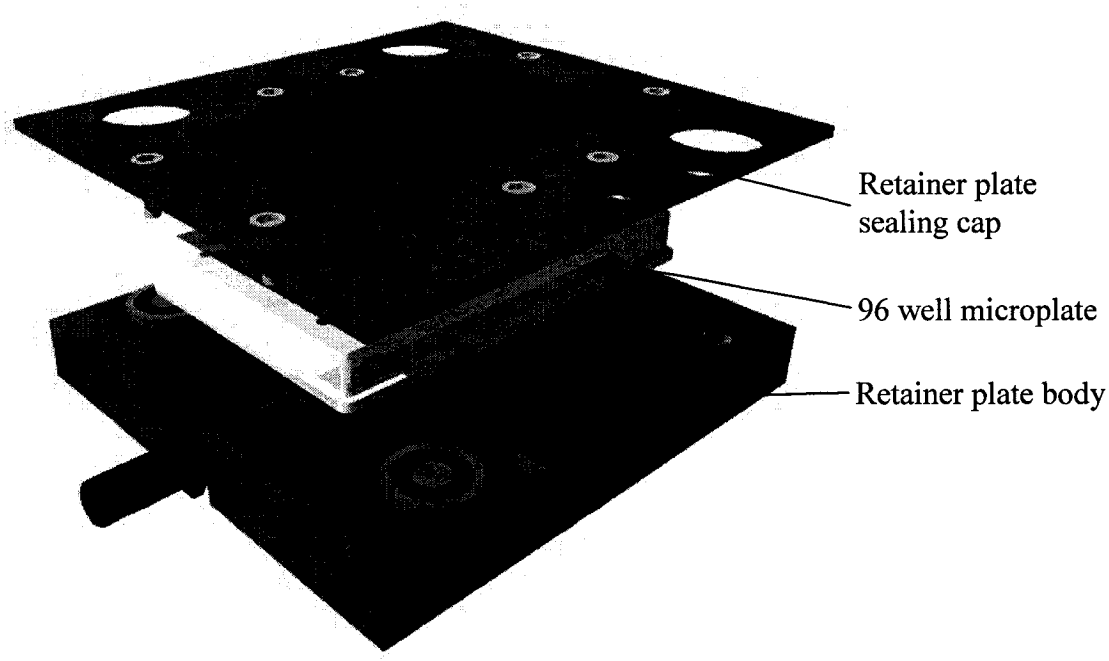

Figure 4.8: Illustration of the retainer plate components. An Epon loaded 96 well microplate is held within the recess and sealed at every well location by an EPDM gasket on the bottom of the retainer plate cap.

The body incorporates a rectangular recess to fit the microplate. Through holes are located in the four corners of the recess for removal of the microplate. Otherwise, the retainer plate body is equipped with standard core mechanism components.

A 1.6 mm thick EPDM gasket on the bottom surface of the sealing cap provides intra-plate sealing to the Epon-loaded wells of the microplate and the standard inter-plate sealing arrangement of O-rings is located on the top surface of the cap that interfaces with the filter plate.

4.2.6 Inter-plate Positioning

Figure 4.9 shows the method for plate assembly. Although the procedures for sample processing, delivery and embedding employ different plate configurations, the method of assembly utilizes the components described in this section and is identical in all cases.

The filter plate is located at the center of all plate configurations and contains all the plate interaction components. Eight high-power permanent magnets built into the filter plate create the compressive force for inter-plate static sealing. Corresponding electromagnets located in the other plates permit automated de-coupling (see Figure 4.17). Locating pins on the surfaces of the filter plate ensure internal alignment of the

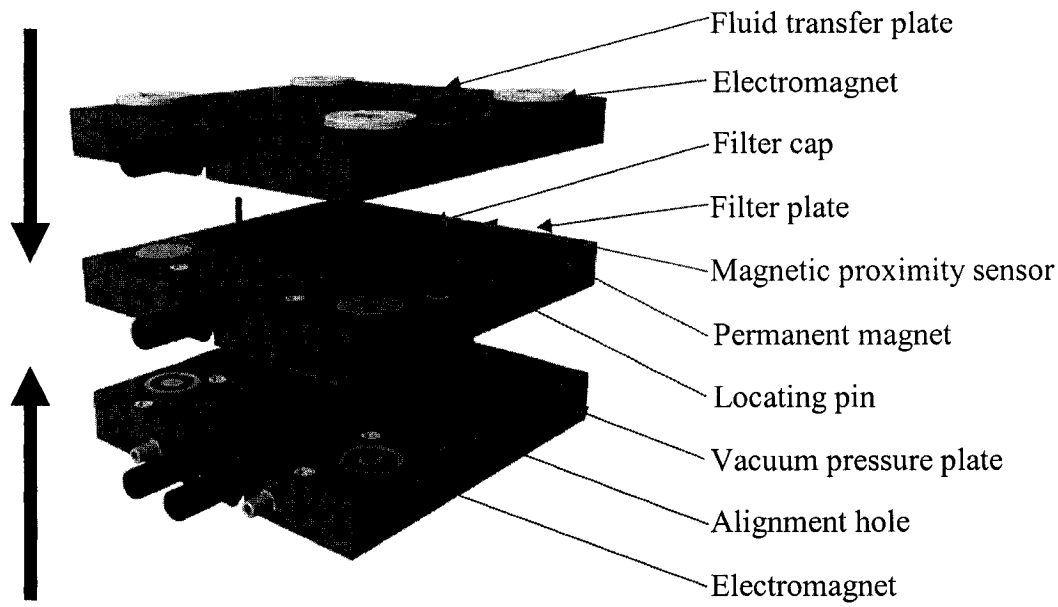

Figure 4.9: Illustration of the processing configuration showing the method of plate assembly for all core mechanism configurations. The centrally located filter plate contains all components for coupling, alignment and plate sensing. The large arrows on the left hand side show how other plates interface directly to either surface of the filter plate.

core mechanism *via* interaction with corresponding alignment apertures in other plates. In addition, magnetic proximity sensors embedded in the filter plate detect corresponding magnets in the other plates to signal plate alignment to the robot controller.

4.3 Cooling Subsystem

Figures 4.10 and 4.11 illustrate the layout of the cooling subsystem on the EMPOP robot, which maintains the operating temperature of the core mechanism at 4°C.

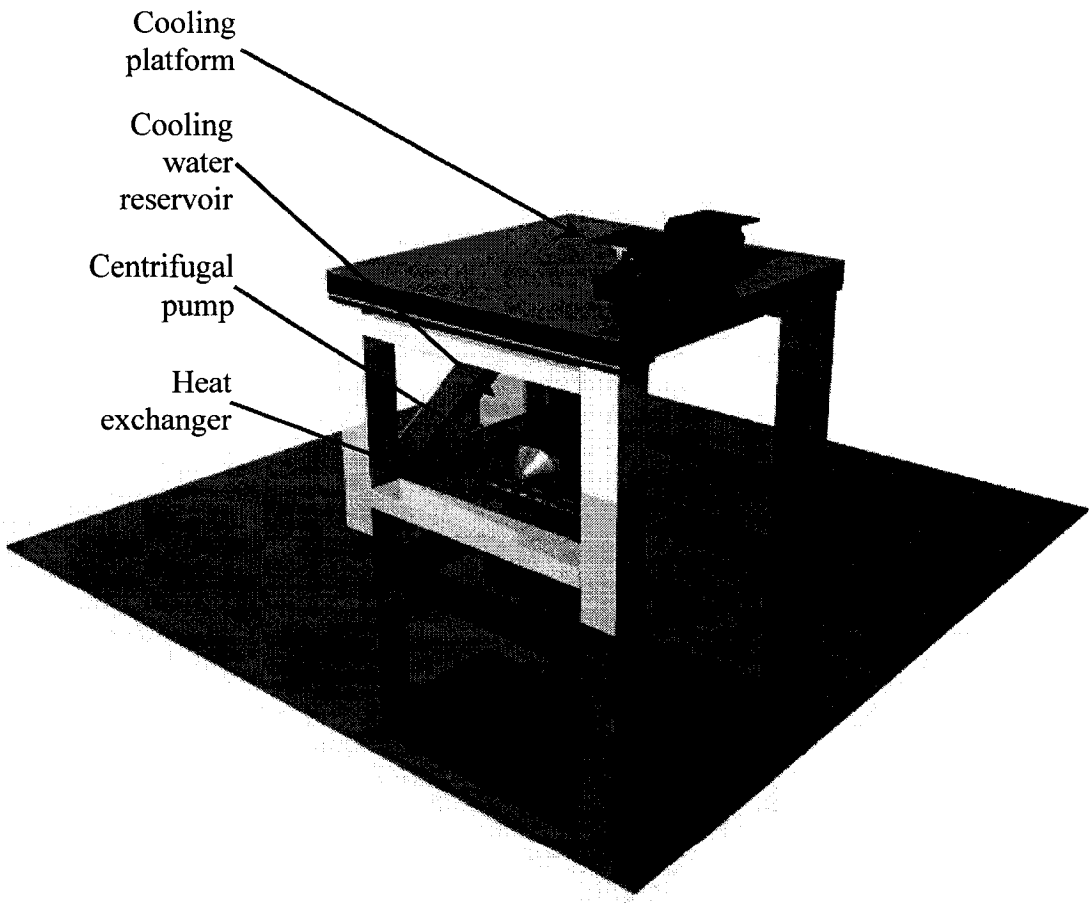

Figure 4.10: A front perspective rendering of the EMPOP robot showing the cooling platform subsystem layout.

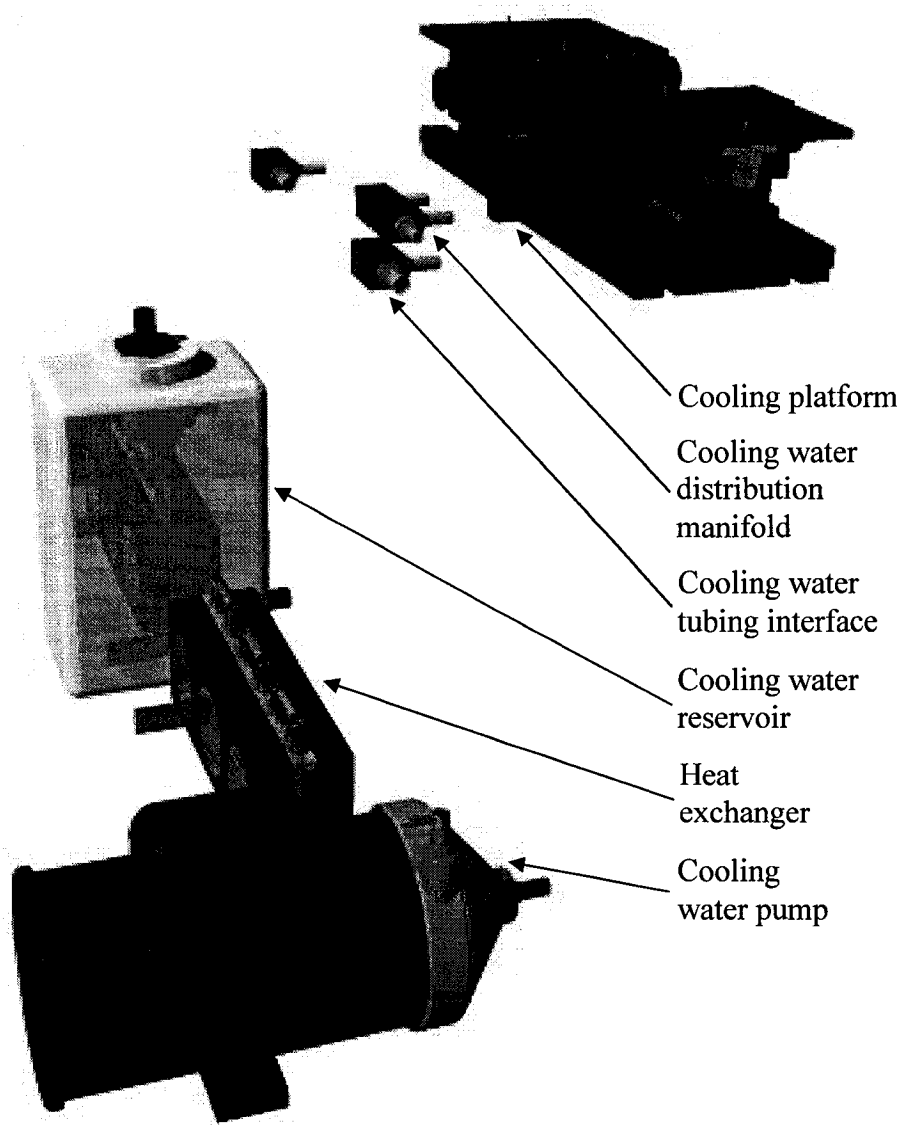

Figure 4.11: Illustration of the spatial arrangement of the subsections of the cooling platform subsystem. The cooling platform integrates with the core mechanism geometry for localized cooling and plate positioning. The cooling water recycling subsection continuously pumps water through the cooling platform to remove heat produced by operation of thermoelectric coolers. Cooling water is recycled through five components: (i) a reservoir with a top return and bottom outlet (ii) a centrifugal pump, (iii) tubing interfaces and a distribution manifold function to direct cooling water in and out of the cooling platform and immobilize fluid lines, and (iv) a heat exchanger assembly composed of a bank of three, 4-pass, compact, finned, aluminum radiators fitted with six high-velocity fans.

The central assembly of the subsystem, the cooling platform, interfaces to the core mechanism geometry for localized cooling as well as plate positioning and stabilization for reconfiguration of the core mechanism.

Cooling takes place only within the center of the platform assembly, where thermoelectric coolers (TECs) [206, 208] are located within the three surfaces facing the core mechanism. Liquid cooling blocks secure and compress the TECs against the inner walls of the platform cooling surfaces. Water circulates continuously through the subsystem within a serial loop of cooling blocks and heat exchangers to maintain the thermal gradient produced by the TECs [206, 208, 209].

The cooling platform is also equipped with mechanisms for retraction and compression of the vertical cooling faces to interact with the electromagnetic arm for plate positioning and interchange. Retraction, achieved by linear pull-type solenoid actuators [175, 197], provides clearance for positioning the core mechanism within the cooling platform. Compression of the vertical cooling faces, produced by miniature gas springs, ensures direct contact with the core mechanism for efficient conductive heat transfer [212, 217-220].

Figure 4.12 shows the three subsections of the cooling subsystem: (1) two side platforms, each providing a vertical cooling surface as well as positioning components for cooling surfaces and plates, (2) a central base, providing a cooling surface and electromagnets for stabilization of the core mechanism, and (3) a stabilizing platform.

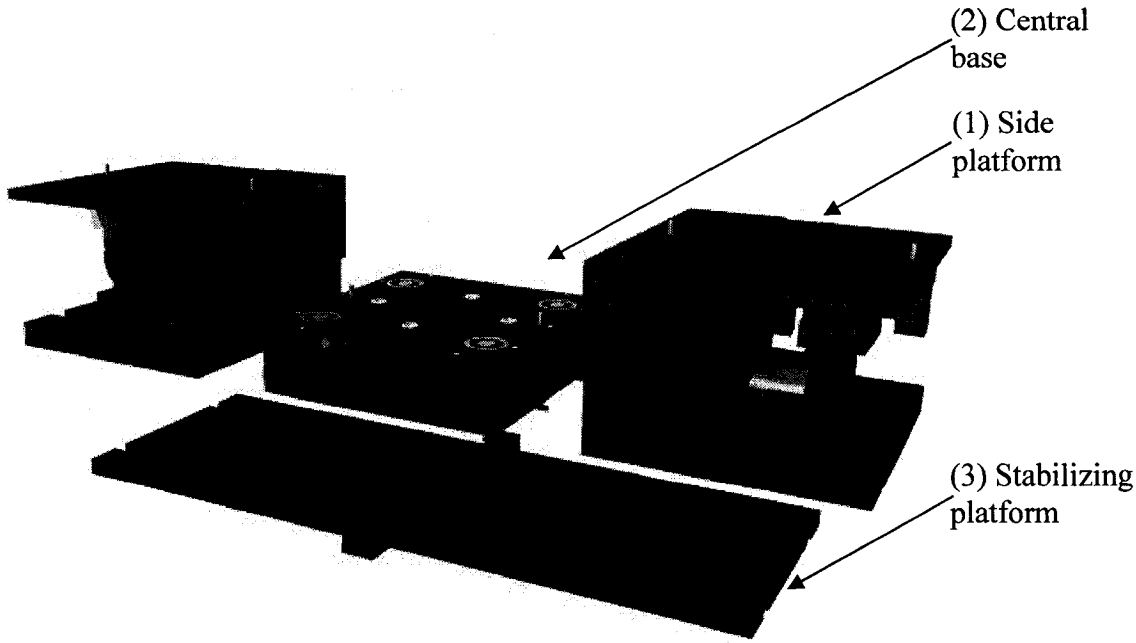

Figure 4.12: Illustration of the cooling platform modules. The central base floor and side platform walls are the cooling surfaces. The central base holds the core mechanism throughout processing and the side platforms retract to provide clearance for plate manipulation and compress against the core mechanism for effective heat transfer. The side platforms also hold plates for retrieval or placement by the electromagnetic transfer arm. The stabilizing platform provides a surface for interconnection of the modules and a means to fasten the entire assembly to the antivibrational table.

(1) The side platforms, illustrated in Figure 4.13, are identical and provide stabilization, positioning and cooling by way of six principle components or sub-assemblies:

(i) Mounting base. This sub-assembly stabilizes the side platform to the antivibrational table and holds the positioning components for retraction and compression of the side platform. Two miniature linear slides carry the side platform; actuating a manifold of tubular pull-type linear solenoids retracts it

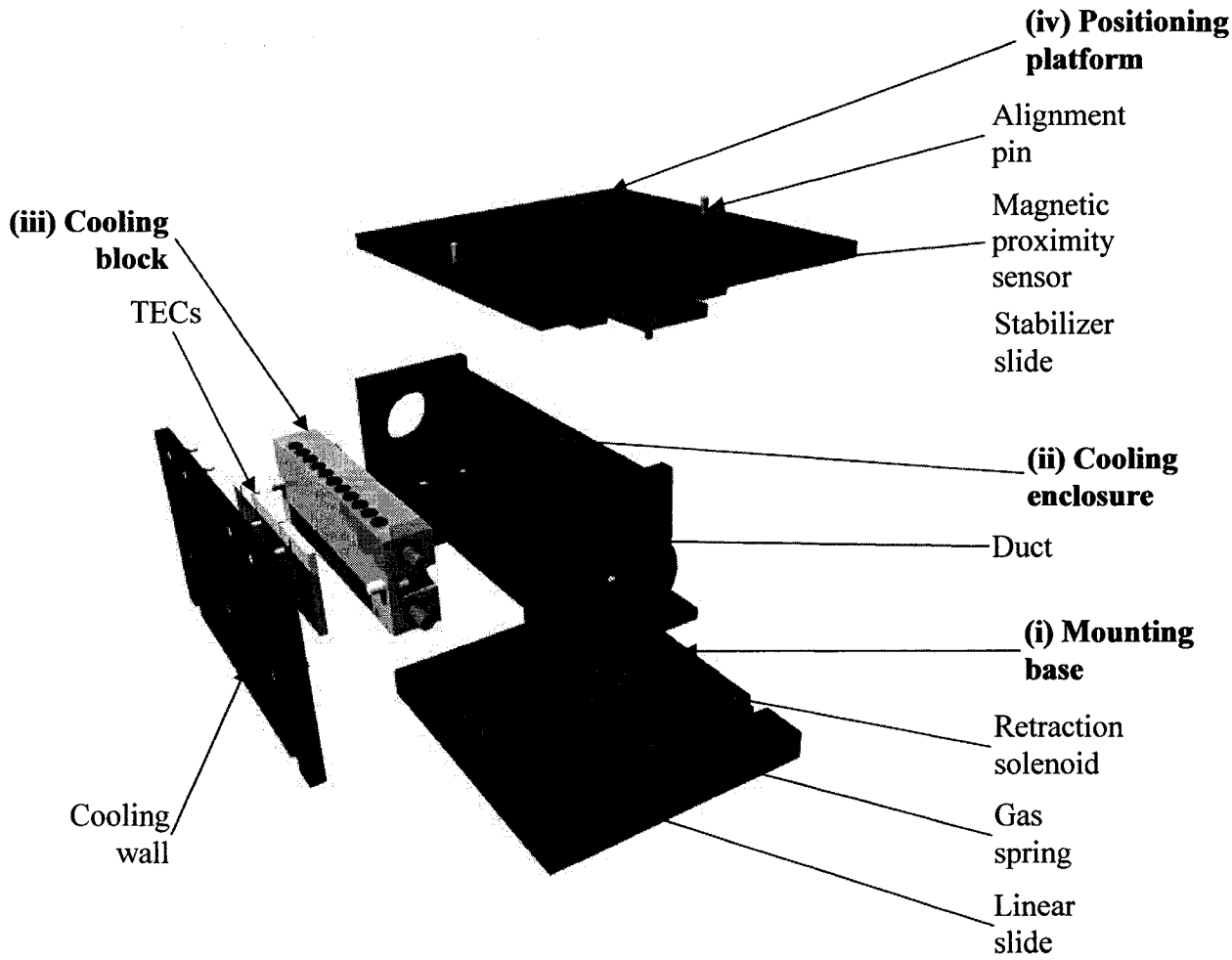

Figure 4.13: Illustration of the cooling platform side platform components. The cooling enclosure holds three 40 mm x 40 mm TECs with a maximum heat pumping capacity (Q_{max}) under maximum current (I_{max} = 6A) and voltage (V_{max} = 15.4V) of 51.4 W; totaling ~150 W of cooling power under efficient operating conditions. The power to the modules is also converted to heat ($Q_{power} = I_{max}V_{max} \sim 60W$); totaling ~180 W that must be removed with the pumped heat ($Q_{Total} = Q_{max} + Q_{power} \sim 330$ W) to maintain the thermal gradient of the TEC.

The side platform rides on two miniature, 1 in. stroke, linear ball slides for retraction *via* a manifold of two continuous duty, 25 mm pull stroke, 7.25 N, linear solenoids and compression by two 25 mm push stroke, 2.25 N, micro-compression gas springs. The solenoid plungers and gas spring shafts fasten to the cooling wall to pull or push the assembly. The side platform structure is supported further for motion a linear slide and rail, which is mounted on the bottom of the positioning platform.

to the clearance position; otherwise it is maintained in the cooling position by the force from a manifold of micro compression gas springs. The mounting base also has a set of step-tapered alignment apertures the serves as coupling locations to the central base of the cooling platform.

(ii) Cooling enclosure. The enclosure is composed of four interconnected faces (side, bottom, two ends and the cooling wall). It holds three 40 mm square TECs and a cooling block (see below) that are fastened against the inner surface of the cooling wall. It provides the surface for heat exchange between the TECs and the core mechanism. Temperature sensors and couplings for the retraction and compression motion components are mounted in the cooling walls.

(iii) Side platform cooling block. Figure 4.14 illustrates the large internal surface area provided by the cooling blocks for heat transfer from the hot faces of the TECs to the cooling water, which passes through multiple channels along the length and width of the block.

(iv) Positioning platform. This sub-assembly is used to store plate not used in the current core mechanism configuration. The surface geometry and positioning mechanisms match those of the core mechanism. Alignment pins locate plates *via* the core mechanism plate-to-plate alignment apertures and the plate-to-plate proximity magnets actuate the magnetic proximity sensor to signal plate presence to the robot controller. This sub-assembly completes the structure of the side platform.

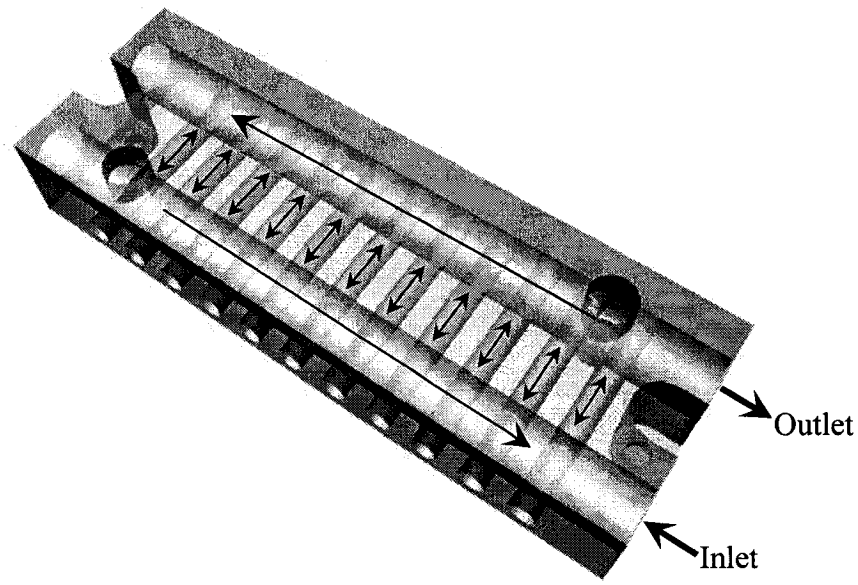

Figure 4.14: Illustration of a cooling platform side platform cooling block and flow through the cooling water channels. Cooling water flows through multiple channels to provide a high surface area for heat transfer and flow communication across the heat sinking surface; two large diameter, inlet and outlet channels (d_l = 10 mm) as well as 11 small diameter (d_s = 10 mm) channels. Combined with the high flow rate of cooling water (~ 10 L/min), the high thermal conductivities of the aluminum block ($k_{Al\ alloy\ 6061,\ 25°C}$ ~ 170 W/m°C) and cooling water ($k_{H2O,\ 25°C}$ ~ 0.606 W/m°C) produce a low thermal resistance (θ_s ~ 0.001 to 0.01 °C/W) for efficient heat sinking [211, 217-220].

(2) Figure 4.15 shows the central base, composed of three principle sub-assemblies to cool and stabilize the core mechanism.

(i) Cooling enclosure. The enclosure is comprised of five interconnected faces that accommodate a bank of five 25 mm square TECs and a cooling block (see below). All faces are interconnected and the bottom face has two sets of alignment pins located on the side edges for immobilization of the two side platforms.

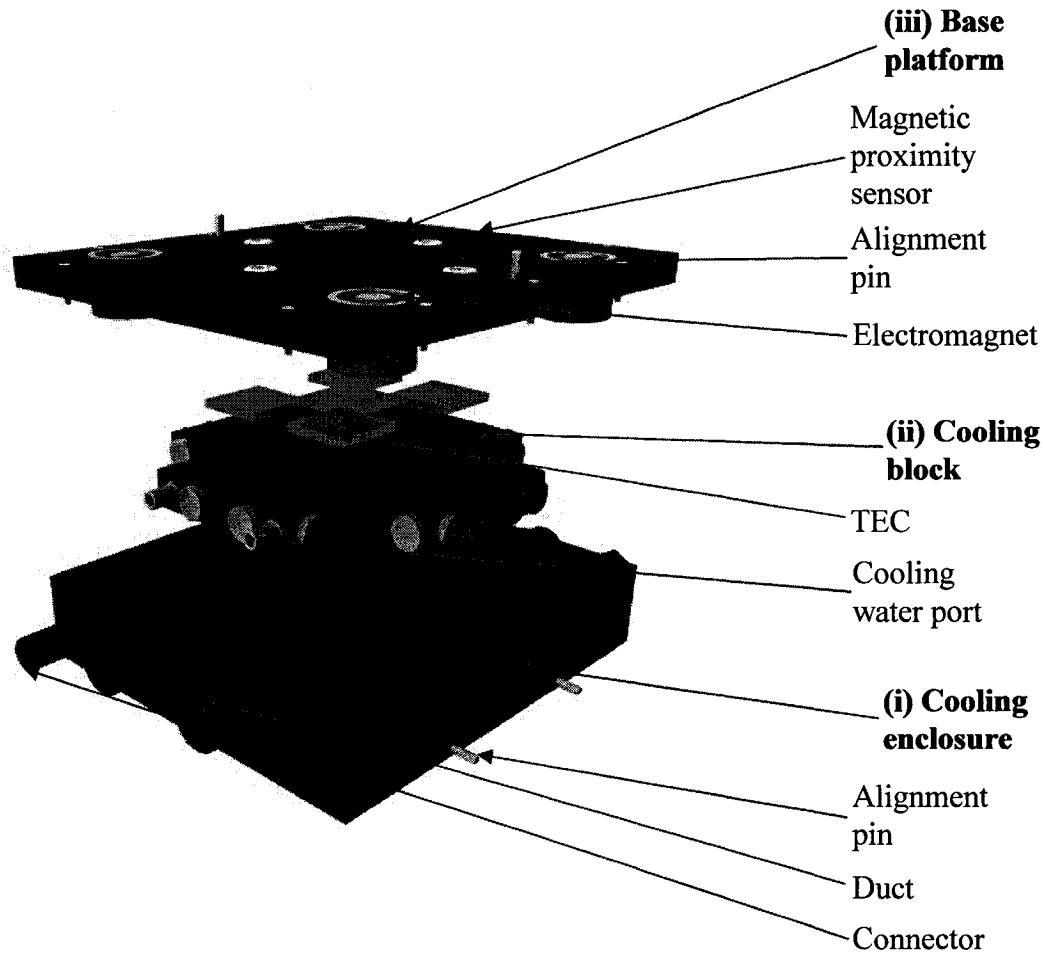

Figure 4.15: Illustration of the cooling platform central base components. The cooling enclosure holds five 25 mm x 25 mm TECs with the following specifications: Q_{max} = 33.4, I_{max} = 3.9A, V_{max} = 15.4V. To maintain the thermal gradient of the TECs, ~ 460 W of heat (Q_{Total}) must be removed.

The central base is also equipped with four surface-contact, round, island-pole electromagnets to supply a counter-force during plate decoupling steps. The electromagnets secure the core mechanism to base platform while the electromagnetic transfer arm removes the top, decoupled plate.

(ii) Central base cooling block. Figure 4.16 illustrates the cooling block and the paths for cooling water. It supports the TEC heat transfer requirements in the same manner as that for the side platforms.

(iii)Base platform. Identical to the structure of the side platforms, the surface geometry and positioning mechanisms of the sub-assembly match those of the

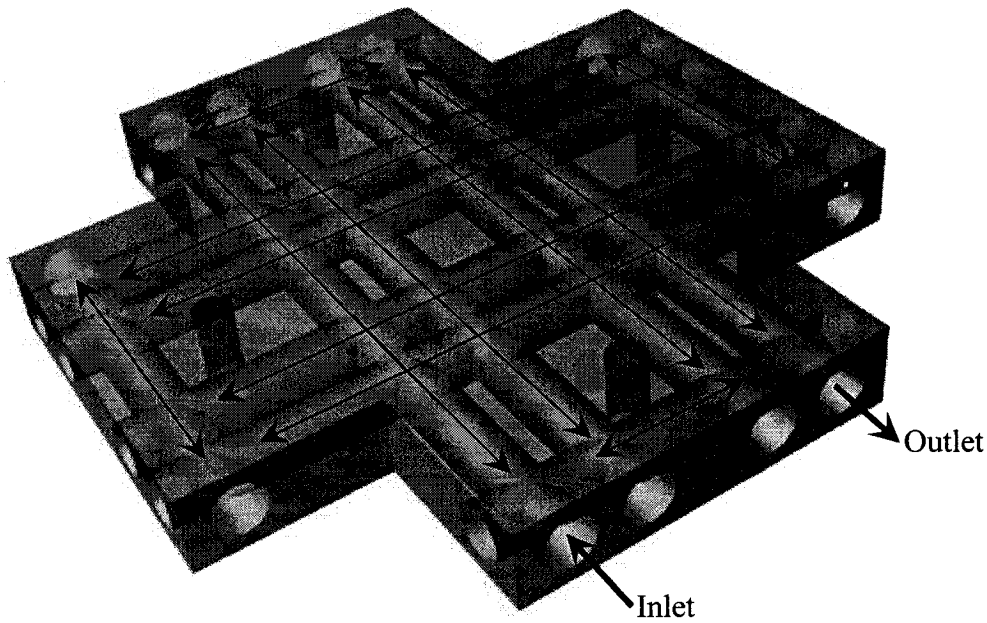

Figure 4.16: Illustration of the cooling platform central base cooling block and flow through the cooling water channels. Cooling water flows through a network of uniform diameter channels (10 mm) that provide a high surface area for heat transfer and flow communication across the heat sinking surface.

core mechanism core mechanism for plate alignment and sensing. The base platform is also equipped with four surface-contact, round electromagnets that stabilize the core mechanism during plate interchange; these immobilize the bottom surface of the core mechanism while top plates are decoupled and coupled during reconfiguration of the core mechanism (see Figure 4.17).

(3) The stabilizing platform assembly is the common coupling interface between the side platforms/central base assembly and the antivibrational table.

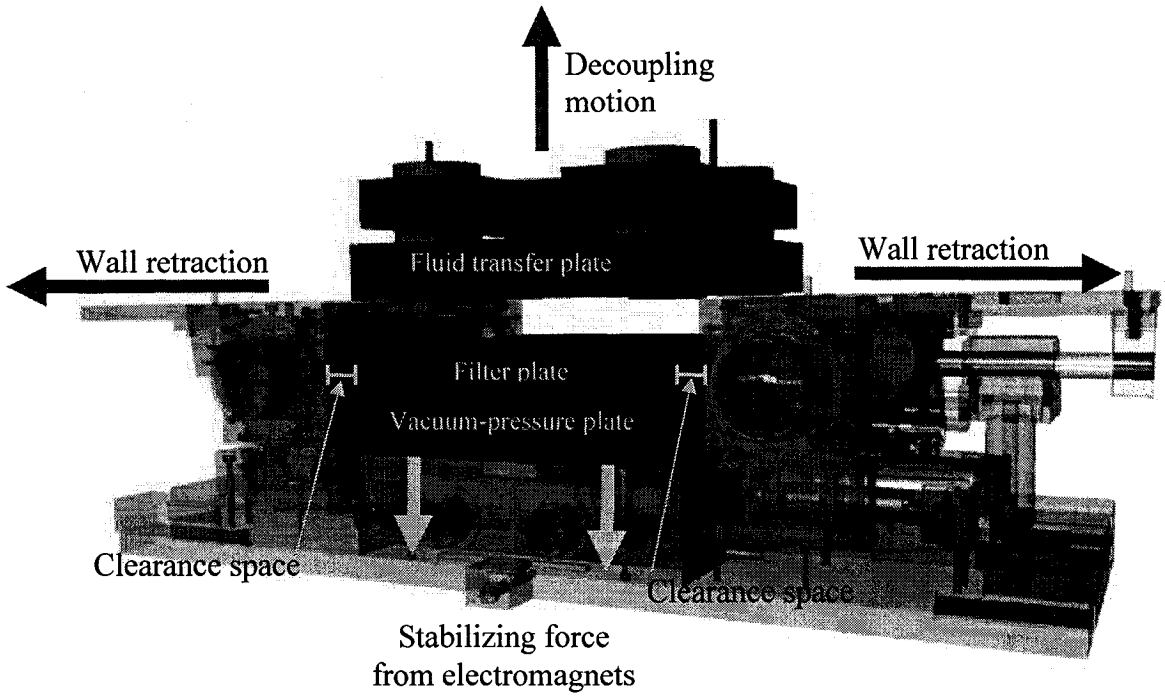

Figure 4.17: Illustration of the cooling platform during plate decoupling. The walls of the cooling platform retract for clearance. The cooling platform stabilization electromagnets secure the remaining plates of the core mechanism to the central base of the cooling platform. Horizontal bars indicate clearance spaces and the arrows indicate the directions of motion.

4.3.1 Thermoelectric Cooling

Although a vapor-compression refrigeration system (composed of a compressor, evaporator and a condenser) [210, 216] has a competitive advantage over TECs for high-power cooling (>200 W), [207, 209] this approach was not used here. The use of a TEC system permits electronic regulation high-power density cooling in a localized and narrow zone around the core mechanism (see Figure 4.18).

Due to their small size, low weight and reliability, TECs provide a means for customized cooling solutions in prototype instrumentation. Accordingly, three factors determined the thermoelectric cooling approach: (1) space limitations within the compact

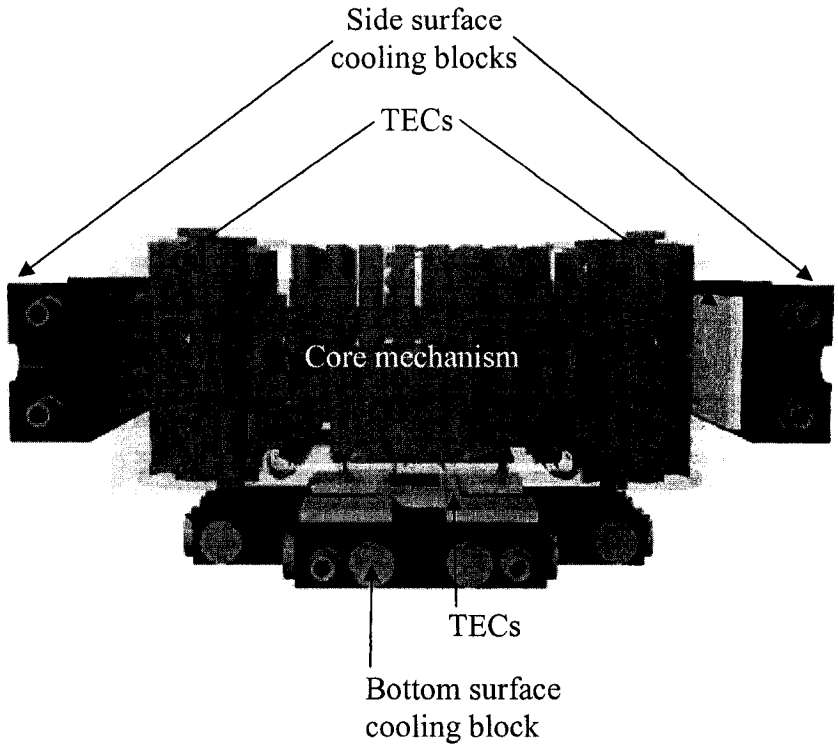

Figure 4.18: A 3D CAD rendering illustrating the arrangement of TEC/cooling block modules that produce the thermal gradient to cool the core mechanism. The thermal gradient that cools the core mechanism (semi-transparent rendering) is produced by TECs situated with their cold surfaces facing the core mechanism and their hot surfaces facing the cooling blocks. The TEC/cooling block module located against the bottom surface is hidden in this illustration.

Compared to a vapor-compression refrigeration system, in a TEC system, a semiconductor material replaces a liquid refrigerant, a heat sink replaces a condenser, and a DC power source replaces a compressor. Based upon the Peltier effect [206] (current passing through two different conductors produces a temperature change), application of DC power to a thermoelectric module causes electrons to move through the semiconductor material from high (n-type) to low (p-type) energy level elements [206, 208]. The electron movement on one face absorbs heat (the cold face) and expels it on the hot face. The level of heat absorption is proportional to the number of thermoelectric couples and the current applied.

cooling platform structure, (2) the motion requirements of the side platform walls, and (3) the remote and confined location of the platform on the robot.

To satisfy the steady state cooling requirement of maintaining the temperature at 4°C, the system was designed for worst-case conditions of ambient environment (25°C)

and heat load; the latter specified according to the maximum power input to the TECs (the product of maximum current and voltage, $I_{max}V_{max}$). Although it is possible to use many TECs to force the temperature down, the power applied to drive the TECs converts to heat ($Q_{power} = I_{max}V_{max}$) that must be removed [209, 214]. Therefore, to maintain the compact geometry of the platform and avoid the need for a large heat sink system, a practical limit for the number of TECs (see Figures 4.13 and 4.15) was determined by the layout of the platform. Furthermore, under worst-case heat load conditions, heat sinking and discharge must be efficient enough to permit all TECs to operate with a low difference between cold face (T_c) and hot face (T_h) temperatures (dT) and consequently, operate near their maximum heat pumping capacity (Q_{max}) [206, 208]. The total heat generated at a TEC hot face (Q_{Total}) is then the sum of the two contributions ($Q_{Total} = Q_{power} + Q_{max}$).

Thermal management of the TEC hot face is the absolute determinant parameter of its application [206, 208, 209, 214]. Due to their high thermal resistance (θ_s), natural convection or forced air heat sinking methods could not remove enough heat from the system to maintain the thermal gradient needed for 4°C steady state cooling [211]. Inadequate heat sinking diminishes the rate of TEC heat pumping as the maximum dT is approached [206, 208]. Moreover, these methods negate the gradient produced by the TECs, because they discharge heat locally.

The indirect liquid cooling method of the platform circumvents these issues by utilizing the high thermal conductivity of water flowing through the cooling block intermediate to heat sinking structures [173, 211]. Heat pumped by the TECs transfers to the cooling blocks by conduction and to the pumped water by forced convection. The

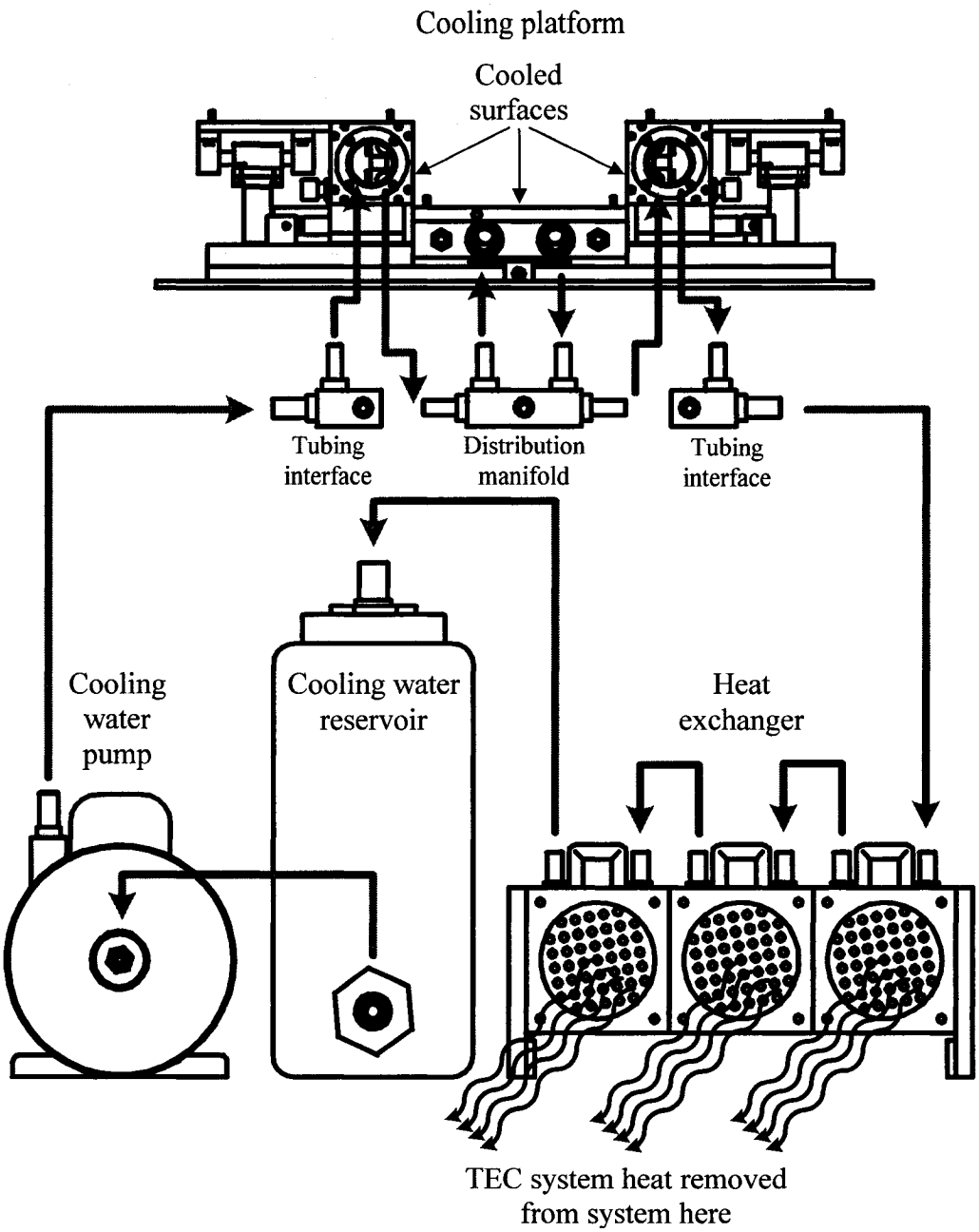

Figure 4.19: Schematic illustration of the cooling water recycling flow path. Water is pumped from the reservoir *via* a centrifugal pump [227, 228]; to provide adequate power to compensate for the pressure drop through the system as well as provide a turbulent flow rate within the cooling blocks (~ 10 L/min, Re > 2300, see Figures 4.14 and 4.16). The high flow rate removes heat quickly, while the turbulence decreases the fluid/thermal boundary layer [211] and eliminates stagnation in the cooling blocks [211, 217-220]. Circulating water continuously returns *via* the top of the reservoir and is pumped from the bottom. In addition to providing a large volume of water for cooling, the reservoir provides a location of thermal expansion of the liquid as well as a means to remove air for more effective heat transfer [212] and to avoid damage to the pump by cavitation [227, 228].

high efficiency of heat sinking minimizes the dT, permitting the TECs to approach their Q_{max}. Figure 4.19 illustrates how, downstream of the cooling blocks, forced air convection is used to discharge heat from the water *via* the bank of three fan equipped, finned heat exchangers [213]; each rated to discharge ~ 500 W of heat [213].

Because there is no active heat load (i.e. no heat generated by the core mechanism) and no insulation surrounding the platform and core mechanism, all heat loads are passive (i.e. parasitic loads). However, Teflon gaskets insulate the cooling surfaces from the remainder of the platform. Therefore, convection from exposed surfaces to ambient air is the predominate parasitic load [211, 212]. Convective heat loss is estimated *via* Newton's law of cooling [212, 217-220],

$$Q = hA\Delta T. \tag{4.1}$$

Where,

Q is the heat transferred to or from ambient air,

h is the convection heat transfer coefficient ($h_{Air,\ 25°C} \sim 21.7$ W/m^2°C) [211, 212],

A is the exposed surface area of all plates and cooling surfaces (0.24 m^2) [171], and

ΔT is the difference between ambient air (25 °C) and the exposed surface (4 °C).

Although determination of the total passive heat load is complicated, the worst case estimate above results in Q ~ 110 W, which is much less than the quantity of heat the TECs can pump (~ 475 W, see Figures 4.13 and 4.15) under worst case, steady state cooling conditions and conservative levels of TEC and heat sinking performance.

4.4 Fluid Handling Support Subsystems

Successful sample processing on the EMPOP relies on coordinated fluid handling for sample filtration, reagent dispensing and aspiration, needle cleaning, waste removal, and sample delivery. For effective completion of these tasks, three fluid handling support subsystems, illustrated in Figure 4.20, provide controlled fluid handling for: (1) processing reagent handling, (2) pneumatics and (3) cleaning and waste management.

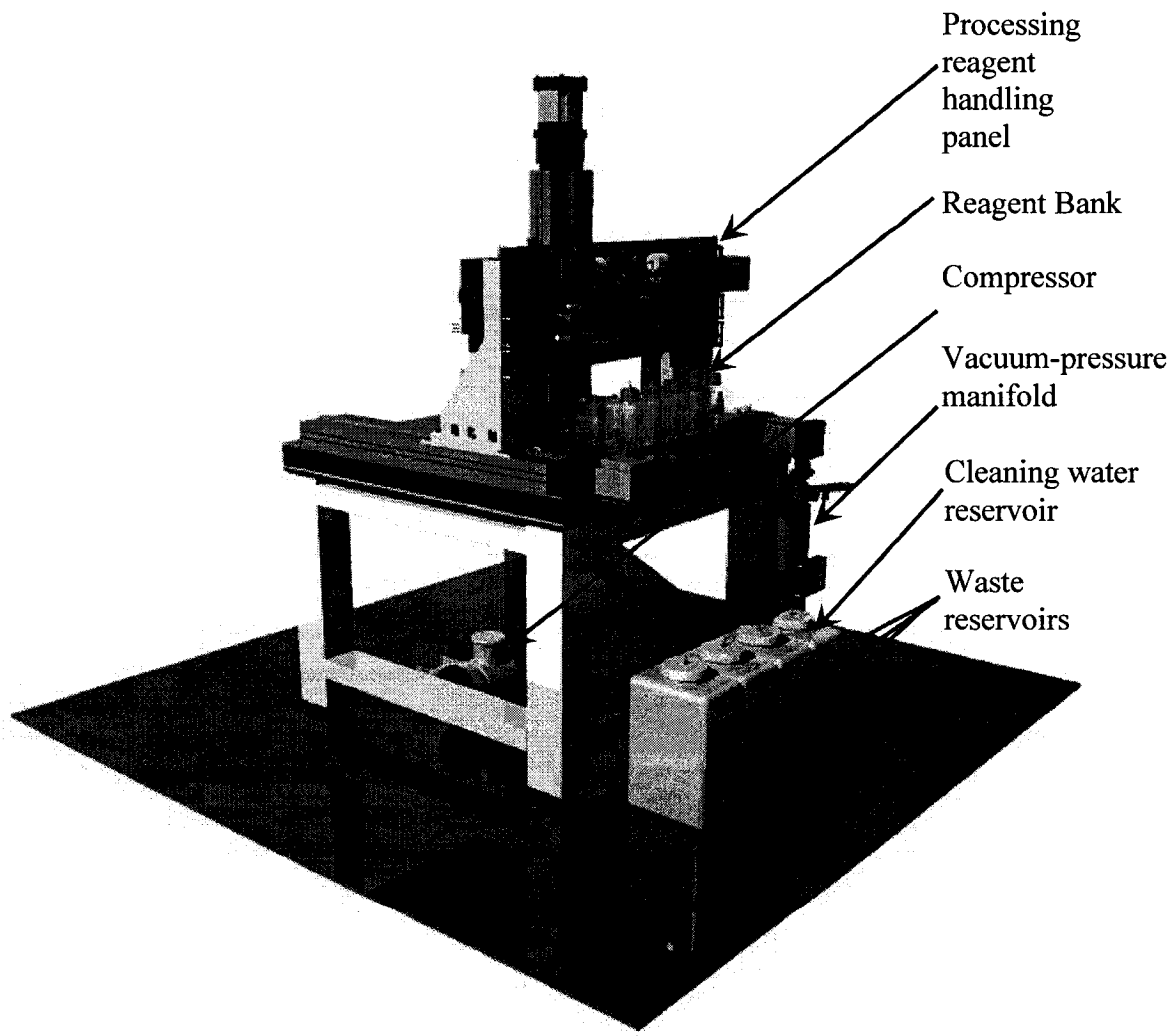

Figures 4.20: A rear perspective rendering of the EMPOP robot illustrating the fluids handling subsystems layout.

4.4.1 Processing Reagent Handling Subsystem

The processing reagent handling subsystem provides for the pumping, mixing and dispensing of all reagents to the processing channels of the core mechanism. Successful automatic sample processing requires a liquid handling arrangement that delivers microliter-range volumes of specific reagents (or mixtures) and provides flexible flow control to develop protocols and maintain the structural integrity of the samples. Development of the subsystem followed five general criteria to meet these requirements:

(1) Volume minimization. To handle small liquid volumes efficiently, the subsystem employs only miniaturized components.

(2) Full automation. To support operator-defined liquid handling requirements for dispense sequence, volume and velocity; all actuated components are modular and addressable to control the flow of individual reagents.

(3) Chemical compatibility. To eliminate component failure due to reaction of materials with reagents, the subsystem employed only materials compatible with all processing reagents for the wetted parts of subcomponent.

(4) Mechanical compatibility. To avoid loss of dispensing efficiency due to large pressure differentials, all subsystem components operate with a similar cross sectional area for flow. Also, to avoid sample disruption, the subsystem utilized components specified to impose minimal mechanical perturbations on the processing samples.

(5) Integration. To localize reagent handling as near as possible to the processing samples, reduce reagent consumption and consolidate occupied space, the subsections are integrated with the motion control subsystem.

Reagent dispensing to the processing channels of the core mechanism follows a flow path that leads through three subsections:

(1) Reagent bank. Figure 4.21 shows the 17 reservoirs located in a rack. Three reservoir sizes (100, 250 and 500 ml) provide flexibility for the choice of reagent volumes used in processing as well as a standard locations for those reagents used in the standard protocols supported by the robot. Miniature fittings, tubing and a vent modify the cap of each reservoir for reliable pumping and interconnection to flow control valves.

(2) Reagent handling panel. Figure 4.22 shows the panel of automated liquid handling components that is the interface controlling reagent flow from the 17 reservoirs to two output fluid lines that lead to a set of dispensing needle manifolds. The panel fastens to the Y-axis of the motion control sub-system and consolidates reagent flow control to a system of four symmetrically organized component groups:

(i) Solenoid valves interfaced with directional manifolds. Figure 4.23 illustrates the valve arrangements used to access individual reagents (from their respective reservoirs) and divert them to one of the panel pumps *via* a single

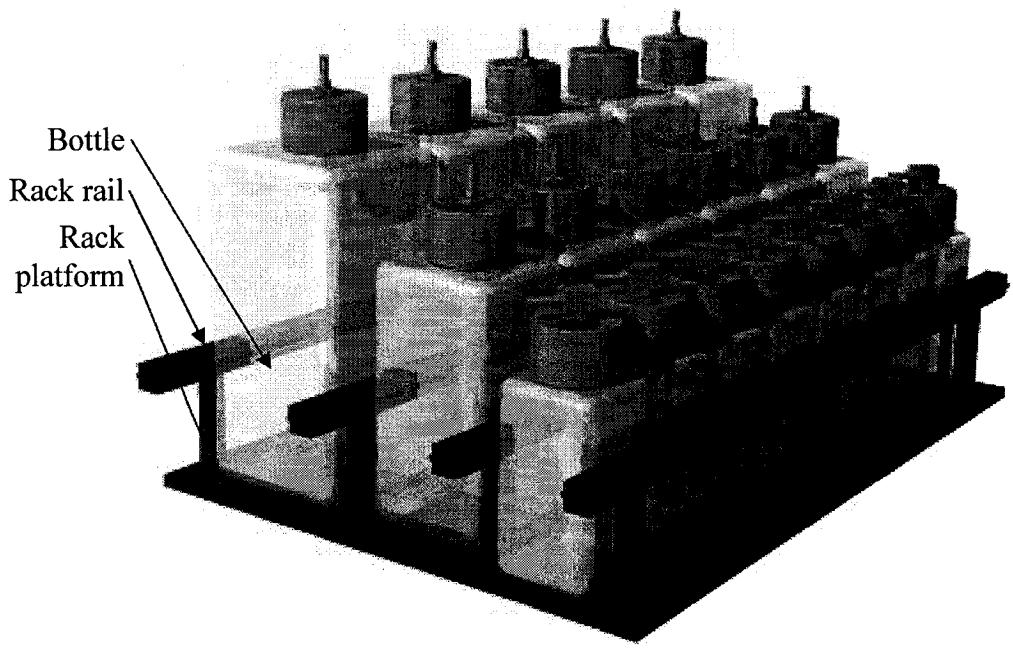

Figure 4.21: Illustration of the processing reagent handling system reagent bank. The racks is composed of a platform and four rails, which each stand on three spacer rods, and are fit with vibration-damping, square-ring material on the bottle-contacting surfaces. The rack provides adequate space for 17 Pyrex square bottles (500 ml, 250 ml and 100 ml). The caps of all bottles were modified with a miniature bulkhead fitting with corresponding barbed fittings for 1/16 in. I.D. PTFE tubing on the inside and outside surfaces of the cap. Tubing was installed on the inside faces of the caps to reach the bottom surfaces of the bottles. For pressure relief, a 1.5 mm diameter vent passes through the surface of each cap.

fluid line. The arrangements consist of six, miniature, 2-way, normally-closed, solenoid valves [224-226] that serve as automated gates to the corresponding ports of the 6-inlet/single outlet directional manifolds. Directional manifold 3 supports six fluid lines (for dehydration and embedding reagents). Directional manifolds 1 and 2 interface to create one outlet port that supports 11 fluid lines (for water and chemical processing reagents). Directional manifold 4 serves as the interface to direct flow from

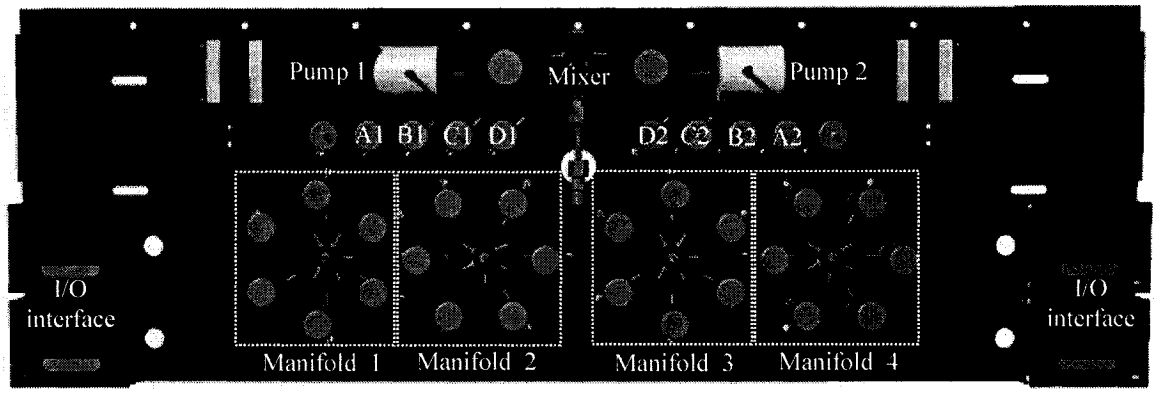

Figure 4.22: Illustration of the processing reagent handling subsystem reagent handling panel. The organization three fluidic subassemblies is indicated by (1) the dashed-line boxes indicating the four directional manifolds, (2) the two variable volume stepper pumps and their associated support valves (A_n, B_n, C_n and D_n), and (3) the mixer, which is located to interface with the output of both pumps. The I/O interfaces consolidate all component wires and cables in four screw terminals, which are connected to the robot control electronics with four corresponding cables.

the panel to the dispense needle manifolds, located on the θ-axis of the motion control subsystem

(ii) Stepper pumps. Figure 4.24 illustrate the pumping arrangements that interface the directional manifolds. The panel holds two variable-volume stepper pumps, which each using a bank of three 2- and one 3-way, normally-closed solenoid valves to coordinate pump aspiration (from directional manifolds 1 and 3) and dispense cycles as well as divert pumped reagents directly to directional manifold 4 or by way of the mixer. The stepper pumps (positive displacement piston pumps) are self-priming [227-229] and, with interfacing inlet and outlet valves, they move relatively large volumes (2650 μl/stroke) quickly and efficiently. Additionally, the level of automated control (the pumps are controlled as virtual axes by the robot controller, see

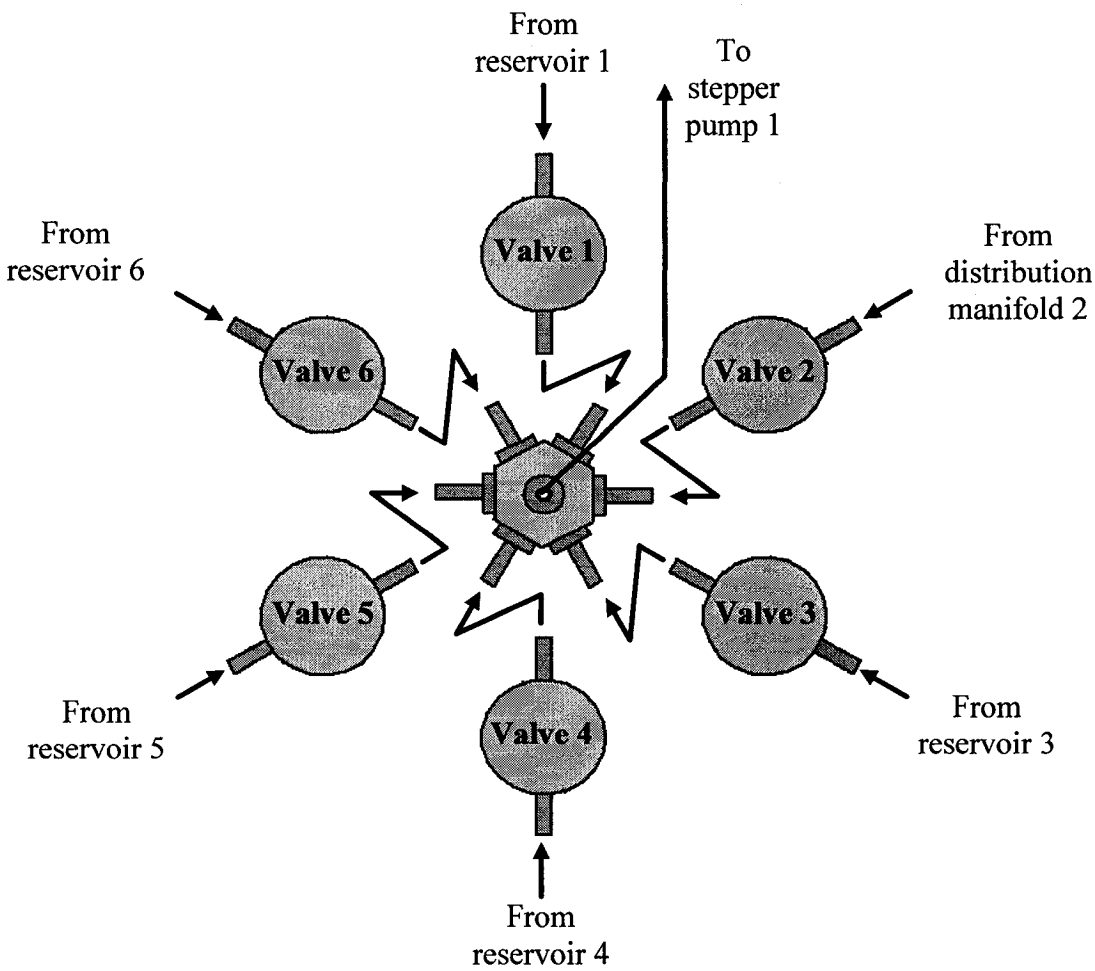

Figure 4.23: The liquid handling components are arranged such that three, 6-inlet directional manifolds are each interfaced with six miniature, 2-way, normally-closed, direct-acting solenoid valves (PTFE and EPDM wetted parts) fit with miniature barbed fittings for 1/16 in. I.D. PTFE tubing; each serving to isolate a particular reagent reservoir and, upon actuation, allow free passage of liquid to the pump. A set of 2-way solenoid valves are arranged with directional manifold 4 to direct pumped processing reagents to the reagent dispensing needle manifolds, located on the θ-axis of the motion control system.

Section 5.6.1) permits reliable and quantitative dispensing of reagents through the network of valves and tubing to the individual processing channels of the core mechanism.

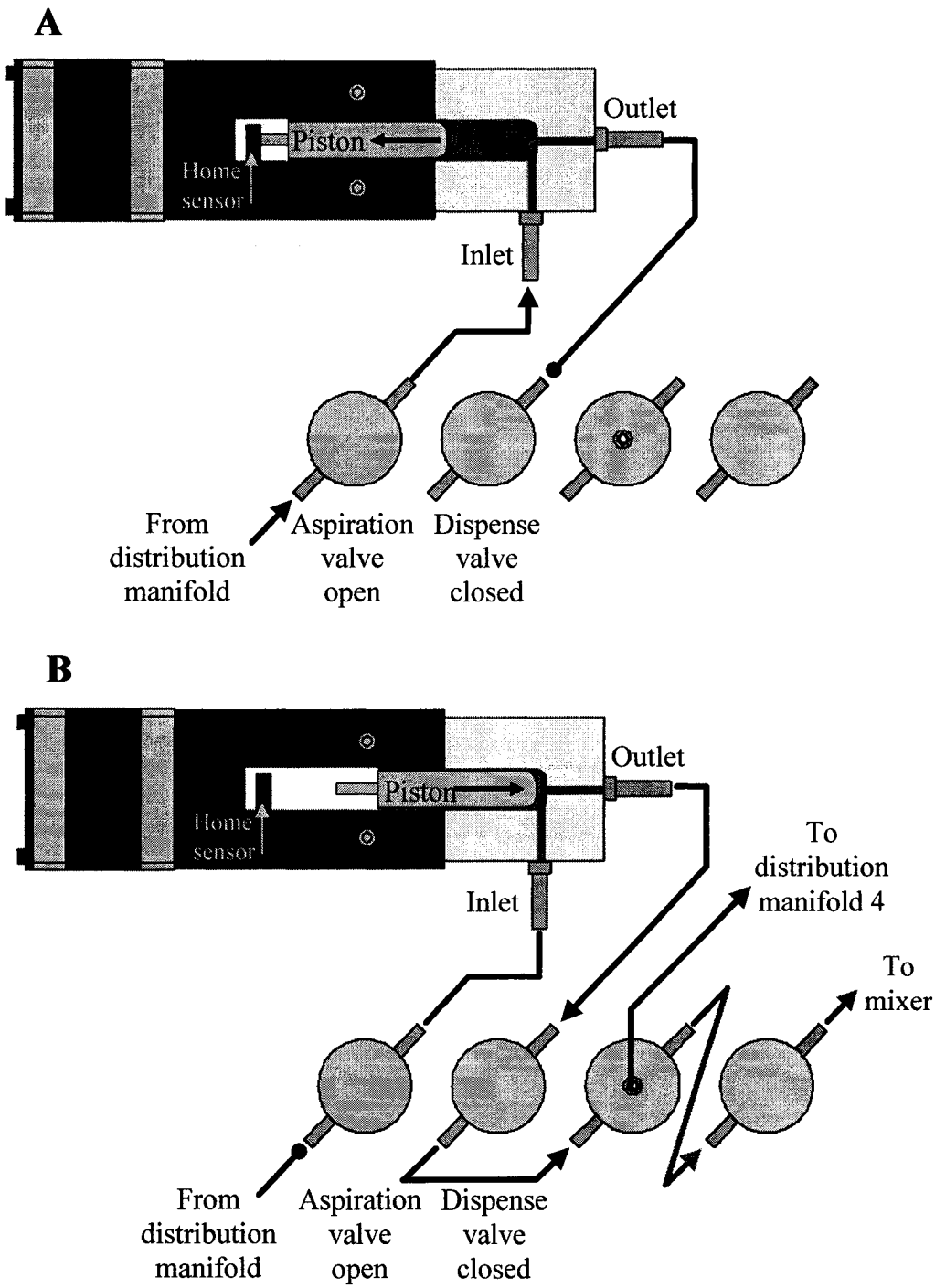

Figure 4.24: Schematic illustration of pump operations for reagent (A) aspiration and (B) dispensing. The outlet ports from directional manifolds 1 and 3 are interfaced with two corresponding 2650 µl stroke, variable volume stepper pumps (PEEK, Zirconia and polyethylene wetted parts) by way of a two banks of three 2- and one 3-way, direct-acting solenoid valves. All components are fit with miniature barbed fittings for 1/16 in. I.D. PTFE tubing.

The 2-way valves serve as gates to the inlet and outlet ports of a pump [229]. Figure 4.24A illustrates the aspiration cycle, where the aspiration valve (A_n) (dispense valve B_n is closed) is actuated to permit passage to the pump chamber. The displacement of the pump's axial piston drives the fluid motion. Figure 4.24B shows how the dispense cycle occurs in the opposite manner; the dispense valve (B_n) is actuated (while valve A_n is closed) to permit the piston to force fluid from the pump chamber. Next, the 3-way valve C_n diverts the reagent to directional manifold 4 or the mixer (*via* valve D_n).

(iii) Mixer. Figure 4.25 illustrates the two stages of the reagent mixer, where two processing reagents are simultaneously introduced to a vortex mixer [230] and then forced through a miniature helical static mixer [231]. The outlet of the mixer leads directly to directional manifold 4.

(iv) I/O interfaces. Four screw terminals located on the panel are used to connect valve and pump electrical leads to the robot controller (see Section 5.5.1).

(3) Reagent dispensing needle manifolds. Figure 4.26 shows the structure of a needle manifold. It permits reagent dispensing to the individual processing channels core mechanism *via* a four channel assembly of blunt-end or radial flow needles (see Figure 4.27A) and a staged configuration of three 3-way solenoid valves (see Figure 4.27B). The interface valves increase the flexibility and speed of the sample preparation process by addressing the four dispensing channels

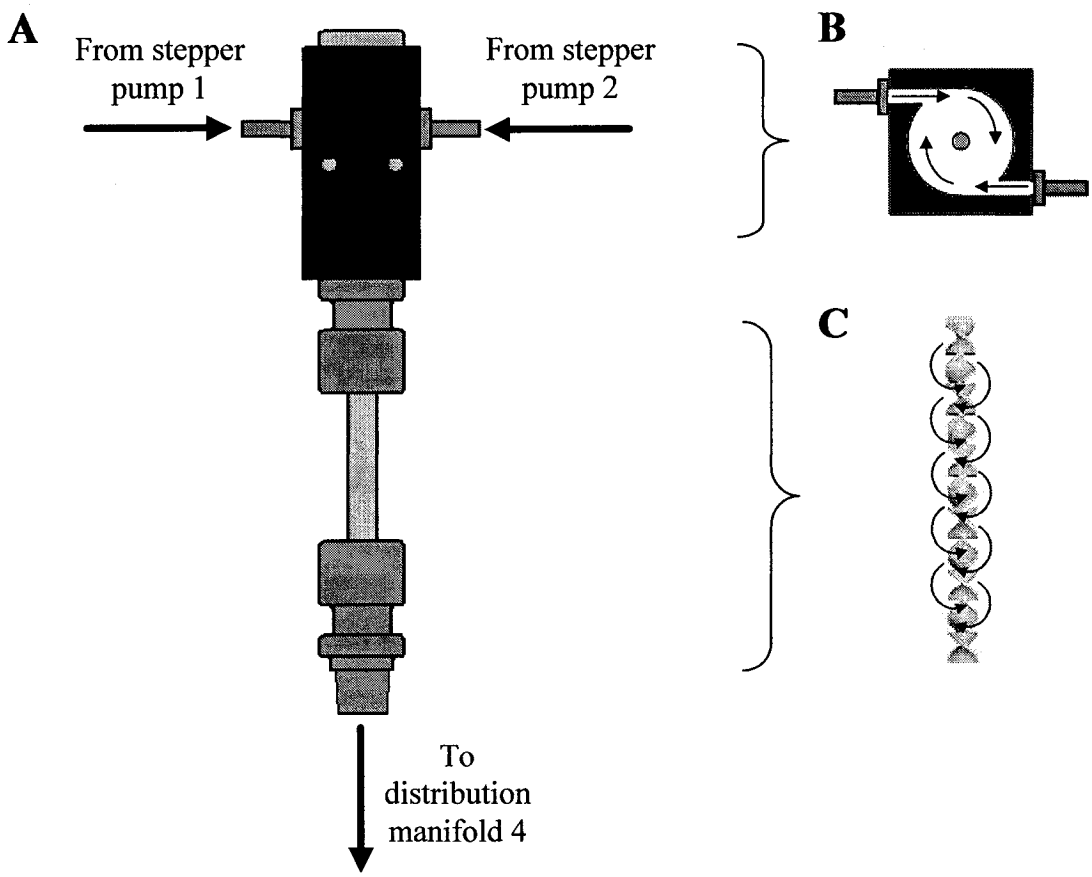

Figure 4.25: Schematic illustration of the mixer and the two mixing stages. Two processing reagents are introduced in (A) a vortex mixer and pumped through (B) an interfacing 3/16 in. I.D. stainless steel tube containing a miniature polypropylene helical static mixer. Arrows indicate the flow direction for mixing.

individually and reducing the motion required for dispensing to each processing channel. The manifold also includes a linear retraction mechanism equipped with a magnetic proximity sensor to detect and compensate for misalignment of needle manifolds (i.e. a collision, see Figure 4.27C); retraction prevents damage to the manifolds while the sensor signals the robot controller for a reverse-direction motion response to pull away from the surface.

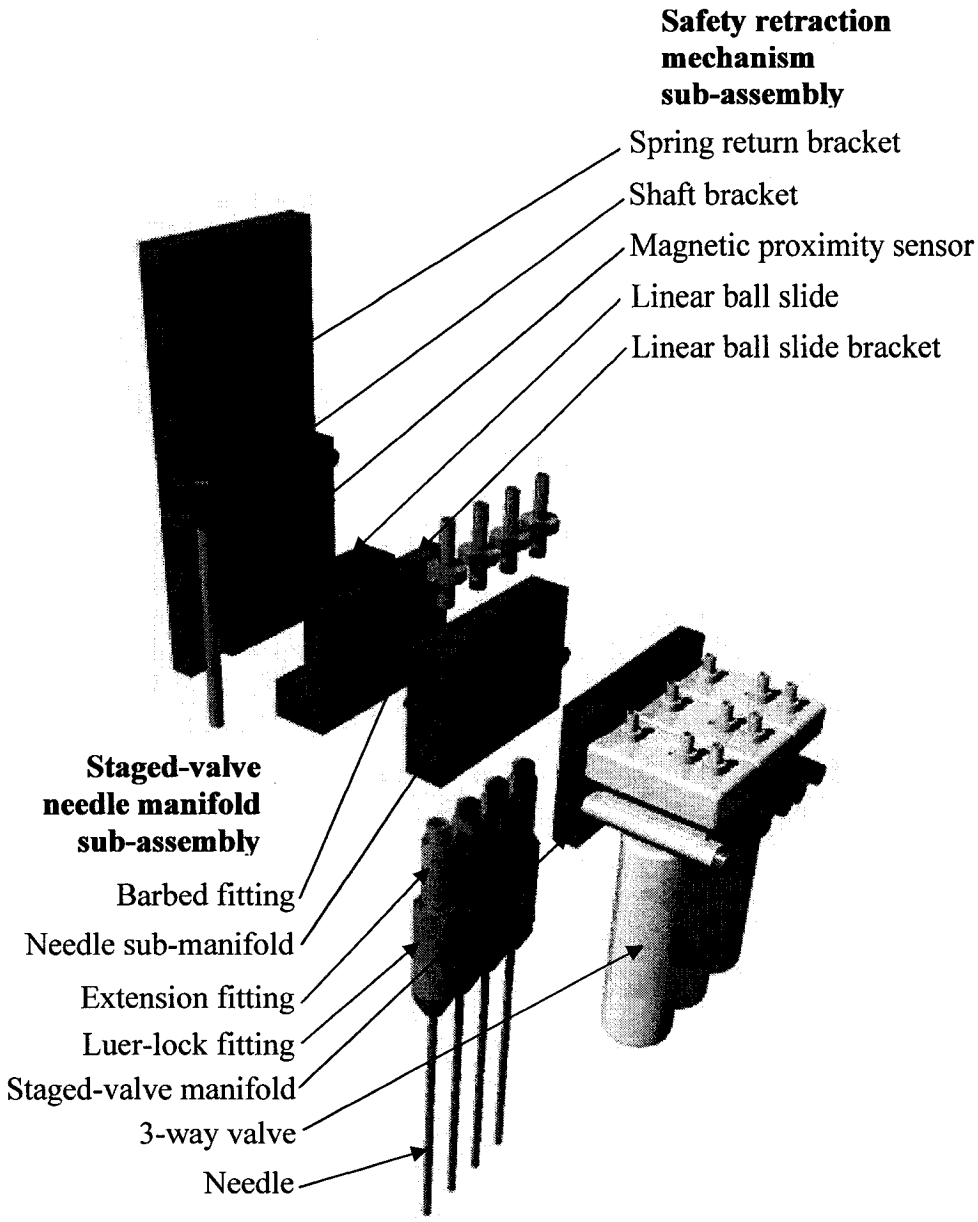

Figure 4.26: Illustration of the reagent dispensing needle manifold components. The needle manifolds accommodate two operations and are composed of two corresponding sub-assemblies: (1) a staged-valve needle manifold to control delivery of processing reagents to the core mechanism *via* the four needles, and (2) a safety retraction mechanism to compensate for and detect misalignment of the dispensing needles to prevent damage to the manifold and signal the robot controller for a response.

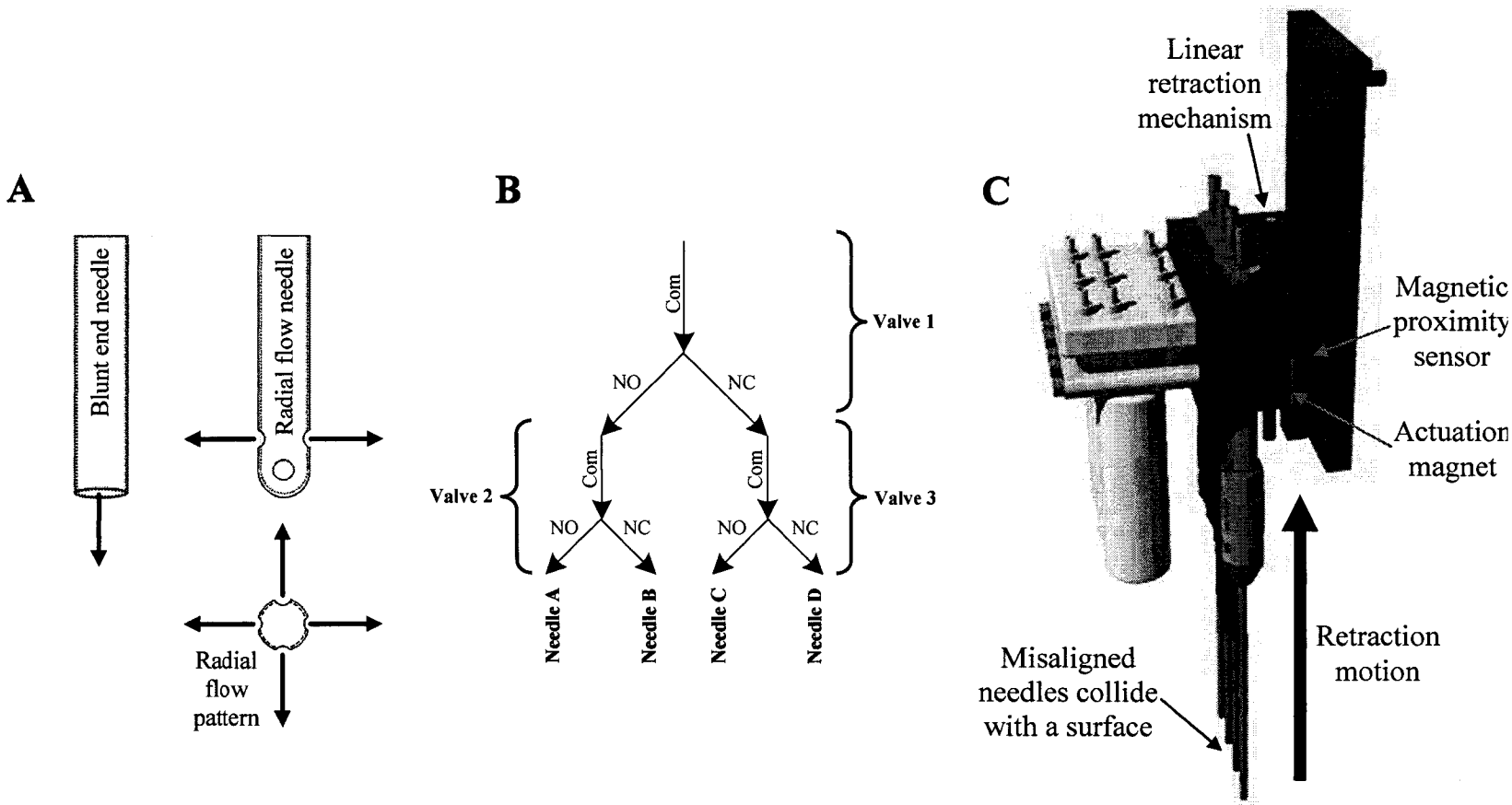

Figures 4.27: Schematic illustrations of dispensing needle manifold components. (A) Structure and flow pattern of blunt-end and radial flow needles. The cumulative cross-sectional area for radial flow (holes offset by 90°) is equal the area for the blunt end needles. Unlike flow from blunt ended needles, radial flow does not directly impinge on the samples. (B) Flow diagram for the manifold 3-way staged solenoid valves. Liquid delivered from the processing reagent handling panel is introduced to the needle manifold *via* the common (Com) port of valve 1. Liquid passes though either the normally open (NO) normally closed (NC) port to the Com port of either valves 2 or 3. The same arrangement is used for valves 2 and 3 to distribute the liquid to needles A, B C or D. (C) A retracted reagent dispensing manifold during a collision event. When the manifold retracts, the magnet actuates the proximity sensor, which signals the controller for a motion response.

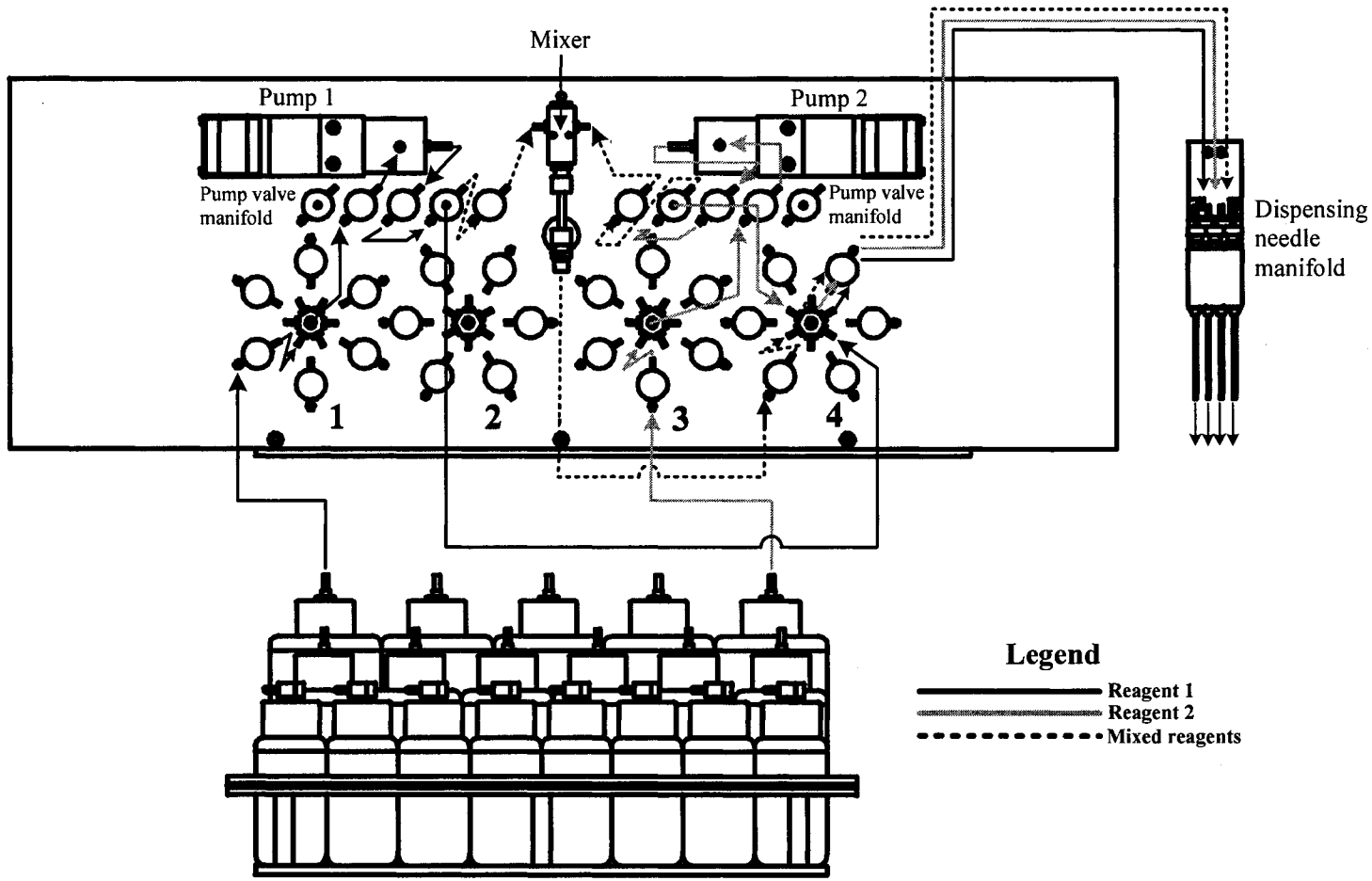

Figure 4.28: Schematic illustration of reagent dispensing flow paths for single and mixed reagents. Distribution manifolds are indicated by the numbers "1, 2, 3 and 4". For clarity, the figure shows only one dispensing needle manifold and neglects all non-fluidic components. Reagents 1 and 2 follow independent flow paths *via* pumps 1 and 2. Alternatively, pump support valves divert both reagents to flow simultaneously through the mixer. In either case, valves at manifold 4 direct reagents to either of the two needle manifolds, located on the θ-axis.

4.4.1.1 Operation of the Processing Reagent Handling Subsystem

Figure 4.28 illustrates the flow paths of two reagents through the subsystem for individual or mixed delivery. To deliver a single reagent, the robot selects and actuates the solenoid valve on the directional manifold that is in-line with the appropriate reagent reservoir. The aspiration/dispense cycles of the pump and pump support valves moves the liquid through the network to directional manifold 4. Actuation of a manifold solenoid valve then diverts the liquid to one of the needle manifolds, where it is dispensed into the core mechanism.

Reagents are mixed by synchronized operation of two pumps following the sequence for single reagents. However, before arrival at manifold 4, both reagents are diverted and introduced to the mixer. Afterward, the mixed reagents follow the normal dispensing route to the core mechanism.

4.4.2 Pneumatic Subsystem

The pneumatic subsystem controls pressurized air and vacuum levels from one manifold. Isolated and multitasked use of the localized pressure and vacuum sources is supported by solenoid valve-interfaced fluid lines extending to the core mechanism and the cleaning and waste management subsystem. Figure 4.29 illustrates the five components that compose the pneumatic subsystem:

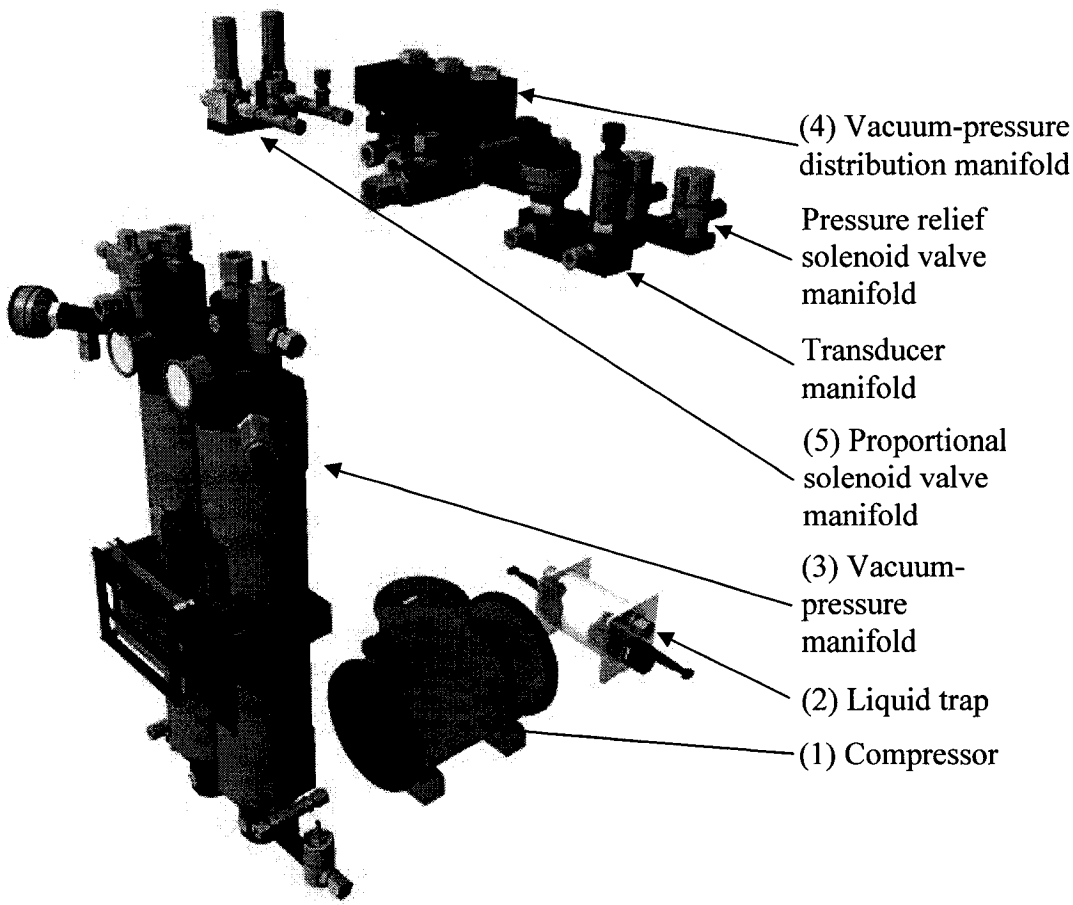

Figure 4.29: Illustration of the spatial arrangement of the pneumatic subsystem. The compressor charges the two reservoirs of the vacuum-pressure manifold. To localize the vacuum and pressure sources within to the robot workspace, ½ in. I.D. fluid lines connect each reservoir to the vacuum-pressure distribution manifold on the surface of the antivibrational platform. From there, air flow to and from the core mechanism is regulated by proportional solenoid valves and a corresponding manifold of pressure relief valves, which are interfaced with transducers to monitor pressure levels applied to the core mechanism. Also, the vacuum line is shared on the distribution manifold to provide a direct, high velocity source to the needle dry station (see Section 4.3.3).

(1) Compressor. To avoid use independent pressure and vacuum sources, the inlet and outlet lines of the compressor are distributed to charge the vacuum and pressure reservoirs. The sources are never used simultaneously. The combined compressor/vacuum pump arrangement [234, 237] consolidates components and

adequately supports the intermittent use of pressure and vacuum within the automated process.

(2) Liquid trap. A trap precedes the compressor inlet to collect and isolate any misdirected liquid waste introduced to the vacuum reservoir [237] during a sample processing run. The trap prevents loss of efficiency or damage to the compressor and stops the introduction of liquid to the pressure reservoir (*via* the compressor outlet).

(3) Vacuum-pressure manifold. Vacuum and pressurized air are similarly developed, stored and distributed within the subsystem. Figure 4.30 illustrates the structures of the vacuum and pressure manifolds, which are built around 1L air reservoirs. The application requires use of a range of selectable flow rates and pressures for sample filtration, sample delivery, cleaning and waste removal. Storage of pressure and vacuum in reservoirs eliminates pulsation and compensates for the volumetric inefficiency of a compressor or vacuum pump [232-237]. Direct monitoring of pressure and vacuum levels also permits a level of control that is otherwise unachievable. Moreover, the low volume of the reservoirs accelerates pressurization [232, 234, 235, 237] and the pump down rate for generation of vacuum [233, 236, 237].

(4) Vacuum-pressure distribution manifold. The reservoir-stored sources are coupled directly to the components located on the surface of the antivibrational table *via* 0.5 in. ID semi-rigid tubing (to avoid flow restriction) to a manifold of three, 2-way, normally-closed, direct acting solenoid valves [224-226]. The vacuum source is divided on the manifold to two of the solenoid valves. The manifold

then controls the vacuum source to the dry station of the cleaning and waste management system (see Section 4.4.3) as well

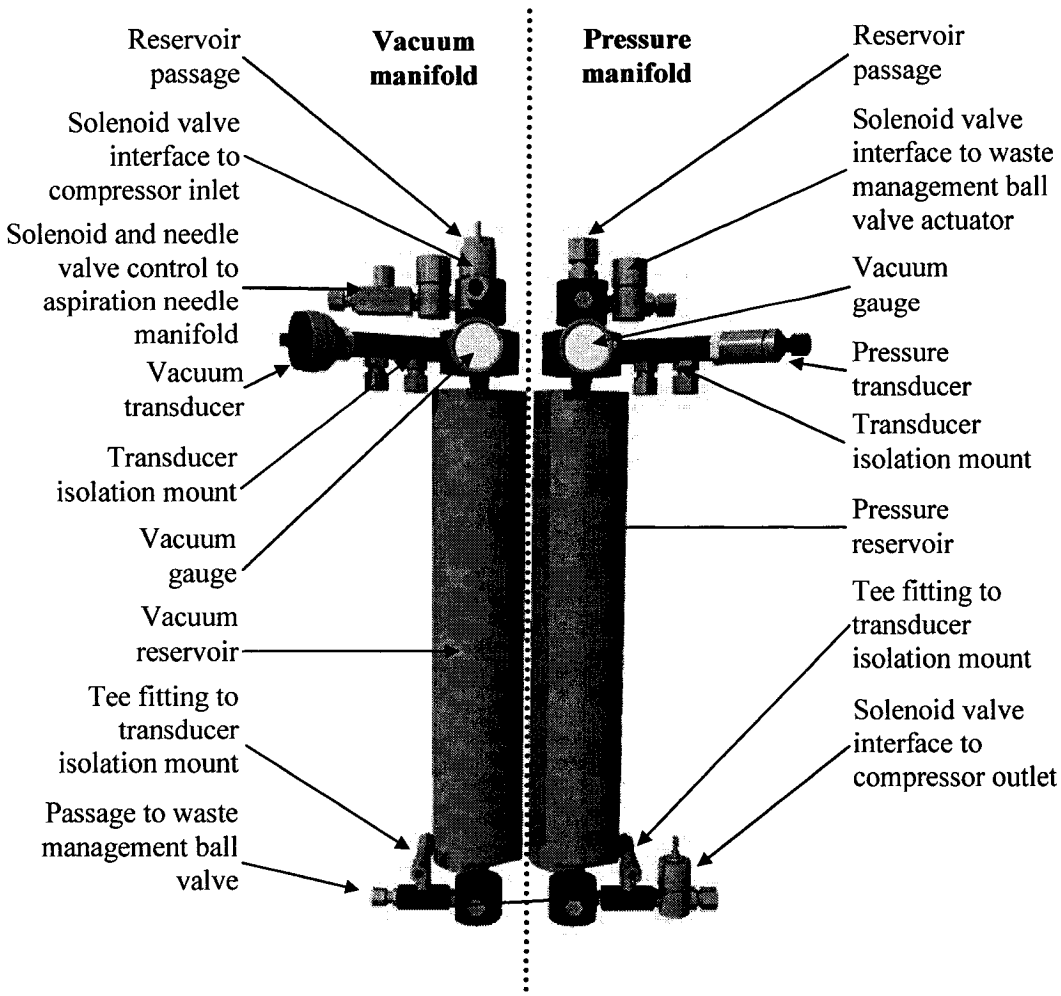

Figure 4.30: Illustration of the vacuum-pressure manifold. The manifolds have similar structure and with six components or component groups. Each manifold has three similar sub-manifolds equipped with (1) a reservoir passage leading to the vacuum-pressure distribution manifold, (2) a pressure gauge and a transducer, and (3) a fitting for isolation fluid line connections to the transducer. Each manifold also has a 3-way solenoid valve interface to the compressor. The three remaining components regulate flow to the components of the cleaning and waste management subsystem: (4) A coupled solenoid and needle vale to open and regulate vacuum to the aspiration needle manifold, (5) the vacuum-reservoir drain for removal of accumulated liquid waste (*via* the waste removal manifold), and (6) a pilot solenoid valve for actuation of the ball valve interfacing the waste removal manifold.

as the introduction of vacuum and pressurized air to the proportional solenoid valve interface to the core mechanism.

(5) Proportional valve interface to the core mechanism. For automated control of air flow under vacuum or pressure, the core mechanism interfaces to the pneumatic subsystem by a manifold of two proportional solenoid valves [222, 224, 256, 257].

For quantitative control of vacuum and pressure levels delivered to the core mechanism, each proportional solenoid valve is fitted with a tee compression fitting that connects the fluid lines to a manifold of two transducers, identical to those used on the vacuum and pressure manifolds. Furthermore, for pressure relief in the core mechanism, the fluid lines passing the transducers are interfaced to a manifold of two, 2-way, miniature solenoid valves that vent accumulated pressure or vacuum to atmosphere after sample filtration or delivery step completes.

4.4.2.1 Operation of the Pneumatic Subsystem

Figure 4.31 shows the flow diagram for vacuum and pressurized air among the components of the subsystem. Two 3-way solenoid valves connect the inlet and outlet ports of the compressor interface to the vacuum and pressure sub-manifolds. The 3-way valves are oriented to allow free passage of air to the compressor *via* their common-to-normally-open port paths. Reservoirs are charged when one of the valves is actuated to its common-to-normally-closed port path; the other permits free passage of air to the

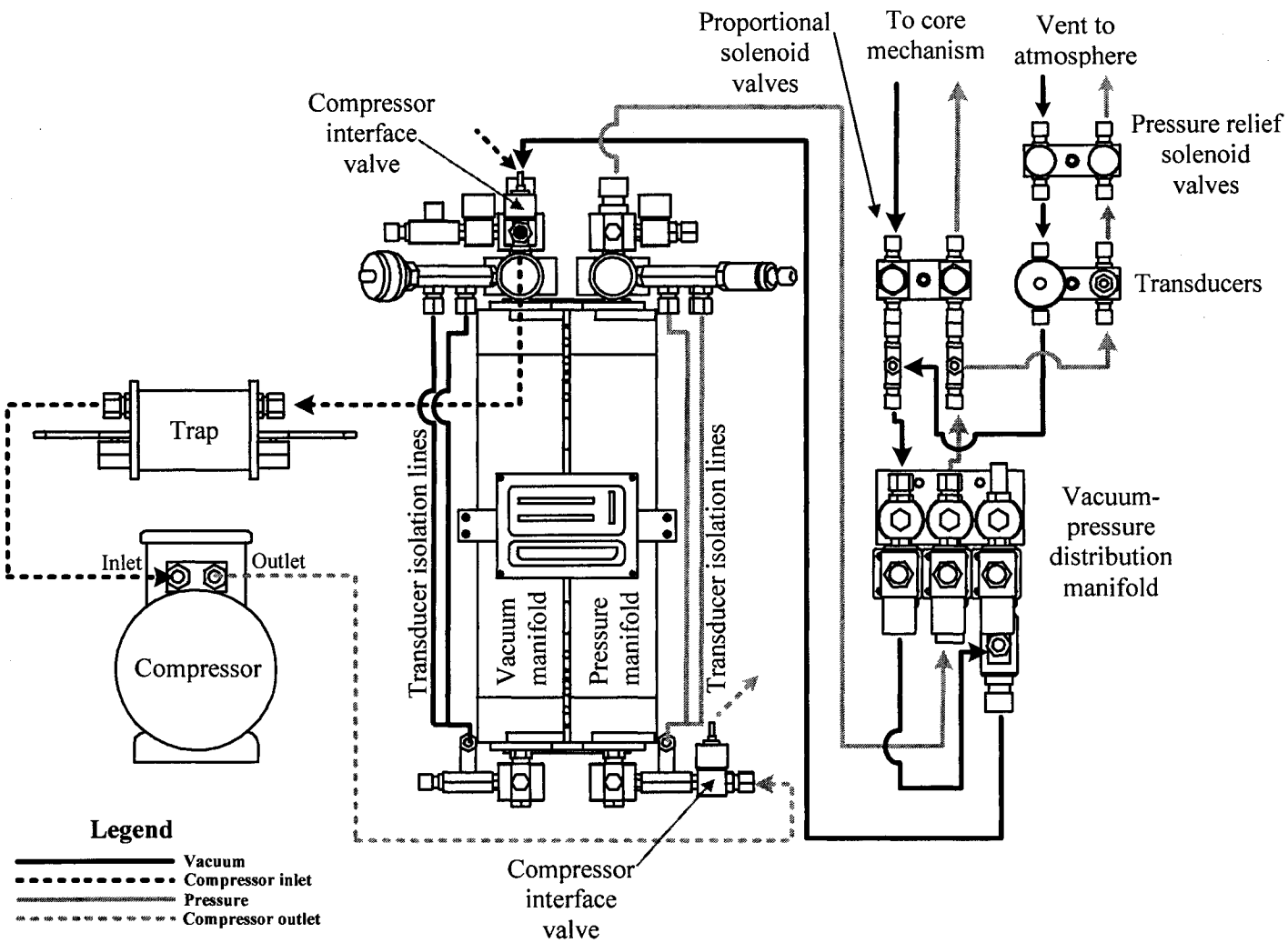

Figure 4.31: Schematic illustration of the pneumatic subsystem flow paths. The compressor inlet and outlet ports interface to the vacuum and pressure reservoirs *via* 3-way solenoid valves, which permit the free flow of air to or from the compressor while one of the reservoirs charges. Vacuum and pressure extend to the vacuum-pressure distribution manifold, which opens the sources to the proportional solenoid valves interfacing the core mechanism. Proportional valve fluid lines branch to pressure relief solenoid valves and interfacing transducers, which vent and monitor accumulated pressure in the core mechanism to atmosphere.

opposing compressor port; the arrangement does not permit simultaneous charging. The vacuum and pressurized air reservoirs connect to the vacuum-pressure distribution manifold, which connects the sources to proportional solenoid valves that regulate the flow to and from the core mechanism.

4.4.3 Cleaning and Waste Management Subsystem

The cleaning and waste management subsystem moves excess processing reagents to waste. Most of the subsystem components use vacuum or pressurized air to remove liquid waste and, as Figure 4.32 illustrates. The system is integrated with the pneumatic subsystem and shares the same features for quantitative and automated control. The cleaning and waste management subsystem comprises three subsections to clean needles, remove reagents from the core mechanism, and deliver all liquid to waste reservoirs.

(1) The clean station. The exterior surfaces of dispensing and aspiration needles are washed and dried at one location, which also serves as a location for deposition of processing reagents from the reagent dispensing manifolds (during reagent line priming (see Section 6.4.3). Figure 4.33 shows the structure of the clean station, which is composed principally of a body that is supported by adjustable leg assemblies and covered with a needle-ported cap.

Figure 4.34 illustrates interaction between the needle manifold and the clean station as well as the design and operation of the sub-sections for: (i) needle wash and (ii) needle dry:

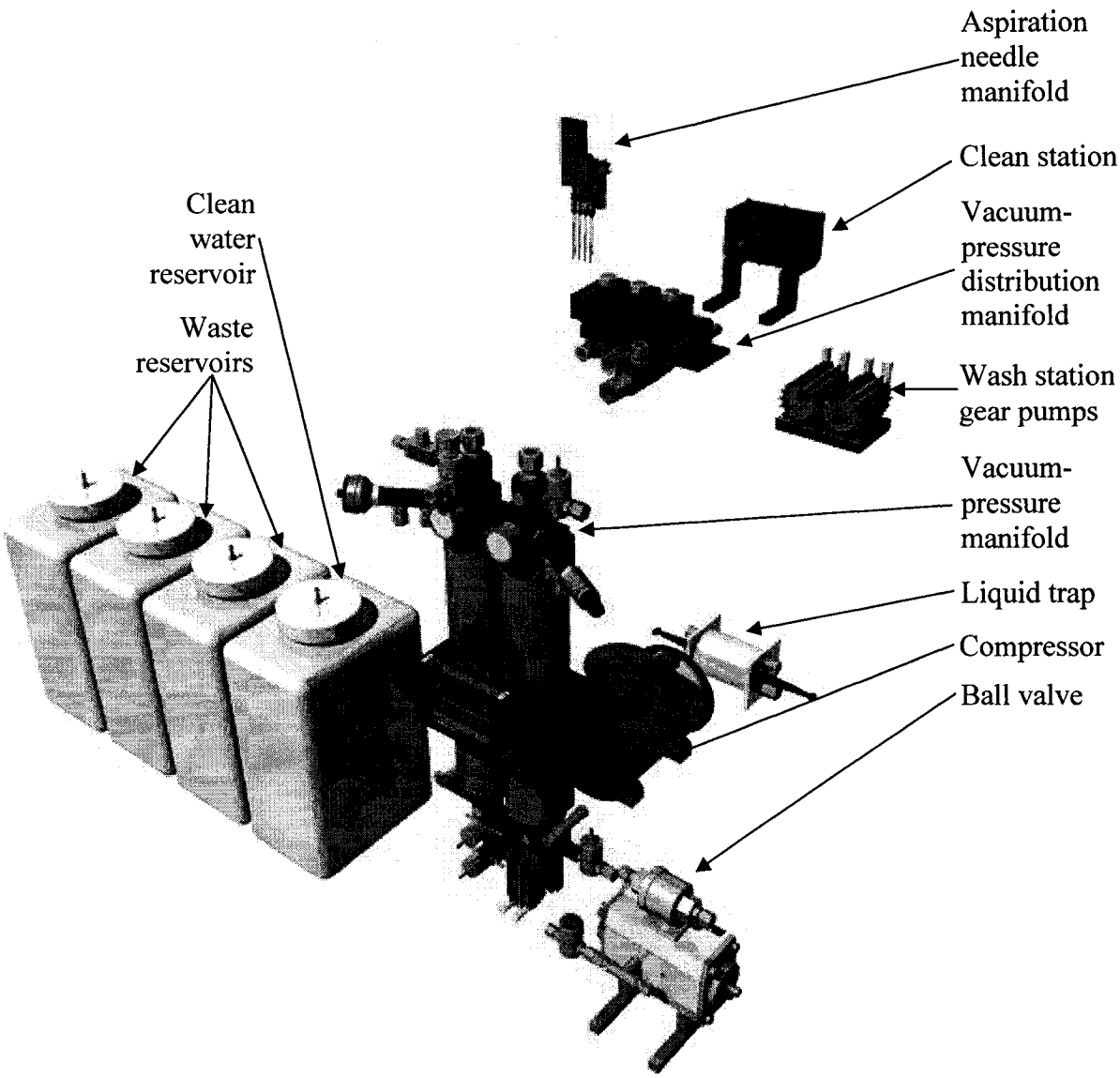

Figure 4.32: Illustration of the spatial arrangement of the cleaning and waste management subsystem and integration with the pneumatic subsystem. Five principle components or component groups comprise the subsystem: (1) the aspiration needle manifold to remove spent reagents from the core mechanism by way of a coupled solenoid and needle valve connection to the vacuum reservoir, (2) the needle dry station interfacing the vacuum-pressure distribution manifold, which permits high velocity evacuation of the dry station chamber and removal moisture from needle surfaces, (3) the wash station with two interfacing miniature gear pumps for delivery and removal of cleaning water (from the cleaning water reservoir), (4) a ball valve, actuated *via* the pressure source, permitting passage of accumulated liquid waste from the vacuum reservoir, and (5) the waste removal, which pumps liquid waste from the vacuum reservoir and separates it to three waste reservoirs.

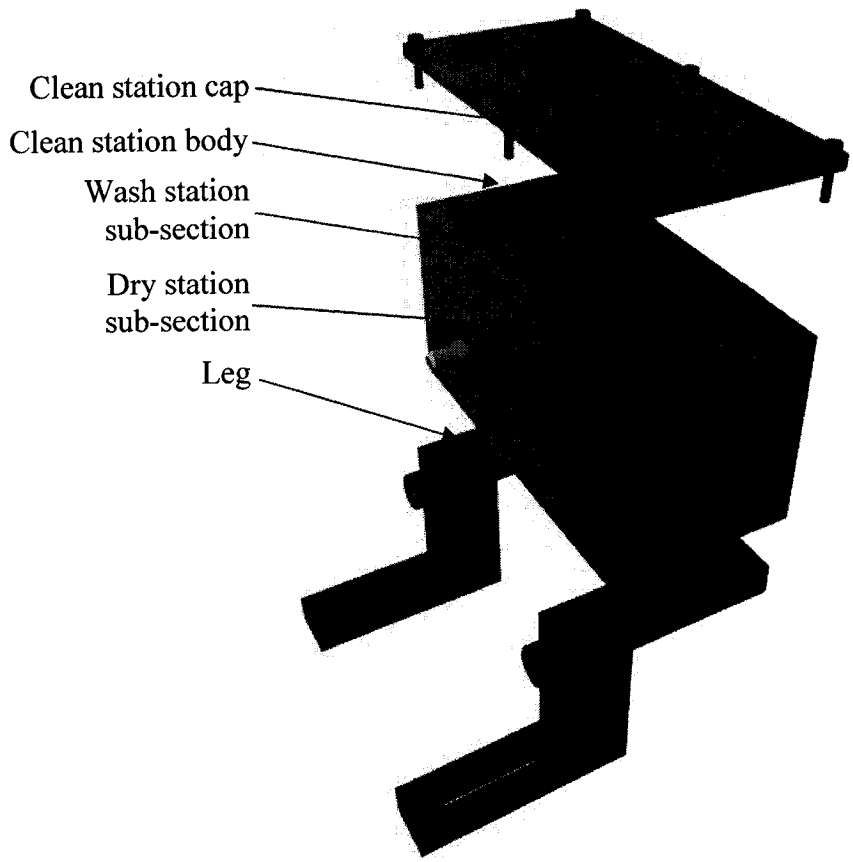

Figure 4.33: Illustration of the cleaning and waste management subsystem clean station components. The cap has surface dimensions identical to the body and two sets of four tapered though-holes for needle clearance. The clean station legs have and bottom sections that allow flexibility for horizontal and vertical positioning of the clean station onto the antivibrational table.

The schematic in Figure 4.34B shows the overflow design of the needle wash station. Water is introduced into the wash station basin by a cleaning water reservoir support pump. The needles are washed in a continuous stream of cleaning water that overflows into the wash station drain, where a second support pump removes it to a waste reservoir.

(i) The needle dry station, in Figure 4.34C, is composed of a single chamber. The chamber has a low cross-sectional area to maintain a high volumetric

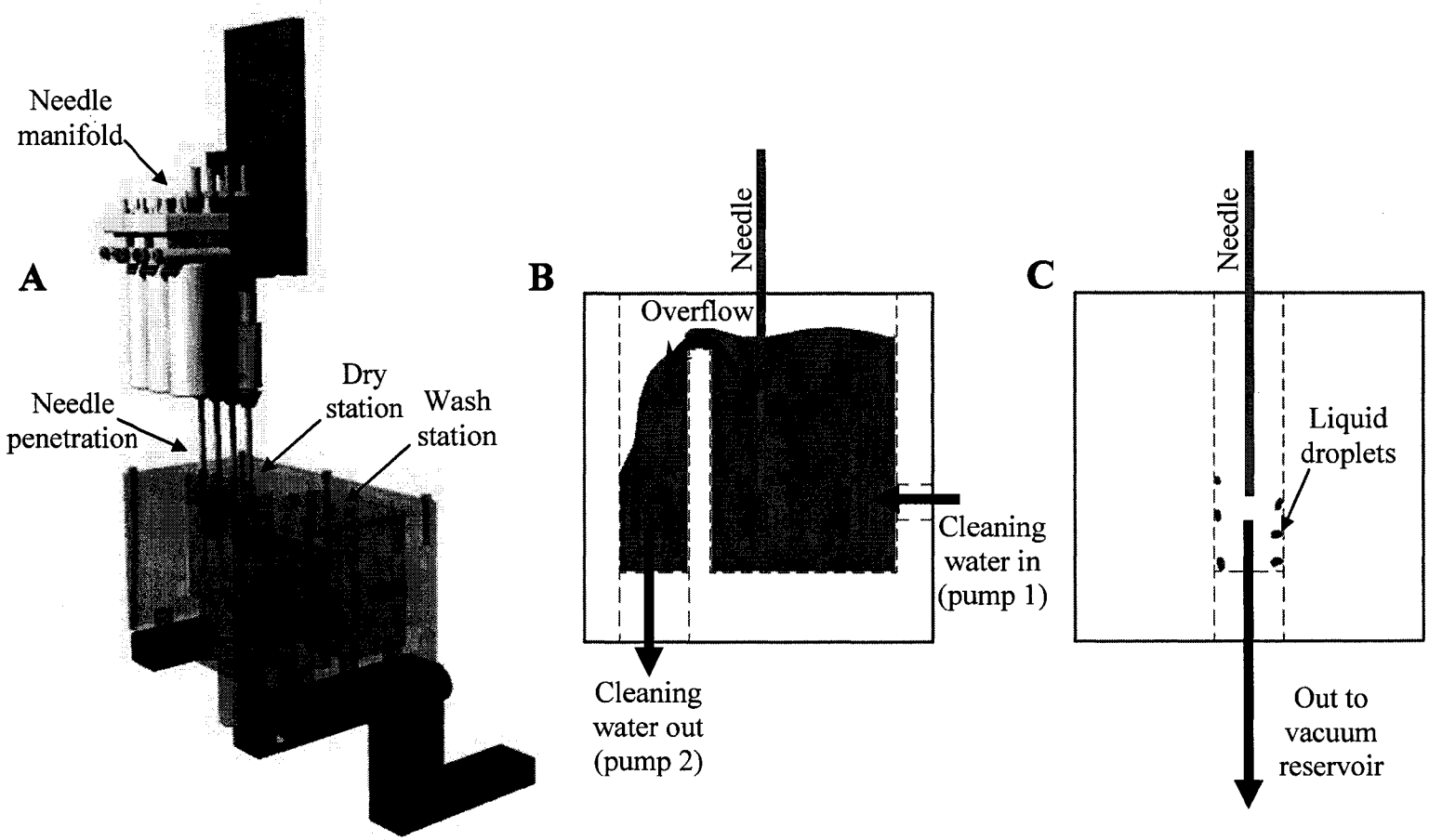

Figure 4.34: Needle manifold interaction and operation of the clean station. (A) A transparent 3D CAD rendering of the clean station showing a needle manifold penetrating into the dry station, (B) cross-sectional schematic of the wash station showing the minimum liquid level maintained by the overflow of pumped cleaning water from the basin to the drain, and (C) cross-sectional schematic of the dry station showing the method of liquid removal by rapid evacuation of the dry station chamber.

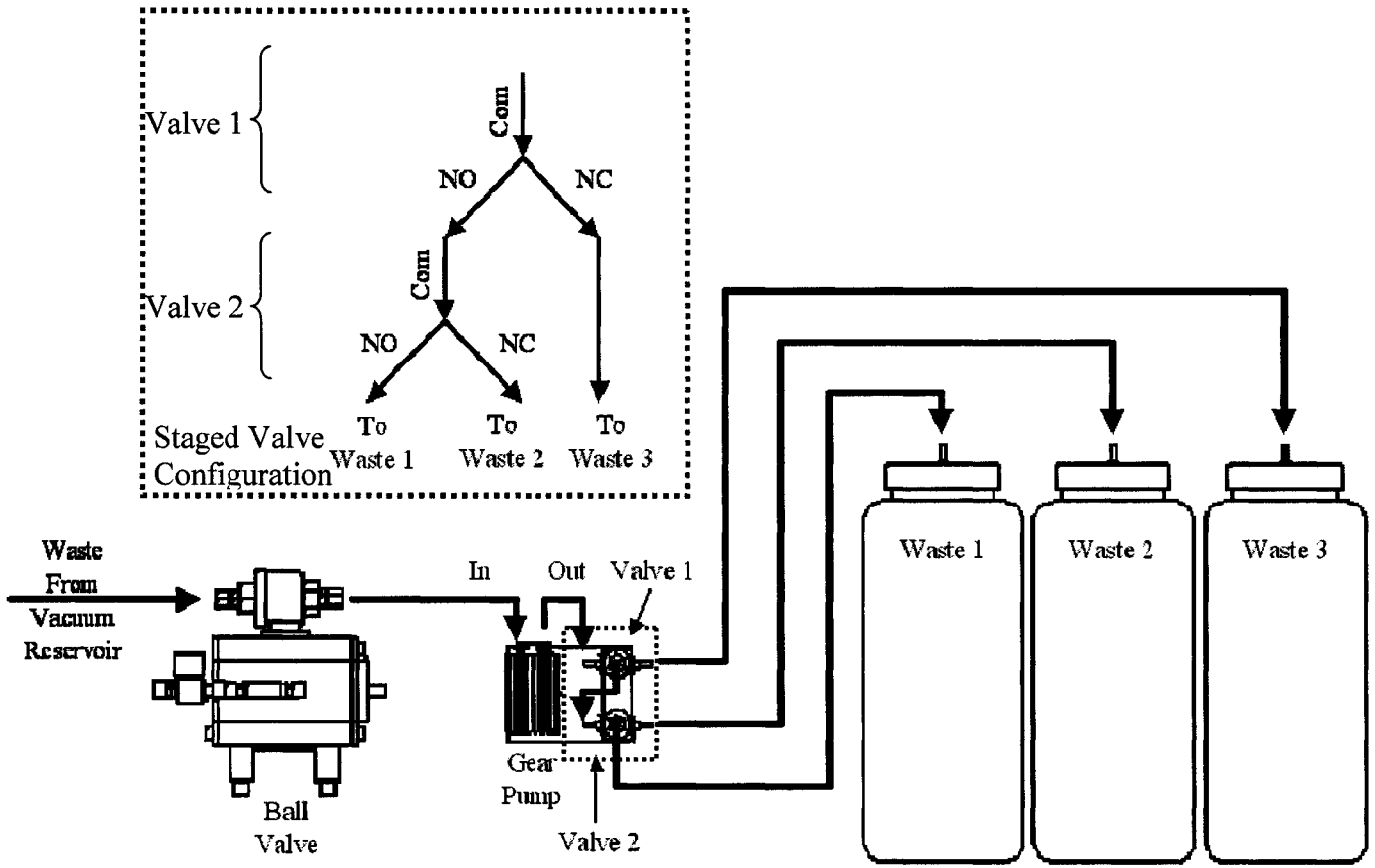

Figure 4.35: Method for removal of vacuum reservoir accumulated liquid waste *via* the waste removal subsection. The ball valve opens the fluid line from the vacuum reservoir to the waste removal manifold. A gear pump moves waste to a staged configuration of two, 3-way solenoid valves (within the dashed line), which divert the liquid to three reservoirs designated for different levels of toxicity.

flow (and a correspondingly high velocity) [217-220] for rapid evacuation of the chamber and removal of residual moisture from the needle surfaces. Air flow is provided by actuation of a solenoid valve (in the vacuum-pressure distribution manifold), which is directly in-line with the charged vacuum reservoir. The vacuum reservoir also serves as a temporary storage site for waste until it is removed with the waste removal subsection (see below).

(2) Aspiration needle manifold. Vacuum aspiration of reagents from the processing channels of the core mechanism utilizes a needle manifold that is the same design as the delivery needle manifold of the processing reagent handling subsystem (see Section 4.4.1). The manifold operates identically (with either needle structure in Figure 4.27A), but liquid flows backward to the vacuum reservoir, where in-line solenoid and needle valves open the vacuum source and regulate flow, respectively.

(3) Waste removal subsection. Figure 4.35 illustrates how accumulated waste is removed from the vacuum reservoir through a series of three sub-components (i) a ball valve, (ii) the waste removal manifold and (iii) a bank of three waste reservoirs.

(i) The frequent and abrupt changes in the gas load and direction of liquid waste flow at the interface of the vacuum reservoir and the waste manifold mandate the use of a valve with a robust mechanism for sealing and actuation [233]. This ball valve is actuated pneumatically *via* a pilot solenoid valve feed [224-

226] from the pressure manifold; permitting passage of the vacuum reservoir contents to the waste manifold. An identical solenoid valve vents the actuation pressure to the spring-loaded valve armature [225, 226] to close the fluid line; sealing the vacuum reservoir and stopping passage of waste.

(ii) The waste manifold comprises a miniature gear pump [227, 228] and two, staged, 3-way, miniature solenoid valves that direct waste to three different fluid lines.

(iii)The three fluid lines exiting the waste removal manifold lead to three reservoirs reserved for waste of different levels of toxicity.

4.4.3.1 Operation of the Cleaning and Waste Management Subsystem

Figure 4.36 illustrates the integrated operation of the cleaning and waste management with the pneumatic subsystem and the flow paths for the three subsections:

(1) Aspiration needle manifold. The subsection simultaneously utilizes vacuum to evacuate spent reagents from the core mechanism, and the vacuum reservoir as an accumulation trap for waste. The compressor supplies a continuous source of vacuum to the needle manifold, while a solenoid valve controlled fluid line from the needle manifold delivers the waste to the vacuum reservoir, where it is temporarily collected. To avoid disruption of the processing samples, the in-line needle valve restricts the flow of air (manually adjusted) for gentle evacuation of the waste from the channels of the core mechanism.

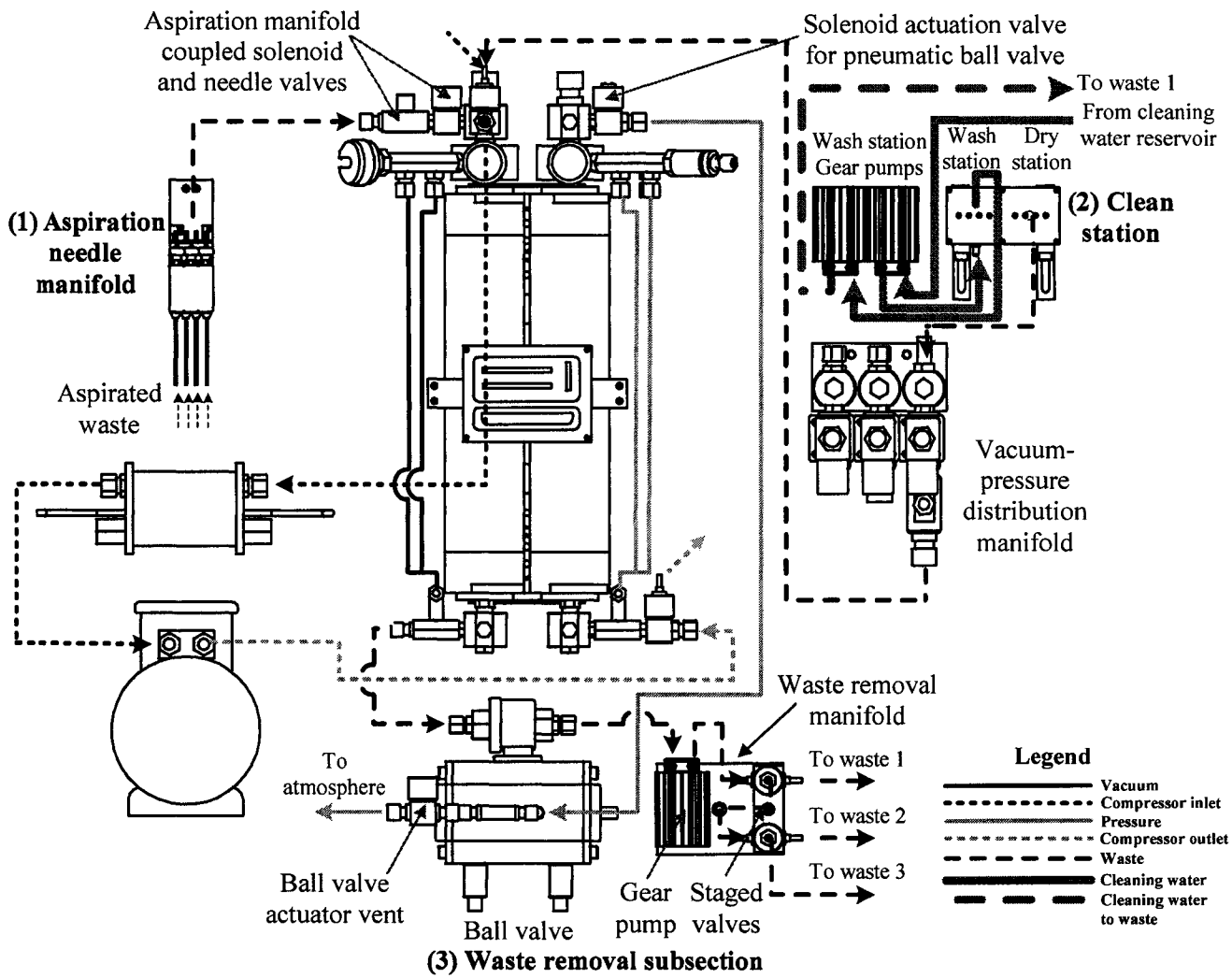

Figure 4.36: Schematic illustration of cleaning and waste management subsystem flow paths. For clarity, pneumatic subsystem components are not labeled (**see Figure 4.31**). Vacuum and pressure are maintained by normal operation of the pneumatic subsystem.

(2) Clean station. Cleaning water passes through the needle wash station *via* two parallel operating gear pumps. One pumps from the cleaning water reservoir while the other removes the spent cleaning water to waste reservoir 1 (reserved for low toxicity waste).

Vacuum is supplied to the dry station by way of a high flow solenoid valve in the vacuum-pressure distribution manifold. A large-bore (0.5 in. ID) fluid line couples the dry station to the valve for high-velocity evacuation and effective removal of residual moisture from the needle surfaces.

(3) Waste removal subsection. Operation of the aspiration needle manifold and the needle dry station accumulates liquid waste in the vacuum reservoir, which is removed periodically to the three waste reservoirs. The waste removal manifold pump moves liquid from the vacuum reservoir drain and through a ball valve. Downstream from the pump, the staged arrangement of two, 3-way valves diverts the liquid to one of three waste reservoirs.

4.5 Positioning Support Subsystems

Implementation of the automated sample preparation process requires coordinated positioning for core mechanism reconfiguration as well as repeated needle manifold positioning at the clean station and across the array of core mechanism processing channels. Three integrated support subsystems (see Figure 4.37) fulfill the positioning requirements while imposing minimal mechanical perturbation on the samples: (1) the

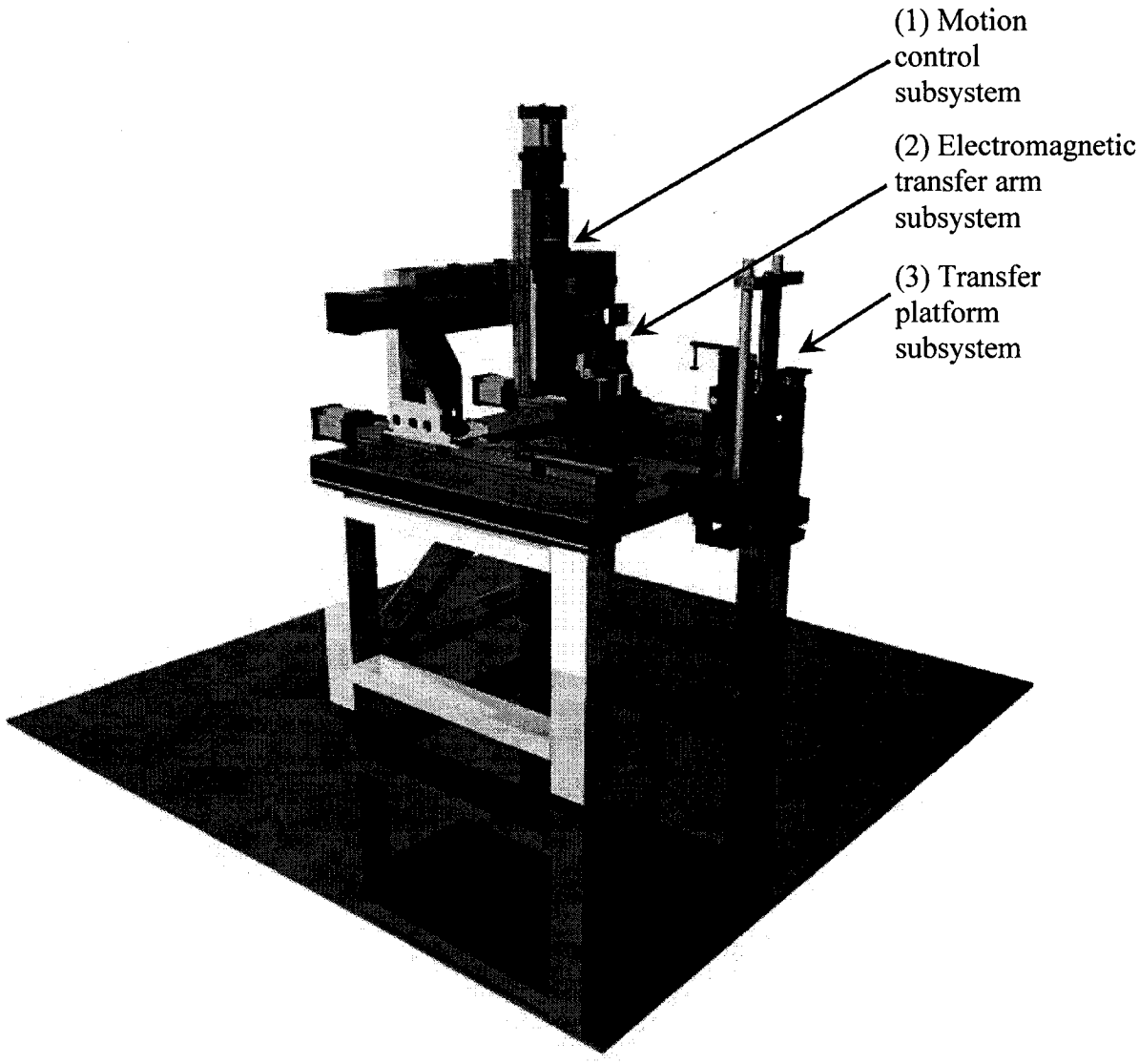

Figure 4.37: A front perspective rendering of the EMPOP robot illustrating the positioning subsystems layout.

motion control subsystem, (2) the electromagnetic transfer arm, and (2) the transfer platform.

The motion control subsystem supports use of the electromagnetic transfer arm and transfer platform for reconfiguration. Otherwise, the motion control subsystem operates to position reagent dispensing and aspiration needle manifolds in a workspace over the cooling platform, core mechanism and clean station.

4.5.1 Motion Control Subsystem

The motion control subsystem provides flexible Cartesian and rotational positioning of the core mechanism and fluid handling tools. Figures 4.38 and 4.39 show the arrangement and range of motion of the five serially coupled, servo-driven axes.

The X-, X'-, Y- and Z-axes comprise the arrangement for translational motion, where the two synchronized X- and X'-axes (500 mm travel), mount onto the antivibrational platform, to carry the perpendicular Y- and Z-axes (500 and 200 mm travel, respectively) on two vertical-right angle mounting bracket assemblies. The Z-stage fastens directly to the Y- stage carriage and a vertically adjustable interface bracket, mounted on the Z- stage carriage, carries the θ– and ϕ– rotational stages.

A 6 in. diameter rotary table serves as the θ-axis. The ϕ-axis couples to a bracket mounted on the surface of the rotary table, which also supports the needle manifolds at three 90° offset mounting locations. The ϕ- axis is a pivot mechanism [238] providing >90° of rotational motion to support the electromagnetic transfer arm and core mechanism payload. The axis couples to its motor by a parallel mount for a compact geometry that does not intrude on the workspace of the core mechanism and needle manifolds.

The serial axis arrangement keeps the core mechanism static throughout most of processing; reducing its motion requirements to the plate interchange and inversion steps. The pick-and-place Cartesian axes provide a large workspace for the two rotational axes, which carry all tools. Furthermore, servo motors provide resolution, accuracy and repeatability [246-252] throughout the subsystem.

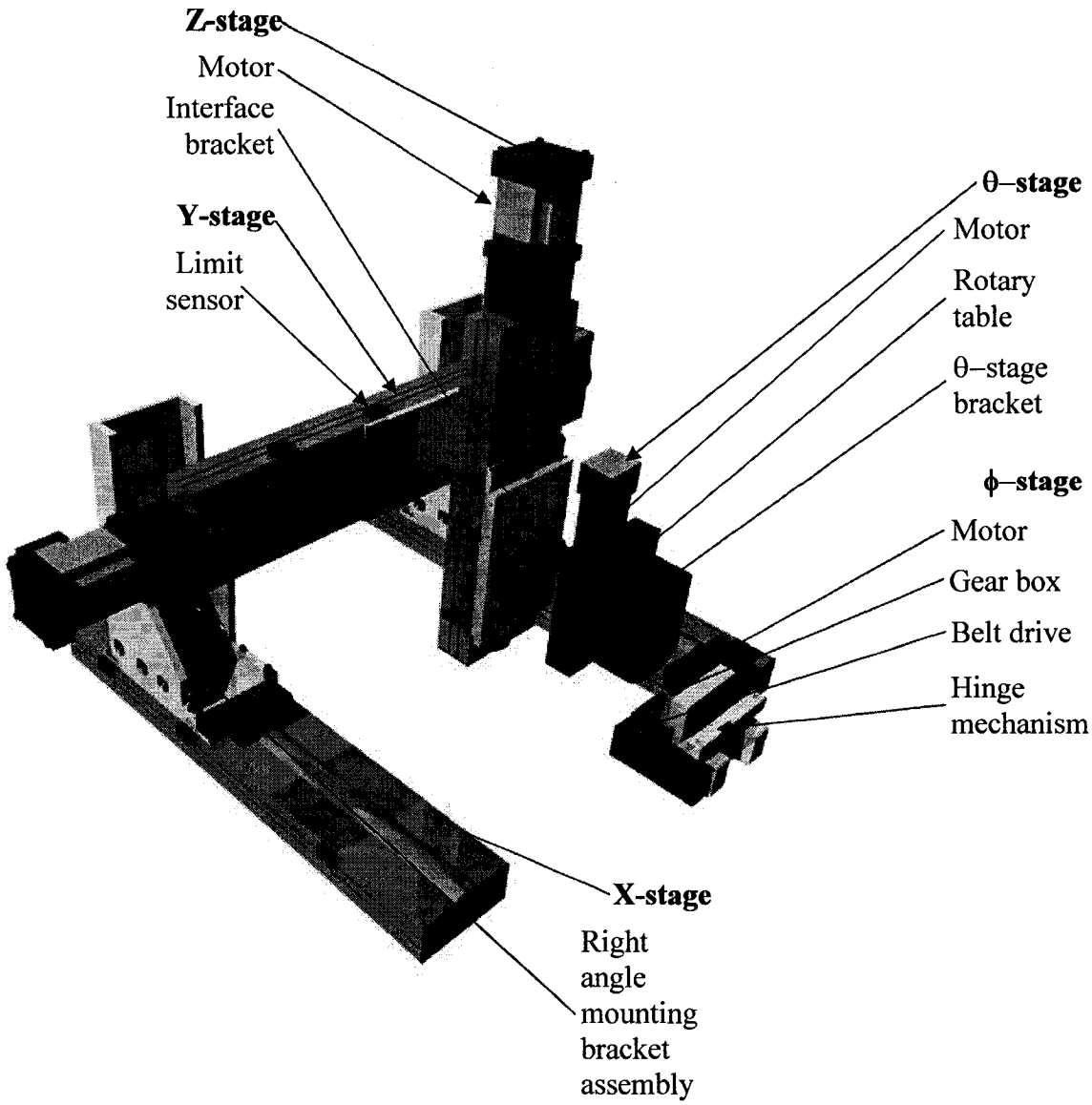

Figure 4.38: Illustration of the serial arrangement of the six axis, five degree-of-freedom, servo motion control subsystem. The X/X'-, Y- and Z-axes are square rail linear bearing positioners with 5 mm lead ballscrews for mechanical transmission. The Cartesian system couples to rotational axes *via* the Z-axis carriage and operates to position the θ- and ϕ-axes, which the carry fluid handling and positioning tools for interaction with the core mechanism.

The θ-axis is a 90:1 worm gear driven, 6 in. diameter rotary table with a surface bracket that supports the ϕ-axis and the three needle manifolds. The bracket also as underside-clearance for cables and tubing that are progressively channeled though the rotary table thru-hole and the Z- axis interface bracket. The ϕ- axis is a pivot mechanism that carries the electromagnetic transfer arm through ~90° of rotational motion, and supports the core mechanism payload *via* a parallel mounted servo motor with 25:1 in-line planetary gearing.

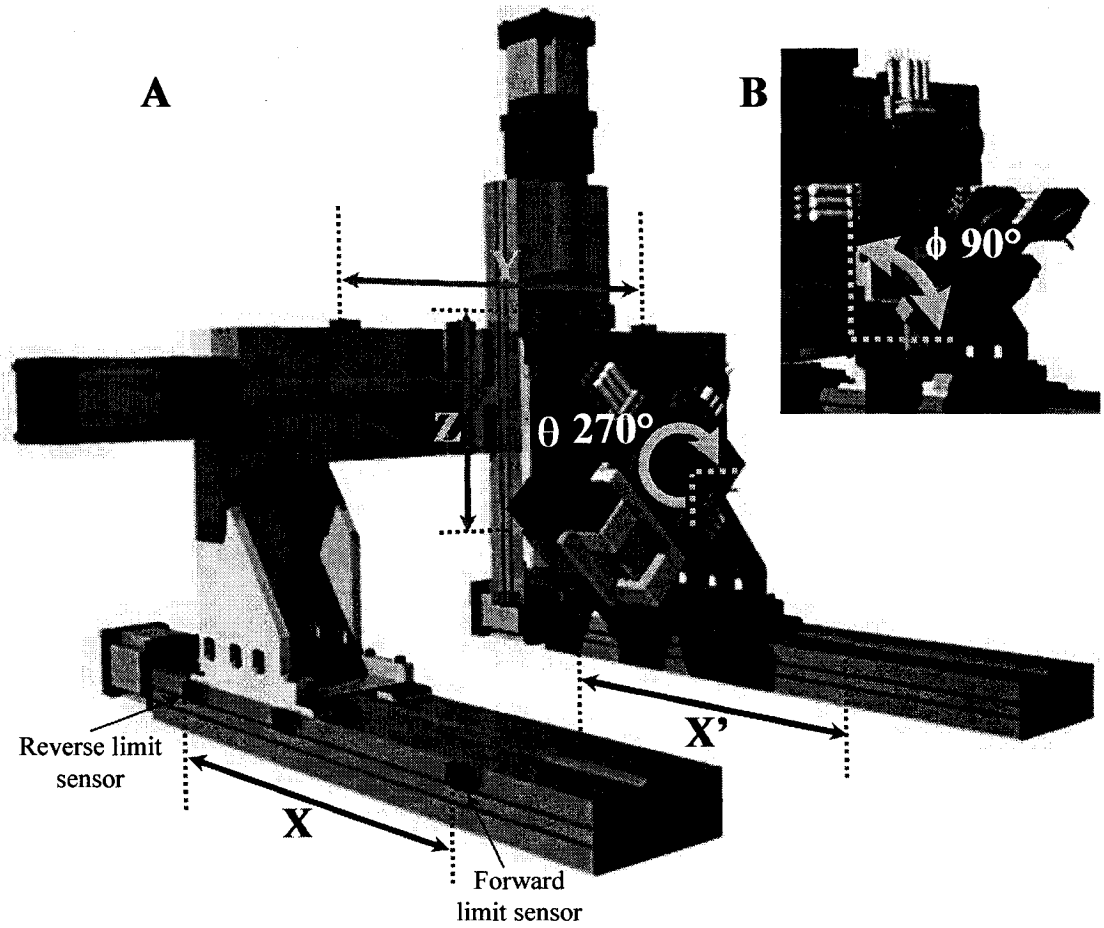

Figures 4.39A and B: Illustration of the assembled motion control subsystem illustrating: (A) the range of motion between linear axis forward and reverse limit sensors and the mechanical limit of the θ-axis, and (B) the range of motion between mechanical limits of the ϕ-axis. For positioning reference, the X-, Y- Z- and ϕ-axes are equipped with NPN inductive home, forward and reverse limit sensors. The θ-axis uses a single magnetic home sensor and the synchronized X/X'- axes share one set of limit sensors. For accuracy and repeatability within the limits of motion, linear and rotational axis motors are equipped 2000 and 1000 line encoders, respectively.

Specifications for the rotational axes were defined by the torque requirements for worst-case rotational positioning under maximum load (i.e. inversion of the core mechanism, see Figure 4.40); within motor rated torques and all component duty-cycles.

Specifications for the Cartesian axes were determined on the basis of trapezoidal velocity profile positioning [246-250] for the loaded rotational axes. Moreover, due to the higher requirement for translational positioning within the process, subsystem load, torque and inertia [243] parameters were considered for Cartesian axes stage/motor/drive sizing.

The ϕ-axis positions the electromagnetic transfer arm into its active (horizontal) state. It must provide enough torque to remain positioned for plate decoupling, interchange, and core mechanism inversion. An in-line, 25:1 planetary gearbox [238, 241] augments the motor static torque [247, 250] to support the electromagnetic transfer arm/core mechanism payload. The configuration produces a 2.5/10-fold torque margin

Figure 4.40: Illustration of core mechanism inversion with the motion control and electromagnetic arm subsystems. The inversion step imposes the greatest loads, moments and inertia across the positioning subsystems. Therefore, for stable, high-performance positioning under all circumstance, the motion control subsystem components were designed to accommodate this "worst-case" condition.

(for continuous/peak motor torque levels), ensuring stable positioning of the arm and coupled plates.

The θ-axis provides torque to invert the ϕ-axis and coupled core mechanism. A 90:1 worm gear-drive [238, 241] built into θ-axis supports positioning requirements under maximum load. The high gear ratio supports the moment and corresponding inertial load [247, 249, 250] imposed by the ϕ-axis/arm/core mechanism during inversion (while providing 1 to 5-fold torque margin).

The Cartesian axes carry the subsystem load, which builds through the serial axis progression. Accordingly, the structure of the linear stages is more robust to accommodate normal and axial loads; as reflected by the synchronized X-/X'-axes that carry all other axes of the subsystem. Furthermore, for high performance positioning under maximum load, the load inertia reflected to the motors (*via* axis ballscrews) was also considered. For a stable, power efficient system, the load inertia (J_L) should be similar to the motor inertia (J_M). A typical inertial matching design target for the load inertia-to-motor inertia ratio is

$$2.5J_L \leq J_M/N^2 \leq 10J_L, \tag{4.2}$$

where N is the gear ratio [247, 250, 257, 258]. Specifications for all Cartesian axis motors produced ratios < 4. As a consequence of inertial matching under worst-case conditions [171], the torque margin for each axis is between 20 to 40-fold.

All motion control subsystem cabling and fluidics subsystems tubing are arranged in cable carriers. They are mounted progressively from the antivibrational table and

along the three Cartesian axes with a series of motor brackets and cable carrier runners, which stabilize their motion (see Figures 3.1).

4.5.2 Electromagnetic Transfer Arm Subsystem

The electromagnetic transfer arm is the end effector of the motion control subsystem [184, 258]. Figure 4.41 shows the arm, which is a magnetic gripper that provides a means for dependable automated positioning of the core mechanism plates and reconfiguration by unilateral interaction with plate surfaces [253, 254].

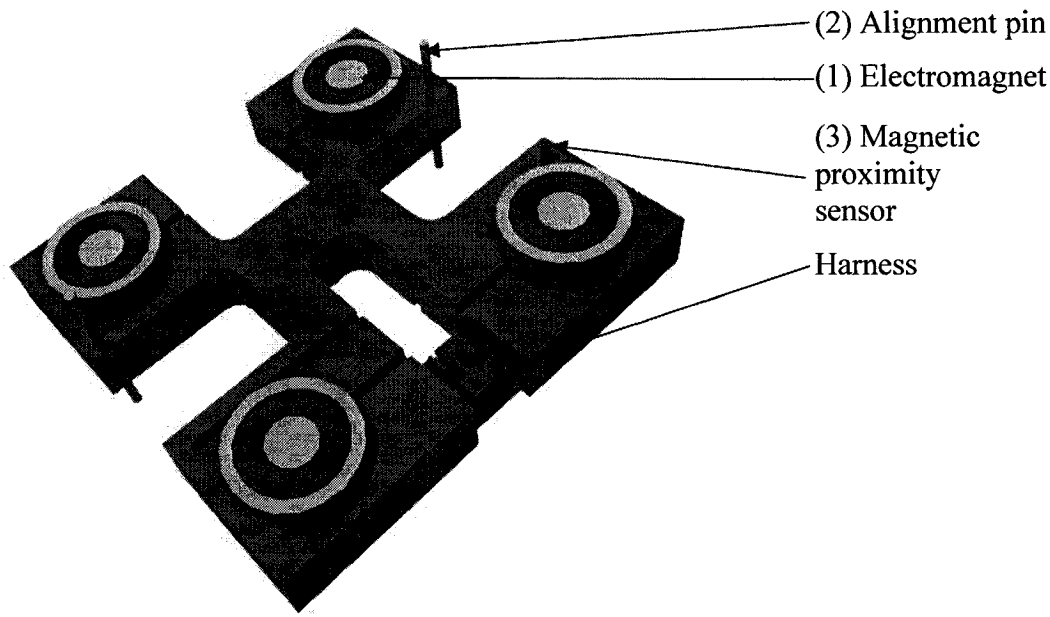

Figure 4.41: Illustration of the electromagnetic transfer arm. The illustration shows the identical group of subcomponents built into each face. A symmetrical array of four1.5 in. diameter x 1/2 in. height, 12 VDC surface-contact, round, island-pole electromagnets; a set of 1/8 in. diameter x 1.25 in. length, steel dowel pins for arm-to-plate alignment; and a miniature cylindrical magnetic proximity sensor for plate detection and signaling the robot controller. All wires from electromagnets and magnetic proximity sensors are localized in a cable harness located on each face.

Electromagnets provide high-force, part-securing interaction in a compact geometry, without moving parts and are controlled easily for low settling-time pickup and quick release of the core mechanism and individual plates (see Section 5.6.2). The arm body is robust enough to eliminate deflection under static and dynamic conditions. Also, as part of the integrated system, the arm geometry also provides clearance for the needle manifolds, the cooling platform walls and the transfer platform positioning surface.

An identical group of subcomponents is built into each face: (1) A symmetrical array of four, 175 N pull-force, surface-contact, round electromagnets to support the core mechanism payload, (2) a set alignment pins for arm-to-plate alignment and stabilization, and (3) a miniature cylindrical magnetic proximity sensor.

The arm fastens to the ϕ-axis of the motion control subsystem for rotation by approximately 90° into its active (horizontal) position (see Figure 4.39) to support interaction with the core mechanism (see Figure 4.17). In the active position, the arm can interact with plates (and detect their presence) on either face. Furthermore, the motion control subsystem can position the arm with coupled plates on horizontal, vertical and rotational planes. When the arm is not in use, it is stowed in the vertical position; parallel to the θ-axis of the motion control subsystem.

4.5.3 Transfer Platform Subsystem

The transfer platform is required for inversion of the core mechanism during the sample delivery stage of automated processing. Restrictions on the range of motion of

the electromagnetic arm and the motion control positioning subsystems made the transfer platform necessary. Thus,

(1) When the core mechanism is inverted, the electromagnetic arm will be on the underside of the plate configuration, and so cannot place the plates onto the cooling platform.

(2) The θ- and ϕ-axes have limited travel in the Z-axis. Thus, when the core mechanism is inverted, it cannot be positioned onto the surface of the cooling platform because it is beyond the range of motion of the Z-axis.

The transfer platform subsystem provides a simple and effective means to complete the core mechanism inversion step with a minimum level of control (see Section 5.6.3). Figure 4.42 and 4.43 illustrate the five sub-assemblies and the range of motion of the device:

(1) Positioning platform. Figure 4.44 shows the sub-assembly that holds the core mechanism during the transfer. The core mechanism is stabilized on the platform surface by two alignment pins and a magnetic proximity sensor signals core mechanism presence to the robot controller. A through-passage in the surface of the positioning platform corresponds to a perimeter trace of the electromagnetic transfer arm geometry.

(2) Rotational actuator. Motion to locate the positioning platform into an active (horizontal) or a stowed (vertical) position is provided by an electromechanical

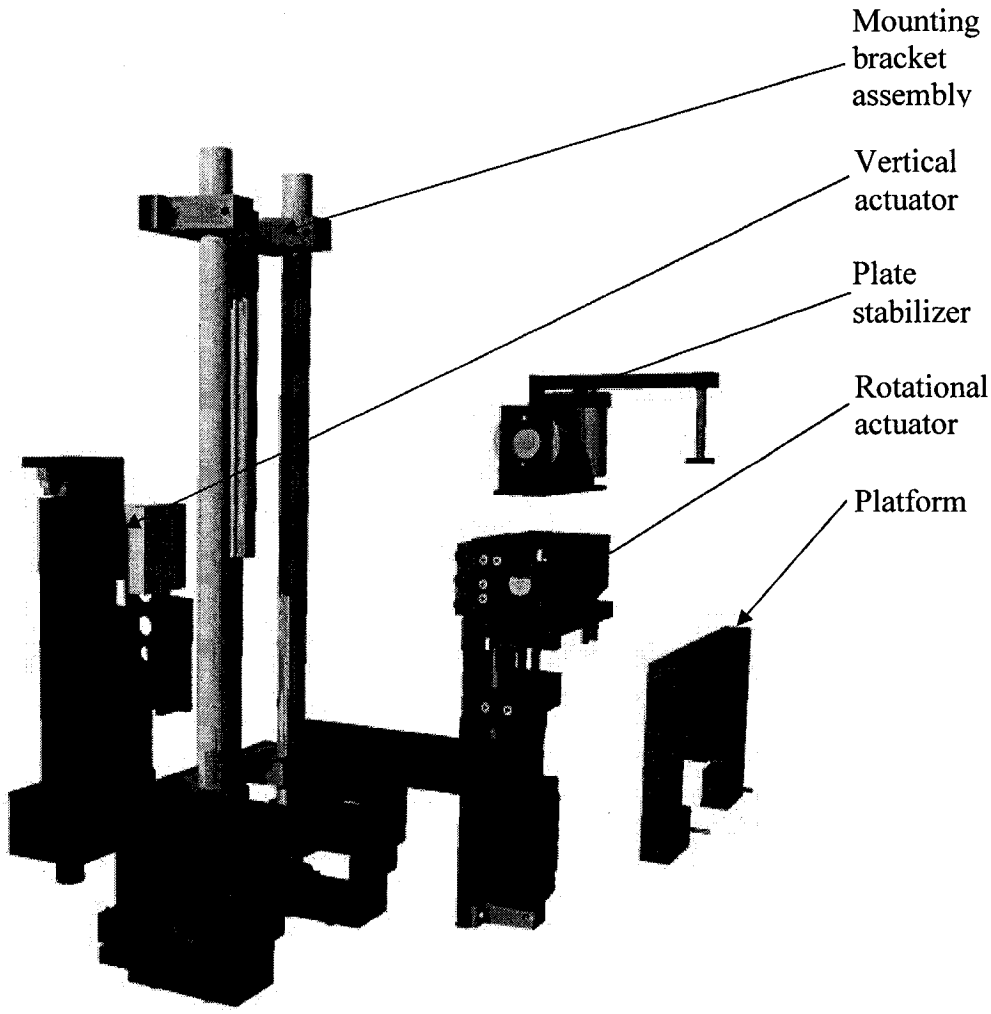

Figures 4.42: Illustration of the transfer platform subsystem components. The subsystem is comprised of five sub-assemblies for transfer and stabilized, vertical positioning of the core mechanism during inversion as well as automatic retraction into a stowed position when unused.

linear actuator. The static torque required to directly maintain the active state of the positioning platform during transfer is high. Therefore, the actuator assembly design followed an alternative approach to provide a high torque margin, high stability and simple control.

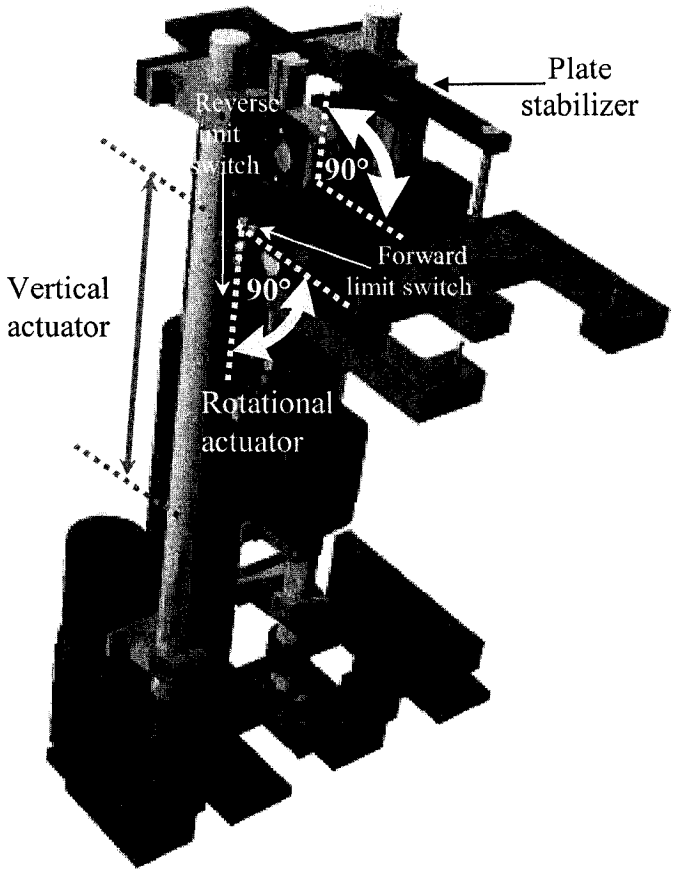

Figure 4.43: Illustration of the transfer platform subsystem illustrating the range of motion between forward and reverse limit switches of the vertical and rotational actuators as well as the mechanical limits of the plate stabilizer. The rotational actuator and plate stabilizer move ~90° between their stowed and active positions, and the vertical actuator repositions the core mechanism with the full 8 in. stroke length of its linear actuator.

Figures 4.45 shows the assembly, which is composed of four interconnected sub-brackets for adjustment and stabilization of the actuator. The slider-crank mechanism [238-242], in Figure 4.45B, permits stable translation of linear motion into the rotational motion necessary to position the platform in its stowed or active positions. Limit switches control power to the actuator and determine the end-of-travel for both positions.

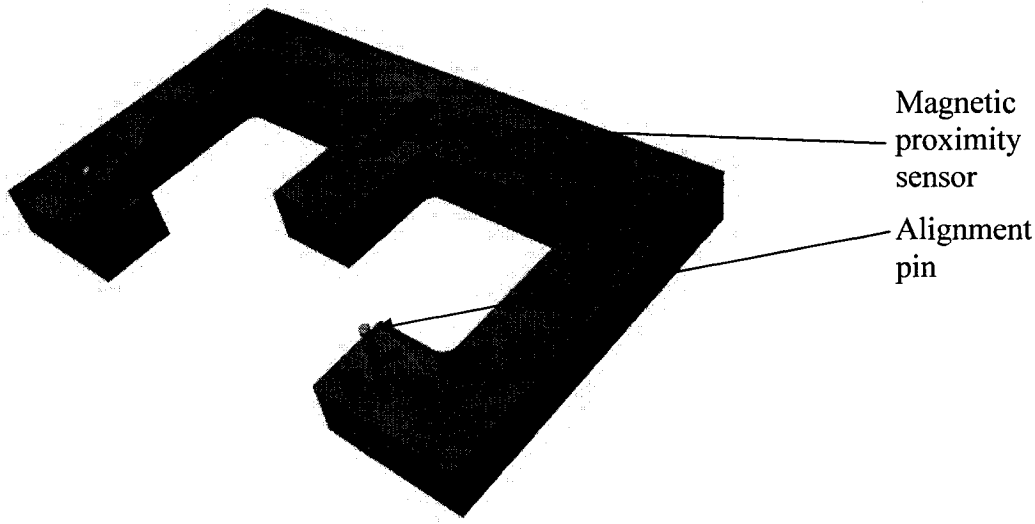

Figure 4.44: Illustration of the positioning platform and components to stabilize and detect the core mechanism on its surface. The electromagnetic transfer arm can pass through positioning platform to leave the core mechanism on the surface (transfer). Two 1 in. x 1/8" diameter steel alignment pins stabilized the core mechanism and a magnetic proximity sensor signals its presence to the robot controller.

(3) Vertical actuator. Figure 4.46 shows the assembly for vertical positioning of the transfer platform. An 8 in. stroke length linear actuator directs vertical motion of the rotational actuator and positioning platform along a linear motion guide. Brackets stabilize motion with the rotational actuator sub-assembly and end-of-travel limit switches control power to the actuator.

(4) Plate stabilizer. Figure 4.47 shows the solenoid driven assembly that immobilizes the core mechanism on the positioning platform during transfer. It has two principle sub-assemblies:

(i) A rotational solenoid actuator that positions the compression solenoid into its active state.

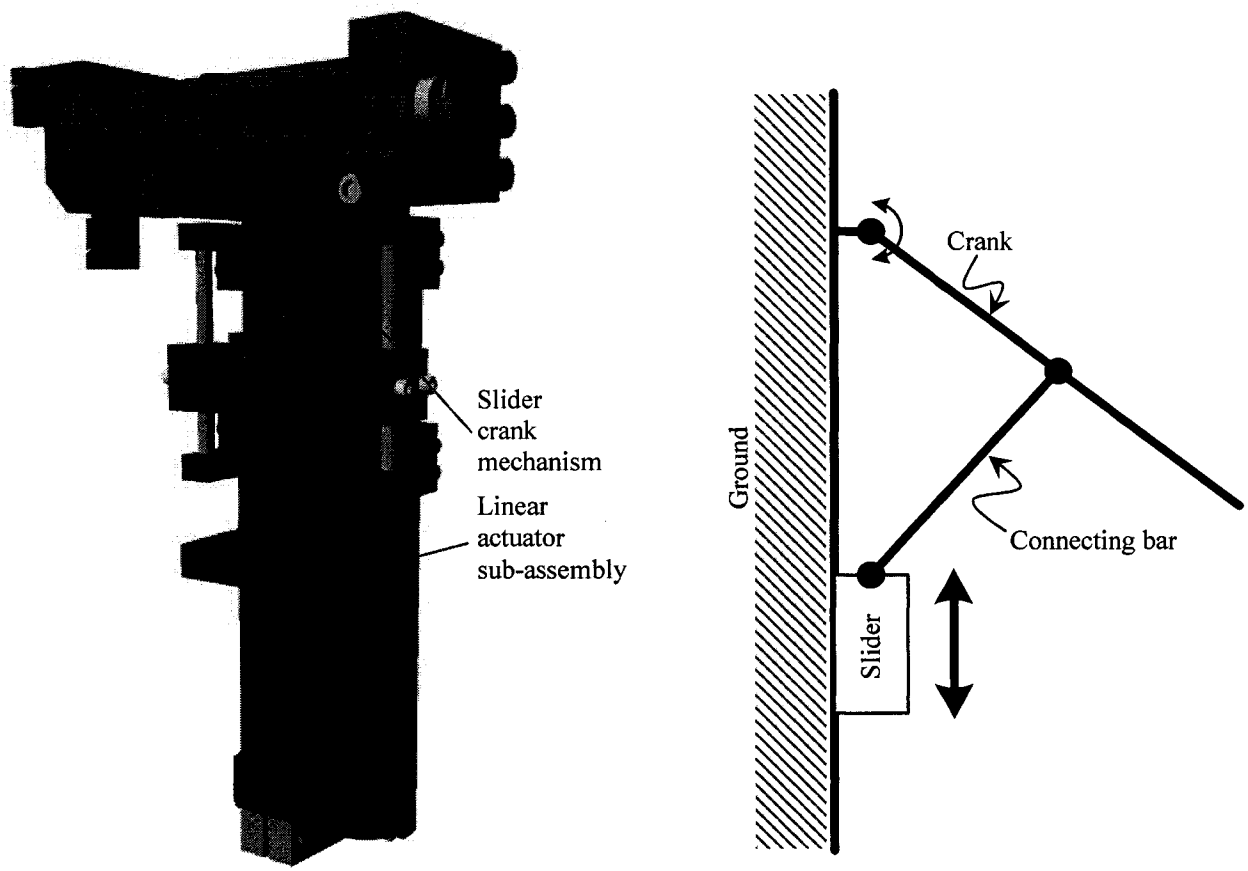

Figures 4.45: (A) Illustration of the transfer platform rotational actuator and (B) schematic illustration of a typical slider-crank mechanism. A slider-crank mechanism is a four-bar linkage with 3 revolute joints and one slider joint that converts rotary motion into reciprocating linear motion, or *vise versa*. The ground link is the "base" of the machine that connects the axis of rotation of the crank with the surface upon which the slider moves. A 2 in. stroke electromechanical linear actuator with 75 lb. a load capacity provides the force for the slider and the static torque to support the core mechanism during transfer and vertical repositioning.

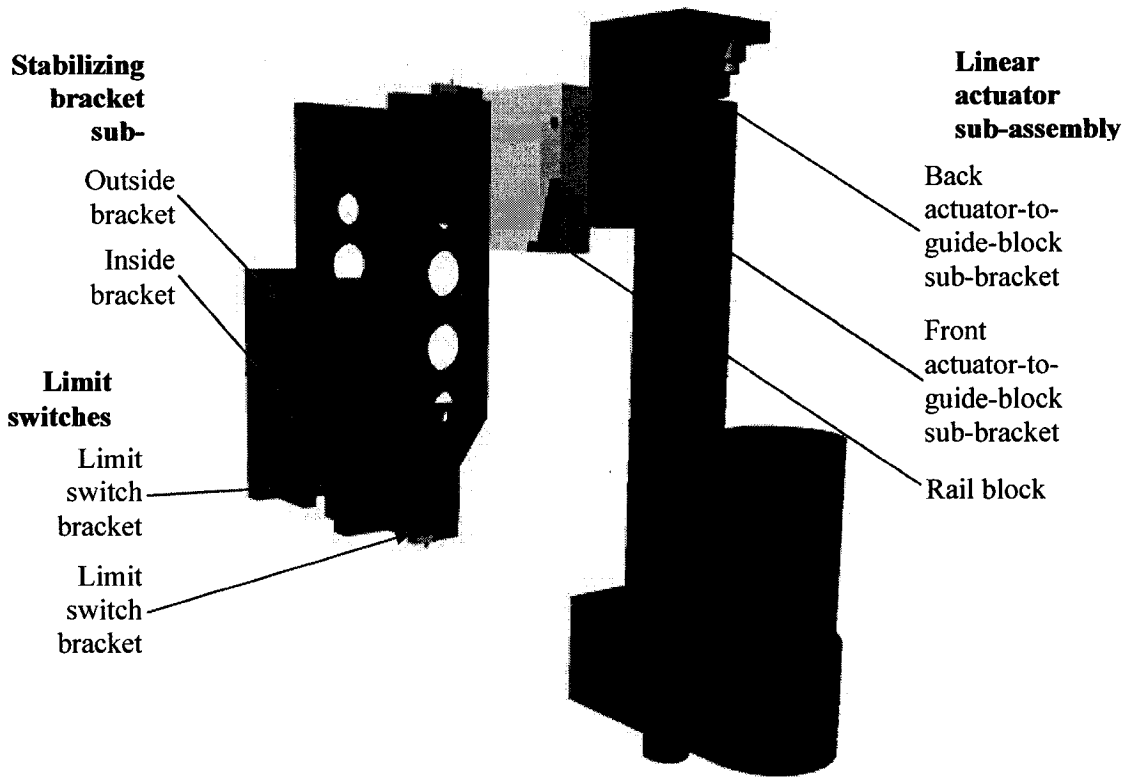

Figure 4.45: Illustration of the vertical actuator. The actuator moves and stabilizes the rotational actuator/positioning platform on a linear rail to retrieve the inverted core mechanism at it top position and present it back to the electromagnetic transfer arm after it is lowered.

(ii) A compression solenoid actuator that forces the stabilizer arm onto the core mechanism holding it in place.

(5) Mounting bracket. An adjustable base stabilizes transfer platform and a sub-assembly of vertical brackets permit adjustment with the range of motion of the remaining positioning subsystems.

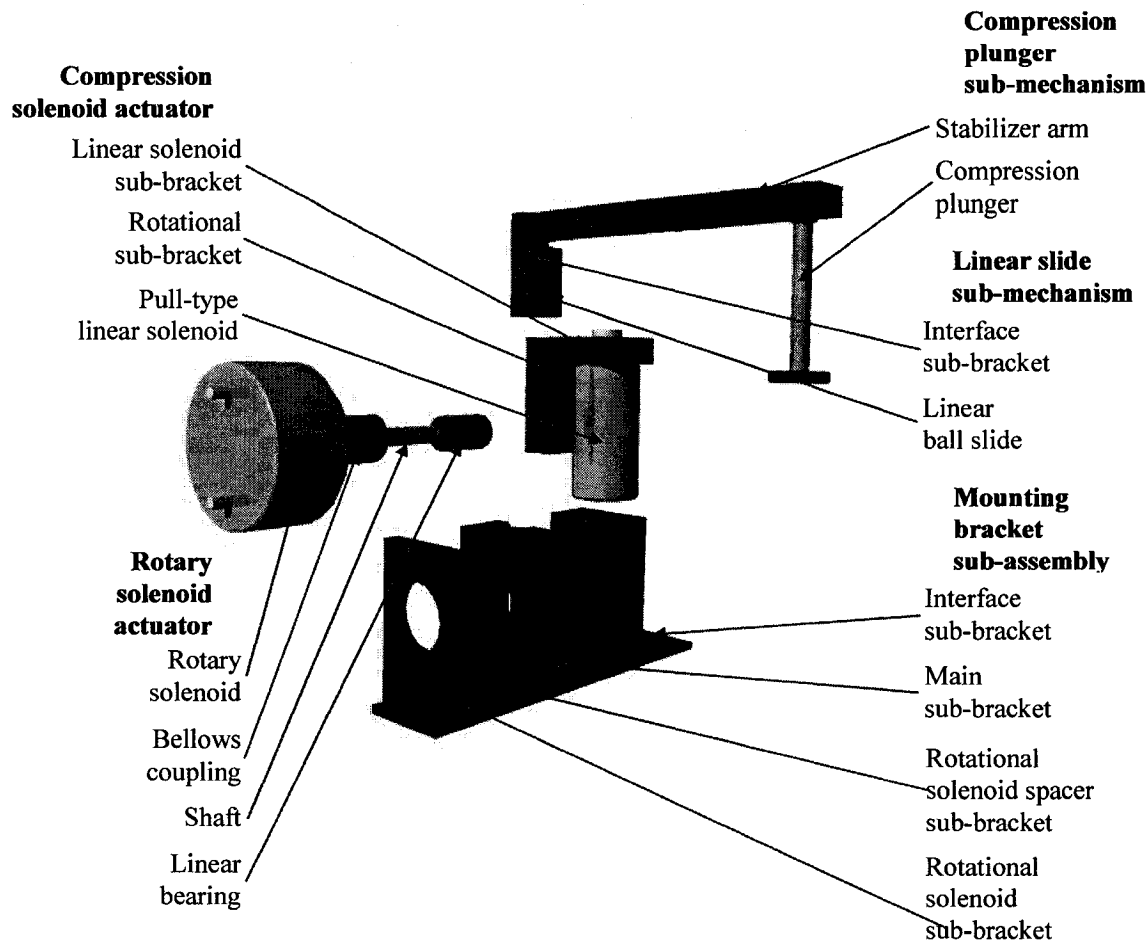

Figure 4.47: Illustration of the plate stabilizer showing the components for rotation of the plunger and compression of the plunger onto the core mechanism. Both solenoids are spring loaded to permit automatic retraction for electromagnetic arm clearance as well as stowed positioning when unused.

The transfer platform overcomes the positioning restrictions of the electromagnetic arm and motion control subsystems. Figure 4.48 illustrates its operation. The vertical and rotational actuators first position the platform to receive the core mechanism. Then the electromagnetic transfer arm, holding the inverted core mechanism, descends into the platform, and passes through it, leaving the plates behind. The plate stabilizer secures the core mechanism onto the platform surface and, when the plates are

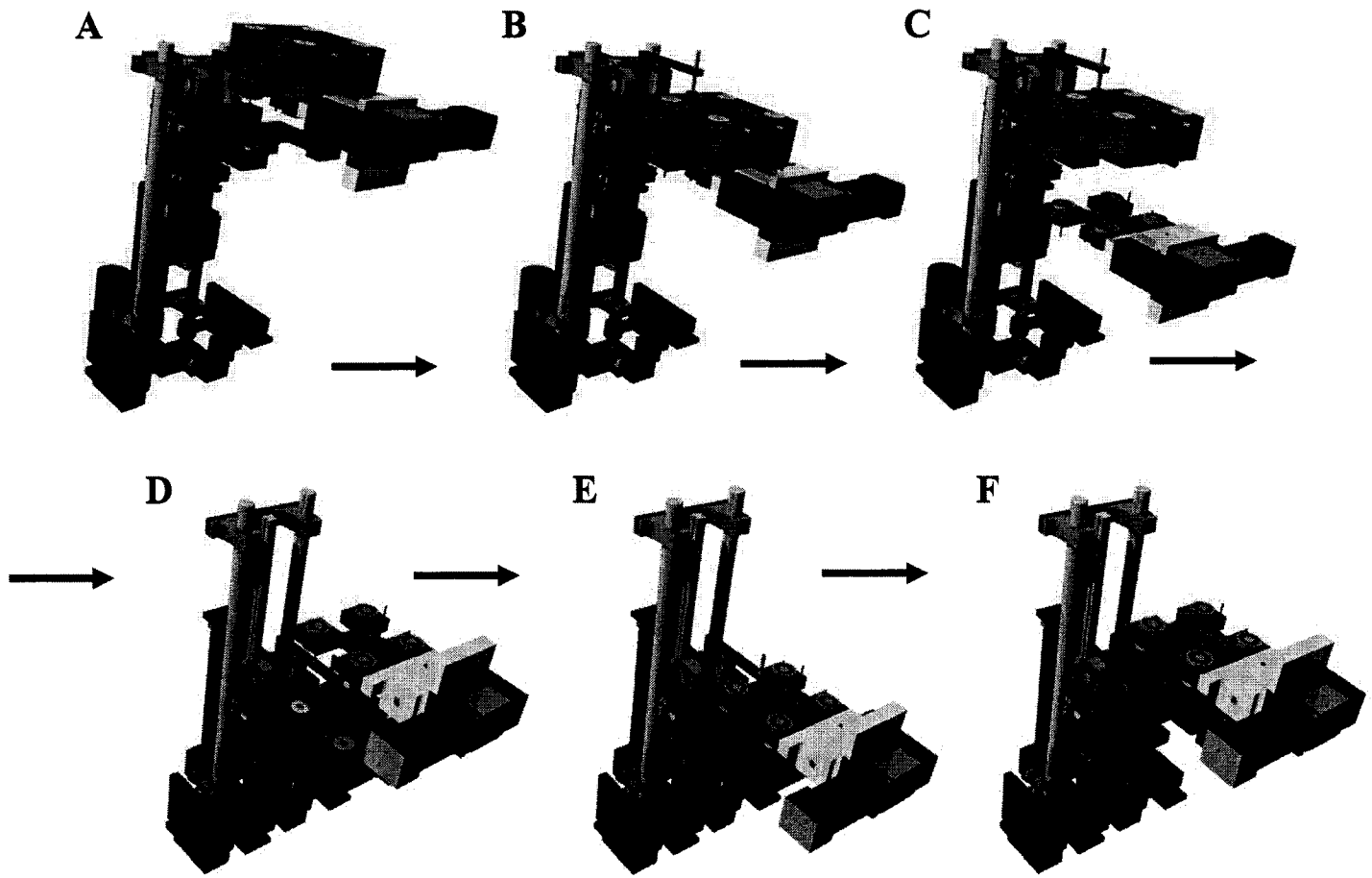

Figures 4.48: Operation of the transfer platform for core mechanism repositioning during inversion. (A) The transfer platform is raised and extended for interaction with the approaching electromagnetic transfer arm and coupled core mechanism. (B) The arm positions the delivery configuration on the transfer platform and the plate stabilizer actuates for compression. (C) The arm releases the delivery configuration and descends for rotation. (D) The transfer platform descends and the rotated arm positions to couple the core mechanism. (E) The arm couples the core mechanism. (F) The arm removes the core mechanism from the transfer platform.

retrieved by the electromagnetic transfer arm, all actuators automatically retract back to stowed positions.

5 EMPOP Robot Electronics

5.1 Overview

This chapter describes the electronics of the EMPOP robot. It first provides an overview of the architecture of the control electronics and power supply systems architecture and describes the robot controller and its input/output capabilities. The remainder of the chapter provides more detailed description of the electronics of the core mechanism and its seven support subsystems. All specific details of electrical construction of the robot are located in the EMPOP robot manual [171].

5.2 Overview of the EMPOP Robot Electronics

Figure 5.1 illustrates the arrangement of the EMPOP robot electronics system and the directions of connectivity and communication between its subdivisions. At the center of the system is the automation control electronics system, which contains the robot controller and interface modules for the core mechanism and seven support subsystems. The surrounding subdivisions are: (1) a host computer that sends information to, and receives status updates, from the robot controller, (2) a power supply subsystem that provides power to the control electronics and electromechanical actuators, and (3) the robot that receives power and control signals from the control modules and sends status input to the robot controller *via* feedback devices.

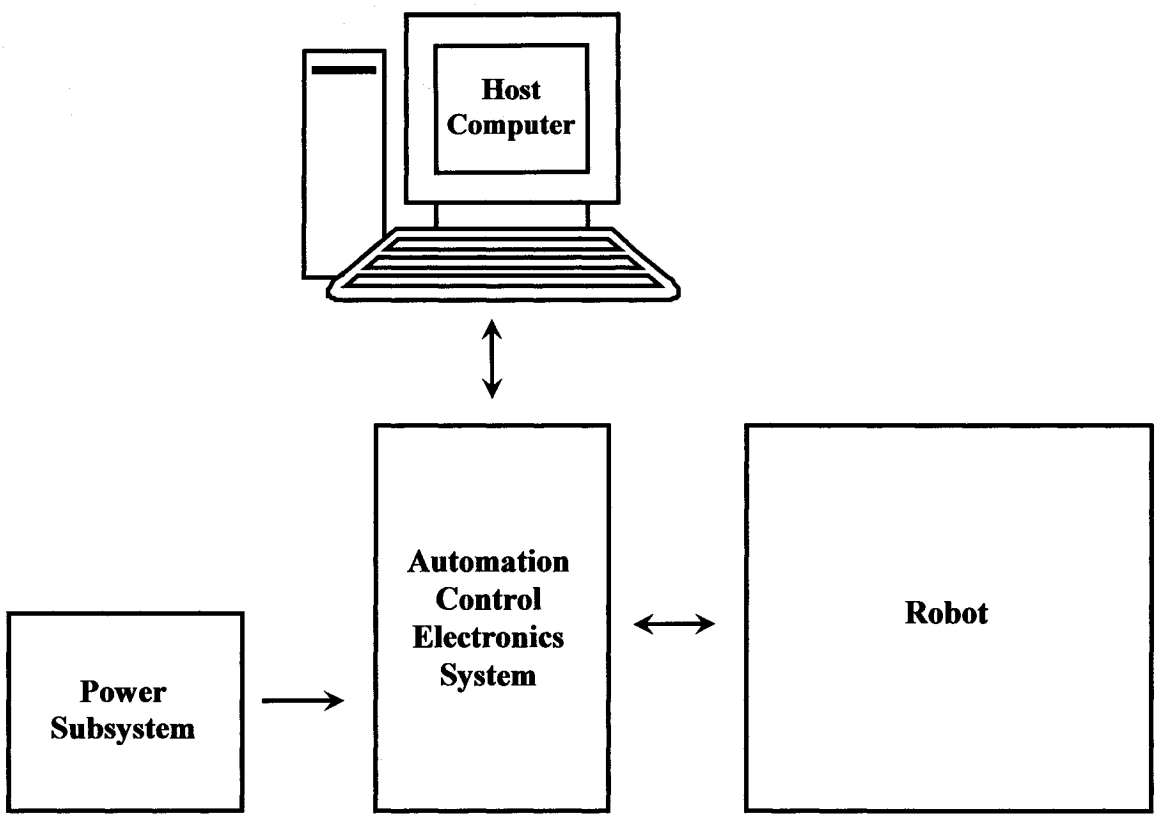

Figure 5.1: Generalized arrangement of the EMPOP robot electronics system, showing the directions of connectivity and communication between the automation control electronics system and the surrounding subdivisions.

5.2.1 Automation Control Electronics System

The automation control electronics system is modularized to simplify development of the prototype (i.e. testing, troubleshooting, repair and modification). All control modules and components are consolidated in one centralized enclosure that permits interconnection of all control electronics and power with both the robot controller and the robot. Figure 5.2 shows the automation control electronics system in its enclosure and Figure 5.3 further illustrate how the control components are arranged in three principle groups for: (1) motion control power, (2) robot control and (3) subcomponent control and interfacing.

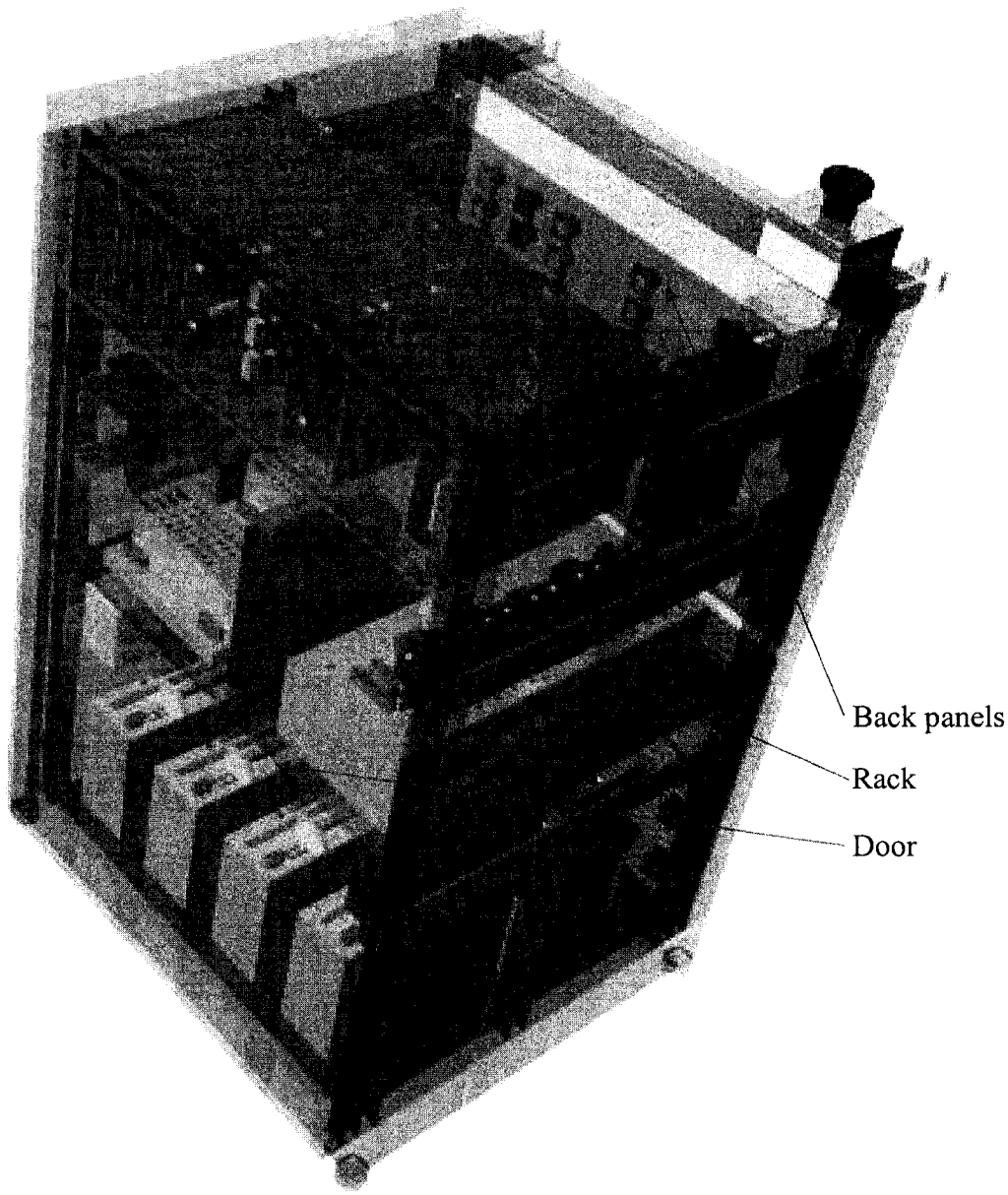

Figure 5.2: Illustration of the arrangement of the automation control electronics system in its enclosure. The enclosure is a 28 in. table-top rack with standard 19 in. mounting locations to hold the control components. The rack is also equipped with a hinged panel rail door and modular back panels for cable interfaces, cooling fans and ventilation.

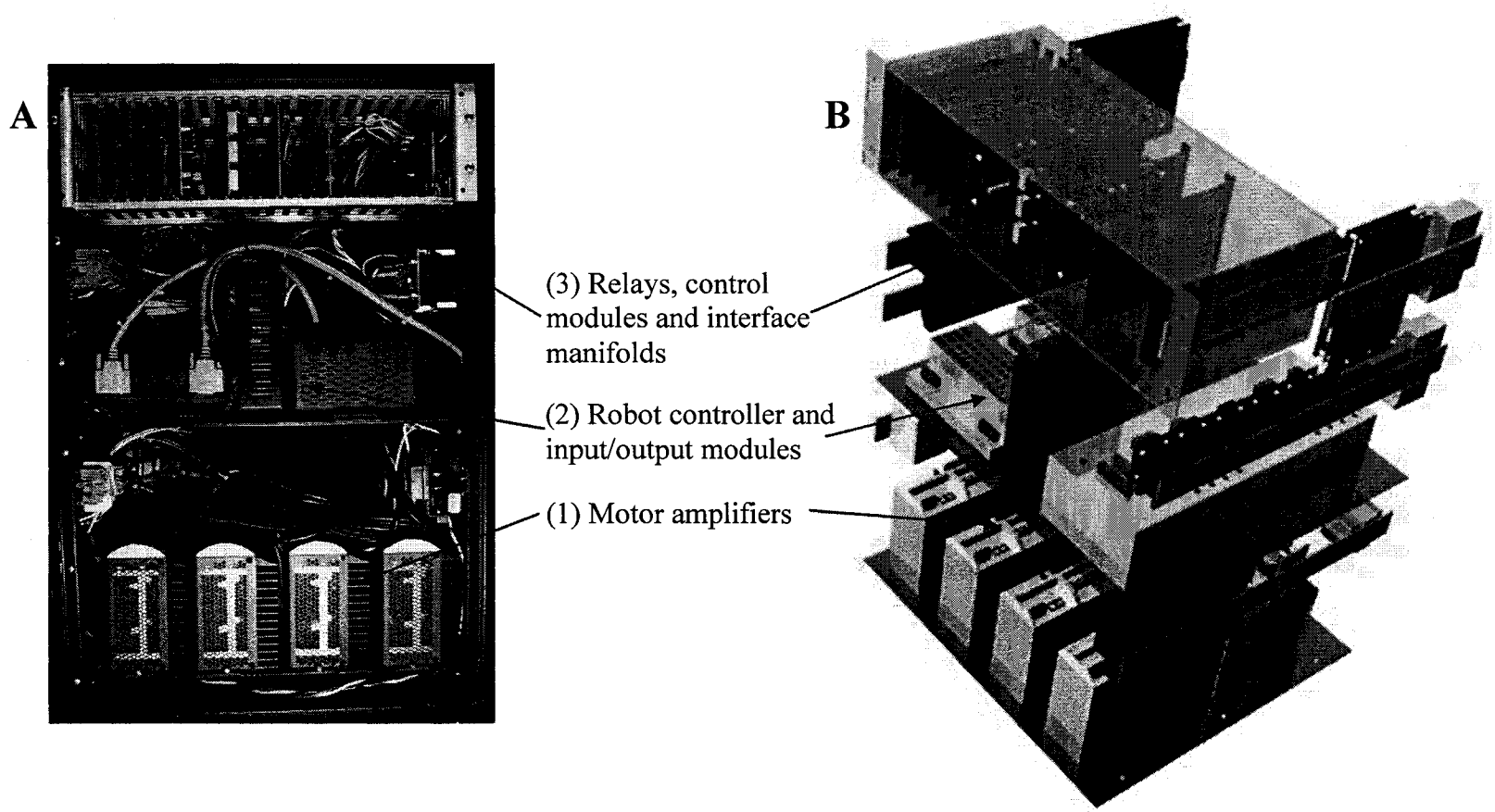

Figure 5.3: Illustrations of the three component groups of the automation control electronics system shown in (A) a front view photograph and (B) a 3D rendering. The organization simplifies interconnection to the centrally located controller and the cable interfaces on the rear surface of the enclosure.

(1) The motion control power group, shown in Figure 5.4, is composed of: (i) four Cartesian axis (X, X', Y, Z) motor amplifiers, (ii) two rotational axis (θ and ϕ) motor amplifiers, (iii) two stepper pump axis motor amplifiers, (iv) a 110 VAC power distribution terminal block and (v) power fuses for each axis amplifier.

(2) Figure 5.5 shows the robot control group, comprising: (i) the robot controller, (ii) three extended input/output (I/O) modules, (iii) a power supply, and (iv) a bank of limit sensor screw terminals.

(3) The subcomponent control and interfacing group in Figure 5.6, is comprised of:

(i) A card cage sub-rack, shown in Figure 5.7, occupies most of the enclosure's upper level and contains: (A) five banks of low signal relays, which permit digital actuation of all direct-acting solenoid valves, solenoids and electromagnets by connection with 12 VDC power; (B) proportional solenoid drivers; (C) DC gear pump controllers; (D) plate electromagnet decoupling controllers; (E) arm electromagnet controllers; and (F) four DC input-AC output solid state relays for AC-isolated actuation of components operating with 110 VAC [269].

(ii) The remaining relays and control modules, illustrated in Figure 5.8, are mounted along the enclosure walls in six groups: (A) a set of two high-power relays and corresponding fuses for control of the transfer platform linear actuators; (B) a DC input-DC output solid state relay that interfaces power to the plate electromagnet decoupling controller; (C) a bank of five TEC

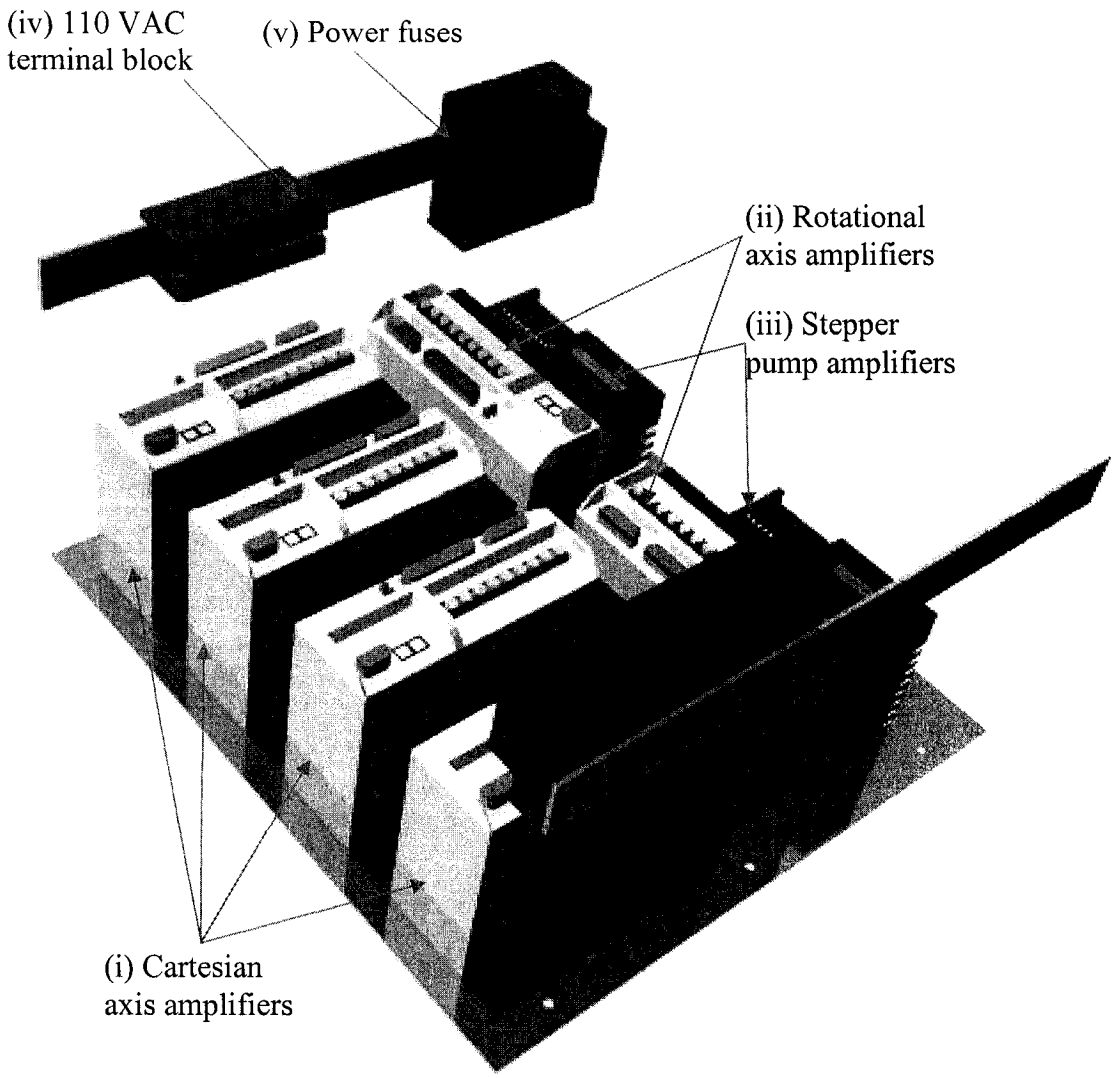

Figure 5.4: Illustration of the motion control power group. Amplifiers are arranged in banks for Cartesian, rotational and stepper pump (virtual) axes. The 110 VAC power is distributed through a distribution terminal block, comprised of a bank of DIN rail-mounted, 5 mm screw-clamp modular terminal blocks connected with jumpers into three sets for positive, neutral and ground conductors. The positive and neutral power conductors connect to the amplifiers *via* two banks of power fuses, while a grounding lug connects the enclosure chassis to the 110 VAC ground.

controllers; (D) two temperature transmitters to signal cooling temperatures; (E) a latching relay to power the cooling subsystem; and (F) a 24 VAC step-down transformer to power the temperature transmitters.

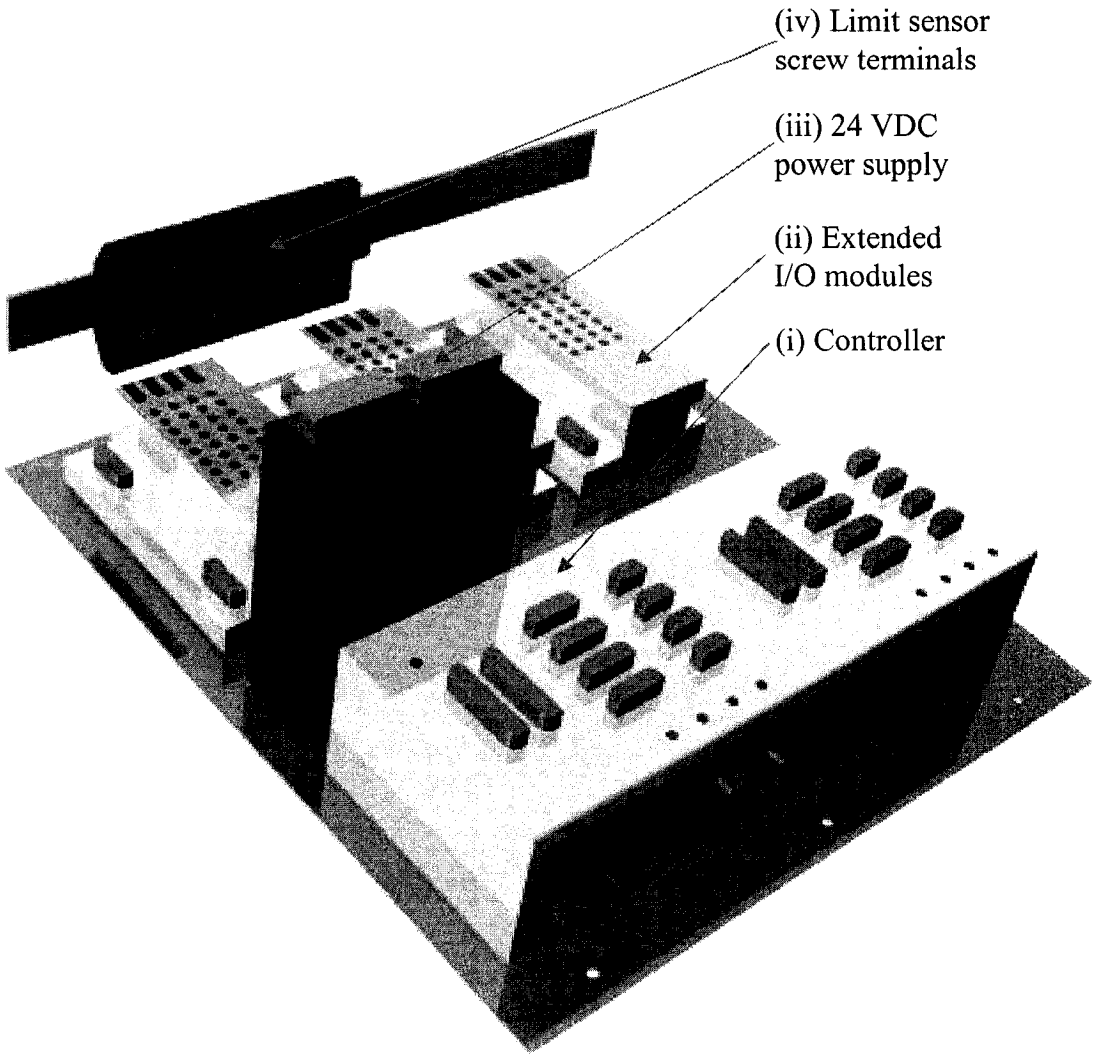

Figure 5.5: Illustration of the robot control group. All robot control components are located in the center of the system to facilitate interfacing with components above and below as well as for direct connections to the cable interface panel at the rear of the enclosure.

(iii)The enclosure also contains four screw terminals that serve as consolidated interface manifolds for: (A) I/O for the processing reagent handling subsystem panel, (B) I/O for the pneumatic, cleaning and waste management, and cooling subsystems, (C) DC power distribution and (D) high power lines to TEC controllers.

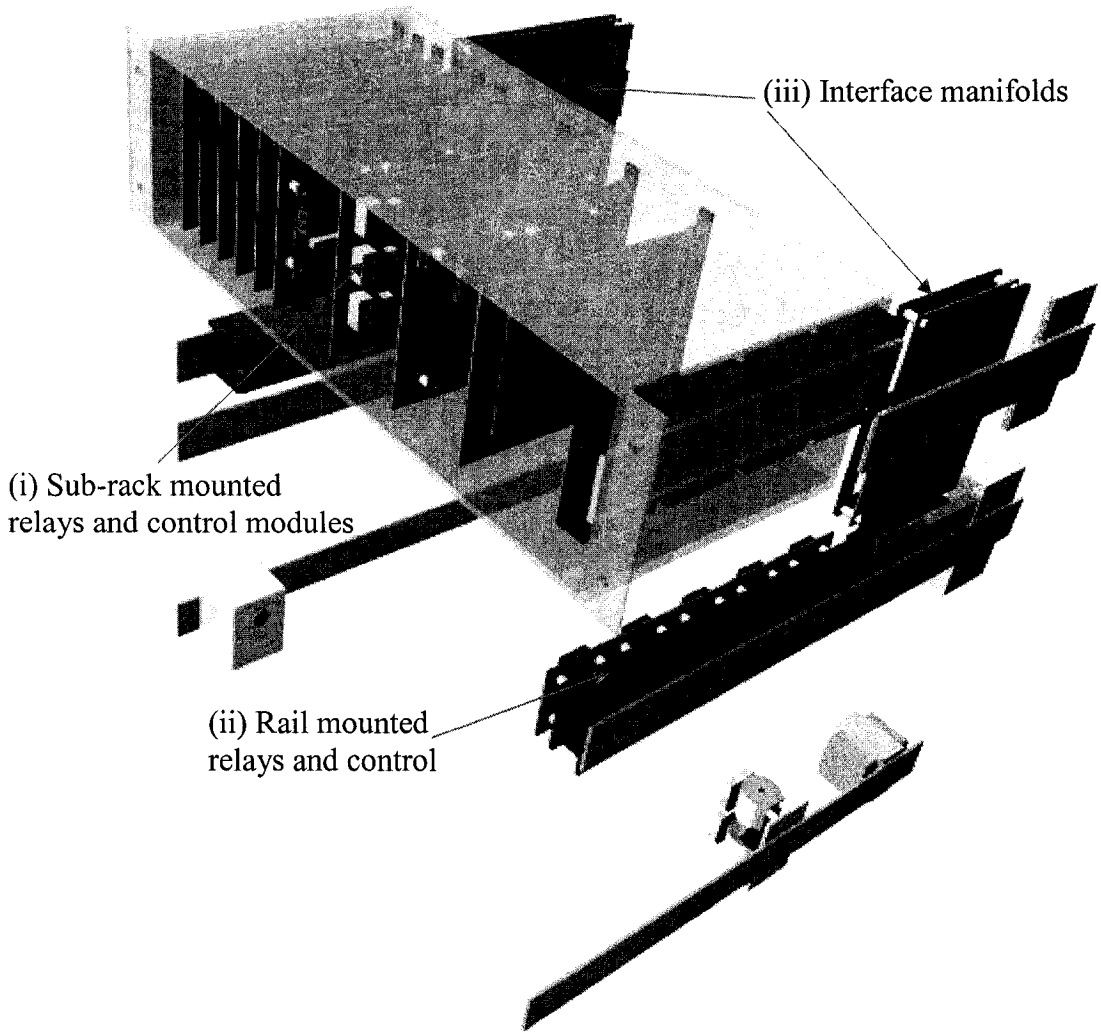

Figure 5.6: Illustration of the subcomponent control and interfacing group. The group is comprised of relays, control modules and consolidated cable interfaces for all robot subcomponents (except those from the motion control subsystem).

The back surface of the automation control enclosure, illustrated in Figures 5.9, is composed of modular panels for enclosure cooling and cable interfacing.

System cooling is provided by a 5.25 in. fan panel fitted with two 110 VAC 80 mm sq. tubeaxial fans, controlled by a thermostat located inside the enclosure. Velcro strap cable organizing panels and steel cable rings secure and arrange all cables.

Clearance space between panels permits ventilation and cable access to the three consolidated screw terminal interface manifolds.

All robot components not accommodated on the screw terminal interface manifolds connect to the back surface of the automation control enclosure *via* connector panels for: (1) AC actuated components and (2) DC actuated components.

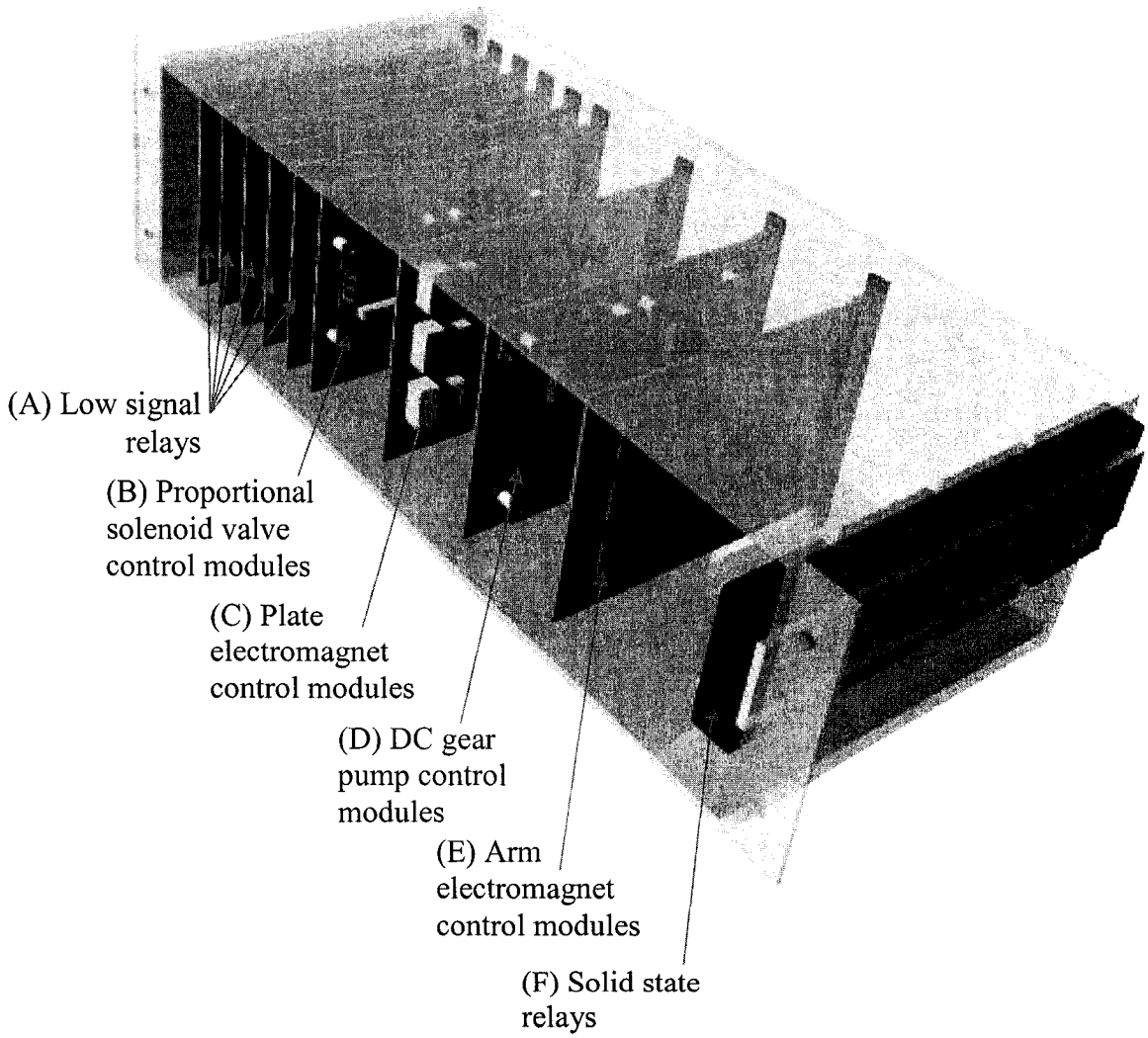

Figure 5.7: Illustration of the card cage sub-rack. The rack consolidates most relays and control modules in accessible bank for system organization. The arrangement also makes the components accessible for testing, troubleshooting and repair.

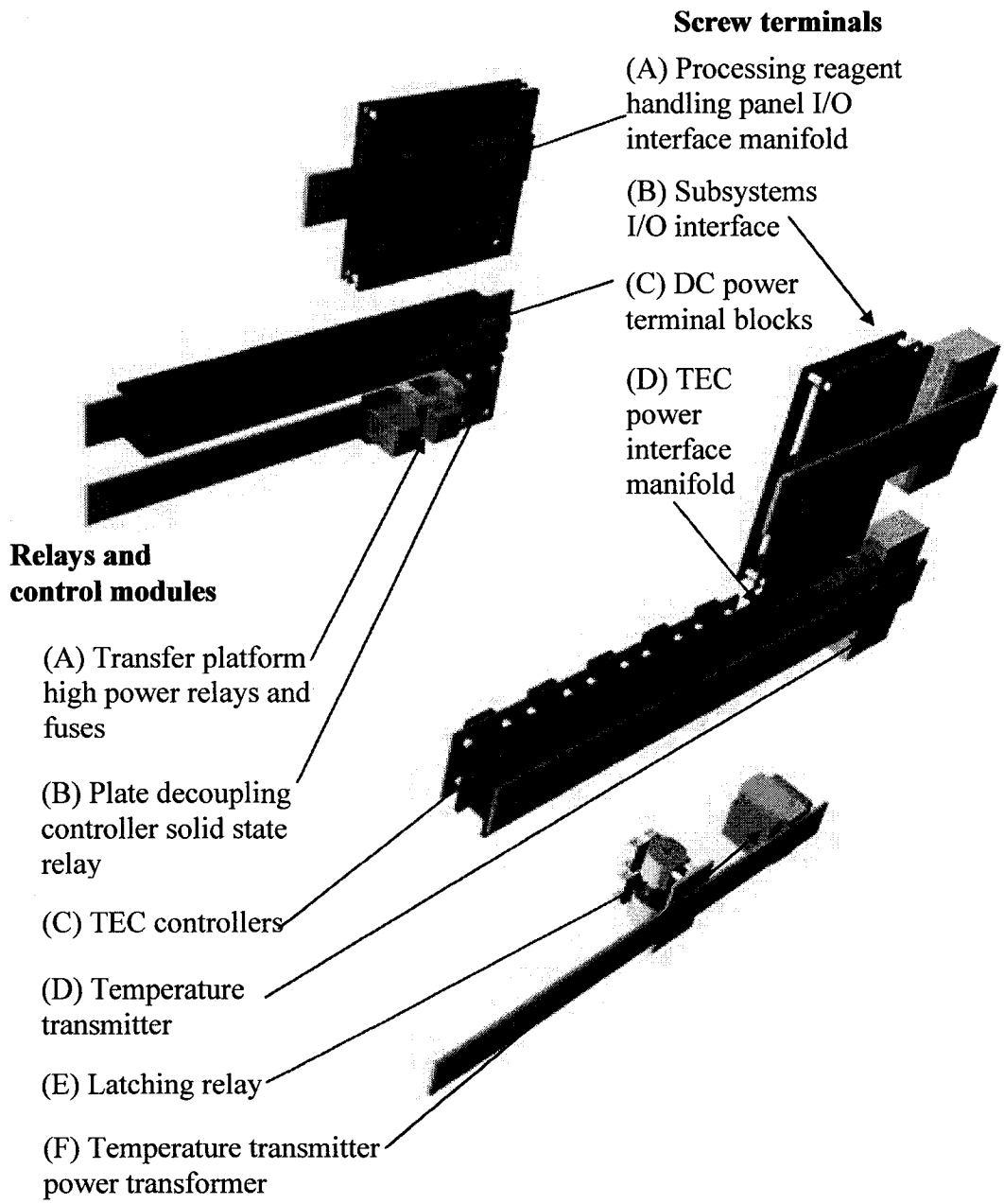

Figure 5.8: Illustration of the rail mounted relays and interface manifolds. The rails are a convenient location for holding large control electronics devices as well as terminal block for distribution of power and consolidated I/O connections.

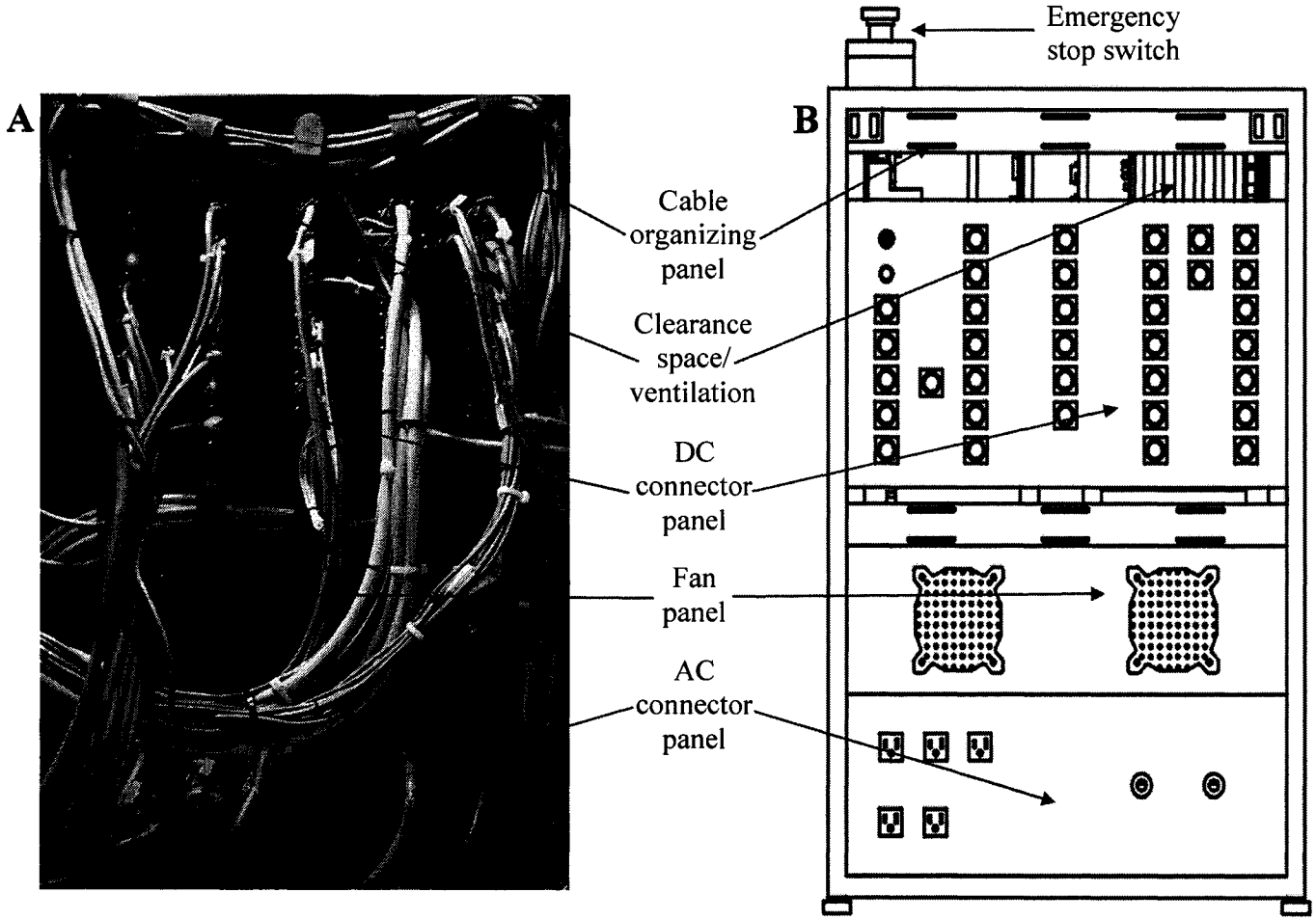

Figure 5.9: Organization of the automation control electronics enclosure rear surface. Two panels support interconnection of cables for feedback devices as well as AC or DC actuated subcomponents. Cables for devices connecting to the interior interface manifolds pass through clearance spaces, which also serve as ventilation for passage of the air forced through the enclosure by the cooling fans.

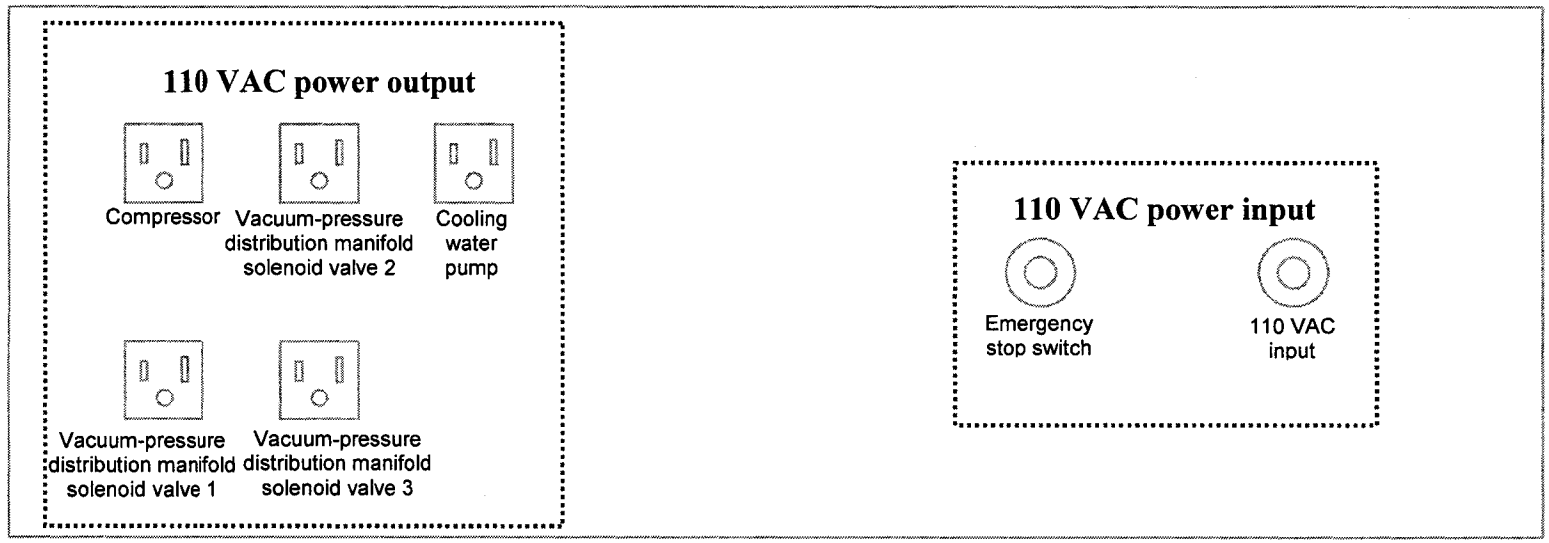

Figure 5.10: Schematic illustration of the automation control enclosure interface panel for robot components actuated with 110 VAC.

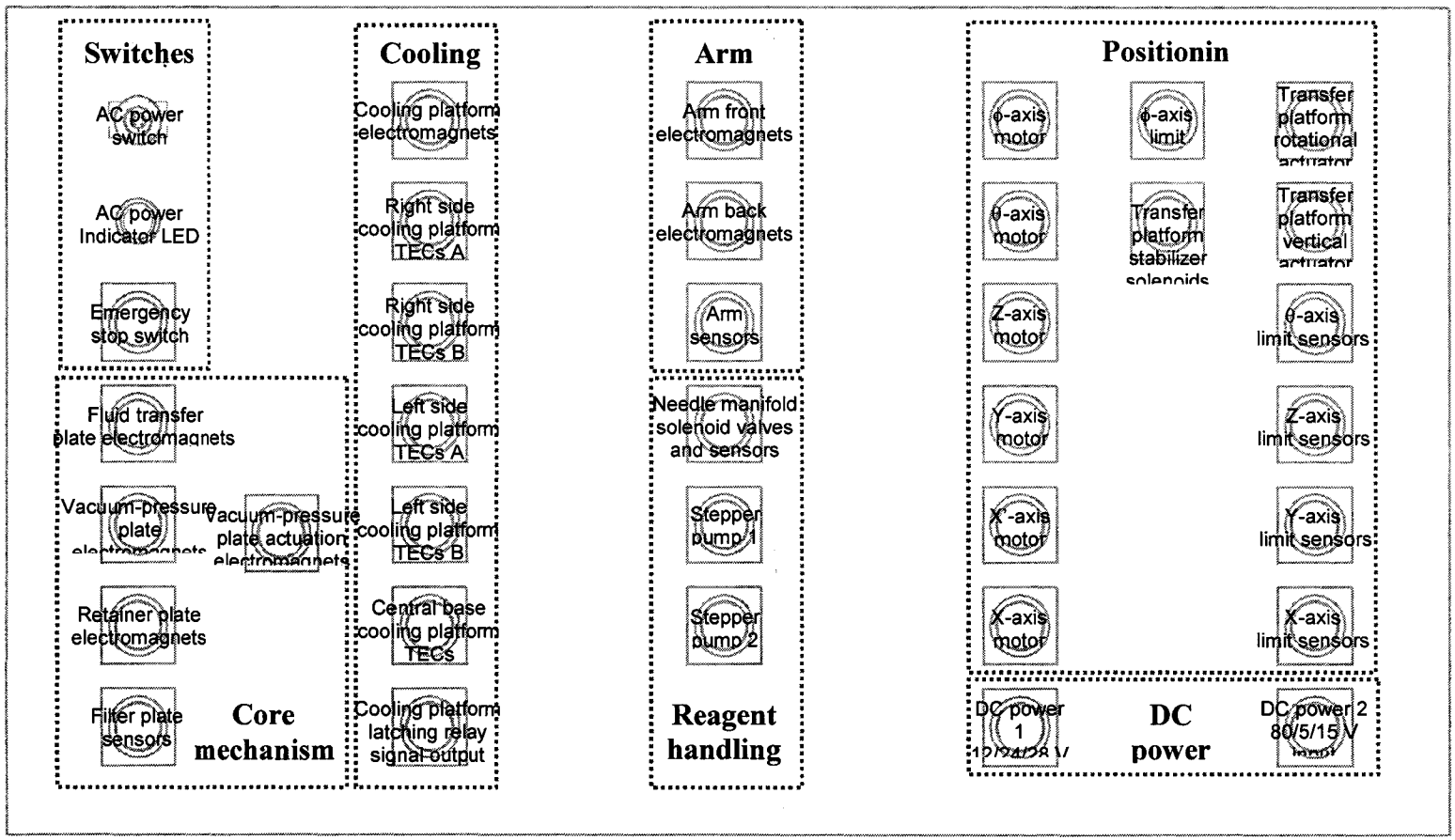

Figure 5.11: Schematic illustration of the automation control electronics enclosure interface panel, showing the organization of connections for robot feedback devices and DC actuated components.

(1) A 7.5 in. panel, illustrated in Figure 5.10, provides the interface for: (i) AC power to the automation control enclosure and (ii) power to AC actuated robot components.

(i) The 110 VAC power cable is equipped with an in-line, enclosure-mounted, emergency stop switch to disable the system (see Figure 5.9B).

(ii) The components powered with 110 VAC interface to the lower AC panel *via* five receptacles for: (i) the pneumatic subsystem compressor, (ii-iv) the solenoid valves of the vacuum-pressure distribution manifold and (v) the cooling water pump.

(2) A 10.5 in. panel, illustrated in Figure 5.11, is the interface for: (i) switches for AC power and the controller emergency stop, (ii) core mechanism power and feedback, (iii) cooling subsystem power and signaling, (iv) electromagnetic arm power and feedback, (v) processing reagent handling power and feedback, (vi) positioning subsystems power and feedback, and (vi) DC power input to the automation control enclosure.

5.2.2 Power Supply Subsystem

Several power supplies were used to support the individual control modules and electromechaical devices of the EMPOP robot. Due to their size, they are organized in a second enclosure that sources power to the automation control components.

The power subsystem enclosure, illustrated in Figure 5.12, holds six DC power supplies for the control electronics and the EMPOP robot components. Figures 5.13A and B show the shelves and DIN rails are used to arrange the power supplies and components on two levels.

(1) The upper level holds two power supplies: (i) an unregulated 12 VDC, 75 A

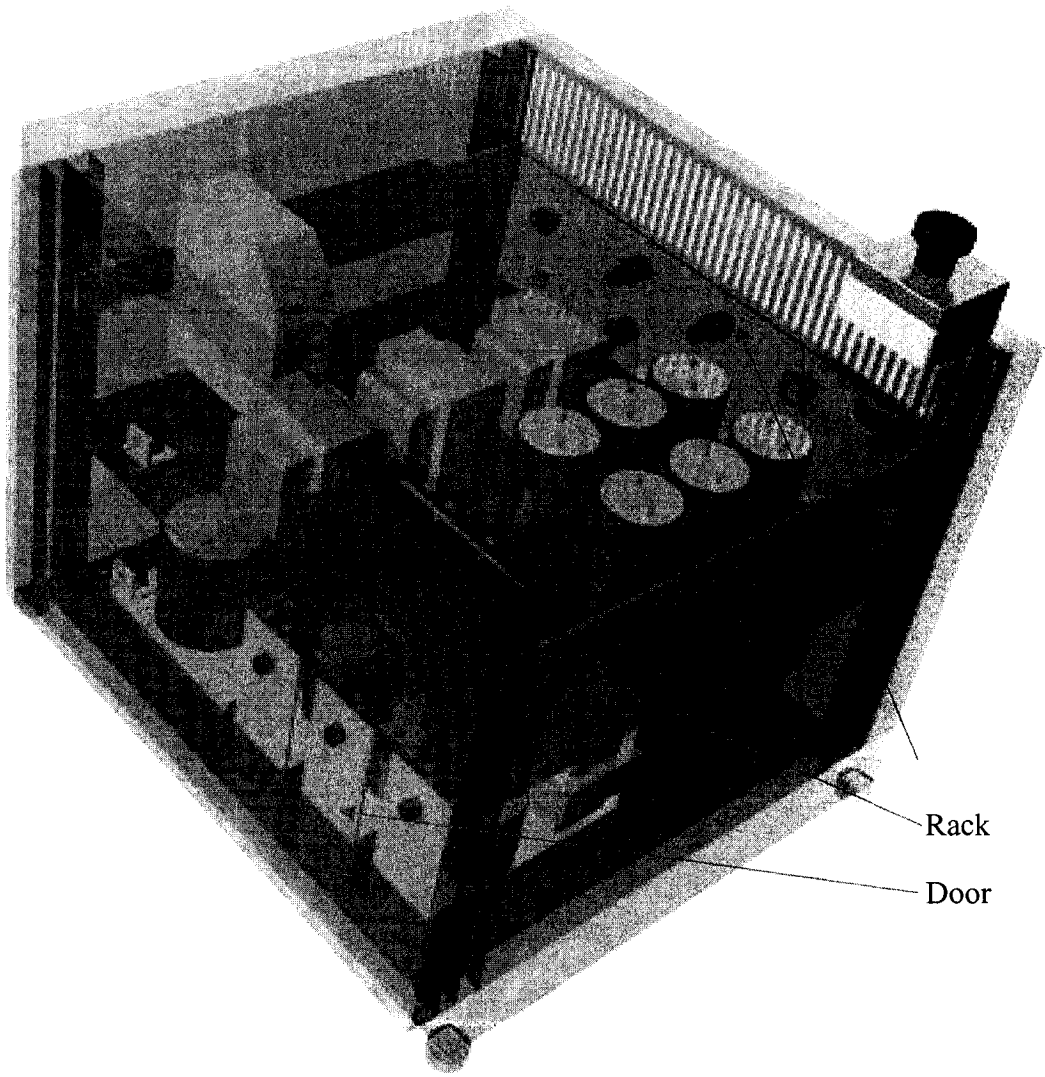

Figure 5.12: Illustration of the arrangement of the power subsystem in its enclosure. The enclosure is a 14 in., table top rack with standard 19 in. mounting locations to hold components. The rack is also equipped with a hinged panel rail door and modular back panels for cable interfaces, cooling fans and ventilation.

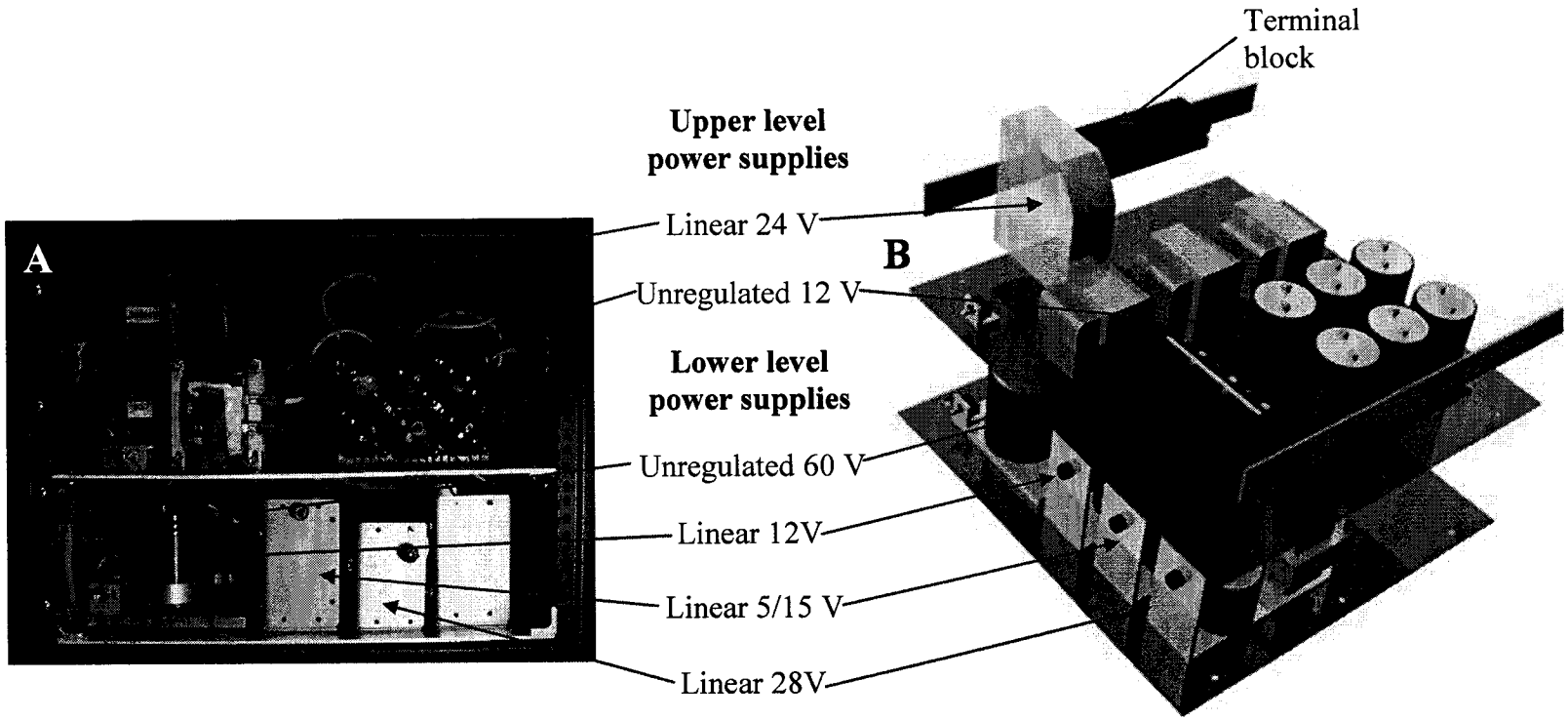

Figure 5.13: Illustrations of the power subsystem organization, shown in (A) a front view photograph and (B) a 3D rendering. All 110 VAC input power is distributed to the power supplies through a terminal block. The enclosure chassis connects to the 110 VAC ground by way of a grounding lug mounted on the enclosure frame and the positive AC power connects to all power supplies *via* time delay fuses. All DC power is directed to the automation control electronics *via* cables extending from the rear surface of the enclosure.

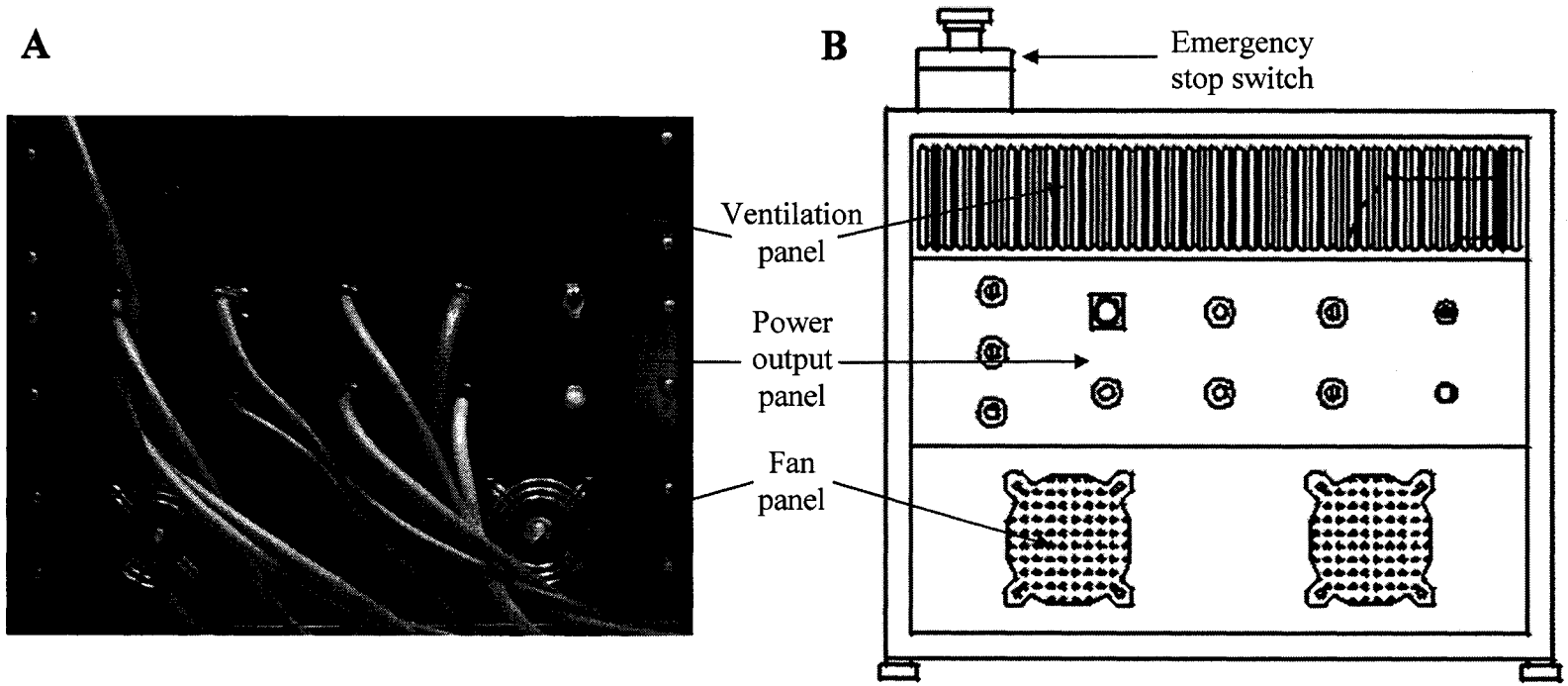

Figure 5.14: Organization of the power subsystem enclosure rear surface, shown in (A) a front view photograph and (B) a 3D rendering. Multi-conductor output cables for DC power are supported on one panel. The cooling arrangement is identical to that of the automation control enclosure; except that a slot panel provides ventilation and prevents access to the interior of the enclosure.

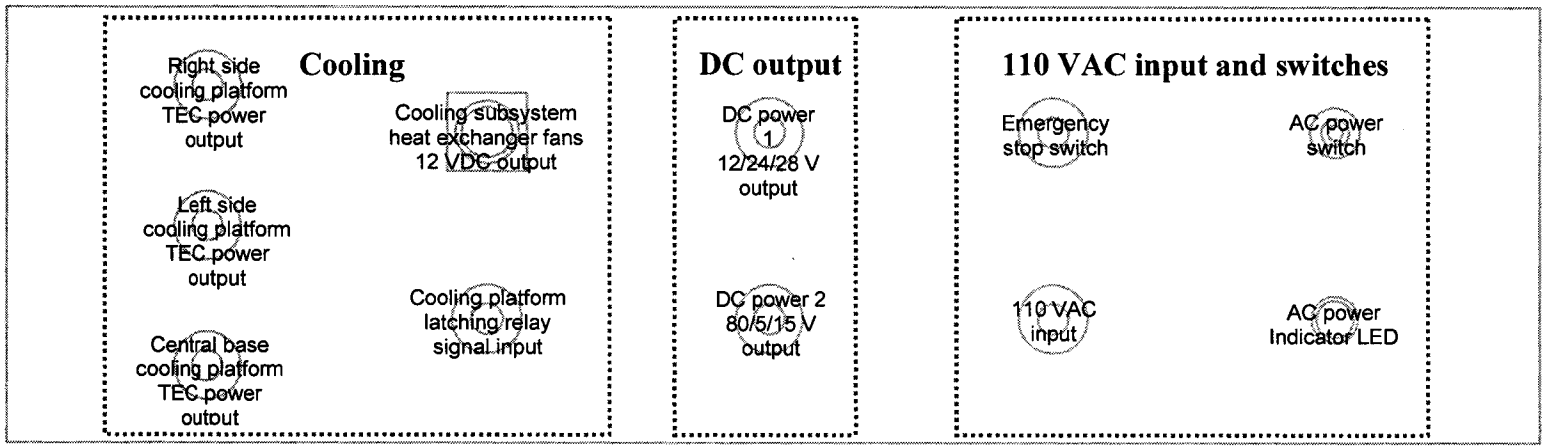

Figure 5.15: Schematic illustration of the power subsystem enclosure output panel, showing support for the cooling subsystem and all DC power directed to the automation control electronics.

power supply for the cooling subsystem TECs and (ii) a 24 VDC, 2.5 A power supply for additional power to the robot controller and extended I/O.

(2) The lower level holds: (i) a 60 VDC, 3.75 A unregulated supply for the plate decoupling electromagnets, (ii) a 12 VDC, 10.2 A linear supply for the direct-acting solenoid valves, solenoids, electromagnets, and gear pumps, (iii) a 5/15 VDC, 2 A supply for the control electronics and pressure transducers and (iv) a 28 VDC, 2 A linear supply for proportional solenoid valves and vacuum transducers.

Figure 5.14 shows the back surface of the power enclosure, which is composed of modular panels for cooling fans, ventilation as well and cable interfacing. A 5.25 in. panel, illustrated in Figure 5.15, is the interface for: (1) cooling subsystem power, (2) DC output power to the automation control system and (3) AC input power and switches.

5.2.3 Robot Controller and Extended I/O

A Compumotor 6K8 controller interfaced with three EVM32-II extended I/O modules [261] controls the robot in real time. The controller and I/O modules, shown schematically in Figure 5.16, support the 6 servo and 2 stepper motor driven axes (see Section 5.6.1) as well as 96 channels of digital and analog I/O. The three I/O modules hold 12 boards that support the robot components. Each module holds four boards each supporting 8 channels of either: (1) digital input, (2) digital output, (3) analog input or (4) analog output.

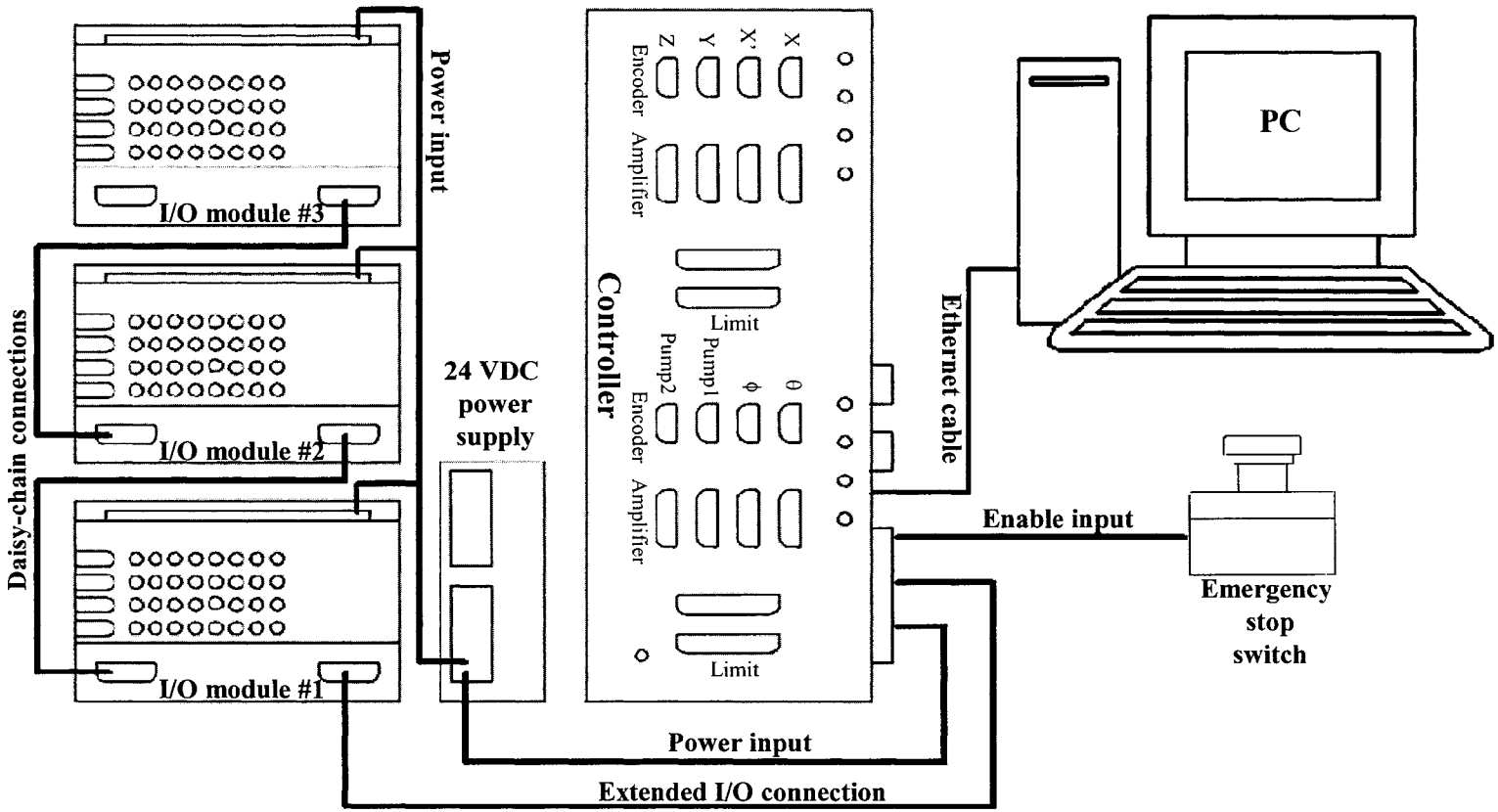

Figure 5.16: Schematic illustration of the robot controller connections to the subdivisions of the robot control group. The extended I/O modules connect to the controller *via* a single cable to the first I/O module; other modules connect in a daisy-chain arrangement. All I/O connections are made to the screw terminals of the modules. All motion control amplifier, encoder and limit sensor interfaces are located on the top surface of the controller a PC equipped with a 10/100 Mbps network card interfaces to the controller *via* an Ethernet cross-over cable. To disrupt operation of the motion control capacity of the controller, the enable input connects to ground *via* two serially connected emergency stop switches.

(1) Digital inputs (24 channels) operate within 0-24 VDC with low and high voltage switching levels at ≤1/3 V+ and ≥2/3 V+ and a maximum sampling rate of 500 Hz (limited by the update rate of the 6K8 controller).

(2) Digital outputs (56 channels) operate within 0-24 VDC range and provide a maximum of 300 mA of current per channel.

(3) Analog inputs (8 channels) use a 12 bit A/D converter over a 0 to 10 VDC and a maximum sampling rate of 500 Hz (limited by the update rate of the 6K8 controller).

(4) Analog outputs (8 channels) use a 10 bit D/A converter over a 0 to 10 VDC unipolar voltage range.

All subcomponents and control modules are digitally actuated unless indicated; only the proportional solenoid valves (see Section 5.5.2) are actuated by analog output signals. Four pressure transducers (see Section 5.5.2) and two temperature transmitters (see Section 5.3) form the analog inputs. The signals are averaged in the robots control software (see Section 6.4.3) to remove large, rapid fluctuations [256]. The digital inputs come from the robot's magnetic proximity sensors and stepper pump home sensors. These are either digital high (24 VDC) or low (0 VDC) signals, and are not filtered.

5.3 Core Mechanism

Due to its role as the focus for sample processing, the core mechanism is a special case for control electronics, because it incorporates components used for cooling, fluid

handling, and positioning subsystems. The electronic components are used for: (1) proximity and temperature sensing, (2) vacuum-pressure plate actuation, and (3) plate decoupling.

(1) The core mechanism employs two sensor systems embedded in the filter plate for (i) plate-to-plate proximity sensing and (ii) temperature sensing.

(i) The two magnetic proximity sensors [256-258, 263-265], located on the top and bottom surfaces of the filter plate are used to monitor plate coupling and signal to the robot controller by way of two digital input channels. As illustrated in Figure 5.17, the sensors are actuated by plate-to-plate proximity sensor actuation magnets, located in the top and bottom surfaces of the other plates of the core mechanism. This method of plate detection is simple and reliable. Similar magnetic proximity sensors are used on the plate-interaction surfaces of the cooling platform, electromagnetic transfer arm, and transfer platform. The method is also used for retraction/collision detection on the dispensing and aspiration needle manifolds.

(ii) A miniature platinum resistance temperature detector (RTD) [256-258, 263-265], embedded in the bottom surface of the filter plate, reports the temperature of the cooled core mechanism to the robot controller by way of a temperature transmitter (see Figure 5.18). The temperature transmitter converts the signal from the RTD into a proportional 0 to +10 VDC analog signal that is read as an analog input by the controller.

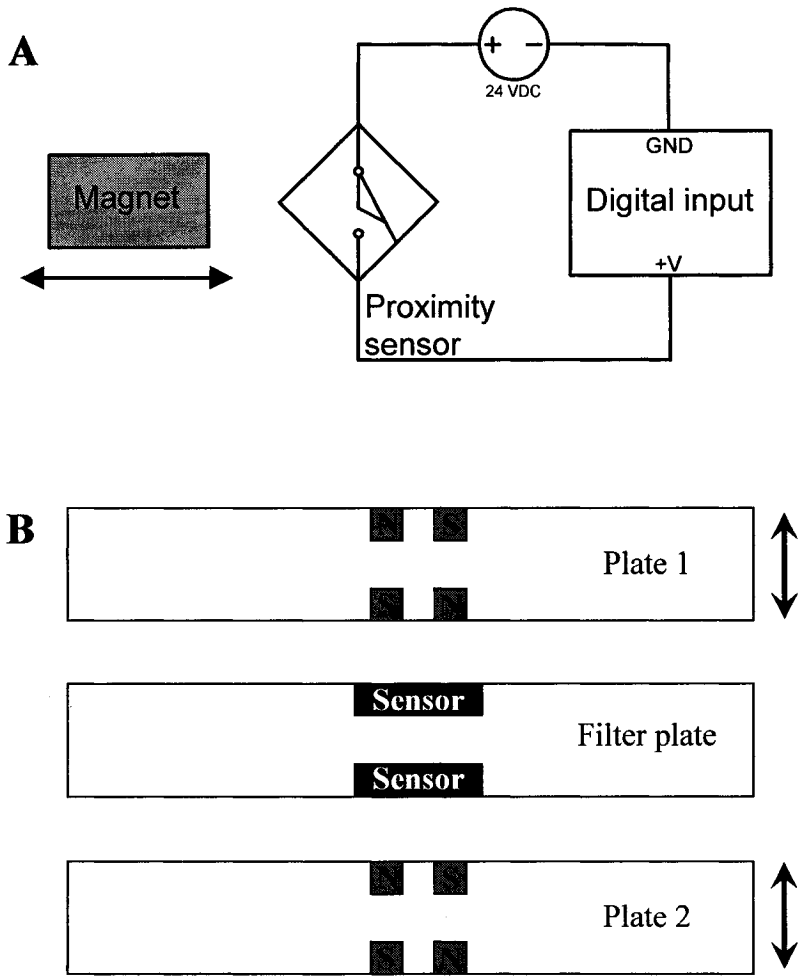

Figure 5.17: Schematic illustrations of the magnetic proximity sensing method used to detect core mechanism plate coupling and decoupling. (A) The sensor is a normally–open magnetic reed switch [263-265]. When the magnetic field is applied, the contacts close on the sensors, allowing plate-to-plate proximity detection to read as a digital input on the controller I/O. (B) The system of filter plate proximity sensors and the actuation magnets on all other plates permits detection and monitoring of core mechanism plate interactions. The same method is used to detect plate interactions and needle manifold collisions in five of the subsystems.

(2) The stopper mechanism retraction electromagnets of the vacuum-pressure plate (see Section 4.2.4) are digitally actuated by way of a low signal relay.

(3) Plate decoupling is actuated by applying a 60 VDC pulse to the four plate decoupling electromagnets. The resulting magnetic fields have the same polarity as the four plate-coupling, permanent magnets of the filter plate and so mutual repulsion produces a gap between the magnetic surfaces (see Figure 4.4B) to allow the electromagnetic transfer arm to separate the plates (see Figure 4.17).

Figure 5.19 show a schematic of the plate electromagnet decoupling controller. A digital signal triggers a decoupling pulse within the circuit, and power is directed to the electromagnets from the 60 VDC unregulated power

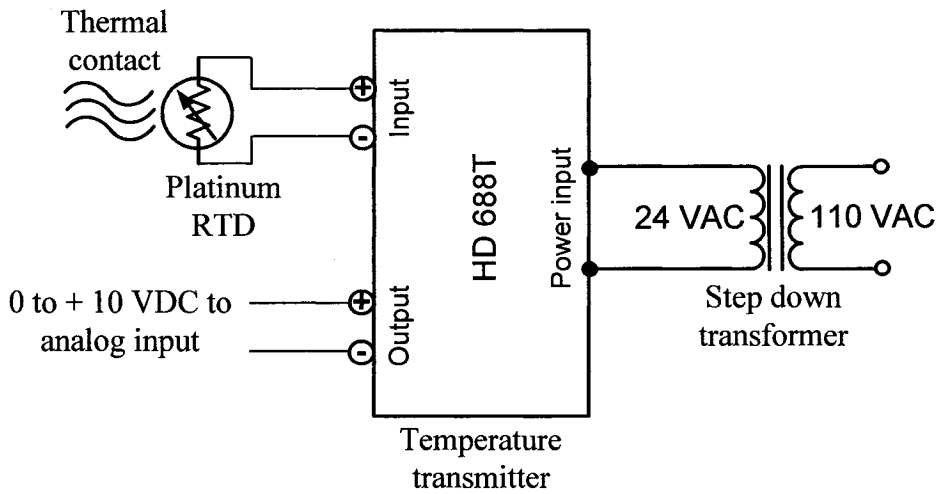

Figure 5.18: Schematic of the RTD/temperature transmitter arrangement used to monitor the temperature of the core mechanism. To represent the core mechanism temperature, a platinum RTD is used to accurately sense the temperature of the filter plate (platinum has a linear range for resistance between -200°C and +850°C, and is accurate to 0.01°C [205, 258, 263-265]). A transmitter (set for a 0°C to 50°C range), collects the RTD signal and delivers proportional 0 to +10VDC signals to an analog input channel on the robot controller I/O.

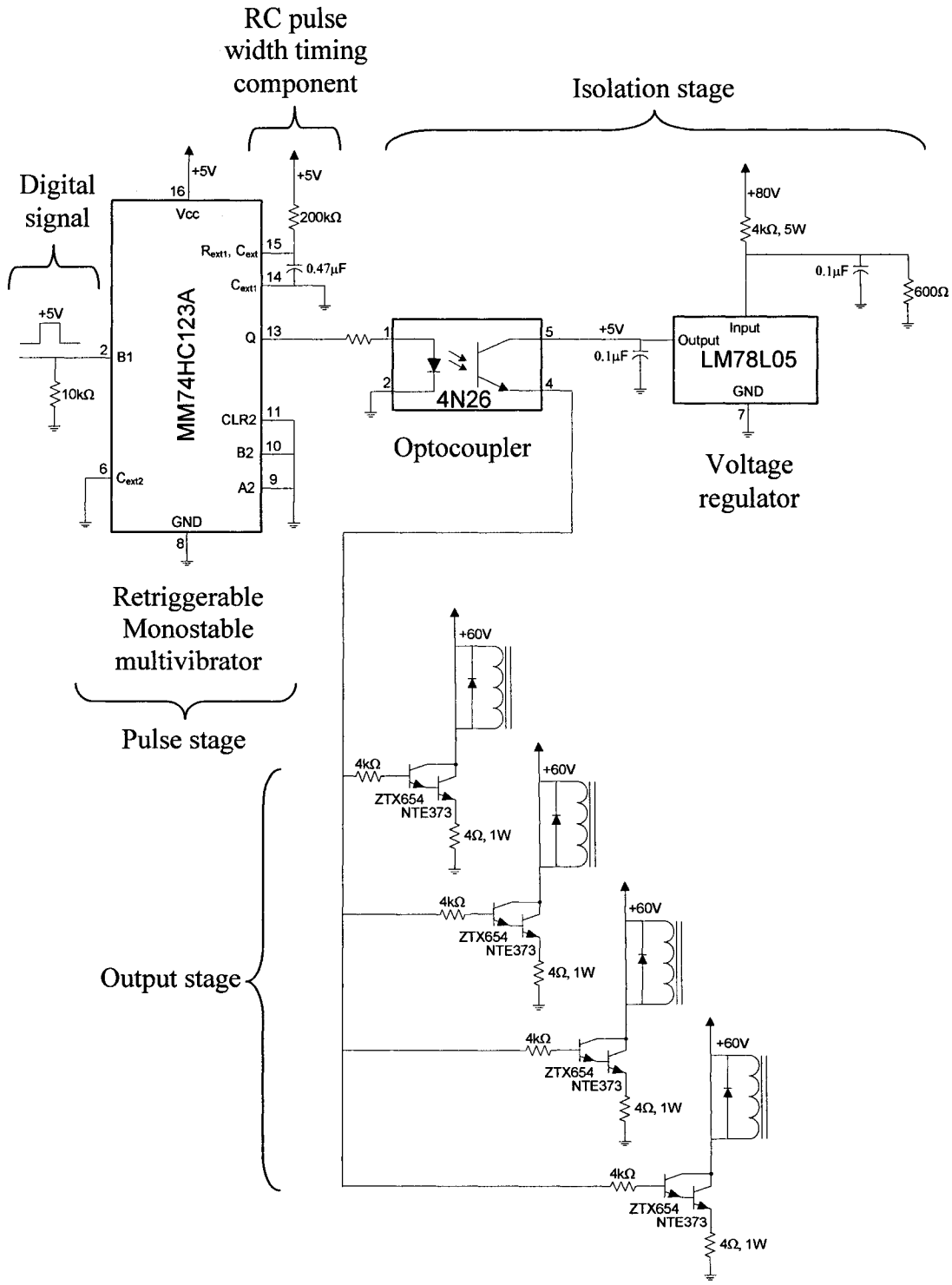

Figure 5.19: Schematic of the plate electromagnet decoupling circuit. The Darlington transistor arrangement provides a minimum current gain [269] of 3000 on the 5V optocoupler signal to complete the high power pulse to the electromagnets. The electromagnets are rated for continuous-duty operation with 1.4 W of power (12 VDC, 120 mA). Therefore, to protect them from shorting under high power (~ 35 W), the Darlington emitter is connected to a 4Ω, 1W resistors to ground.

supply (see Figure 5.20). The decoupling circuit is organized in three stages: (i) the pulse stage, (ii) the isolation stage and (iii) the power output stage.

(i) The pulse stage is a single shot, retriggerable, monostable multivibrator [258, 269] that produces a 100 ms pulse, where width is controlled by an external RC pulse width timing component [267-270]. Since the integrated circuit is retriggerable, an extended pulse or pulse train may be used for plate separation.

(ii) The isolation stage eliminates unwanted loss of efficiency or damage to the circuit; the pulse is transmitted to the high-voltage output stage by way of an optocoupler [268, 269]. A 5V voltage regulator [267-270] supplies power to the optocoupler output transistor to control the voltage from the 60 VDC unregulated power supply to the electromagnets.

(iii)The output stage amplifies the signal to drive the electromagnets with a

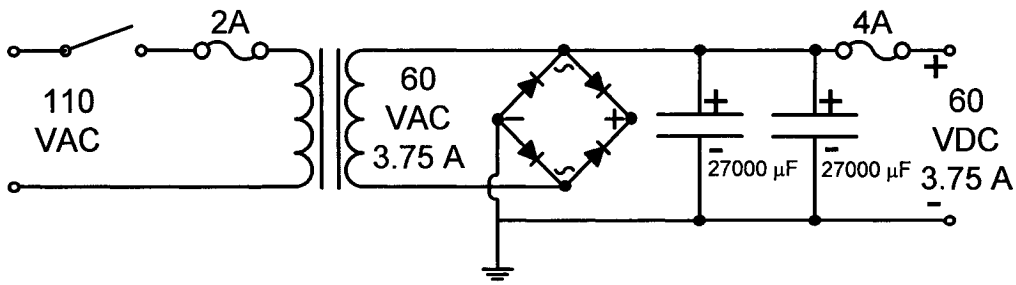

Figure 5.20: Schematic of the 60 VDC plate decoupling controller, unregulated power supply. It is composed of a 60 VDC, 3.75 A toroidal power transformer with the output voltage full-wave rectified and filtered by two parallel large-can capacitors [266]. For operator safety and to prevent damage to the supply, the positive 110 AC input to the transformer is equipped with a time delay fuse and a SPST 10 A toggle switch. Furthermore, to prevent damage to the plate decoupling circuit due to overheating, a DC input-DC output, solid-state relay interfaces the 60 VDC supply to the plate decoupling controller (see Figure 5.8). This relay connects power to the circuit before a plate decoupling event, and disconnects it immediately afterward.

high-power pulse (~35 W). It is composed of four Darlington power transistors [269], one for each plate de-coupling electromagnet.

5.4 Cooling Subsystem

The cooling subsystem maintains an "ice-cold" environment for the processing samples in the cooling platform. The platform also holds plates and retracts for clearance during reconfiguration with the electromagnetic transfer arm. The electronics of the subsystem provides the means for: (1) proximity and temperature sensing, (2) side platform retraction, (3) plate stabilization, and (4) cooling and temperature control.

(1) Two sensor systems are embedded in the side platforms and central base to sense (i) plate proximity sensing and (ii) cooling surface temperature.

(i) The magnetic proximity sensors used for the cooling platform are located on the top surfaces of the central base and the two side platforms. They are identical to those used in the filter plate of the core mechanism (see Section 5.3). Employing the proximity sensor actuation magnets embedded in the plates of the core mechanism, they continuously report plate positioning on the cooling platform to the robot controller *via* three digital input channels.

(ii) A platinum RTD, located in the cooling wall of the left side platform, senses the cooling surface temperature, which is used as the representative temperature for all cooling surfaces of the cooling platform. The

temperature sensing system is identical to that used for the filter plate of the core mechanism (see Section 5.3).

(2) The side platforms of the cooling platform are retracted by two sets of 12 VDC linear solenoids, to provide clearance for the electromagnetic transfer arm and positioning of the core mechanism (see Section 4.3). The solenoids are digitally actuated *via* two low signal relays.

(3) Plate stabilizing, 12 VDC electromagnets secure the core mechanism to the central base of the cooling platform during plate interchange/decoupling events that occur during reconfiguration of the core mechanism (see Figure 4.17). The electromagnets are digitally actuated *via* two low signal relays.

(4) All instrumentation for cooling and temperature control is set into operation by a momentary, digital output signal to two DPST latching relays [202-205, 269], which connect power to the system. Cooling operates during most of a processing run. For that reason, use of latching relays avoids continuous occupation of a digital output channel on the robot controller. Also, because cooling runs in parallel with all other operations, when powered, the subsystem operates independently of the robot controller *via* three subsections:

(i) 12VDC power. As Figure 5.21 shows, the power supply for the cooling subsystem is composed of three identical 12 VDC, 25 A unregulated power supplies. The three supplies operate in parallel to provide enough power to

the TECs on the three cooled surfaces of the cooling platform according to the worst-case conditions for the subsystem design (see Section 4.3.1).

(ii) TEC control. For efficient temperature control within a small bandwidth (±1°C), each group of TEC is equipped with dedicated controller(s) and a feedback sensor. The schematic in Figure 5.22 illustrates the arrangement whereby proportional-integral (PI) [202-205, 256-258] TEC controllers with corresponding thermistor temperature probes maintain the TEC cooled surfaces at 4°C by way of a pulse width modulated (PWM) output [256-258].

(iii) Cooling water recycle and heat dissipation. The cooling water pump requires 110 VAC power for continuous recycling of water and the fans of the heat

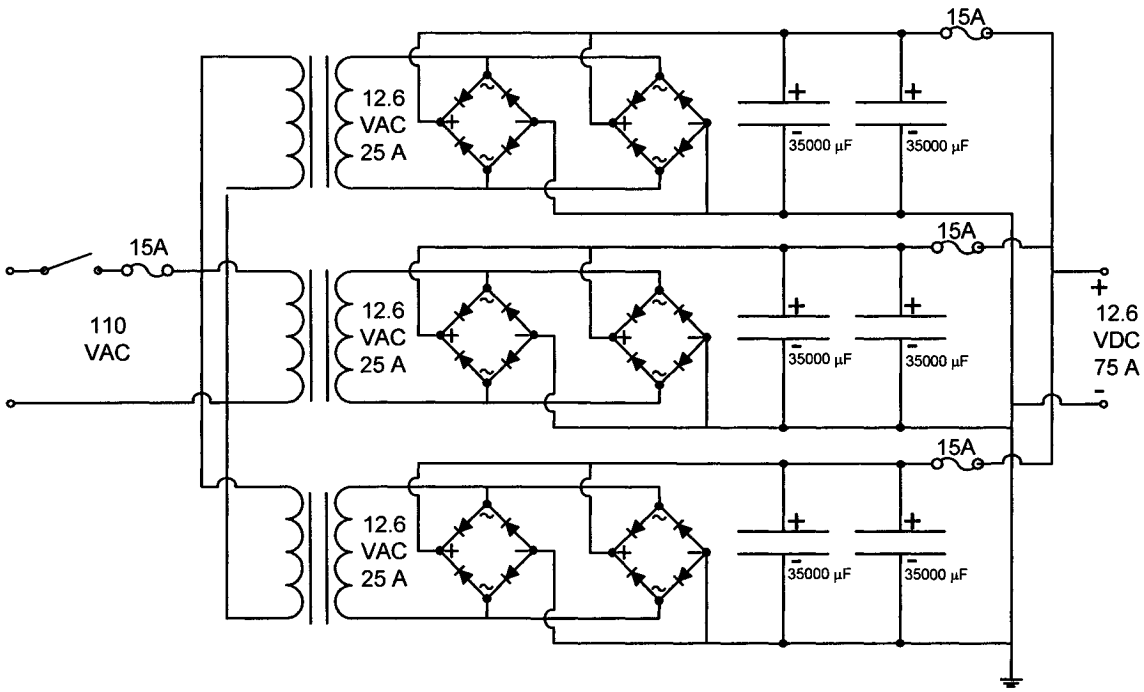

Figure 5.21: Each supply uses a 12 VDC, 25 A power transformer with output voltage full-wave rectified and filtered by dual rectifiers and two parallel large-can capacitors [266]. For operator safety and to prevent damage to the supply, the positive 110 AC input to the transformer is equipped with a time delay fuse and a SPST toggle switch.

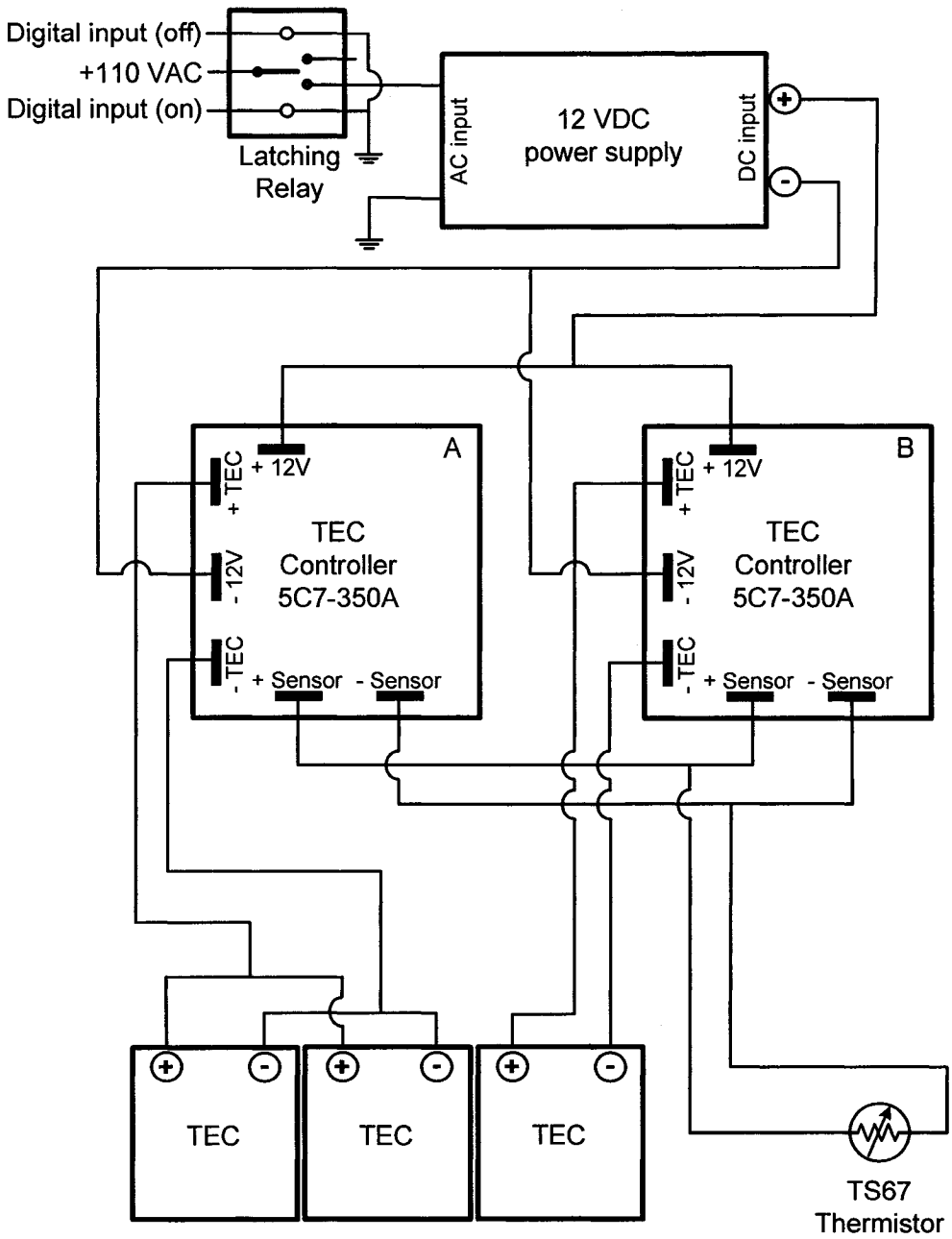

Figure 5.22: Schematic of the TEC controller arrangement used for the cooling platform side platforms. Two parallel controllers are used for the three high power TECs located in each side platform with one temperature probe providing feedback to both (the smaller TECs of the central base operate with one controller and a temperature probe). With proper heat sinking, the controllers provide over 10A of current to the TEC modules. Accordingly, all controllers are fitted with fin matrix heat sinks that are cooled by impinging flow from a coupled cooling fan.

In operation, proportional-integral control [202-204] permits adjustment of the bandwidth for temperature control and adjustment of the offset to maintain the 4°C set temperature. PWM [256-258] is an efficient means of powering the TEC as they approach the lower temperature of the proportional bandwidth (4°C), by modulation of the duty-cycle.

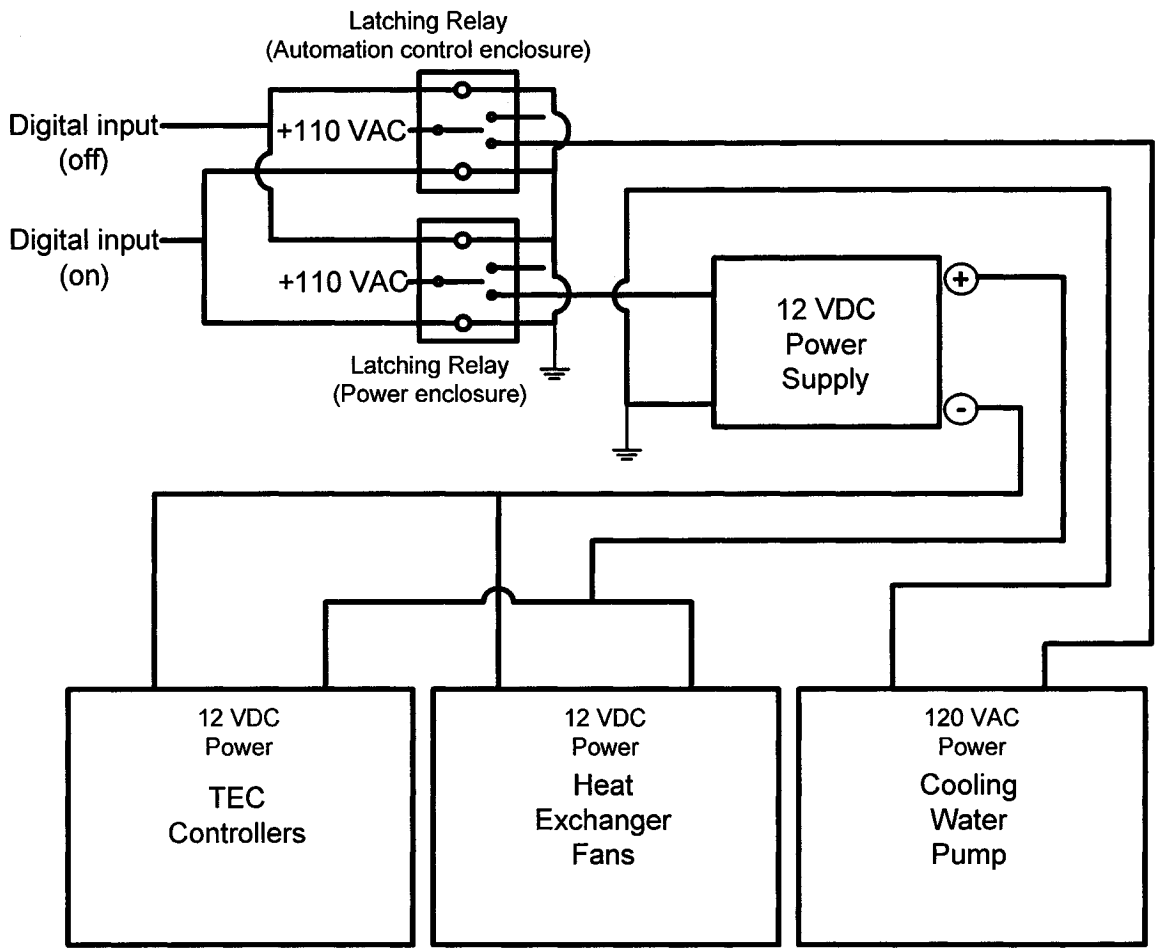

Figure 5.23: Schematic of the cooling subsystem power distribution to TEC controllers, heat exchanger fans and the cooling water pump. A set of latching relays, actuated by the same digital signal, connect 110 VAC to the subsystem for operation. When powered, the TEC controllers regulate 12 VDC power to the TECs.

exchanger assembly are powered by the 12 VDC source for the central base thermoelectric temperature controller and TECs.

The schematic in Figure 5.23 illustrates power distribution through the cooling subsystem. Two latching relays, actuated by the same digital signal, provide 110 VAC power to the 12 VDC power supply and the cooling water

pump. The 12 VDC power is distributed to the five thermoelectric temperature controllers, the TEC controller heat sink fans, and the six high-velocity of the heat exchanger assembly.

5.5 Fluid Handling Subsystems

The fluid handling subsystems interact directly with processing samples. Accordingly, they require specialized components to fulfill their tasks for reagent, air and waste fluid handling. All fluid control relies on the coordinated, digital actuation of miniature, 2- and 3-way, direct-acting solenoid valves; permitting or restricting the flow of pumped liquid or compressed air through fluidic lines and components. More sophisticated control signals and electronics are employed for quantitative fluid handling aspects such as microvolume dispensing, proportional volumetric control and pressure level feedback.

5.5.1 Processing Reagent Handling Subsystem

The specialized electrical components used for automated operation of the processing reagent handling subsystem are: (1) miniature solenoid valves and (2) two variable volume stepper pumps.

(1) Thirty eight miniature, 12 VDC, 2- and 3-way solenoid valves are coordinated (*via* digital actuation) to restrict or direct liquid from the reagent reservoirs to the core mechanism. All subsystem valves interface with the controller I/O modules in two groups:

(i) Processing reagent handling panel valves. For organization of all wiring, valves interface to the control electronics *via* four I/O screw terminals with corresponding cable connections to the consolidated screw terminal interface manifolds located in the automation control enclosure (see Figure 5.8).

(ii) Needle manifold staged solenoid valves. To consolidate cabling to the theta-axis, all three sets of valves are connected to the automation control enclosure DC actuation panel by a single, 4 conductor, cable (see Figure 5.11). Because only one needle manifold can work at a particular time, the corresponding valves on the remaining manifolds can be actuated without any ramifications on the process. This arrangement permits control of all valves on all needle manifolds *via* three digital output channels.

(1) The motion control capacity of the robot controller controls the two variable volume stepper pumps of the processing reagent panel (see Section 5.6.1). For precise control of liquid dispense velocity and volume, microstepping step motor amplifiers drive the pumps. Additionally, each pump is equipped with a home limit sensor (see Figure 4.24); together, occupying two channels of digital input.

5.5.2 Pneumatic Subsystem

Automation and quantitative control of the pneumatic subsystem necessitates coordinated actuation and feedback from four components: (1) a compressor, (2) direct–acting solenoid valves, (3) proportional solenoid valves, and (4) vacuum and pressure transducers.

(1) Compressor. To depressurize or pressurize the reservoirs of the vacuum-pressure assembly, the compressor is digitally actuated by way of a solid state relay that connects 110 VAC power.

(2) Solenoid valves. All solenoid valves are digitally actuated *via* relays. The pneumatic subsystem employs two types of direct-acting solenoid valves: (i) miniature valves and (ii) high-power valves.

(i) Four miniature valves are digitally actuated to control the flow of air in the vacuum-pressure assembly and vent pressurized air from the core mechanism.

(ii) The vacuum-pressure distribution manifold employs high-power valves to extend vacuum and pressure sources to the pneumatic components of the antivibrational table. They are all digitally actuated *via* solid state relays that connect 110 VAC power.

(3) Proportional solenoid valves. The two proportional solenoid valves that interface to the core mechanism rely upon proportional solenoid drivers to control the flow of air. The proportional solenoid valves are actuated by 0 to +10 VDC analog output signals to the drivers. The drivers employ a 28 VDC PWM output to the valves for positioning of the solenoid plunger, which adjusts the flow orifice area and produces the proportional rate of flow. Both valves interface to the drivers by way of the I/O screw terminal interface located on the antivibrational table to the consolidated screw terminal interface manifolds in the automation control system enclosure (see Figure 5.8).

(4) Transducers. Feedback for reservoir evacuation and pressurization as well as monitoring of subsystem performance during sample filtration and delivery events is provided by:

(i) Two vacuum transducers with a -14.7 to 0 psig pressure range, powered with 28 VDC, transmit proportional 0.5 to 5.5 VDC analog signals.

(ii) Two pressure transducers with a 0 to 100 psig pressure range, powered with 5 VDC, transmit proportional 0 to 4.5 VDC analog signals.

The four transducers interface to their respective analog input channels by way of the consolidated I/O screw terminal interface manifolds leading from the antivibrational table and vacuum-pressure assembly to the automation control enclosure (see Figure 5.8).

5.5.3 Cleaning and Waste Management Subsystem

The cleaning and waste management subsystem integrates with the pneumatic subsystem to utilize vacuum and pressure resources for removal of spent reagents during sample processing. The components dedicated to this subsystem include: (1) direct–acting solenoid valves and (2) gear pumps.

(1) The subsystem employs two types of digitally actuated, direct-acting solenoid valves.

(i) Six miniature valves are used for the waste removal manifold, the aspiration needle manifold and the ball valve actuation vent.

(ii) A high-power valve used for the needle dry station is actuated *via* a solid state relay to connect 110 VAC power.

(2) Gear pumps are used to move cleaning water to and from the needle wash station and to evacuate accumulated waste from the vacuum reservoir. PWM DC motor speed controllers regulate the flow velocity from the pumps, and are powered by way of a digital signal to an on-board low signal relay to connect 12 VDC. The needle wash station pumps share one controller and a second controller is dedicated to the waste removal subsection gear pump.

5.6 Positioning Subsystems

Successful automated sample processing relies on accurate positioning of the core mechanism and needle manifolds. The servo-driven motion control subsystem provides the foundation for accurate positioning on the EMPOP robot. Otherwise, positioning is driven *via* digital actuation of less sophisticated control electronics for the electromagnetic transfer arm and transfer platform. These controllers provide the means for effective and reliable operation of their actuators and sensors to manipulate plates and reposition the core mechanism.

5.6.1 Motion Control Subsystem

The components of the motion control subsystem provide electronic communication and control for closed-loop positioning that supports the automated process. Figure 5.24 shows a schematic of motion control electronics arrangement,

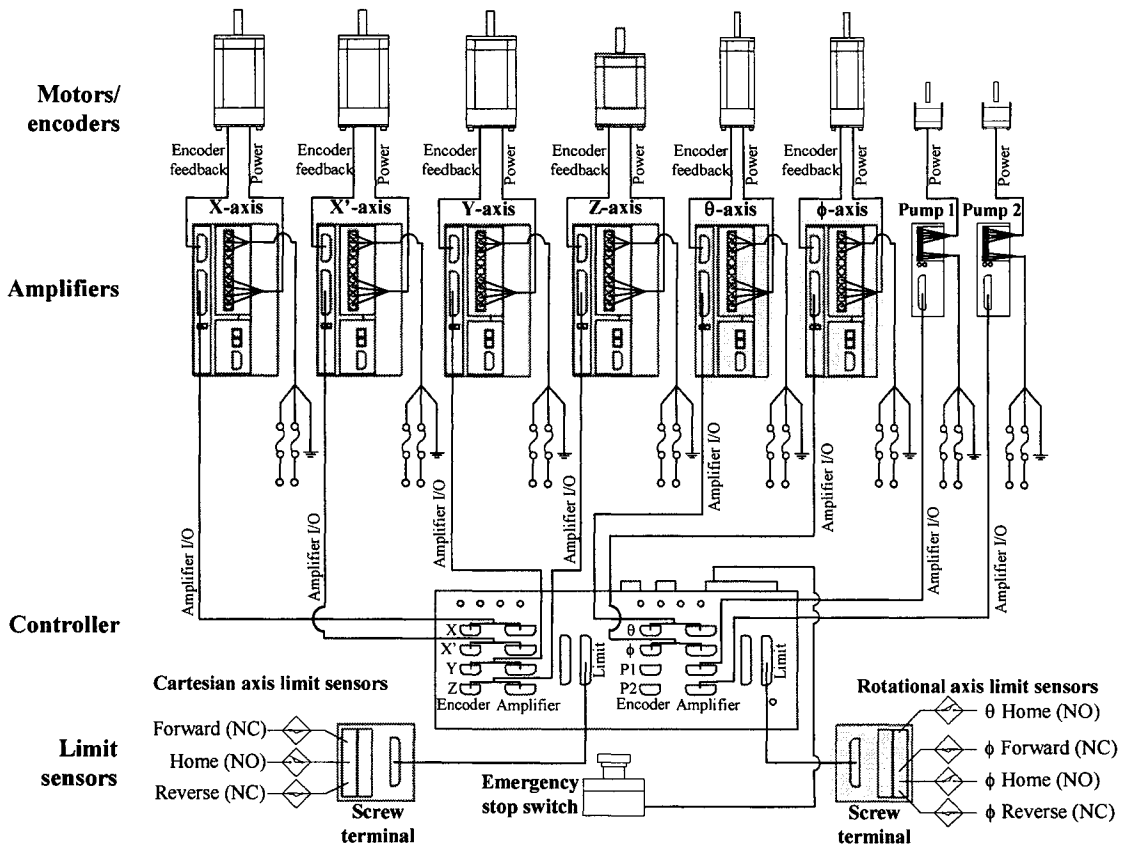

Figure 5.24: Schematic of the interconnection of motion control subsystem components to the robot controller. All subsystem components were purchased from the same manufacturer (Compumotor) [250, 252] and interface to the 6K8 controller *via* D-sub connectors. Cartesian (X, X', Y and Z) and rotational (θ and ϕ) axis motors are equipped with 2000 and 1000 line encoders, respectively. Six digital servo amplifiers power the subsystem motors. Four Gemini GV6K-U6 amplifiers power the Cartesian axes motors, two GV6K-U3 amplifiers are used for the rotational axes and E-AC microstepping amplifiers drive the motors of the variable volume stepper pumps. All axes are equipped with NPN (current sinking) inductive home, forward and reverse limit sensors, except for the magnetic home sensor on the θ-axis. The emergency stop switch interrupts the motion control capacity of the controller by disruption of the enable input.

which is comprised of: (1) the robot controller, (2) amplifiers, (3) encoders and (4) limit sensors.

(1) In addition to the extended digital and analog I/O capacity described above, the 6K8 controller also provides three features that suit it to this application:

(i) It supports the 6 servo and 2 stepper motor driven axes (processing reagent handling subsystem pumps, see Section 5.5.1) with a fast servo update rate of 62.5 μs/axis and ±10V step and direction outputs.

(ii) The controller supports 10 Mbps Ethernet communication *via* the TCP/IP protocol, allowing fast communication with the robot's operator interface *via* a single Ethernet cable. The arrangement also supports network connectivity for access and control from remote locations.

(iii)Controller programming is supported by the Compumotor 6000 programming language platform [262], which permits use of variables and high level math functions for control coding; multitasking of up to 11 parallel tasks for parallel operation of subsystems; and high-speed program logic control (PLC) scanning to monitor sensors and background operations throughout processing.

(2) Amplifiers. Six digital servo amplifiers [252, 255, 256-258, 261] power subsystem motors. All amplifiers operate with 110 VAC and support motor encoder feedback as well as direct drive I/O connectivity to the controller. All

amplifiers match the torque requirements for the specified subsystem's brushless, DC, servo motors (see Section 4.5.1). Accordingly, X/X'-, Y- and Z-axis amplifiers supply 6A continuous and 15 A peak current at 170 VDC and the θ- and ϕ-axis amplifiers supply 3A continuous and 7.5 A peak current at 170 VDC.

Although operated independently of the motion control subsystem, the two variable volume stepper pumps of the processing reagent panel are controlled as "virtual axes" (see Section 5.5.1) and occupy the two remaining motor interfaces of 6K8 controller. Microstepping amplifiers [255, 256-258, 261] drive the unipolar stepper motors of the pumps. Both amplifiers operate with 110 VAC and support direct drive I/O connectivity to the controller. Because stepper motors operation requires only signals for step and direction and operate in open loop, there is no support for encoder feedback.

(3) Encoders. Encoders provide feedback for servo motor positioning and velocity [247, 248, 251, 255, 256-258, 261]. All servo motors are equipped with multi-line rotary incremental optical encoders that provide number a points per revolution for differentiation the motor shaft position. The feedback for linear carriage, rotary table and pivot mechanism positioning (as reflect to the motor shafts *via* their respective ballscrews and gear drives) provides high resolution for accurate placement of the tools carried by the rotational axes, located at the end of the serially coupled arrangement.

Accurate positioning makes a large impact on successful completion of the process. The high resolution is reflected in the robot's capacity to position needle manifolds, which are addressed by rotation of the θ-axis, across the array of

processing channels of different core mechanism configurations. Similarly, the electromagnetic arm is positioned to reconfigure the core mechanism by translational and rotation motion within the robot's workspace, while interacting with two other subsystems.

(4) Limit sensors. Limit sensors signal the controller when an axis approaches its home position or the physical ends of its travel [251, 255, 256-258, 261]. The X-, Y- and Z-axes are equipped with inductive home, forward and reverse limit sensors, which are activated by small steel plates mounted on the carriages of the respective stages. The X'- stage operates in parallel with the X-stage and therefore shares the same set of limit sensors.

Forward and reverse limit sensors are not required for rotary motion. Consequently, only a magnetic home sensor is required on the θ-axis. It is mounted on the rotary table and is activated by a magnet embedded on the side of the rotary table top. The ϕ-axis is limited to approximately 90° of motion and, so is equipped with NPN inductive home, forward and reverse limit sensors. Small steel plates mounted on the hinge mechanism, which couples the electromagnetic transfer arm, activate all ϕ-axis limit sensors.

5.6.2 Electromagnetic Transfer Arm

The electromagnetic transfer arm subsystem is used to position the core mechanism plates and configurations. Each surface of the arm uses two digital I/O channels for: (1) arm-to-plate proximity sensing and (2) arm electromagnet control.

(1) Employing the arm-to-plate proximity sensor actuation magnets embedded in the plates of the core mechanism, magnetic proximity sensors continuously report plate presence to the robot controller *via* two digital input channels.

(2) A magnetic field persists in the arm electromagnets after power is removed. Therefore, to ensure automated plate release after repositioning, the residual magnetism is removed by application of a magnetic field of opposite polarity [187, 198-201, 257]. An H-bridge circuit [256-258, 269, 271] controls the array of four electromagnets on each surface of the arm; permitting continuous actuation of electromagnets for lifting and transfer of plates, followed by a short duration, reversed current pulse. The pulse produces an opposite magnetic polarity in the electromagnets that eliminates the residual field (i.e. coercive force) [185-191] and allows the plates to release by way of gravity.

Figure 5.25A shows a schematic of the arm electromagnet controller. The circuit is comprised of a hex inverting Schmitt trigger IC [257, 258, 269] and a high-power H-bridge IC. The timing diagram in Figure 5.25B illustrates how the hex inverter IC divides the continuous digital signal to the H-bridge direction, brake and PWM inputs. An external RC timing component initially delays the Schmitt trigger input signals to the brake and PWM by 30 ms. The most important aspect of circuit operation occurs when the digital signal to the H-bridge circuit is removed. The 30 ms trailing delay produces a current reversal in the four electromagnets; resulting in a corresponding pulsed reversal of the magnetic polarity [187, 198-201].

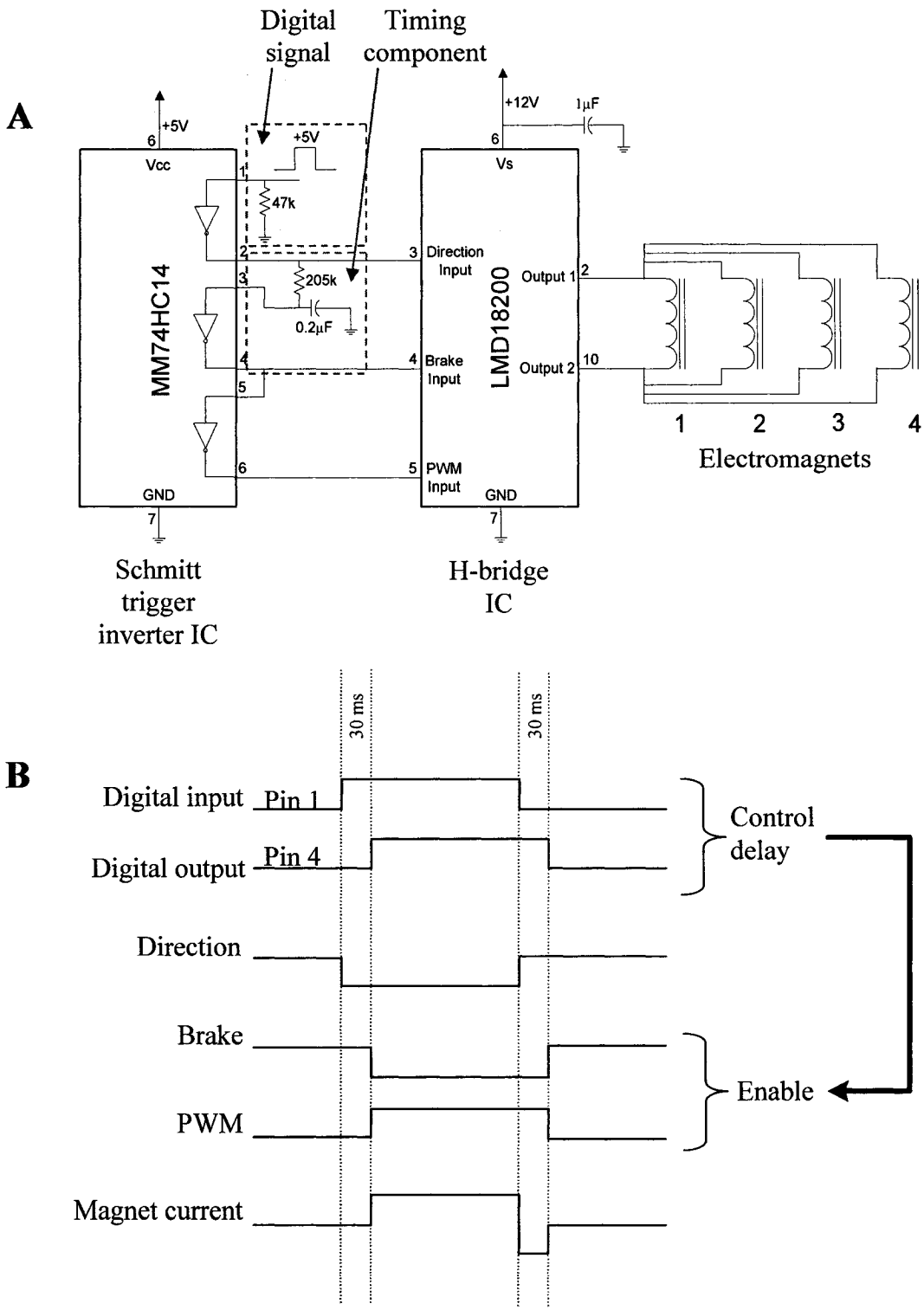

Figure 5.25: Illustrations of (A) the electromagnetic arm controller circuit and (B) the method for generation of a reverse field magnetic pulse. The timing diagram illustrates logic levels and signal delay between the Schmitt trigger inverter and the H-bridge ICs [269, 271]; producing the resultant 30 ms magnetic current reversal when the digital input to the circuit is removed.

5.6.3 Transfer Platform Subsystem

The transfer platform subsystem compensates for the limitations of the other positioning subsystems to vertically reposition the core mechanism during the inversion step of the process. To monitor the core mechanism and control motion of the sub-assemblies, the transfer platform requires: (1) a plate proximity sensor and (2) electromechanical actuators.

(1) Employing the plate-to-plate proximity sensor actuation magnets embedded in the plates of the core mechanism, the sensor reports plate positioning to the robot controller *via* one digital input channel.

(2) The subsystem's electromechanical actuators position components into either the active or stowed positions. Because positioning is controlled only to reach the limits of motion, four digital output signals are used *via* relay arrangements to drive: (i) linear actuators and (ii) solenoids.

(i) The schematic in Figure 5.26 shows the independent circuits, consisting of a DPDT high-power relay and two limit switches, which control the motors of the two linear actuators used for the rotational and vertical actuator assemblies. Because the stowed positions of the linear and slider-crank mechanisms require that their respective actuators move in opposite directions, only reversal of the 12 VDC power source polarities is necessary for the two actuator control circuits. Otherwise, the control circuits are

identical and operate to position the actuators with only one digital signal each; removal of the signal sends the actuators into stowed positions.

(ii) The plate stabilizer assembly employs digitally actuated rotational and linear solenoids [187, 197] to immobilize the core mechanism on the platform. Each solenoid has an internal return spring to force their respective sub-assemblies into stowed positions when no power is applied.

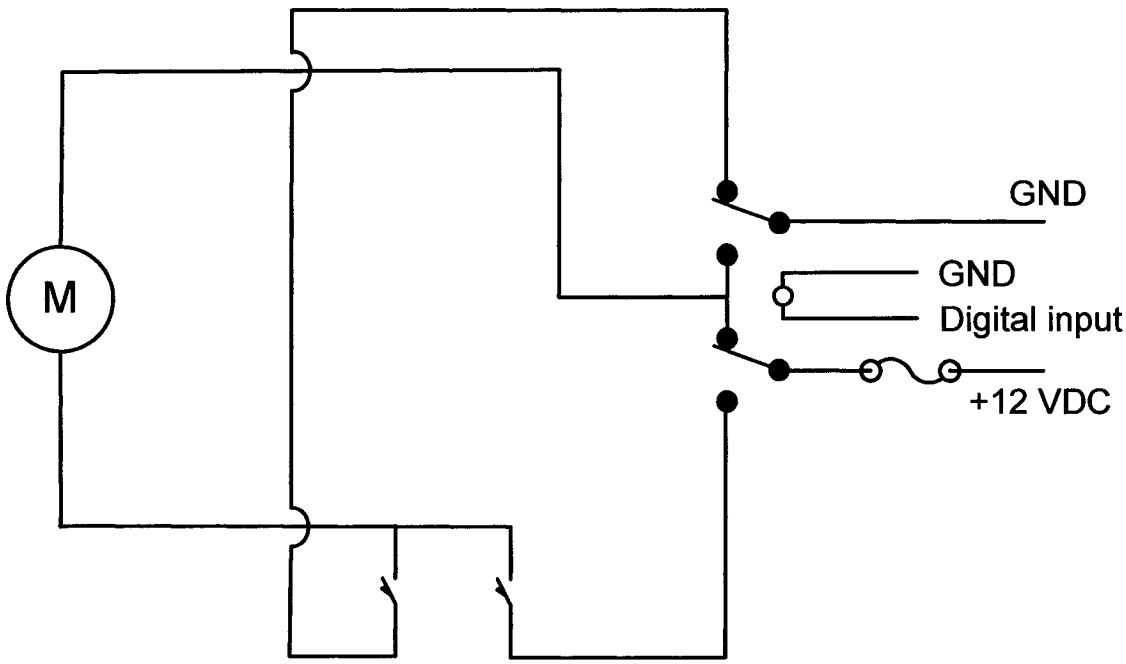

Figure 5.26: Schematic of the transfer platform linear actuator control circuit. A circuit consisting of a DPDT relay and two normally-closed, end-of-travel limit switches (shown open in diagram for clarity) permit extension and retraction of a linear actuator by way of a single digital signal. The relay permits simultaneous switching of voltage polarity to the motor leads while the limit switches permit current flow. When an actuator reaches the end-of-travel, the limit switch is forced into the open position to stop the motor.

6 Operation and Control of the EMPOP Robot

6.1 Overview

This chapter describes the operation and control of the EMPOP robot. The first section shows how the system achieves the sequence of events that comprise a sample preparation run. The second section describes the control software used to implement the automated sample preparation.

6.2 Automated Operation of the EMPOP Robot

The EMPOP robot executes a standard sequence of tasks during a sample preparation protocol. This section describes how the EMPOP robot implements these tasks from two perspectives: (1) the events internal to the core mechanism and (2) its interaction with all subsystems.

Any sample processing run will have four stages: (1) system setup, (2) sample filtration and chemical processing, (3) core mechanism reconfiguration and inversion, and (4) sample delivery and embedding.

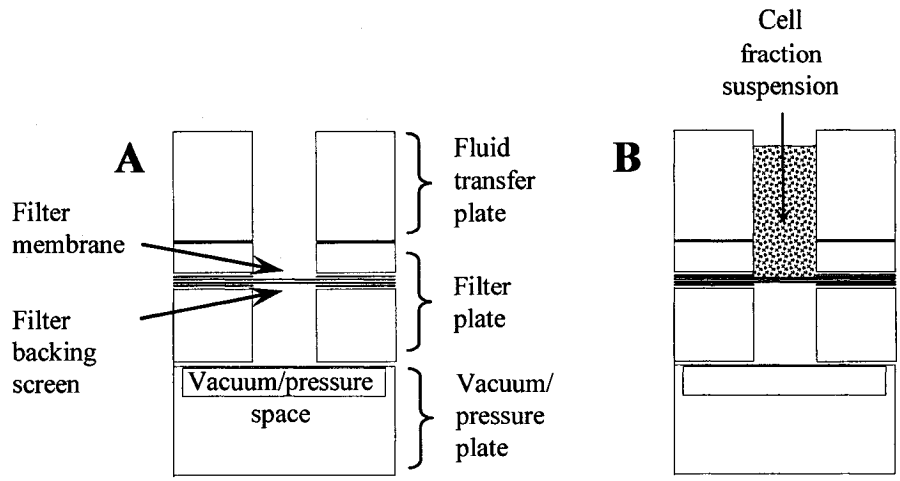

Figure 6.1: Cross-sectional schematics of a single channel of the core mechanism illustrating the manual steps of a processing run. (A) The processing configuration plate arrangement and (B) cell fraction sample loading.

(1) System setup. Two manual steps are required to prepare the system for automated operation. First, as shown in Figures 6.1A and 6.2, the three plates (fluid transfer, filter and vacuum-pressure plates) must be assembled in the processing configuration must be coupled (with the filter and filter backing screen secured in the filter plate). The core mechanism is placed on the cooling platform, cables and fluid lines connected, and cooled to 4 °C. Second, samples are loaded into the processing channels with a pipette (see Figure 6.1B).

(2) Sample filtration and chemical processing. The core mechanism is immobilized in the cooling platform and vacuum filtration is used to deposit the samples onto the filter membrane (see Figures 6.3A and 6.4). Then, as Figures 6.3B & C and 6.5 show, the robot begins cycling through the liquid handling sequence of chemical processing; executing the steps of reagent delivery, needle cleaning, sample

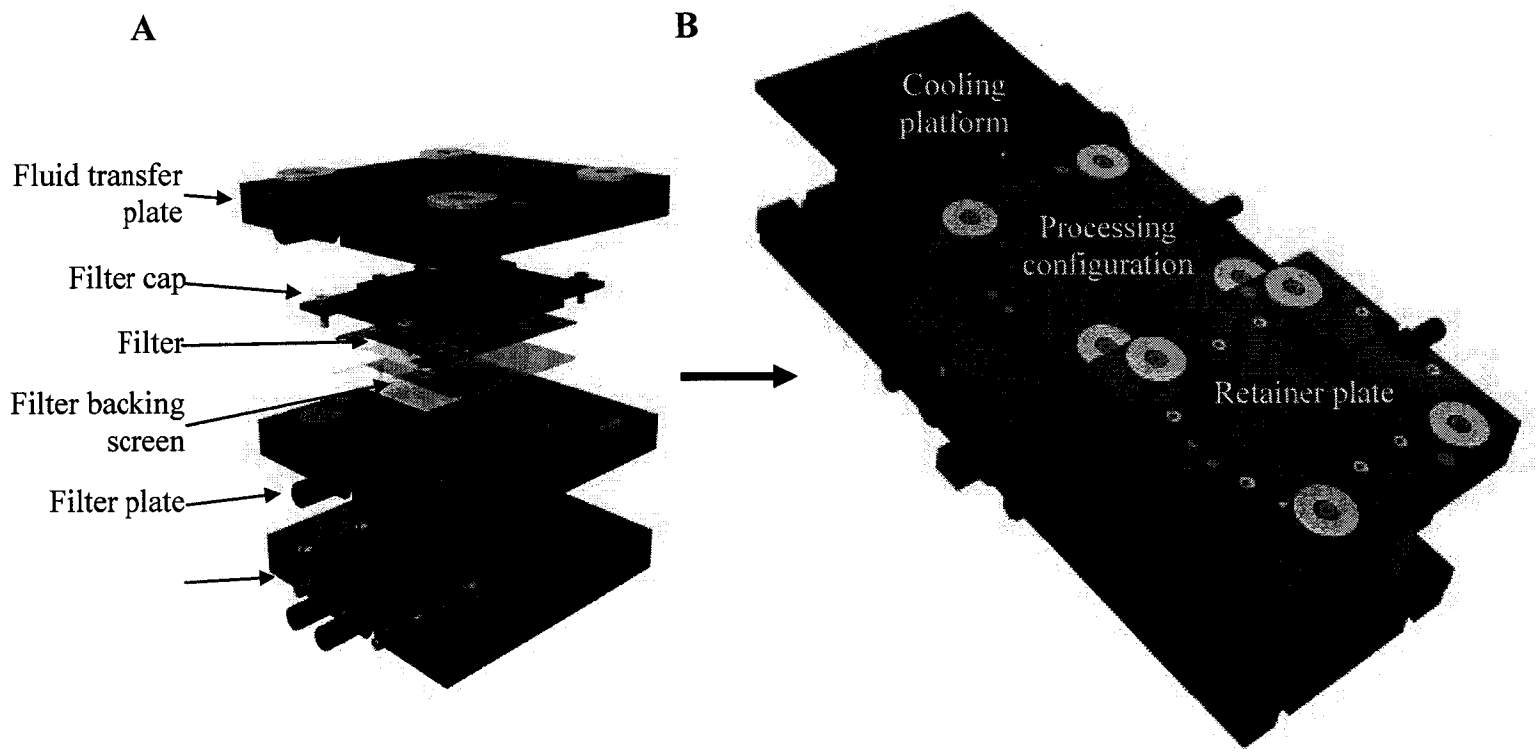

Figure 6.2: Manual steps of a sample preparation run. (A) Creating the processing configuration. (B) The processing configuration and retainer plate positioned on the cooling platform.

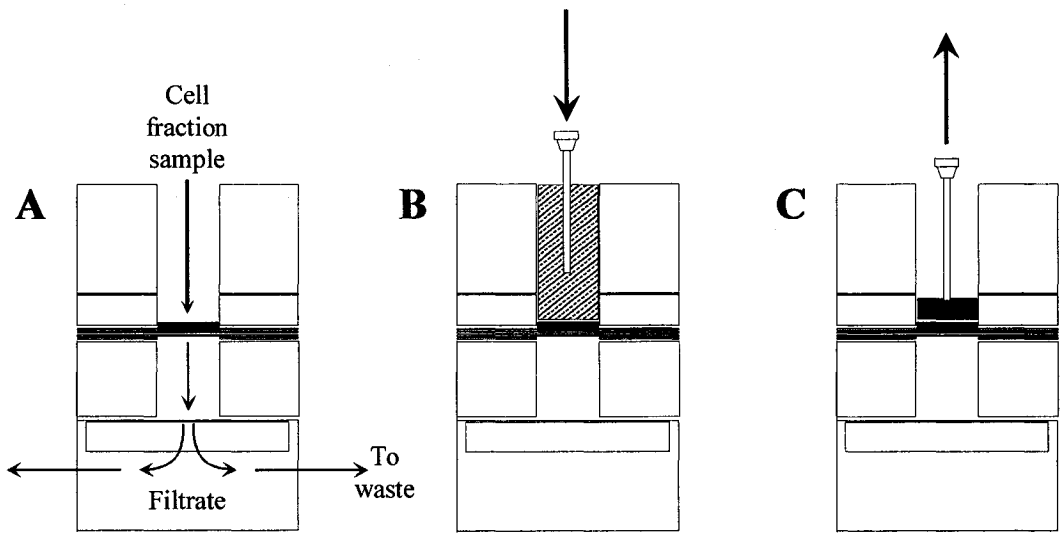

Figure 6.3: Cross-sectional schematics of a single channel of the core mechanism illustrating (A) sample filtration onto charged membrane, (B) reagent dispensing, and (C) reagent aspiration.

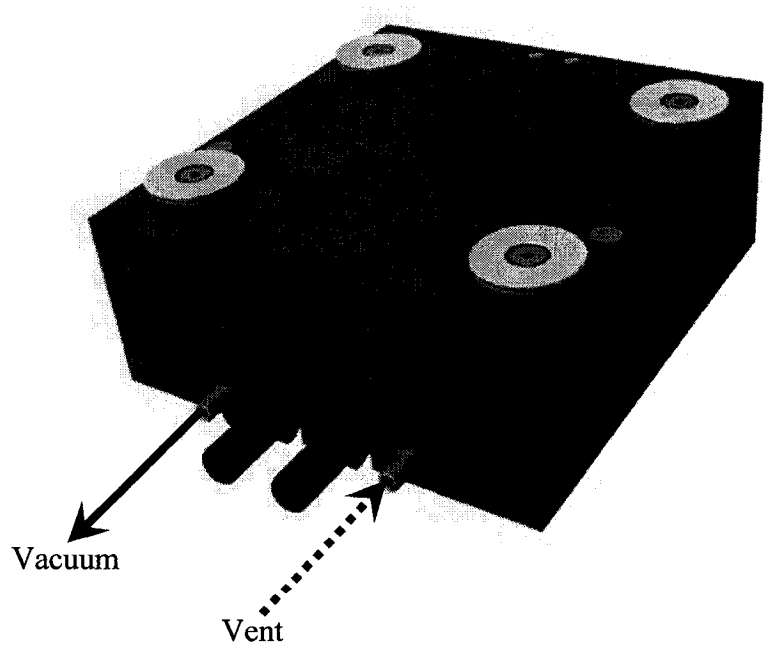

Figure 6.4: Direction of air flow in the processing configuration during the vacuum filtration stage of a sample preparation run.

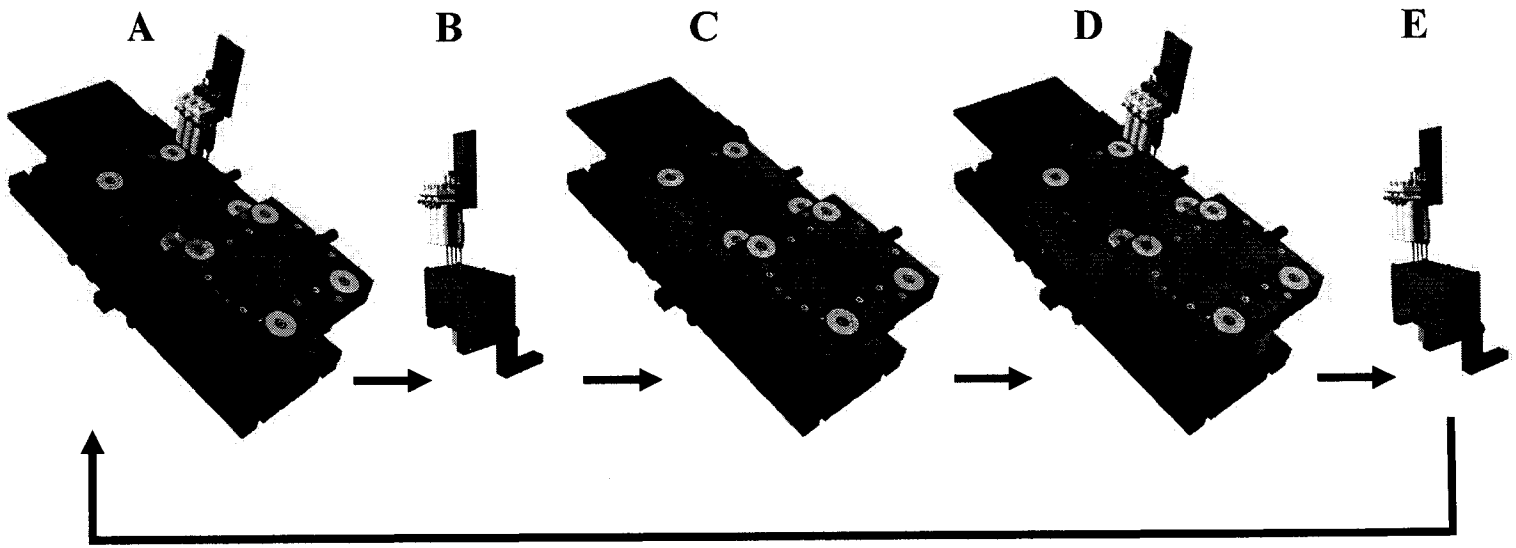

Figure 6.5: The cycle of events for the chemical processing stage of a sample preparation run: (A) reagent delivery, (B) needle cleaning, (C) sample incubation, (D) reagent aspiration, and (E) needle cleaning.

incubation, reagent aspiration, and needle cleaning required for each cycle. The process continues until chemical processing is complete.

(3) Core mechanism reconfiguration and inversion. In preparation for sample delivery and embedding, the robot uses the positioning subsystems to create the embedding configuration *via* a sequence of five events, shown in Figures 6.6 to 6.10:

(i) Plate exchange. The fluid transfer plate is decoupled, positioned on the cooling platform, and replaced by the retainer plate (see Figures 6.6A & B and 6.7). The embedding configuration is then removed form the cooling platform (see Figure 6.7E).

(ii) Inversion. The motion control and electromagnetic arm subsystems rotate the core mechanism by 180° (see Figure 6.8). The core mechanism is then positioned on the transfer platform. Figures 6.9A, B and C show how the inverted core mechanism is placed onto the platform with simultaneous release and through passage of the electromagnetic arm.

(iii)Transfer. The core mechanism is repositioned by the transfer platform to the lower vertical position. Simultaneously, the motion control subsystem rotates the electromagnetic arm by 180° (*via* the θ-axis) and positions it on the Z-axis for approach to the transfer platform Then, the electromagnetic arm picks up the inverted embedding configuration (see Figures 6.6C and 6.9D, E and F).

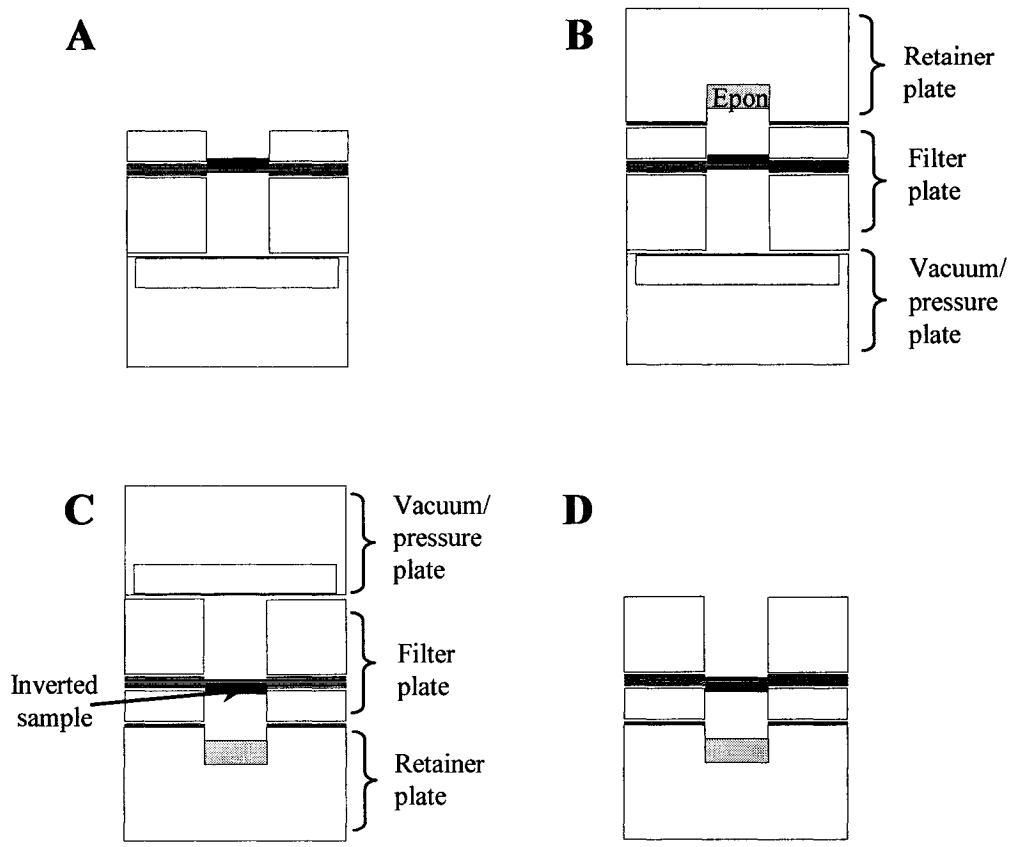

Figure 6.6: Cross-sectional schematics of a single channel of the core mechanism illustrating the steps of the core mechanism reconfiguration and inversion stage: (A) decoupling and removal of the fluid transfer plate and (B) coupling of the retainer plate creating the delivery configuration ready for inversion, (C) the inverted delivery configuration and, (D) vacuum-pressure plate decoupling and removed creating the embedding configuration.

(iv) Repositioning. The arm positions the core mechanism onto the cooling platform and the retainer plate is decoupled to permit execution of the final sample delivery and embedding stages (see Figures 6.6D and 6.10).

(4) Sample delivery and embedding. Before the delivery and embedding sequence begins, further chemical processing takes place to wash the inverted samples

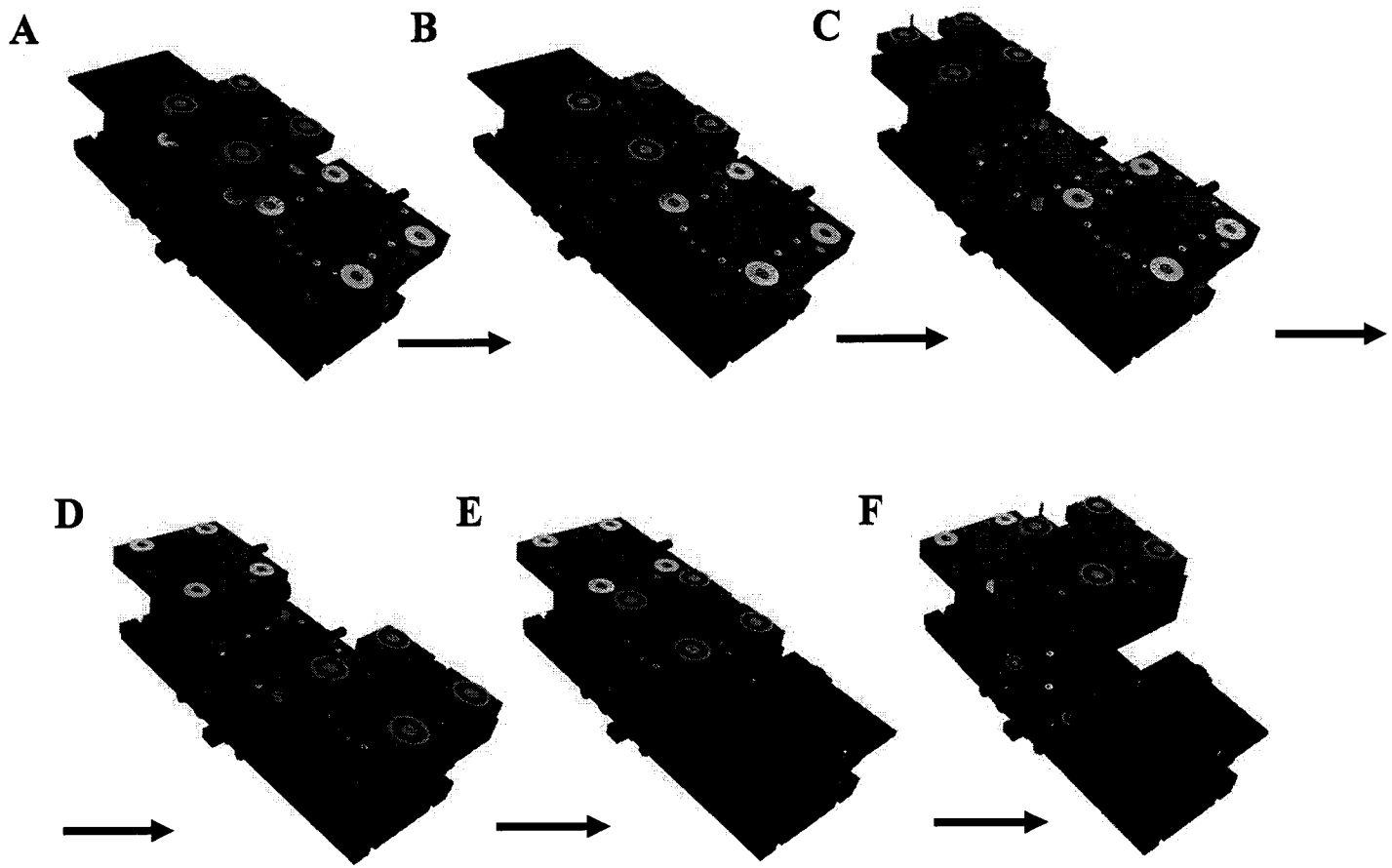

Figure 6.7 The plate interchange steps for assembly of the delivery configuration. (A) The cooling platform walls retract and the arm positions for plate coupling. (B) The fluid transfer plate is decoupled. (C) The fluid transfer plate is positioned on the side platform. (D) The arm positions with the retainer plate and couples for plate repositioning. (E) The retainer plate is coupled to create the delivery configuration. (F) The delivery configuration is removed from the cooling platform for inversion.

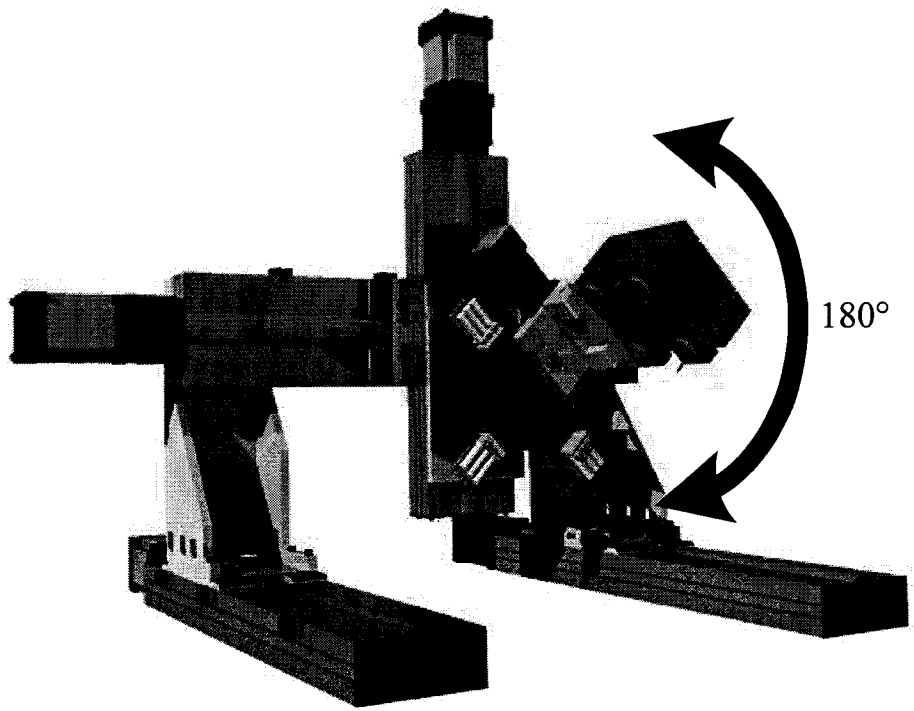

Figure 6.8: The plate inversion step of the core mechanism reconfiguration and inversion step.

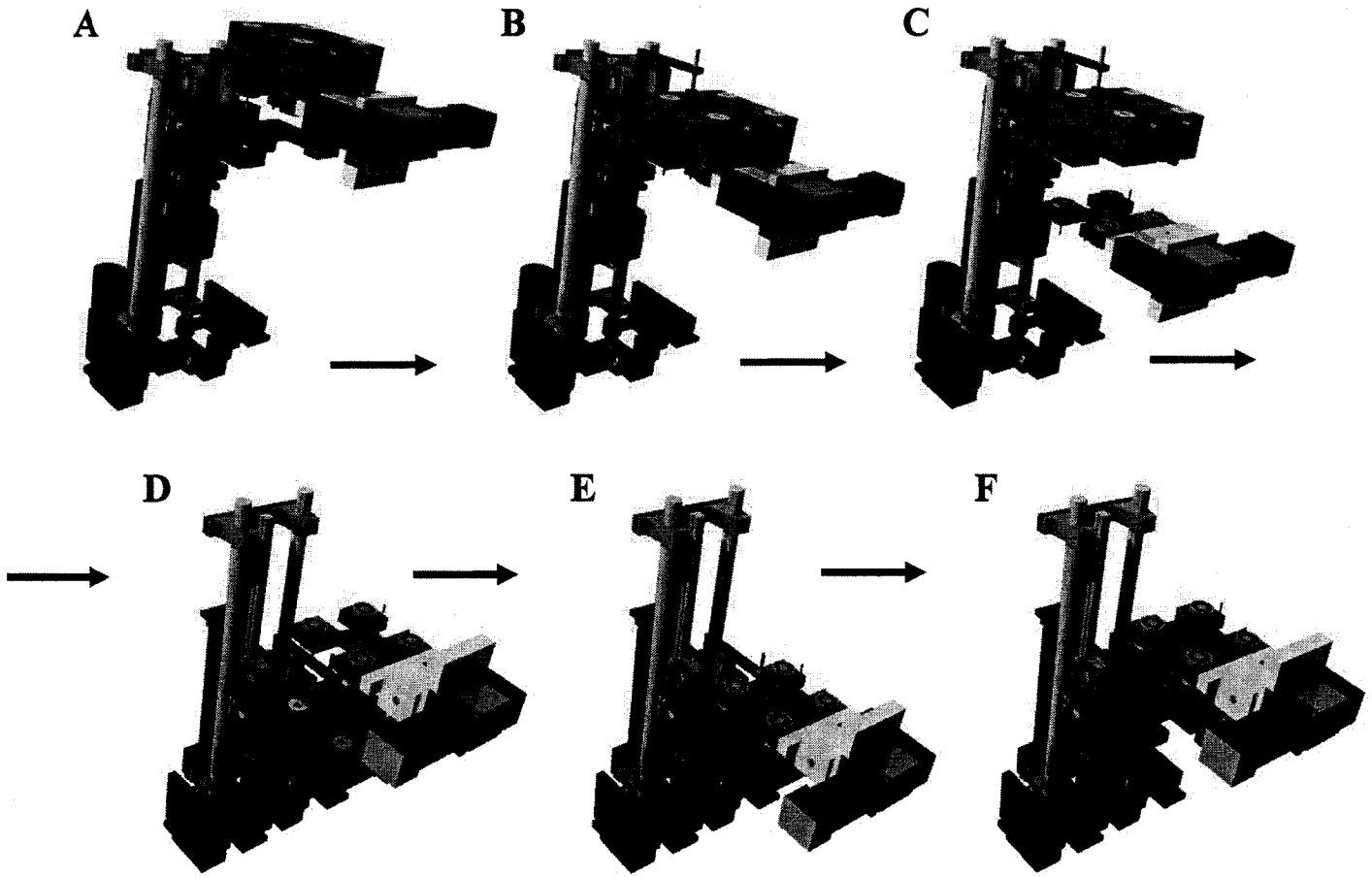

Figure 6.9: Vertical positioning of the delivery configuration with the transfer platform. (A) The arm and coupled delivery configuration approaches the raised and extended transfer platform. (B) The arm positions the delivery configuration on the transfer platform and the plate stabilizer actuates for compression. (C) The arm releases the delivery configuration and descends for rotation. (D) The transfer platform descends and the rotated arm positions to couple the delivery configuration. (E) The arm couples the delivery configuration. (F) The arm removes the delivery configuration from the transfer platform.

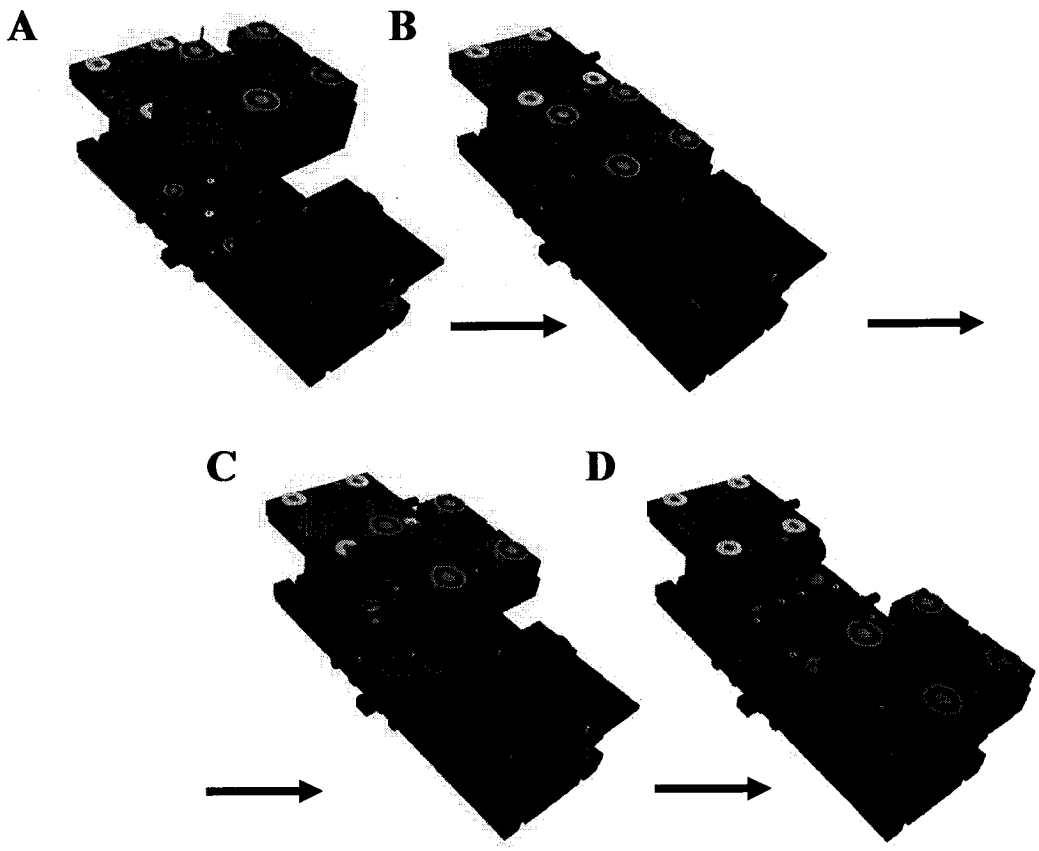

Figure 6.10: Repositioning of the core mechanism. (A) The arm approaches the cooling platform with the delivery configuration. (B) The arm positions the delivery configuration on the cooling platform. (C) The vacuum-pressure plate is decoupled to create the embedding configuration. (D) The arm positions the vacuum-pressure plate on the side platform.

again (see Figure 6.11). Figure 6.12 shows the sequence of events within the core mechanism for the sample delivery and embedding stage. Sample delivery begins when solvent is dispensed to the processing channels and the vacuum-pressure plate is replaced (see Figure 6.13). The samples are delivered with the solvent plug (transferred from the filter plate to the retainer plate) by pressurized air (see Figures 6.12B and 6.14). The vacuum-pressure plate is decoupled and positioned on the cooling platform in preparation for the embedding sequence. For sample

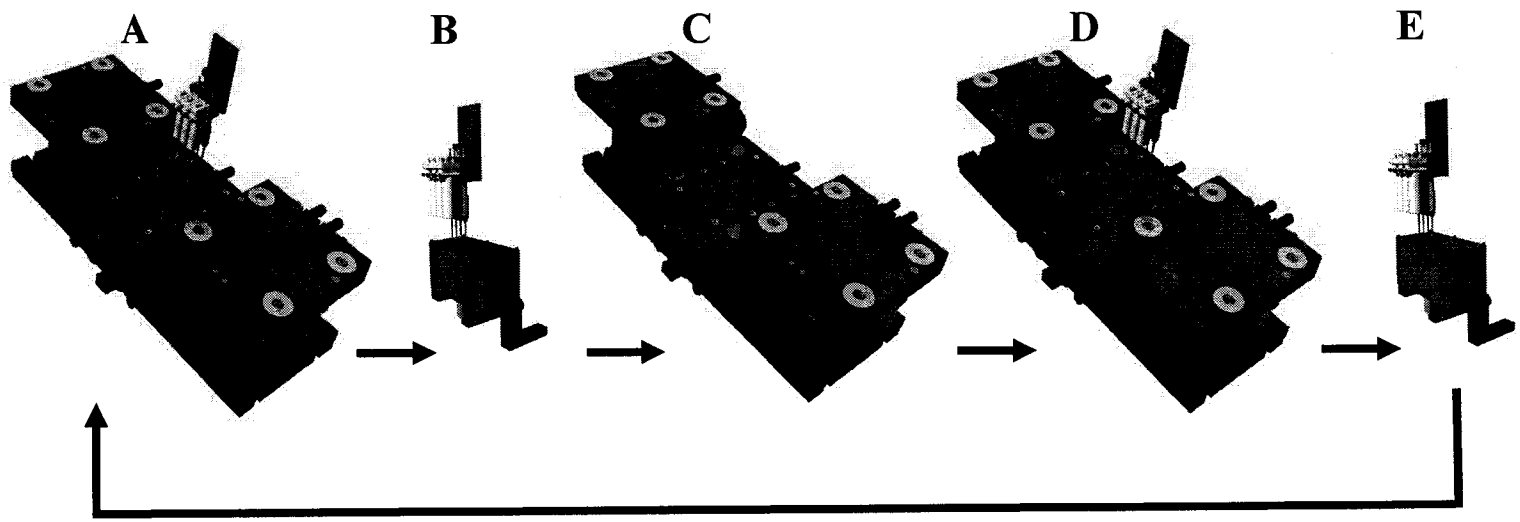

Figure 6.11: The cycle of solvent washing and sample infiltration steps in the embedding stage of a sample preparation run: (A) reagent delivery, (B) needle cleaning, (C) sample incubation, (D) reagent aspiration, and (E) needle cleaning.

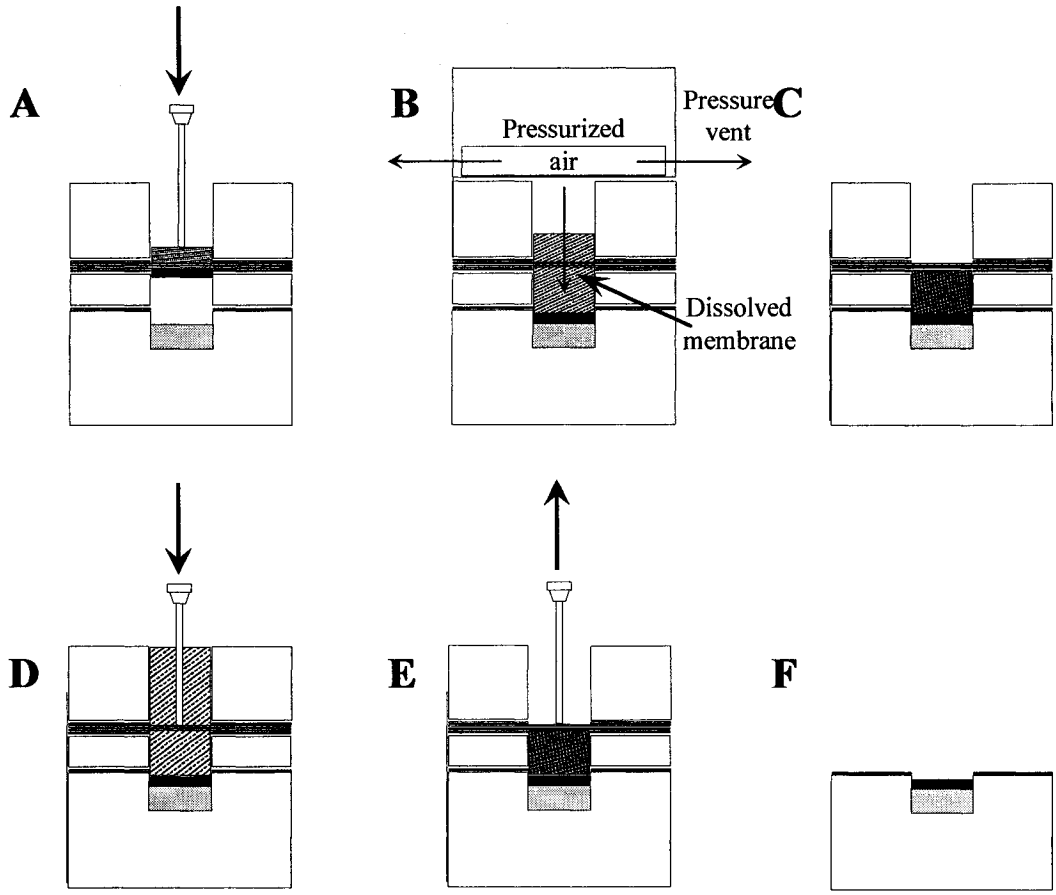

Figure 6.12: Cross-sectional schematics of a single channel of the core mechanism illustrating the sequence of events during for the delivery and embedding stage. (A) Solvent is injected to the filter backing screen to dissolve the filter membrane. (B) The vacuum-pressure plate is coupled and the samples are delivered with a pulse of air. (C) The vacuum-pressure plate is decoupled to removed. (D) Embedding reagents are dispensed across the filter backing screen. (E) Embedding reagents are aspirated across the filter backing screen. (F) The filter plate is decoupled and removed.

embedding, the system loops through events for reagent delivery, needle cleaning, sample incubation, reagent aspiration, and needle cleaning (see Figure 6.11). Sample processing is then complete and the embedding configuration is decoupled, leaving the retainer plate and processed samples on the cooling platform. (see Figure 6.15).

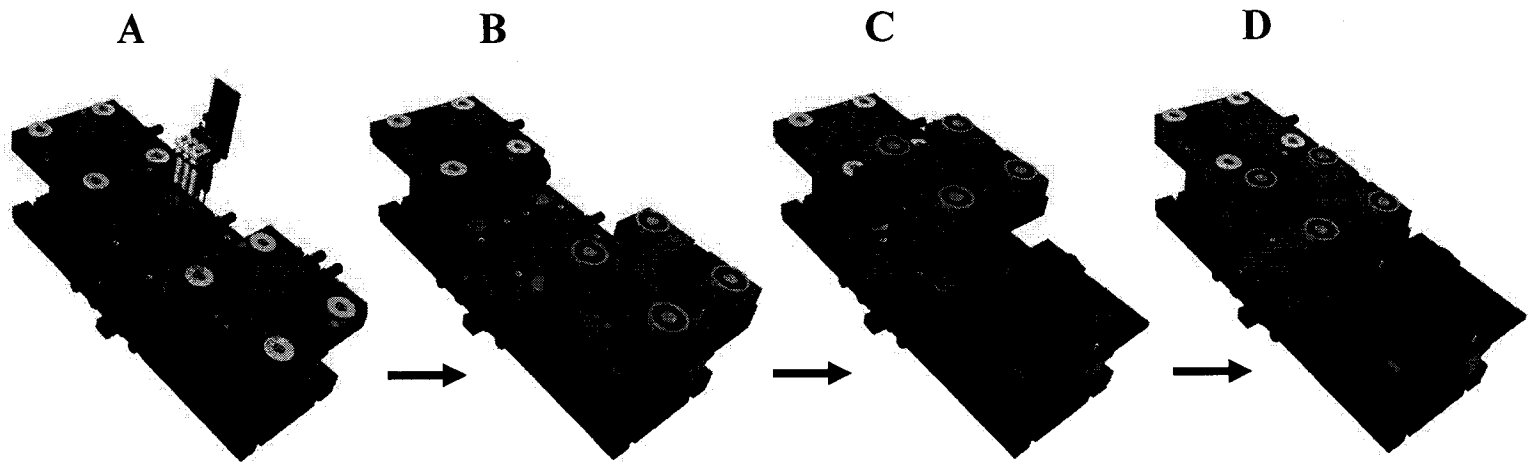

Figure 6.13: The delivery sequence. (A) Solvent is dispensed to the processing channels. (B) The arm positions and couples to the vacuum-pressure plate. (C) The arm positions the vacuum pressure-plate onto the core mechanism. (D) The vacuum-pressure plate couples to create the delivery configuration.

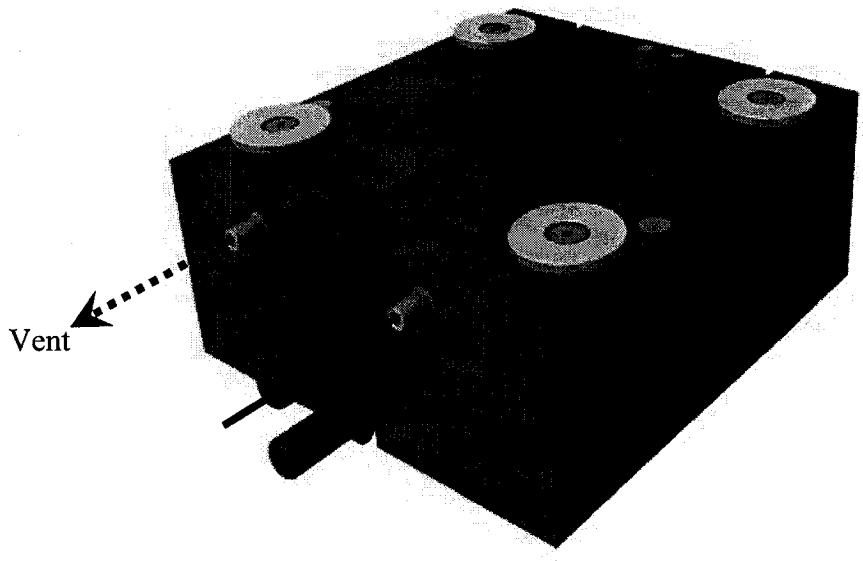

Figure 6.14: Direction of air flow in the delivery configuration during the sample delivery stage of a sample preparation run.

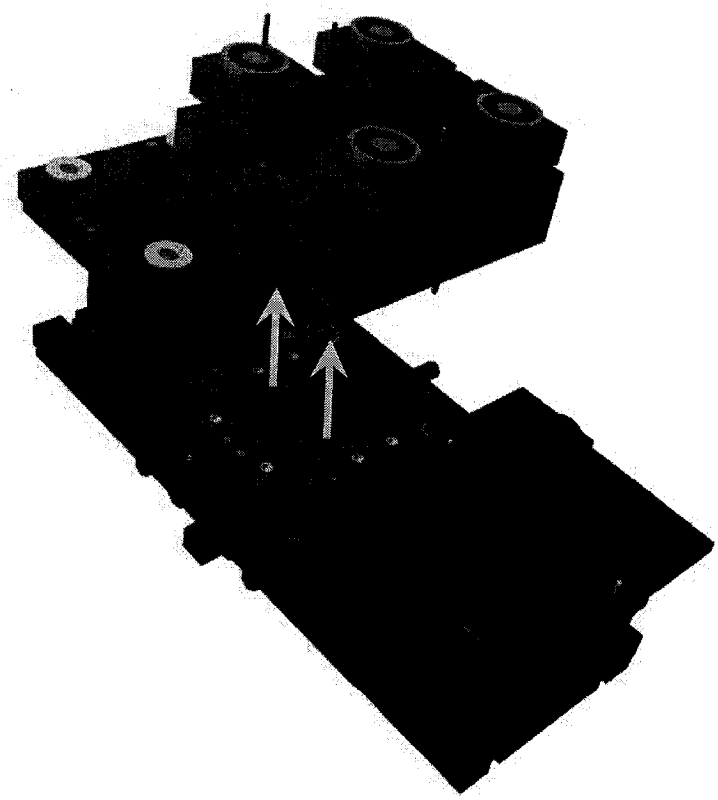

Figure 6.15: The embedding configuration is decoupled, leaving the retainer plate on the cooling platform, to complete the automated sample preparation run. Arrows indicate the direction of motion.

6.3 Automation Control

All software for automated control of the EMPOP robot was developed by Karishma Punwani as her Master's thesis in the Department of Biomedical Engineering at McGill University. All explanations of the control software were derived from her work and all figures in this section were taken from her thesis [172].

6.3.1 Automation Control Software

The robot controller was programmed to execute operator instructions by way of a PC-based automation control scheme based on a two-tier client-server software architecture. The approach permits operation and control *via* two functional levels: (1) the upper/operator level and (2) the low/control level. The scheme reflects the two respective system hardware units: (1) the PC or host computer and (2) the robot; regarded in the programming as the control module, sensors, electronic and mechanical devices (see Figure 6.16).

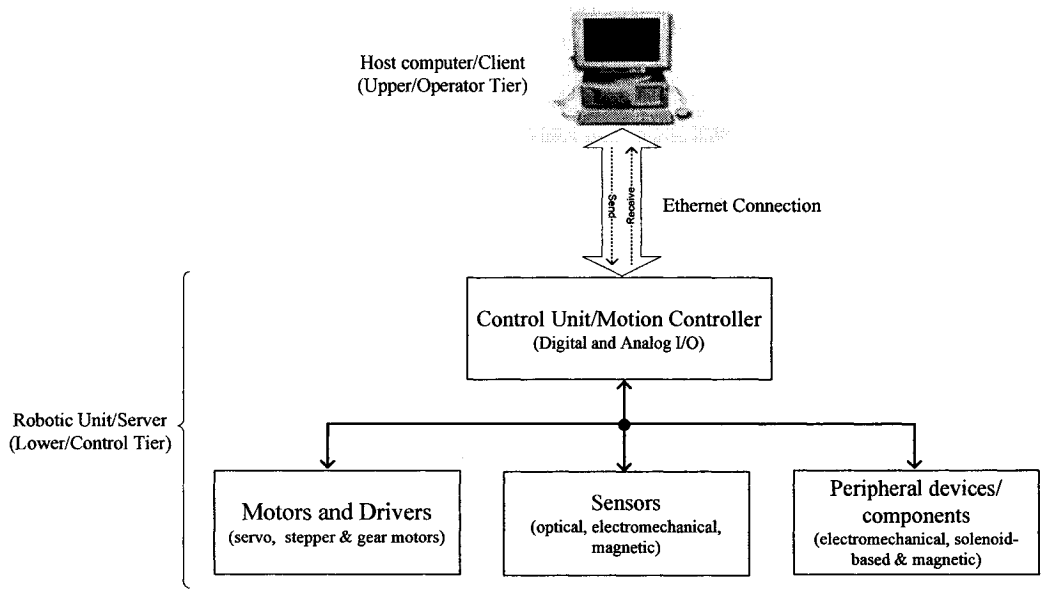

Figure 6.16: Logical diagram of the two-tier PC-based automation control system.

The upper/operator tier (PC and client software) is composed of a human-machine interface (HMI) [275, 276] that provides a user-friendly environment for efficient robot interaction. Furthermore, the HMI prevents access to the system's circuitry and embedded control algorithms by the operator. Following definition of the operational parameters for a processing run, the HMI sends a single high-level command to the robot, which initiates automated processing. From then on, the low/control tier (robot and server software) is responsible for all robotic function.

The HMI application was programmed with Microsoft Visual Basic™ [272, 276] to create a graphical user interface (GUI) for operator interaction with the robot. The system provides for highly flexible setup, operation and control as well as a method for data organization permitting system monitoring and run-to-run performance validation. The robot's controlled elements (motors/amplifiers, sensors and peripheral devices) are coordinated *via* a library of embedded process control routines in the control tier. The routines were developed using Compumotor MotionPlanner™; the language specific to the robot controller [262, 273].

6.3.2 Operator Tier

To support the operator with flexible operation from system start-up to completion of the process, the robot's HMI is comprised of six GUIs for:

(1) Ethernet connection and data management. The host computer and robot communicate using the TCP/IP protocol across an Ethernet link [274]. The Ethernet Connection GUI, shown in Figure 6.17, enables the operator to connect

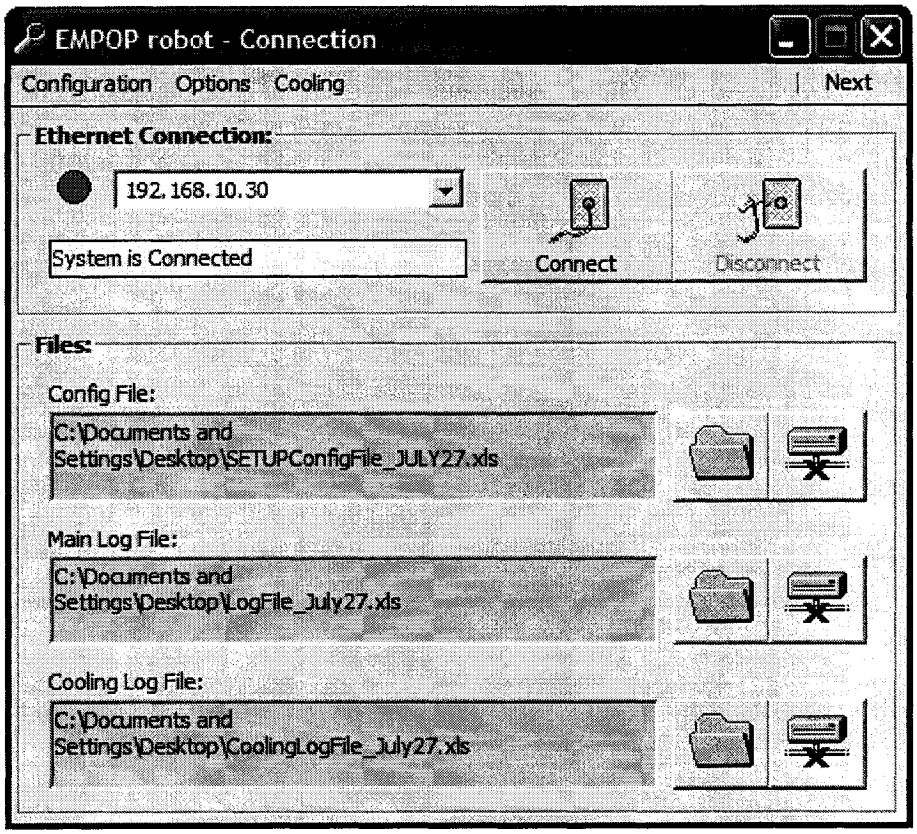

Figure 6.17: The EMPOP robot HMI Ethernet Connection GUI permits the operator to establish communication with the robot controller, upload a configuration file of operational parameters as well as log data for system performance and core mechanism cooling.

to the robot system using its IP address. It also has three dialog boxes that permit the operator to upload a configuration file and/or save performance and temperature data in log files. Configuration files contain all data for system calibration and setup. Use of these data permits repeated and identical execution of sample processing operating conditions.

(2) Calibration Setup. Before a processing run can begin the positions of the dispensing and aspiration needle manifolds as well as the electromagnetic transfer arm must be set using the Calibration Setup GUI shown in Figure 6.18. This

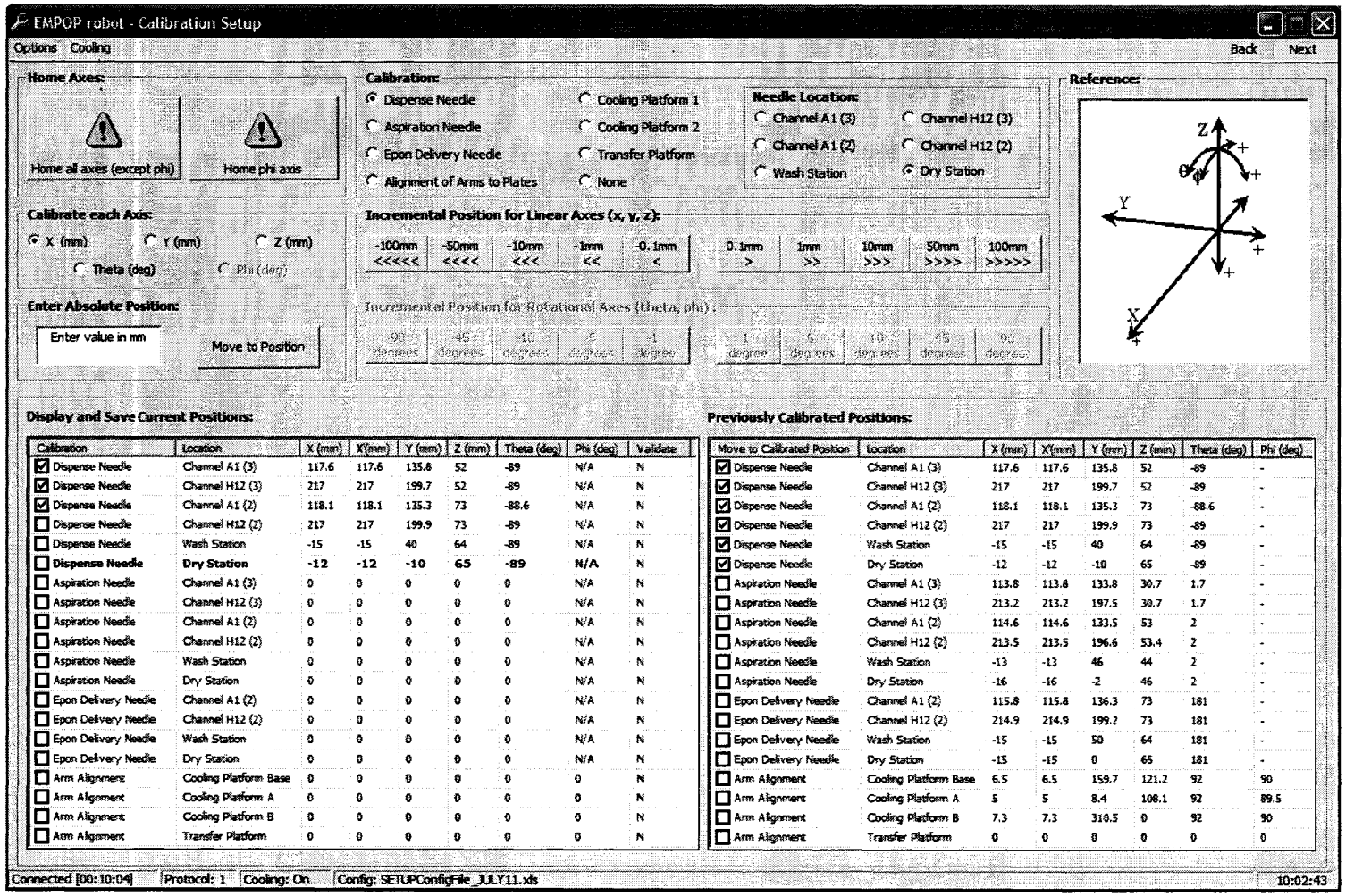

Calibration	Location	X (mm)	X'(mm)	Y (mm)	Z (mm)	Theta (deg)	Phi (deg)	Validate
Dispense Needle	Channel A1 (3)	117.6	117.6	135.8	52	-89	N/A	N
Dispense Needle	Channel H12 (3)	217	217	199.7	52	-89	N/A	N
Dispense Needle	Channel A1 (2)	118.1	118.1	135.3	73	-88.6	N/A	N
Dispense Needle	Channel H12 (2)	217	217	199.9	73	-89	N/A	N
Dispense Needle	Wash Station	-15	-15	40	64	-89	N/A	N
Dispense Needle	**Dry Station**	**-12**	**-12**	**-10**	**65**	**-89**	**N/A**	N
Aspiration Needle	Channel A1 (3)	0	0	0	0	0	N/A	N
Aspiration Needle	Channel H12 (3)	0	0	0	0	0	N/A	N
Aspiration Needle	Channel A1 (2)	0	0	0	0	0	N/A	N
Aspiration Needle	Channel H12 (2)	0	0	0	0	0	N/A	N
Aspiration Needle	Wash Station	0	0	0	0	0	N/A	N
Aspiration Needle	Dry Station	0	0	0	0	0	N/A	N
Epon Delivery Needle	Channel A1 (2)	0	0	0	0	0	N/A	N
Epon Delivery Needle	Channel H12 (2)	0	0	0	0	0	N/A	N
Epon Delivery Needle	Wash Station	0	0	0	0	0	N/A	N
Epon Delivery Needle	Dry Station	0	0	0	0	0	N/A	N
Arm Alignment	Cooling Platform Base	0	0	0	0	0	0	N
Arm Alignment	Cooling Platform A	0	0	0	0	0	0	N
Arm Alignment	Cooling Platform B	0	0	0	0	0	0	N
Arm Alignment	Transfer Platform	0	0	0	0	0	0	N

Move to Calibrated Position	Location	X (mm)	X'(mm)	Y (mm)	Z (mm)	Theta (deg)	Phi (deg)
Dispense Needle	Channel A1 (3)	117.6	117.6	135.8	52	-89	-
Dispense Needle	Channel H12 (3)	217	217	199.7	52	-89	-
Dispense Needle	Channel A1 (2)	118.1	118.1	135.3	73	-88.6	-
Dispense Needle	Channel H12 (2)	217	217	199.9	73	-89	-
Dispense Needle	Wash Station	-15	-15	40	64	-89	-
Dispense Needle	Dry Station	-12	-12	-10	65	-89	-
Aspiration Needle	Channel A1 (3)	113.8	113.8	133.8	30.7	1.7	-
Aspiration Needle	Channel H12 (3)	213.2	213.2	197.5	30.7	1.7	-
Aspiration Needle	Channel A1 (2)	114.6	114.6	133.5	53	2	-
Aspiration Needle	Channel H12 (2)	213.5	213.5	196.6	53.4	2	-
Aspiration Needle	Wash Station	-13	-13	46	44	2	-
Aspiration Needle	Dry Station	-16	-16	-2	46	2	-
Epon Delivery Needle	Channel A1 (2)	115.8	115.8	136.3	73	181	-
Epon Delivery Needle	Channel H12 (2)	214.9	214.9	199.2	73	181	-
Epon Delivery Needle	Wash Station	-15	-15	50	64	181	-
Epon Delivery Needle	Dry Station	-15	-15	0	65	181	-
Arm Alignment	Cooling Platform Base	6.5	6.5	159.7	121.2	92	90
Arm Alignment	Cooling Platform A	5	5	8.4	108.1	92	89.5
Arm Alignment	Cooling Platform B	7.3	7.3	310.5	0	92	90
Arm Alignment	Transfer Platform	0	0	0	0	0	0

Figure 6.18: The EMPOP robot HMI Motion Calibration GUI permits the operator to use predefined calibration positions and/or calibrate positions for the needle manifolds and the electromagnetic transfer arm with the core mechanism, clean station, cooling platform and transfer platform.

permits calibration by single axis and/or simultaneous positioning of all axes to a previously defined calibrated location (from an up-loaded configuration file, see Figure 6.17).

The three needle manifolds are calibrated with respect to the first and last channels (A1 and H12, see Figure 6.19) in the processing and embedding core mechanism configurations (the controller interpolates the locations of remaining 94 channels, A2 to H11). The needle manifolds are also calibrated to the wash and dry sections of the clean station.

Calibration for all manipulation of the core mechanism on the cooling and transfer platforms requires the operator to resolve the system's X, Y-, Z- and θ-axis positions, as well as determine the ϕ-axis extension angle for the electromagnetic transfer arm. In operation, the HMI downloads the axis coordinates into the robot controller as they are determined for each location, and the procedure continues until all have been defined.

(3) System Setup. The GUI shown in Figure 6.19 is divided into three sections for: (i) dispensing and aspiration needle setup, (ii) needle washing frequency and duration, and (iii) processing channel selection. After the parameters are established, the HMI downloads them to the robot controller, where they remain fixed throughout a run.

(4) Reagent Setup. The GUI shown in Figure 6.20 allows the operator to select a preparation protocol as well as specify the reagents located in each of the 17 reservoirs. However, if a pair of reagent is to be mixed, the GUI restricts the reservoir locations to those addressed by opposing pumps. Once all reagents have

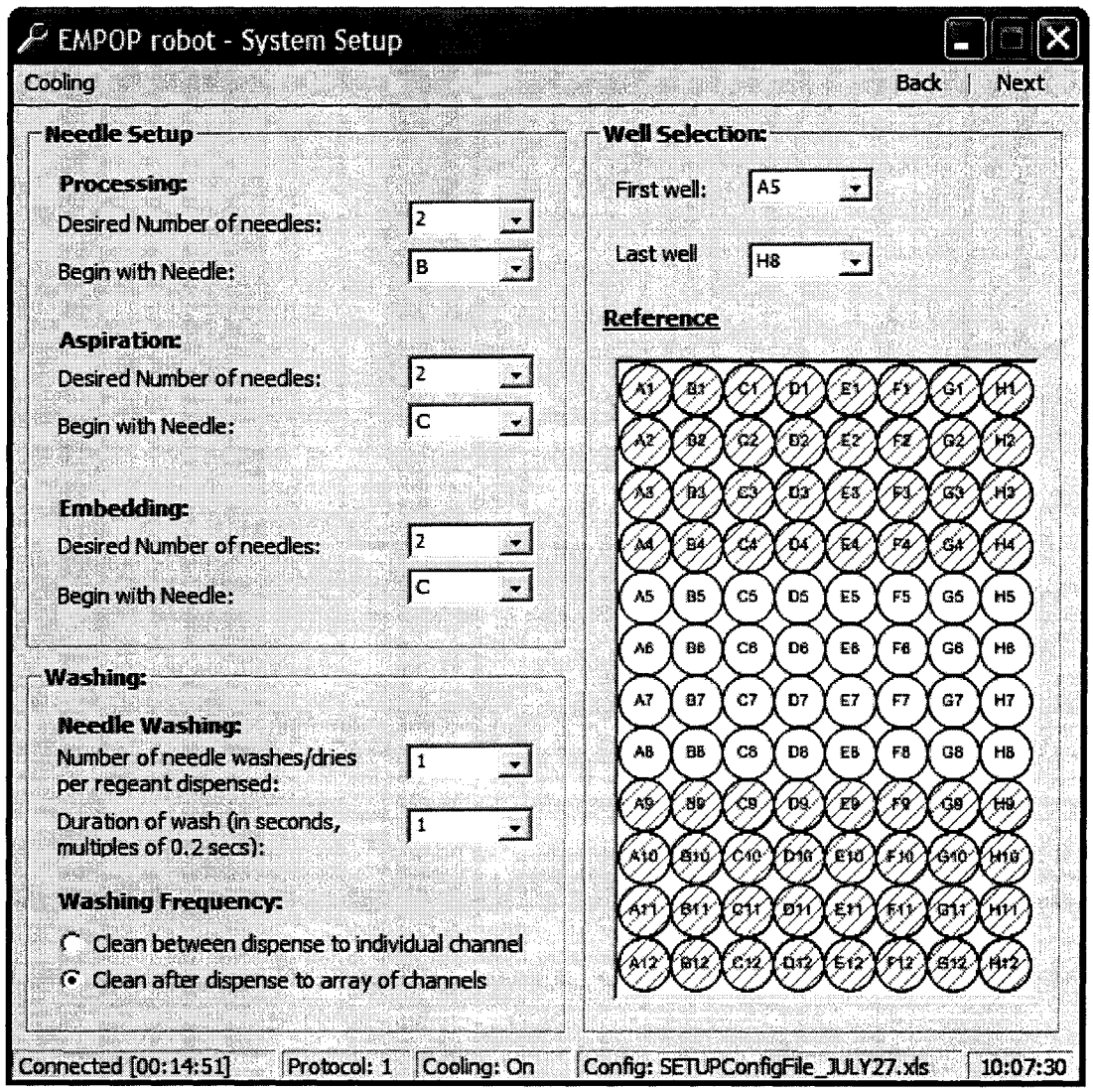

Figure 6.19: The EMPOP robot HMI System Setup GUI permits the operator to configure the needle manifolds and the needle washing steps as well as restrict processing to selected channels.

been assigned to reservoirs, the HMI saves the information to a high-level data structure for use by the Process Monitoring GUI. This data structure includes information regarding:

(i) The link between each reservoir and its corresponding valve on the reagent handling panel,

(ii) The dispensing needle manifold each reagent is dispensed from,

(iii)The core mechanism configuration each reagent is dispensed to,

(iv)The pumping velocity for each reagent.

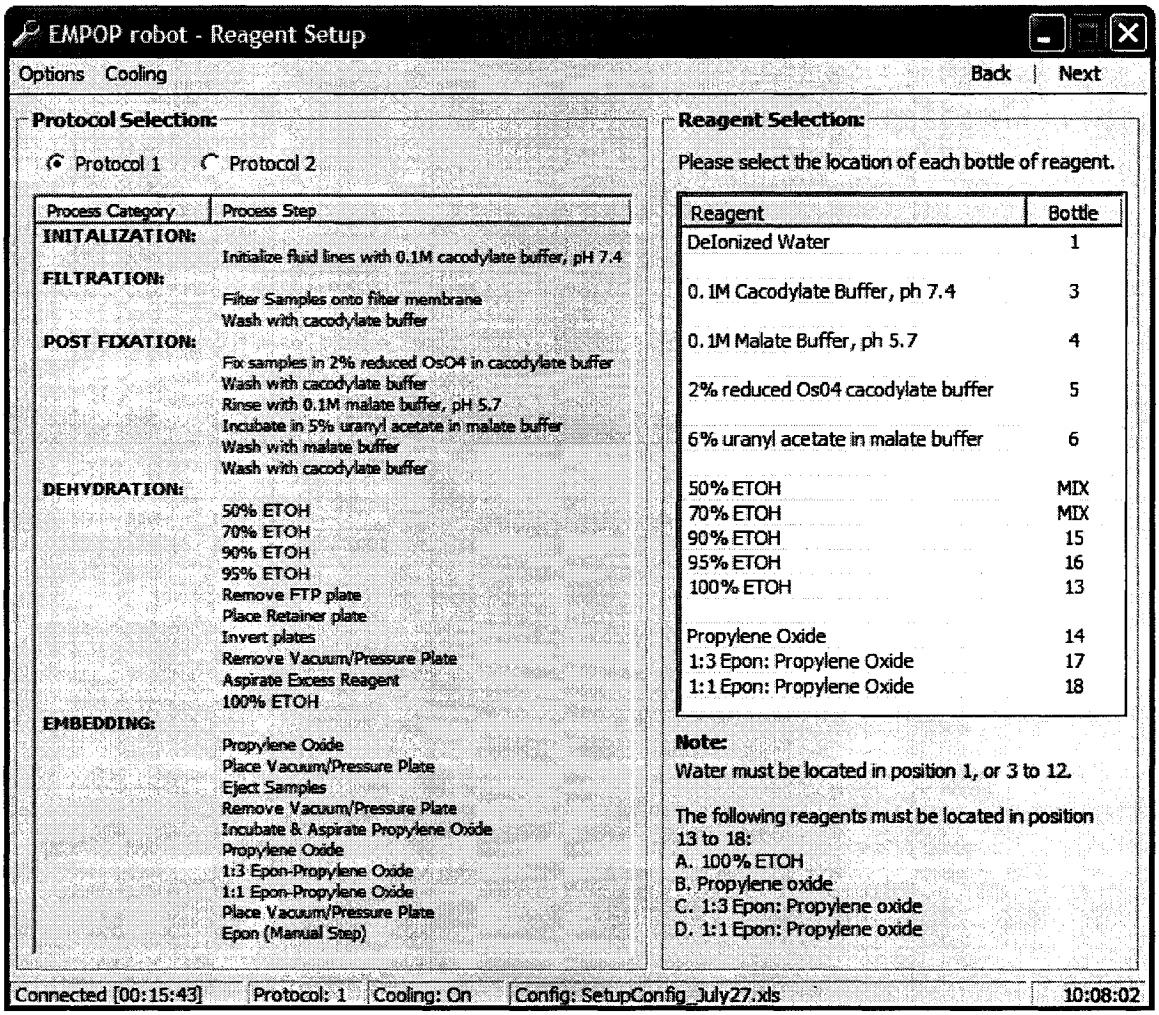

Figure 6.20: The EMPOP robot HMI Reagent Setup GUI allows the operator to set up processing reagents for either of the two protocols according to the reservoirs they occupy.

(5) Process Control. The GUI shown in Figure 6.21 is used to define the mode in which the Process Monitoring GUI (see Figure 6.22) will operate – automatic, manual or combined. In automatic mode, each step of the protocol executes in sequence without intervention. In manual mode the operator

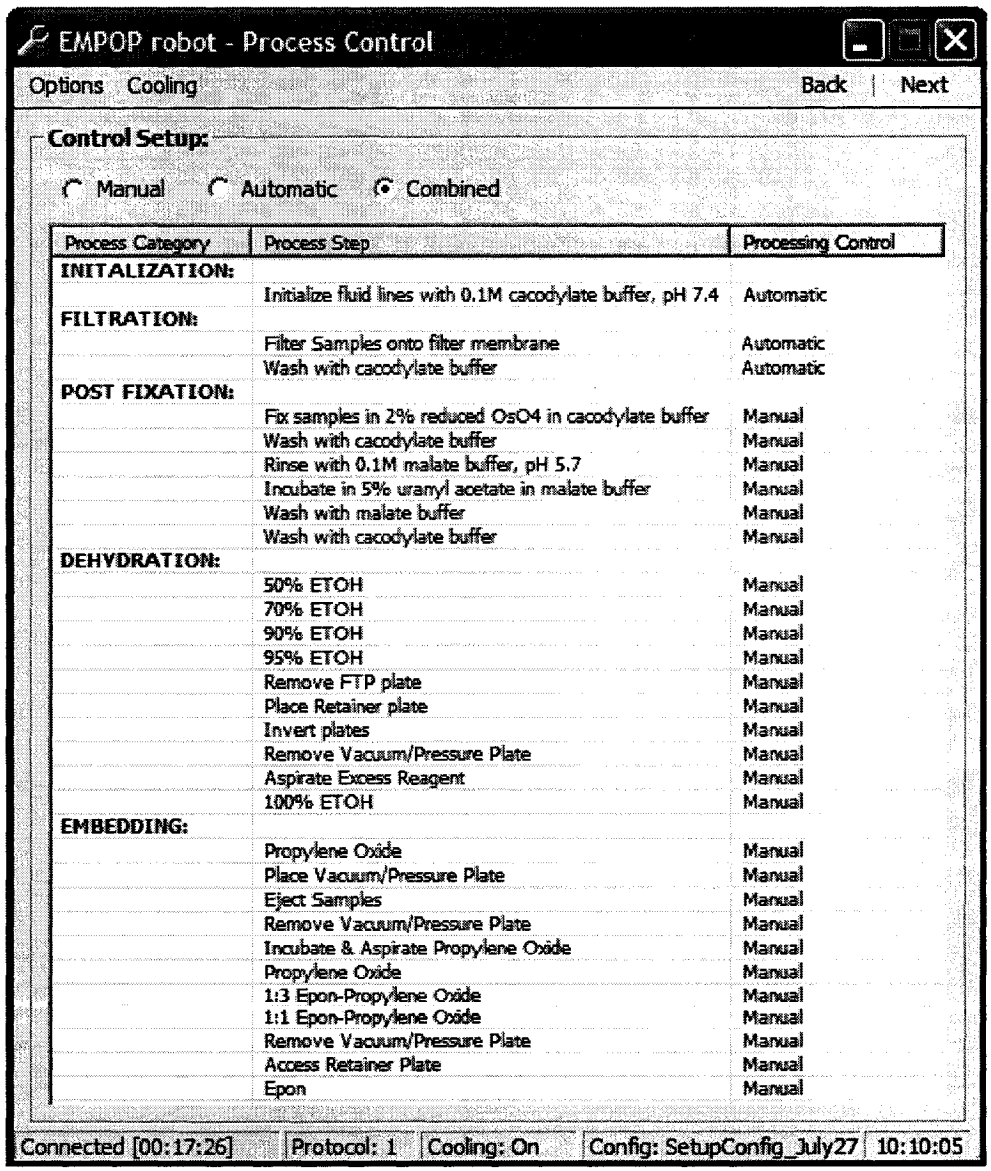

Figure 6.21: The EMPOP robot HMI Process Control GUI allows the operator to select steps to execute automatically and/or manually for step-wise execution of the process.

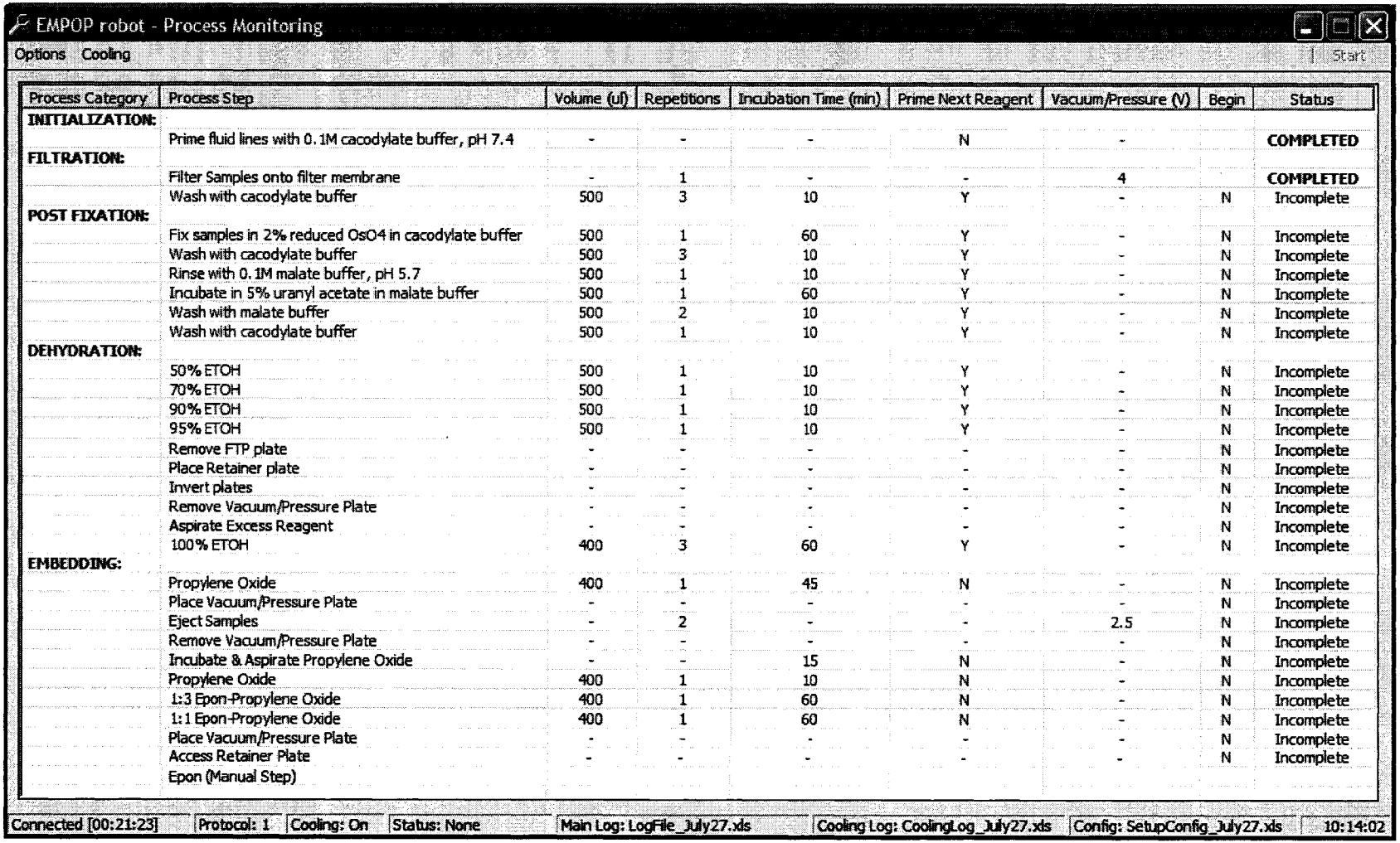

Process Category	Process Step	Volume (ul)	Repetitions	Incubation Time (min)	Prime Next Reagent	Vacuum/Pressure (V)	Begin	Status
INITIALIZATION:								
	Prime fluid lines with 0.1M cacodylate buffer, pH 7.4	-	-	-	N	-		**COMPLETED**
FILTRATION:								
	Filter Samples onto filter membrane	-	1	-	-	4		**COMPLETED**
	Wash with cacodylate buffer	500	3	10	Y	-	N	Incomplete
POST FIXATION:								
	Fix samples in 2% reduced OsO4 in cacodylate buffer	500	1	60	Y	-	N	Incomplete
	Wash with cacodylate buffer	500	3	10	Y	-	N	Incomplete
	Rinse with 0.1M malate buffer, pH 5.7	500	1	10	Y	-	N	Incomplete
	Incubate in 5% uranyl acetate in malate buffer	500	1	60	Y	-	N	Incomplete
	Wash with malate buffer	500	2	10	Y	-	N	Incomplete
	Wash with cacodylate buffer	500	1	10	Y	-	N	Incomplete
DEHYDRATION:								
	50% ETOH	500	1	10	Y	-	N	Incomplete
	70% ETOH	500	1	10	Y	-	N	Incomplete
	90% ETOH	500	1	10	Y	-	N	Incomplete
	95% ETOH	500	1	10	Y	-	N	Incomplete
	Remove FTP plate	-	-	-	-	-	N	Incomplete
	Place Retainer plate	-	-	-	-	-	N	Incomplete
	Invert plates	-	-	-	-	-	N	Incomplete
	Remove Vacuum/Pressure Plate	-	-	-	-	-	N	Incomplete
	Aspirate Excess Reagent	-	-	-	-	-	N	Incomplete
	100% ETOH	400	3	60	Y	-	N	Incomplete
EMBEDDING:								
	Propylene Oxide	400	1	45	N	-	N	Incomplete
	Place Vacuum/Pressure Plate	-	-	-	-	-	N	Incomplete
	Eject Samples	-	2	-	-	2.5	N	Incomplete
	Remove Vacuum/Pressure Plate	-	-	-	-	-	N	Incomplete
	Incubate & Aspirate Propylene Oxide	-	-	15	N	-	N	Incomplete
	Propylene Oxide	400	1	10	N	-	N	Incomplete
	1:3 Epon-Propylene Oxide	400	1	60	N	-	N	Incomplete
	1:1 Epon-Propylene Oxide	400	1	60	N	-	N	Incomplete
	Place Vacuum/Pressure Plate	-	-	-	-	-	N	Incomplete
	Access Retainer Plate	-	-	-	-	-	N	Incomplete
	Epon (Manual Step)							

Figure 6.22: The EMPOP robot HMI Process Monitoring GUI permits the operator to modify each step and follow execution of all steps throughout the process.

can adjust the protocol parameters during processing as well as execute steps in any sequence as many times as desired. This feature offers more control over execution of a protocol for testing and development of optimal parameter settings. Combined mode allows the operator to expedite a processing run by designating some steps to execute automatically and others manually.

(6) Process Monitoring. The GUI shown in Figure 6.22 allows the operator to set and pass operational parameters to the controller. It also calls low-level, embedded control routines to execute sample filtration, fluid handing, plate manipulation and sample ejection. It is the main operator interface for execution of a processing run and is composed of nine columns to permit modification of parameters and execution of each processing step. Columns 1 and 2 specify the processing stage and step. The next five columns allow the operator to set parameters for: (i) reagent dispense volume, (ii) step repetitions, (iii) incubation time, (iv) fluid lines priming for next reagent, and (v) vacuum or pressure levels for filtration or sample delivery. The buttons in column 8 permit execution of processing steps, and the corresponding locations in column 9 display their status.

6.3.2.1 Interaction with the Operator Tier

To use the robot for a sample preparation run, the operator must proceed through the series of GUIs presented in Section 6.4.2. In all GUIs, the operator can begin or stop operation of the cooling subsystem at any time.

In the *Ethernet Connection GUI* (see Figure 6.17), the operator establishes communication with the robot's controller. To expedite system calibration and setup for

the run or repeat a run with identical operational parameters, it is typical to upload a configuration file that provides operational parameters used in the remaining five GUIs. A configuration file is created from previous operation of the robot, where it is an option to save established parameters for repeated execution. The operator also has the option of creating log files with this GUI. The main log file stores system performance data throughout a run and the cooling log file documents the temperatures of the cooling platform and core mechanism.

Using the *Calibration Setup GUI* (see Figure 6.18), the operator must resolve the positions of all axes for all locations interacting with the dispensing/aspiration needles and the electromagnetic transfer arm. After positioning all axes to their home reference positions, all locations must be calibrated and saved to proceed to the next GUI. The operator typically completes this procedure by using the configuration file data, where the pre-calibrated positions can immediately examined, adjusted (if necessary) and saved to proceed to the next GUI. Finally, the options menu of this GUI permits the operator to set needle penetration depths for the fluid transfer and filter plates as well as the wash station.

The operator establishes the method of interaction for the dispensing/aspiration needles with the core mechanism in the *System Setup GUI* (see Figure 6.19). The operator sets number and arrangement of the needles to be used, the needle washing frequency, and the range of consecutive processing channels that must be approached by the needles during the run.

In the *Reagent Setup GUI* (see Figure 6.20), the operator specifies the protocol to be used and the arrangement of reagents as they are accessed by the processing reagent

handling subsystem. In addition, the options menu of this GUI permits testing of all reagent lines.

The operator specifies an automatic or manual control mode for each step of the protocol in the *Process Control GUI* (see Figure 6.21).

The operator interacts with the *Process Monitoring GUI* (see Figure 6.22) for the remainder of the sample preparation run. For each reagent of the specified protocol, the GUI permits the operator to set the dispense volumes, repetitions of the step, incubation times and the option to prime the next reagent in the protocol. Vacuum and pressure levels for sample filtration and delivery steps are adjusted in the same way. These operational settings appear automatically when a configuration file is used. Depending on the control mode specified, the GUI also permits the operator to execute individual steps and reports the status of completion.

The options menu of this GUI allows the operator to:

(1) Set the reagent dispensing velocities and a needle residence time for aspiration (see Figure 7.12)
(2) Set the proportional solenoid valve settings for vacuum and pressure to the core mechanism.
(3) Set the sample delivery settings for the number and duration of pressure pulses.
(4) View status bars to monitor cooling platform and core mechanism temperatures as well as the vacuum and pressure levels of the pneumatic subsystem.
(5) Terminate the run.
(6) Create a configuration file for reuse of all operational parameters in another run.

6.3.3 Control Tier

The control tier is the lower level of the client-server software architecture. It is invisible to the operator and, by way of the robot controller, executes all real-time tasks. The library of process control routines created for the control tier are reusable and modular. Therefore, organization of low-level routines follows a top-down structure; routines in each layer can only call routines in the same or lower layers. The layer assigned to a routine depends upon its role within the robot system; from top to bottom, the routines become more specialized.

Because routines associated with a particular GUI never call the routines of another, their specific control routines are organized into separate top-down structures. Coordination and integration of the Process Monitoring GUI (see Figure 6.22) routines enables execution of the preparation protocols. Its routines are the most complicated and numerous and so are used as an example, where a block diagram of the top-down structure is shown in Figure 6.23.

The HMI calls only first-order routines, ensuring separation between the operator-level and the control-level. First-order routines direct the robot's overall processes for cooling, fluid handling and positioning. Conversely, routines at the lowest levels perform very specific tasks within processes, such as reservoir pressurization and valve actuation. Two types of lower level control routines assist first-order routines. The first type, shown in grey in the block diagram, are activated by the controller and run independently of the main process (*via* the multitasking capacity of the controller and its software development language [261, 262, 273], see Section 5.6.1). The remaining routines are dependent on and only respond to higher-order programs.

6.3.3.1 Independent Control Tier Routines

To control frequently or continuously used operations, or operations necessary to protect the robot from damage due to a failure, the control tier employs an advisory program that mimics a programmable logic controller (PLC) [202-204]. PLC modules are microprocessor-based devices that trigger execution of a user-defined routine associated with a change in state of any I/O channel. Utilizing the multi-tasking capacity of the robot controller, the software framework incorporates the PLC program for efficient automated operation of the robot; allowing the controller to carry out several functions simultaneously, independently of the routine that is currently executing.

Figure 6.24 is a state diagram of the PLC program. In response to state changes of specific I/O channels and/or variable conditions, the program activates one of six different control routines:

(1) Create Vacuum. Activated by signaling from the vacuum transducer, the routine charges the vacuum reservoir to a pre-defined level. It is the first of the ordered PLC program tasks due to its frequent use. To avoid a conflict among different routines that use vacuum, the code implements a pneumatics semaphore, a binary variable that is shared among all routines requiring vacuum, to signal the state of vacuum use. Before any routines requiring vacuum begin their task, they must wait for the pneumatics semaphore to become available and then take possession of it for duration of their activity.

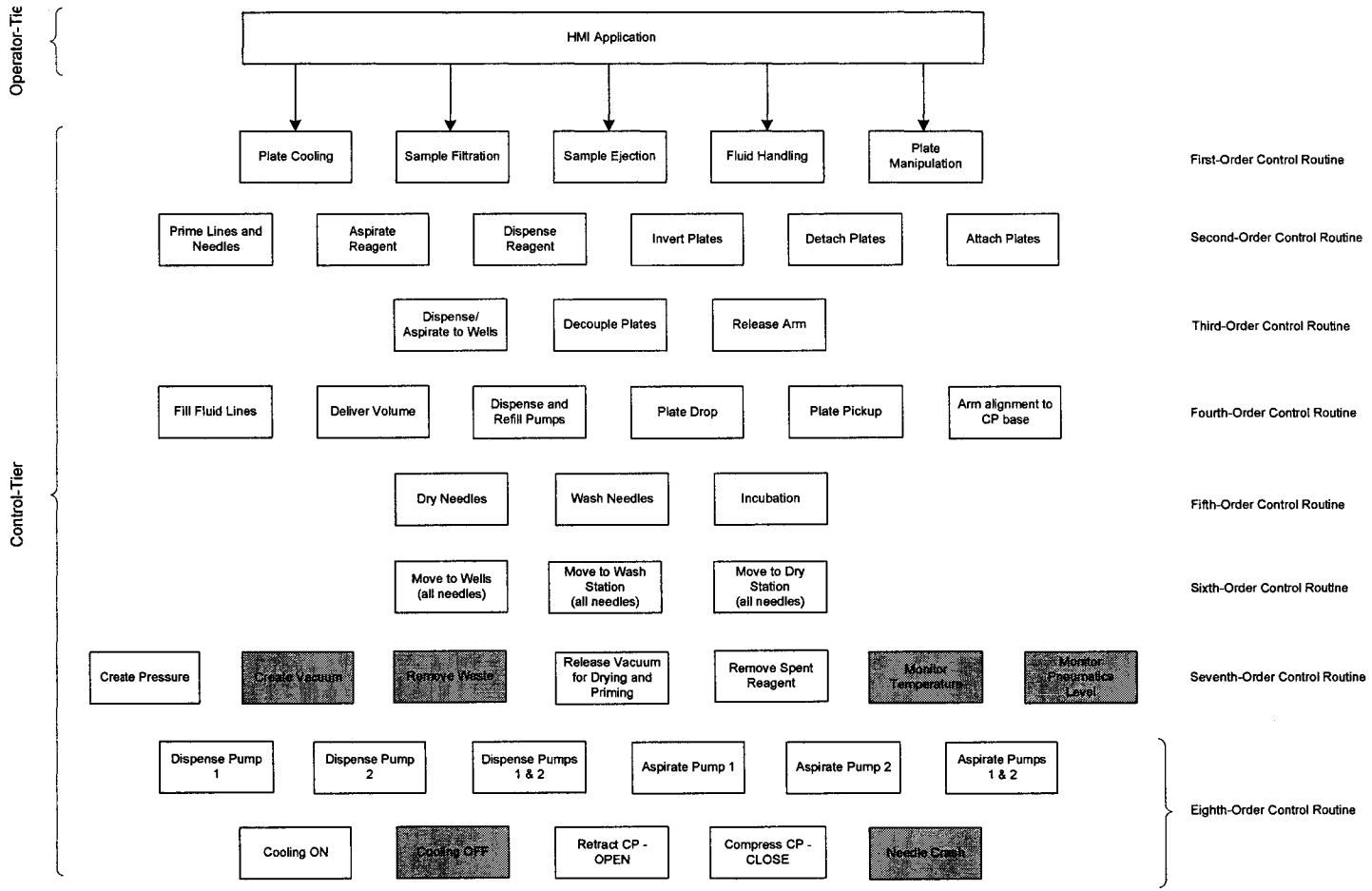

Figure 6.23: Block diagram of the top-down organization of control routines associated with the HMI Process Monitoring GUI. The HMI calls only first-order control routines which are supported by dependent control routines that become increasingly more task-specific at the lowest levels. The grey lower-level control routines indicated with grey-blocks run independently of the main process.

(2) Remove Waste. The "Remove Waste" routine eliminates accumulated waste in vacuum reservoir. Due to its frequent use, it runs in the background. The routine requires full control of the vacuum reservoir and, therefore, must wait for the pneumatics semaphore's to become available before executing.

(3) Cooling OFF. To avoid damage to the thermoelectric cooling system and the biological samples, this routine disables the cooling subsystem immediately if the temperature of the cooling platform or filter plate exceeds 35°C.

(4) Needle Crash. To minimize system damage in the event of a needle manifold collision, this routine is activated by the needle manifold collision sensors and returns all robot motion control axes to their respective home positions.

(5) Monitor Pneumatics Level. The routine reports vacuum and pressure reservoir levels to the Process Monitoring GUI, which provides the operator with a visual indication the pneumatic subsystem performance *via* two continuously updated status bars.

(6) Monitor Temperature Level. The routine reports the temperature of the cooling platform and the filter plate to the cooling log file and the Process Monitoring GUI. Two status bars continuously display the temperature of the cooling platform and the filter plate.

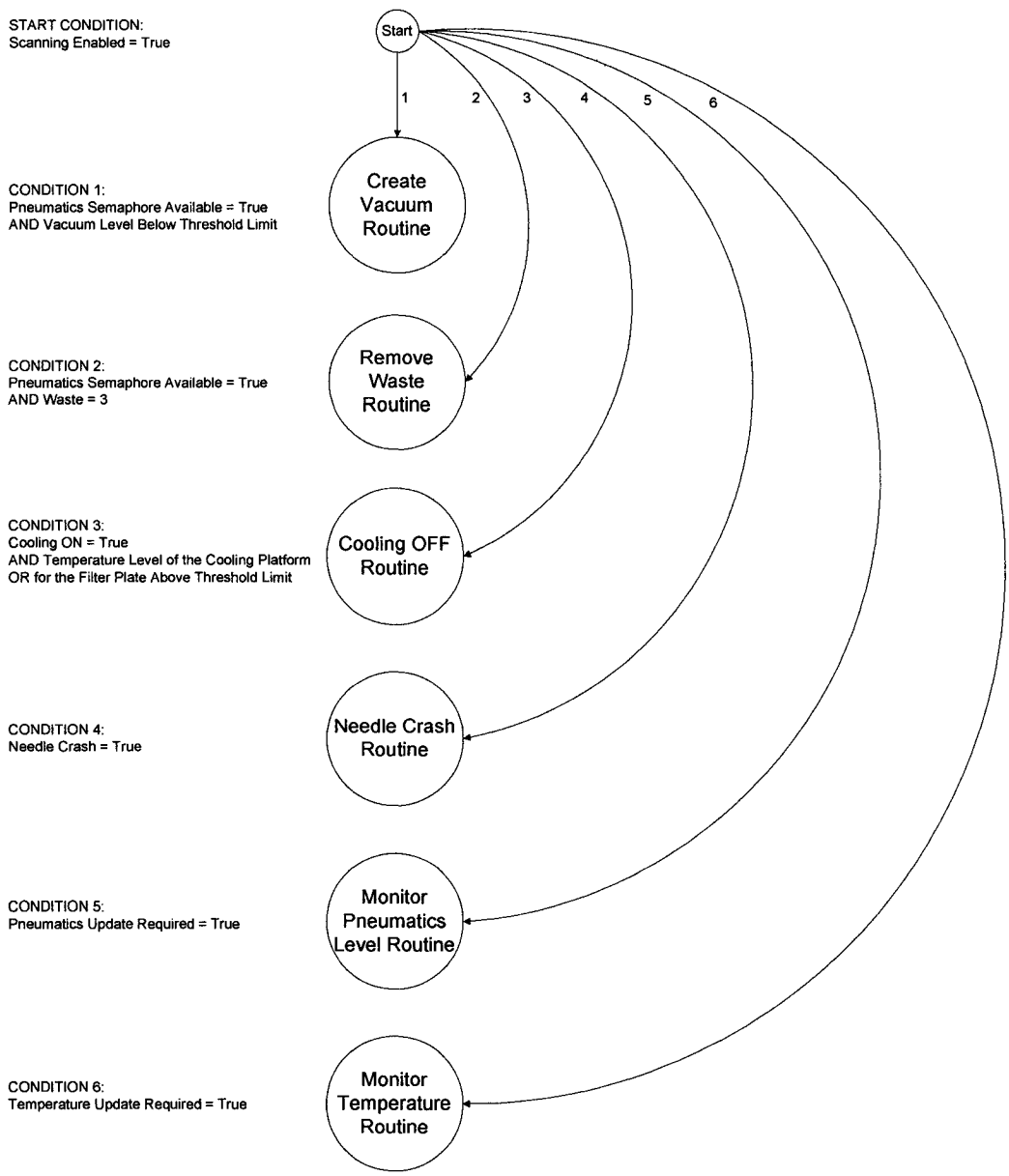

Figure 6.24: State diagram of the control-tier PLC program and activated independent control routines

6.3.3.2 Dependent Control Tier Routines

To ensure separation between the operator and the control-levels, the HMI calls only first-order routines. The algorithms are complex and a complete description of each can be found in "Automated Control of the Electron Microscopy Cell Fraction Preparation Robot" [172]. A general discussion is given here to illustrate how the robot's main processes are controlled by five first-order routines:

(1) Plate Cooling. The cooling subsystem can be activated by the operator at any time during the setup procedure and operates in parallel with all other processes. As Figure 6.25 shows, depending on the operator's request to either initiate or terminate core mechanism cooling, the first-order routine uses only two eight-order control routines – *Cooling ON* and *Cooling OFF*.

(2) Sample Filtration. Sample filtration occurs once during each preparation run. However, for protocol optimization, the *Sample filtration* routine (see Figure 6.26) permits the operator (*via* the Process Monitoring GUI) to repeat filtration sequences automatically or manually with the same or an adjusted vacuum level.

(3) Sample Delivery. Sample delivery occurs once during the protocol, although it can be repeated in a manner similar to that for sample filtration. Additionally, for optimization of the delivery procedure, the operator may also specify the number of pressure pulses and the duration of each pulse for a single pressure release (see Figure 6.27).

(4) Reagent Handling. The *Reagent Handling* first-order control routine is responsible for the execution of about 60% of the steps within a preparation

protocol. Reagent handling is the most complex process to render to automatic control; it requires the integration of many routines within different layers to treat each processing channel.

As Figure 6.28 shows, prior to dispensing, incubation and aspiration of a particular reagent, the HMI must receive confirmation that the control unit has downloaded reagent handling parameters for volume, repetitions, incubation, and priming. In operation, the routine uses these parameters to follow a complex path that calls four lower-order routines.

(5) Plate Manipulation. The *Plate Manipulation* routine executes plate interchange and inversion operations to form the delivery and embedding core mechanism plate configurations. Figure 6.29 shows how the routine calls three second-order control routines that are responsible for (i) plate decoupling, (ii) plate coupling and (ii) core mechanism inversion.

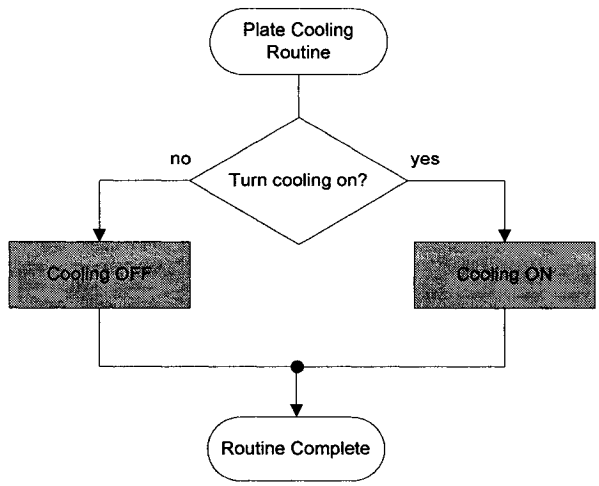

Figure 6.25: Flow chart for the *Plate Cooling* routine first-order control algorithm. Shaded bases indicate the lower-order routines that called by the routine.

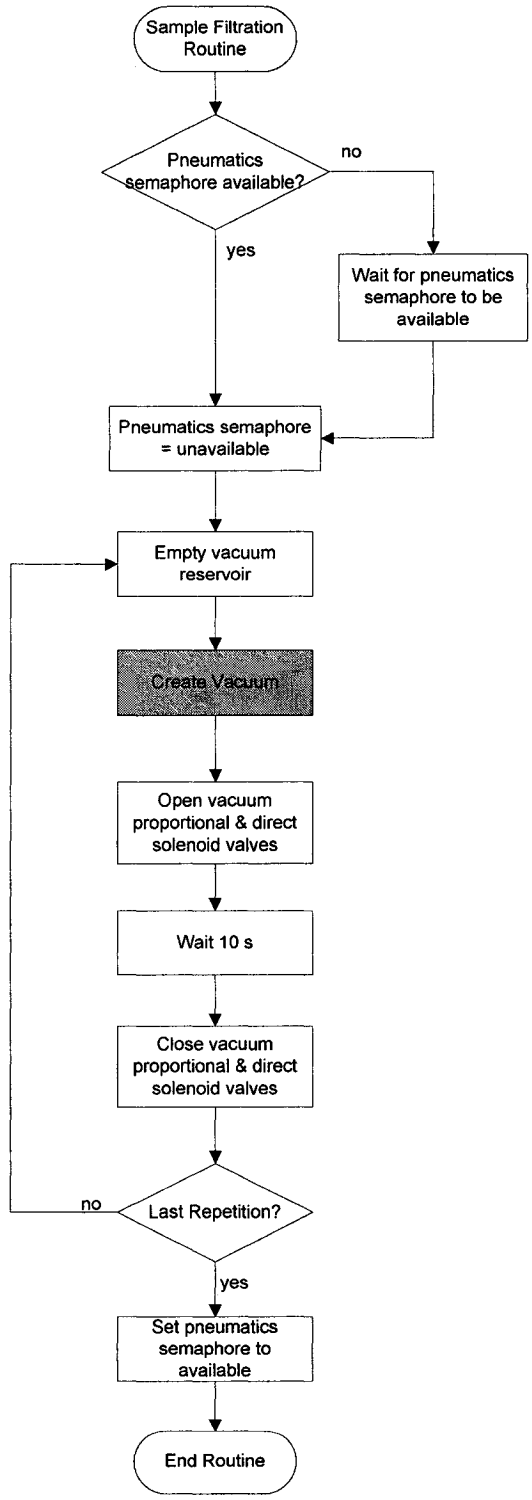

Figure 6.26: Flow chart for the *Sample Filtration* routine first-order control algorithm. Shaded base indicates the lower-order routine that the routine calls.

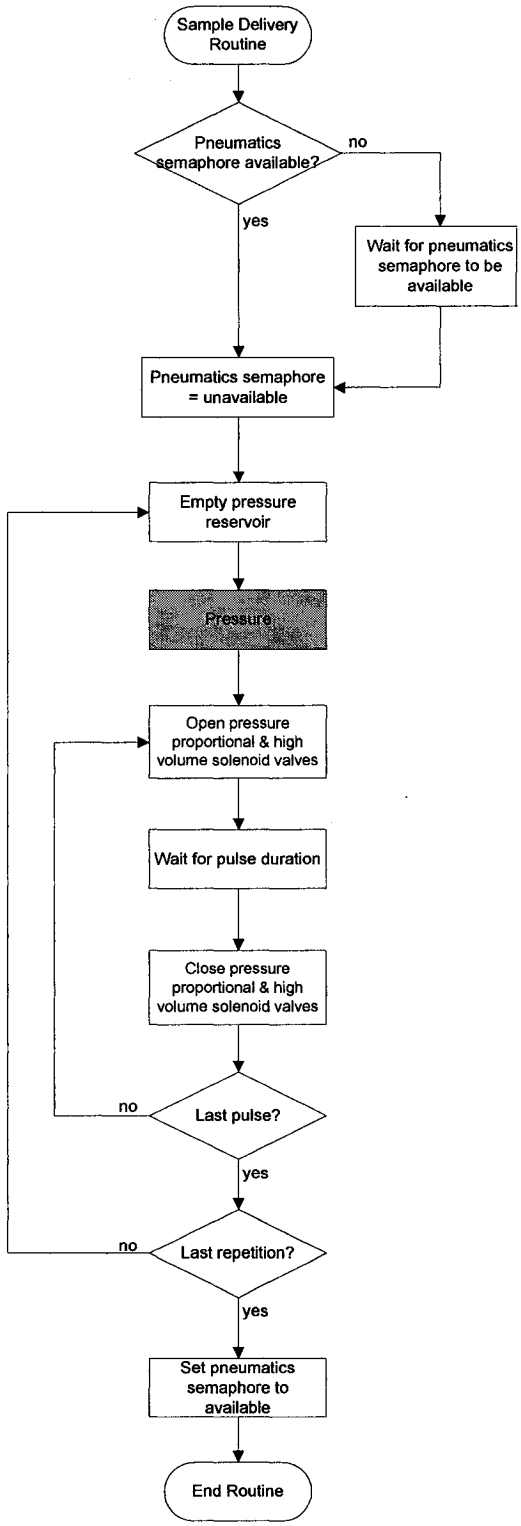

Figure 6.27: Flow chart for the *Sample Delivery* routine first-order control program. Shaded base indicates the lower-order routine called by the routine.

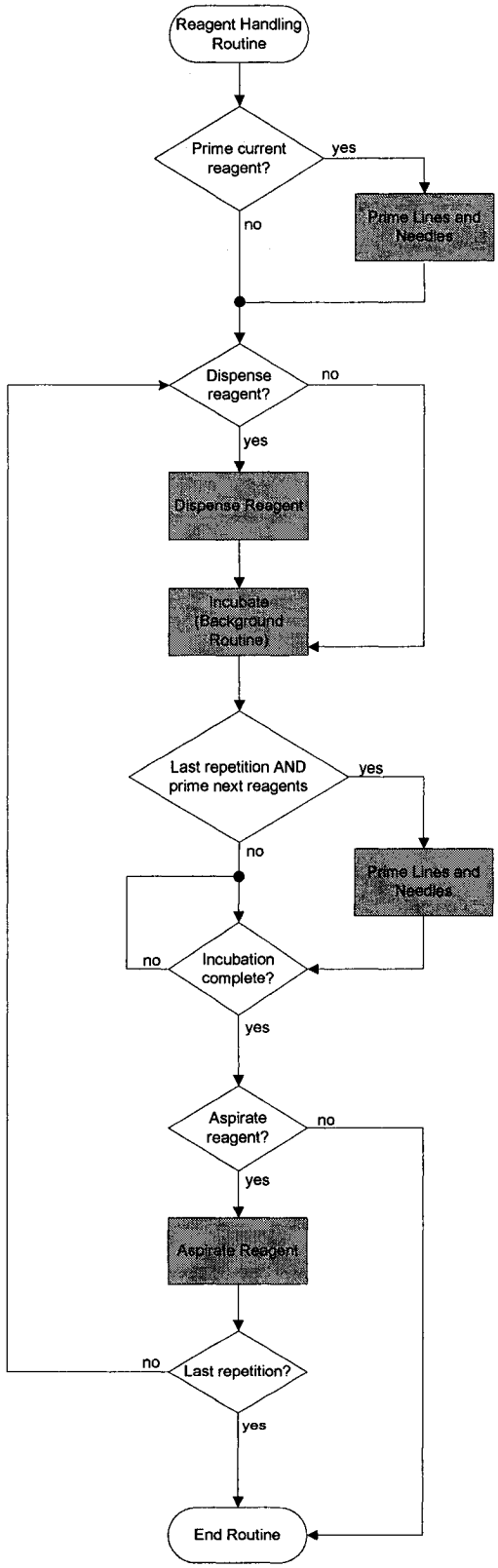

Figure 6.28: Flow chart for the *Reagent Handling* routine first-order control algorithm. Shaded bases indicate the lower-order routines that called by the routine.

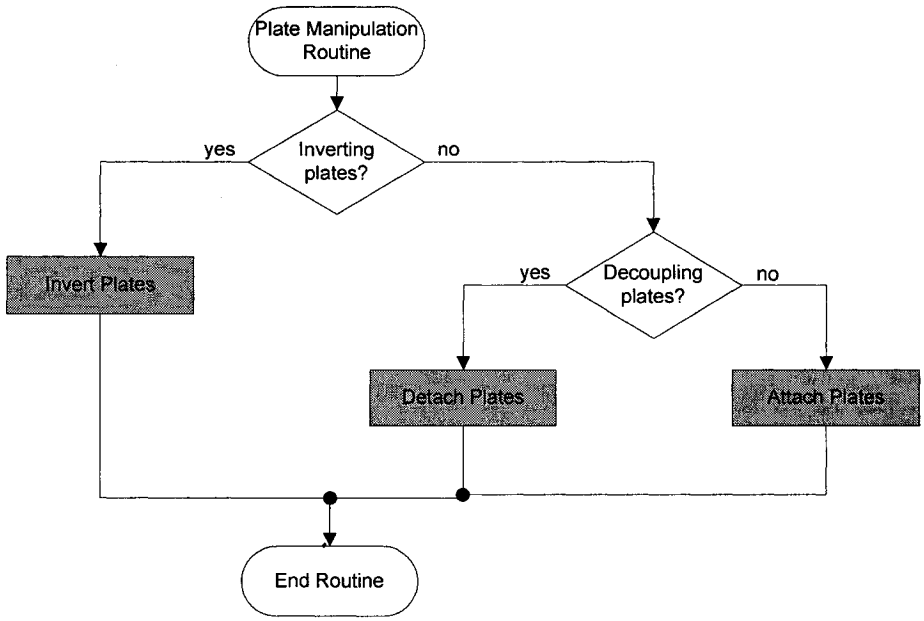

Figure 6.29: Flow chart for the *Plate Manipulation* routine first-order control program.

7 Experimental Results

7.1 Overview

This chapter describes four experiments carried out during the development and validation of the EMPOP robot. Experiment I used a test device that emulated a single processing channel of the core mechanism, to demonstrate feasibility. Subsequent to these experiments, initial trials of the robot demonstrated there was a need to define essential process parameters and determine optimal operating conditions. It was felt that attempting to answer these questions with the full robot would be cumbersome and slow. Consequently, Experiment II used a simplified platform to screen a wide range of operation parameters rapidly. Experiment III used these results to demonstrate that the robot could generate samples successfully. Finally, Experiment IV demonstrated the full capability of the EMPOP robot by generating 96 parallel samples.

7.2 Experiment I: Process Feasibility

The objective of Experiment I was to demonstrate the feasibility of the automated sample processing steps from vacuum filtration through pressurized delivery. For this experiment, a single-channel test device was built to emulate a single processing channel of the core mechanism.

7.2.1 Test Device

Figure 7.1 illustrates the device and its operation. It had four reconfigurable, stacking plates fabricated from 30 mm diameter aluminum rod. Their geometries, O-rings, and filter screen reproduced the internal environment of a core mechanism processing channel. A screw fastening arrangement reproduced the interchangeable design feature of the core mechanism and provided compression for plate-to-plate sealing. Each plate of the device had an identical array of four, aligned threaded holes and corresponding holes for clearance, located on a radius from center of the processing channel. The radial symmetry permitted the use of screws for fastening the interchangeable plates together and fasten the filter and retainer plate caps to their respective plates.

Figures 7.1A and B show the processing configuration of the test device. The geometry and arrangement is identical to a core mechanism processing channel except that the vacuum-pressure plate was replaced by two ports that connected (*via* switch actuated solenoid valves) to a vacuum source and a vent to atmosphere.

For sample filtration, vacuum was applied by way of a switch actuated solenoid valve to deposit the sample on the filter membrane disk in the filter plate. The vent line was opened by way of a second solenoid valve to direct the flow of air from atmosphere for pressure relief and to prevent the samples from going to dryness. After filtration, the tube fittings were replaced by screws fitted with O-rings to seal the processing channel. The chemical processing steps of the sample preparation protocol were done by dispensing and aspirating reagents manually.

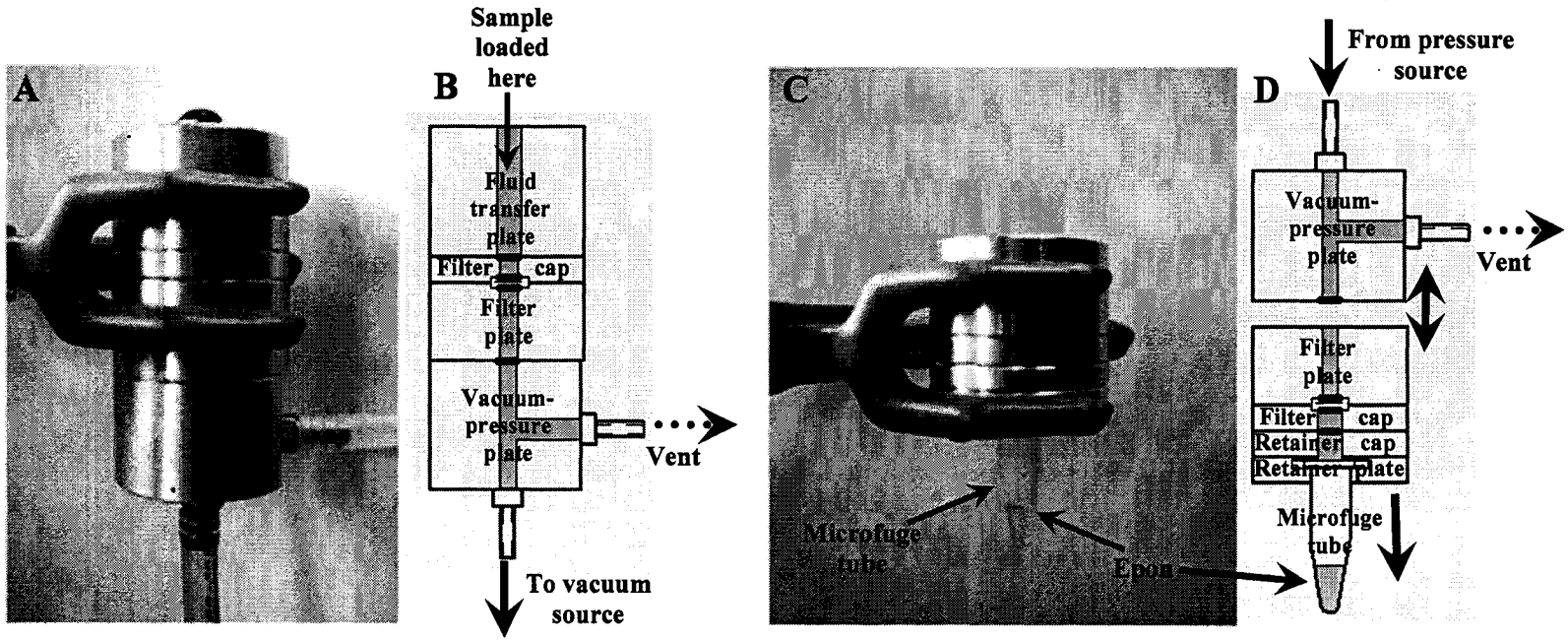

Figure 7.1: Two configurations of the test device emulating a single processing channel of the core mechanism. Photographs and cross-sectional schematics show (A) the assembled processing configuration, (B) the fluid paths (shaded gray) and sample location in the processing configuration, (C) the assembled embedding configuration, and (D) the fluid paths (shaded gray) and sample location in the embedding configuration. The double headed arrow in (D) indicates the method of fastening and release of the vacuum-pressure plate to the embedding configuration to form the delivery configuration.

Figures 7.1C and D show the embedding and delivery configurations of the test device. The arrangement was similar to that of a core mechanism processing channel except that the retainer plate was fitted with a transparent microfuge tube. Because the tube extended from the device, it permitted observation of the sample delivery step and accumulation of the delivered sample on top of the flat surface provided by polymerized Epon. Similar to the processing configuration, a vacuum-pressure plate port was connected to pressurized air for sample delivery and excess pressure was vented to atmosphere.

7.2.2 Experimental Methods

Two validation experiments were carried out to simulate the sample processing steps from vacuum filtration through pressurized delivery. The subcellular fraction samples were processed according to the manual protocol for morphometric analysis (see Table 2.1) and all steps were completed at room temperature. All reagents were manually dispensed and aspirated with 1 ml syringes, and the filtration and delivery steps were executed as described above.

In each experiment, a 50 μg sample of a glutaraldehyde-fixed rat hepatocyte plasma membrane suspension was loaded into the processing configuration of the test platform through the fluid transfer plate. Sample filtration was completed using a -5 psi vacuum source and stopped before the membrane-bound samples were completely filtered to dryness. Then the sample was post-fixed, stained, and dehydrated according to the manual preparation protocol. After application of solvent (propylene oxide) to

dissolve the filter membrane, the sample was delivered using pressurized air. There was approximately 5 minutes delay between the two steps.

7.2.3 Results of the Process Feasibility Experiment

Figure 7.2A shows the results of one experiment. The photograph was taken immediately following application (and removal) of 30 psi of pressurized air to the delivery configuration. Much of the sample has been transferred to the Epon surface in the microfuge tube and fragments of material can be seen settling down. Figure 7.2B shows the entire sample settled to the surface of the polymerized Epon (approximately 10 minutes delay after delivery) with the excess solvent removed.

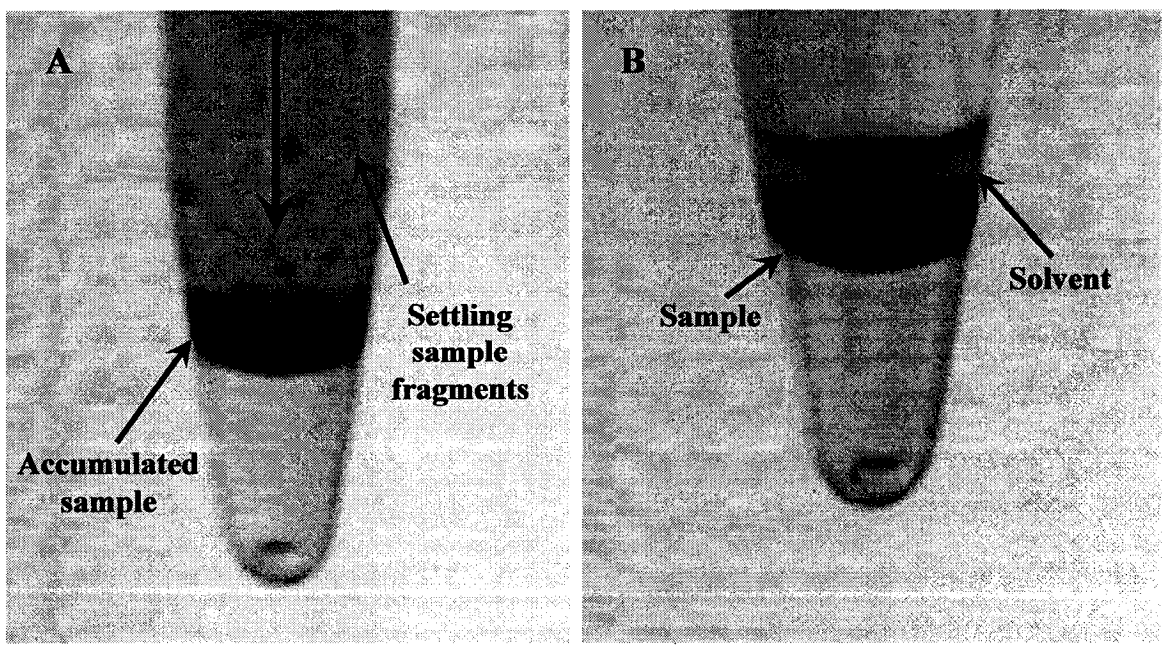

Figure 7.2: Photographs of the retainer plate microfuge tube of the single processing channel test device showing (A) sample delivery immediately after brief pressurization with 30 psi of air and (B) the accumulated sample.

The results of this experiment demonstrated the feasibility of sample processing in the core mechanism from sample filtration through delivery steps. Furthermore, the results illustrated the potential for automation of the process; similar operations can be carried out on parallel samples with the appropriate fluid handling tools and positioning systems.

7.3 Experiment II: Process Screening

7.3.1 Process Validation Experiments

After construction of the robot, troubleshooting electrical and mechanical systems, and debugging code, initial process validation experiments were completed with the robot.

7.3.2 Experimental Methods

In all experiments, subcellular fraction samples of 25 μg of glutaraldehyde-fixed rat hepatocyte plasma membrane suspension were loaded into 24 wells of the core mechanism processing configuration. Using the reagents of manual preparation protocol, the samples were then automatically processed through the entire protocol of filtration (executed with -5 psi vacuum), post-fixation, staining, dehydration, delivery (executed with 30 psi pressurized air), and embedding.

7.3.3 Results of Initial Process Validation Experiments

Figure 7.3 shows an example of the filter, filter screen and delivered samples from an initial experiment. Ideally, the 24 processed and delivered samples should occupy the corresponding Epon-loaded wells of the 96 well plate and appear as darkly stained pellicles covering the surface of the Epon. However, very little sample was delivered to the 96 well plate.

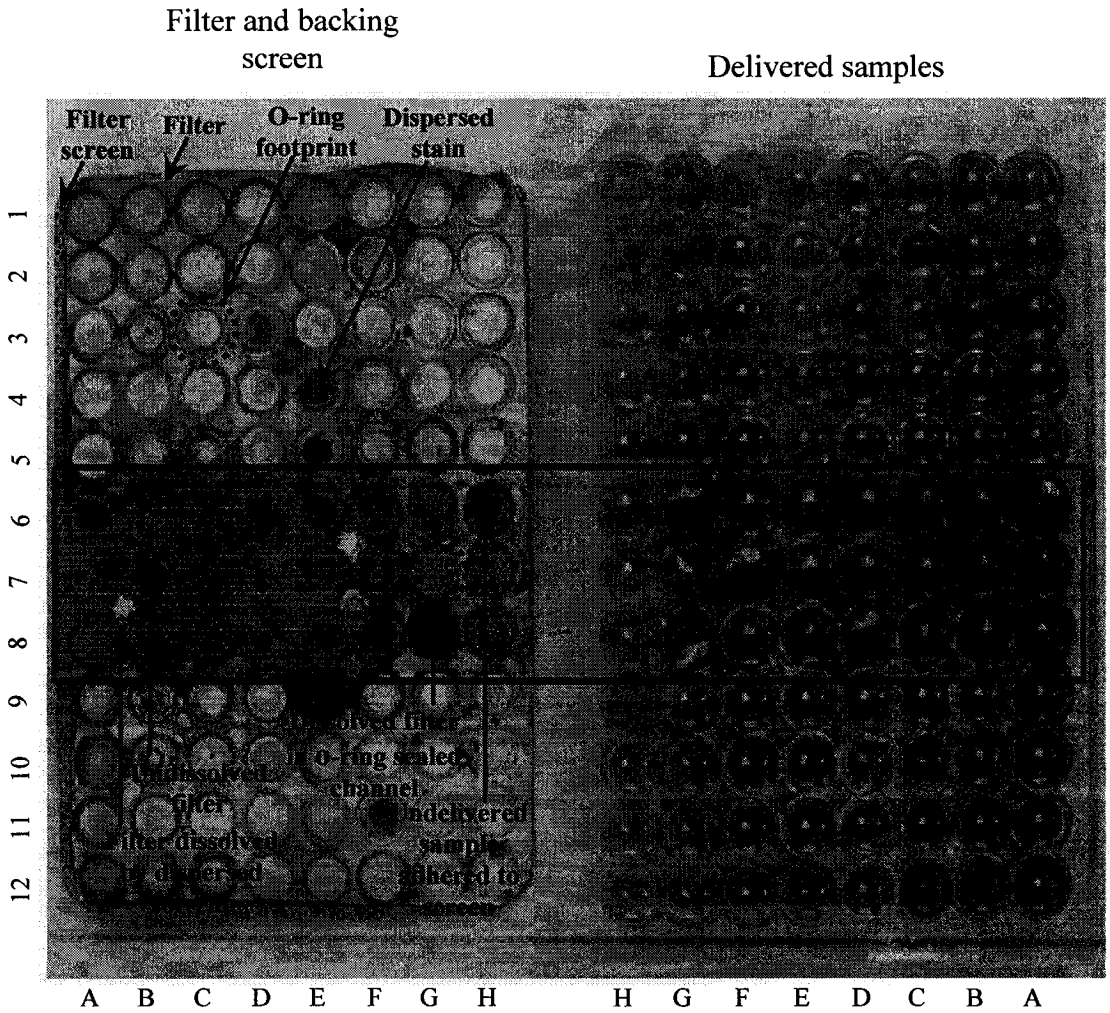

Figure 7.3: Photograph illustrating the filter/filter screen and delivered samples from an initial automated sample preparation experiment. Artifacts from the automated run indicate the necessity for process refinement.

Artifacts from the sample preparation experiment can be seen in the illustration of the filter and filter screen. The O-ring footprints are uniform indicating that sealing against the filter membrane was adequate. However, other artifacts indicating staining and dissolved filter membrane between O-rings, illustrated that there was dispersion of processing reagents over the surface.

The photograph of the filter and filter screen also shows that the membrane dissolution and sample release were not effective. In many of the 24 sample processing locations there is undissolved filter membrane and/or unreleased sample. Although there is little membrane or sample remaining at the sample processing locations, very little appears in the 96 well plate. As membrane sealing was adequate and the samples are trapped in the core mechanism during the delivery step, this result indicates that the samples were lost before delivery, in the reagent dispensing and aspiration steps of the chemical processing stage of sample preparation.

7.4 Conditions for Process Refinement

Although the system was fully operational, the results of the initial experiments were poor. Further analysis indicated that there was a need to optimize fluid handling parameters as well as the methods and supporting materials in the core mechanism. In particular, optimization issues were identified for all three configurations of the core mechanism: (1) processing, (2) delivery and (3) embedding (see Figure 3.2).

(1) Processing. Process optimization of this configuration was needed to maintain the morphological integrity of organelles and the structural integrity of the filter-bound sample in the processing configuration. To do so, it was necessary to:

(i) Define a level of vacuum such that sample filtration stops naturally as the charged filter membrane saturates with organelles. Moreover, it should generate a filtration velocity low enough to saturate the filter and preserve the organelle morphology.

(ii) Determine the reagent dispensing velocity and the dispensing needle penetration depth that would expose the sample to fresh reagents without disrupting them.

(iii) Define the reagent aspiration velocity and aspiration needle penetration depth needed to remove waste effectively (to avoid dilution of successively dispensed reagents) and not disrupt or detach the samples.

(iv) Find a chemically compatible, sealed-filter screen surface that would eliminate liquid dispersion and maintain sample localization within the filter plate.

(2) Delivery. The pressure level, pulse frequency, and duration for sample delivery in the delivery configuration must be defined such that the samples are delivered effectively but are not fragmented or disrupted.

(3) Embedding. To maximize sample delivery and the quality of samples produced from the embedding configuration it was necessary to optimize:

(i) The solvent dispensing velocity, which must be high enough to penetrate the filter screen for adequate filter membrane dissolution, sample release, and maintenance of sample integrity.

(ii) The duration of the pre-delivery solvent incubation must be determined so as to maintain the structural integrity of the samples during the delivery step.

(iii)To deliver unreleased sample from the filter screen and remove dissolved filter membrane from the retainer plate (while avoiding sample disruption and/or removal), the solvent dispensing/aspiration velocities must operate within a standard range, and the embedding configuration, needle penetration depths must be optimized.

(iv)The Epon level in the 96 well plate must be optimized for efficient liquid exchange across the filter screen while imposing minimal perturbations on the samples.

7.5 Process Screening

It was decided that using the robot to do these optimizations would be slow and make it difficult to study individual process steps. Consequently, a screening platform was constructed to provide for the rapid testing and refinement of some of the operational parameters and methods discussed above. Figure 7.4 shows the components of the screening setup and the assemblies required to emulate the three configurations of a

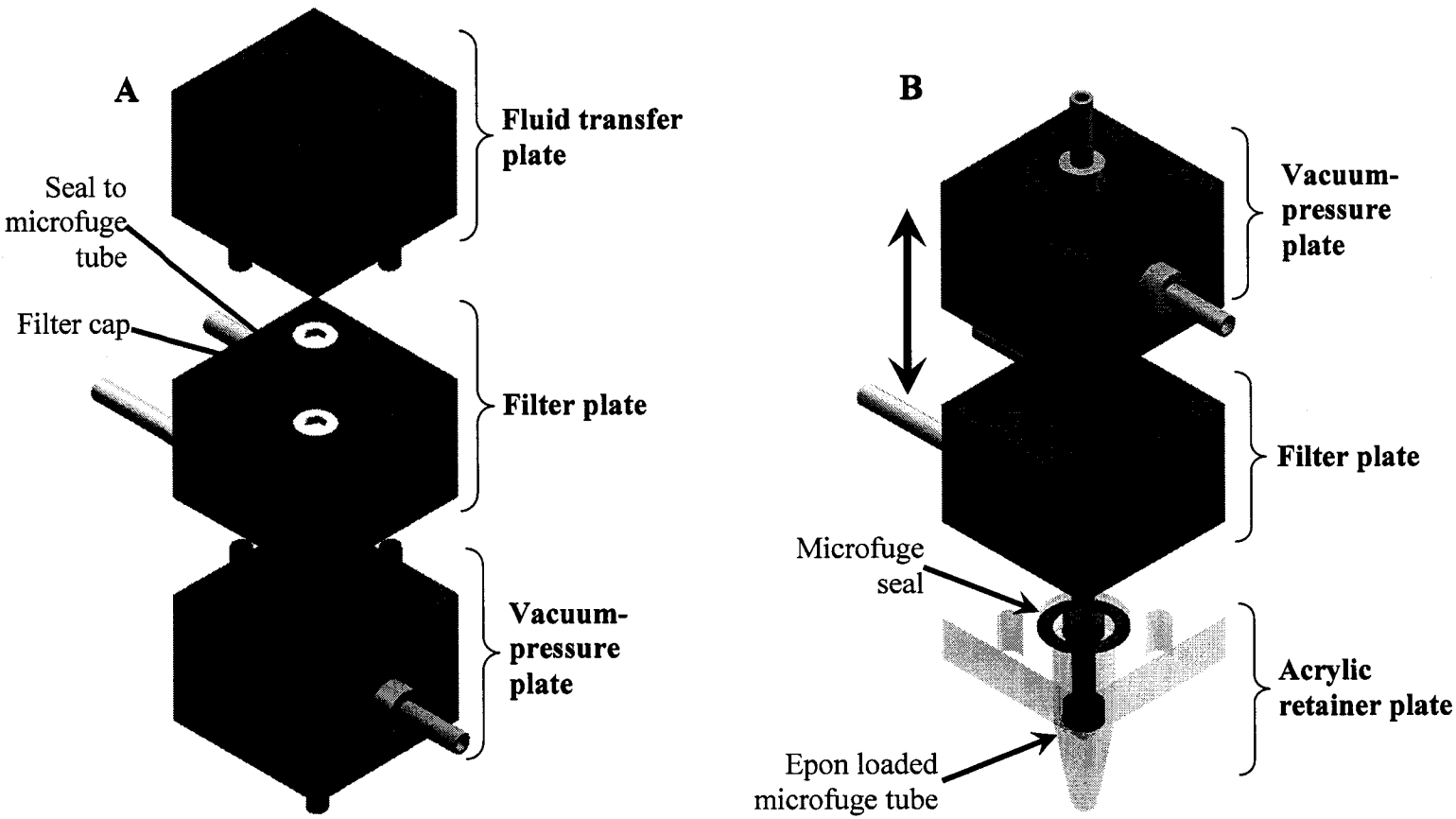

Figure 7.4: 3D CAD renderings of the single processing channel arrangements illustrating the components and assembly of the (A) processing configuration and (B) the delivery and embedding configurations. The double headed arrow indicates how the vacuum-pressure plate fastens to the embedding configuration to form the delivery configuration.

single processing channel of the core mechanism. They are very similar to the device used for the process feasibility experiments discussed in Section 7.2. However, in this case the construction incorporated an acrylic retainer plate to permit direct observation of sample delivery. Figure 7.5 shows the seven identical channels used in the optimization

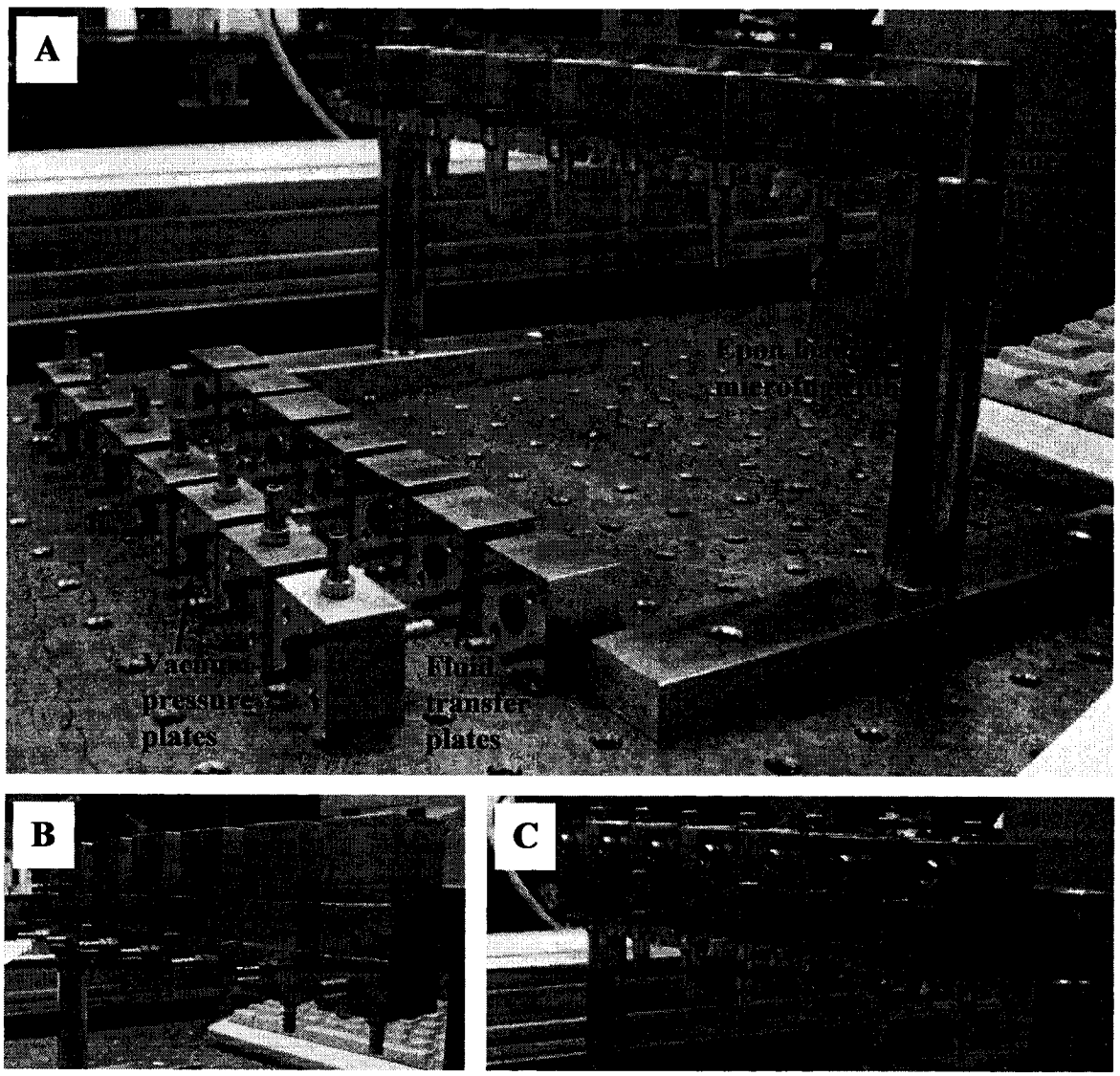

Figure 7.5: Photographs of the screening platform illustrating the seven single processing channel configurations for sample (A) embedding, (B) processing, and (C) delivery.

experiments in each of the three configurations.

Because sample retention was successfully demonstrated in the feasibility experiments, sample delivery was regarded as the relevant step to examine in these experiments. Therefore, seven channels were used to generate sample delivery data over a range of incrementally changed delivery pressures and/or a series of delivery pressure pulses (see Table 7.2). In addition, because most manipulations were performed manually, the timing of the protocol for each channel was identically offset by several minutes in order to process samples in parallel. This imposed a practical limitation on the number of channels that could be examined.

Four experiments were conducted using the screening platform to examine the automated process according to the most effective conditions through sample delivery. Conditions generating the best performance were carried to the next experiment quickly define the conditions for successful processing and sample delivery. The six operations examined in these experiments are indicated in the cross-sectional schematics of Figure 7.6 and the corresponding protocol steps are listed in Table 7.1. These experiments addressed the following issues:

(1) Minimization of vacuum level for filtration. When subcellular fraction samples are filtered with the correct positive pressure using the manual filtration device (see Section 2.4.2), the organelles will eventually saturate the filter membrane and prevent any further passage of liquid (or deposition of organelles). If the pressure is too high, filtration will be too fast and the morphology of the organelles may be damaged or compromised. The conductivity sensors located

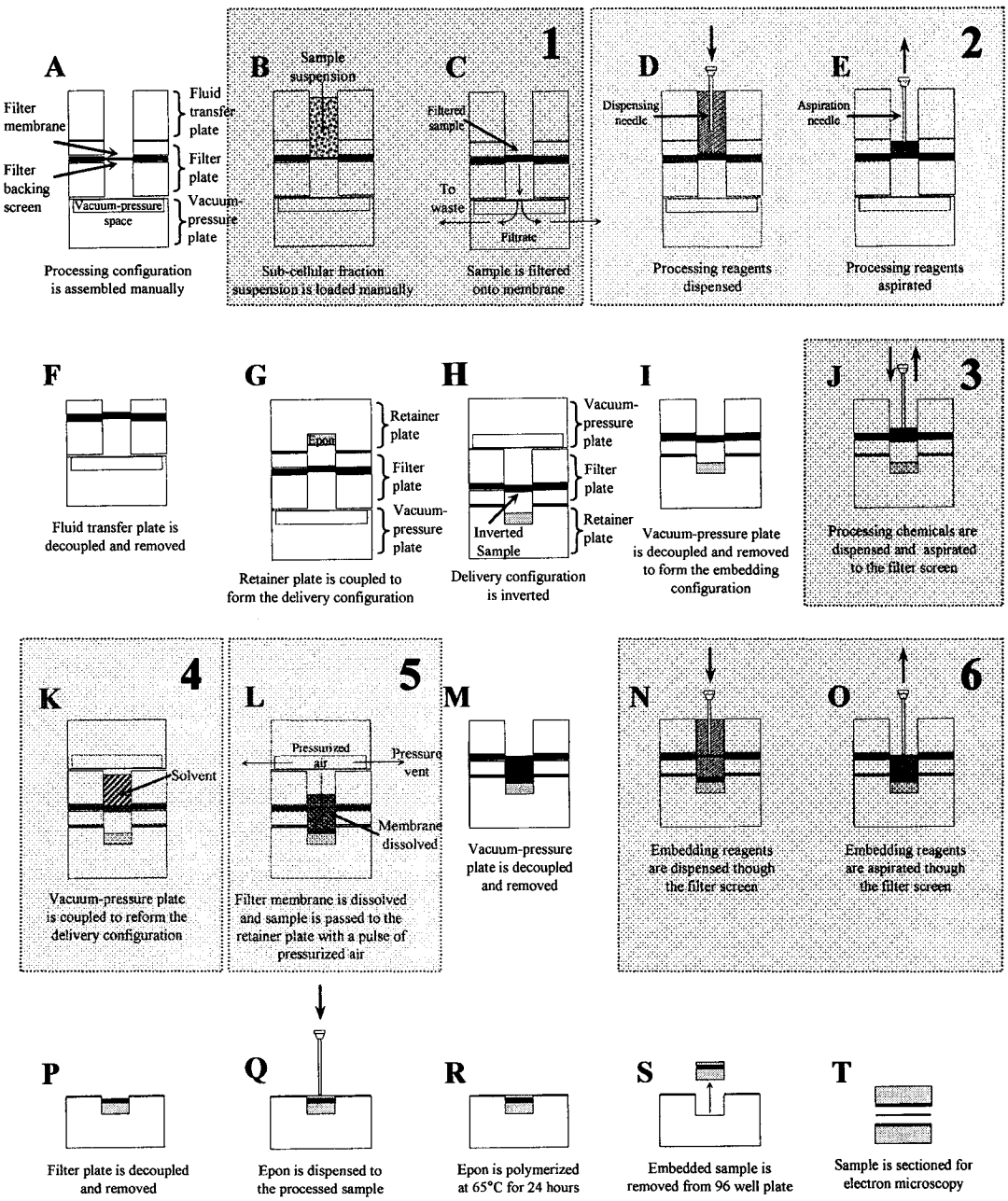

Figure 7.6: Cross-sectional schematics of a single processing channel of the core mechanism illustrating each stage of the automated sample preparation protocol. The grey shaded regions indicate the six issues examined in the process screening experiments: (1) minimization of vacuum level for filtration, (2) effect of reagent dispensing and aspiration velocities, (3) effect of reagent dispensing and aspiration velocities on inverted samples, (4) pre-delivery solvent incubations, (5) sample delivery pressure level, duration, frequency and effect of filter screen material, and (6) solvent dispensing and aspiration across the filter screen.

Table 7.1: Manual subcellular fraction sample preparation protocol for TEM morphometic analysis (91) modified for single processing channel process optimization experiments. The grey shaded regions correspond to the six issues examined in the process screening experiments (see Figures 7.6A to T).

Fixation:

4. Add equal volume of fixative (5% glutaraldehyde, 0.1% $CaCl_2$, 100 mM cacodylate buffer, pH 7.4) to 2 ml of 100 μg/ml protein, store at 4°C.

Filtration:

5. Filter on Millipore™ filter type HA with 0.8 μm pore size. **1**

Post fixation/staining:

6. Wash the filter with bound sample in 100 mM cacodylate buffer, pH 7.4 three times for 10 minutes each.
G. Incubate the samples in 2% reduced osmium tetroxide, 1.5% potassium ferrocyanide in 100 mM cacodylate buffer, pH 7.4 for 1 hour.
H. Wash 3 times with 100 mM cacodylate buffer, pH 7.4 for 10 minutes each.
I. Wash in 100 mM maleate buffer, pH 5.7 for 10 minutes.
J. Incubate in 5% uranyl acetate in 100 mM maleate buffer, pH 5.7 for 2 hours.
K. Wash 2 times with 100 mM maleate buffer, pH 5.7 for 10 minutes each.
L. Wash in 100 mM cacodylate buffer, pH 7.4 for 10 minutes.

Dehydration:

10. Incubate in 50% ethanol for 10 minutes.
11. Incubate in 70% ethanol for 10 minutes.
12. Incubate in 90% ethanol for 10 minutes.
13. Incubate in 95% ethanol for 10 minutes. **2**

14. Incubate in 100% ethanol 3 times for 10 minutes each. **3**

Dehydration/membrane dissolution:

15. Incubate in propylene oxide or acetone for 1 hour.
16. Pressurized delivery to Epon pre-embed block. **4, 5, 6**

Infiltration:

17. Incubate in 1:3 Epon 812:propylene oxide for 1 hour at room temperature.
18. Incubate in 1:1 Epon 812:propylene oxide for 1 hour at room temperature.
19. Incubate in 100% Epon 812 for 1 hour at room temperature.

Embedding:

20. Polymerize at 65°C for 24 hours.

above the filter in the manual device (see Figure 2.7) prevent the sample from filtering to dryness if the pressure is too high (by venting pressure to atmosphere).

The test platform and the core mechanism are not currently equipped with liquid level sensors; but filtration occurs for a fixed time period (10 seconds). For efficient filtration of the samples in the core mechanism (see Figures 7.6B and C), the correct level of vacuum producing organelle saturation of the filter membrane must be determined.

The rate of membrane saturation varies according to the size of the organelle, where smaller organelles readily cover the filter pores to saturate the membrane more quickly than larger organelles. However, the same organelle was used for all experiments in this thesis (rat hepatocyte plasma membrane). Filtration to membrane saturation for this organelle was evaluated by observing the rate of filtration visually and noting whether it stopped before the 10 second duration of the step or before filtering to dryness.

(2) Effect of reagent dispensing and aspiration velocities. Observations of the unsuccessful automated sample preparation runs, such as that in Figure 7.3, led us to believe that reagent dispensing and aspiration velocities were disrupting the samples. The combination of mechanical perturbations imposed by the velocities of reagent pumping and vacuum aspiration displaced the samples from the filter membrane (see Figures 7.6D and E), leaving only artifacts on the filter membrane from sample staining.

This was examined by observing the level of sample retention visually (*via* the top of the fluid transfer plate) after manual dispensing and aspiration of

reagents to the single channel test devices, where all liquid handling employed 1 ml syringes fitted with the same needles used on the robot.

(3) Effect of reagent dispensing and aspiration velocities on inverted samples. Figure 7.6J shows how reagents are dispensed and aspirated on the inverted samples to wash and dehydrate them before delivery. The filter and bound sample should form a relatively impermeable barrier within the processing channel to prevent liquid accumulation in the retainer plate wells. The unoccupied space in the well of the retainer plate is necessary for the passage of solvent (and sample). Any liquid occupying this space limits the effectiveness of the solvent-assisted sample delivery stage (see Figures 7.6K and L).

This was examined by manually dispensing reagents with a 1 ml syringes fitted with the same needles used on the robot and observing the accumulation of any liquid in the transparent retainer plate section of the test device.

(4) Pre-delivery solvent incubations. When exposed to an organic solvent, such as propylene oxide or acetone, the filter membrane becomes gelatinous, however it immediately dissolves when exposed to a high enough volume of the solvent. In the core mechanism, the solvent is used for dissolution of the filter membrane and delivery of the samples, and is injected onto the filter screen side of the inverted samples (see Figure 7.6J). The filter membrane is exposed to very little solvent with this method and, based upon observations for other tests, eventually results in a gelatinous mat of undissolved filter membrane and processed sample that adheres to the filter screen. Therefore, the pre-delivery solvent incubation (see Figure 7.6K) should be short to begin dissolution of the membrane for sample

delivery. The membrane will be dissolved further by exposure to a higher volume of solvent after delivery.

The effect of this parameter was evaluated by visual observation of the extent of sample delivery seen through the transparent retainer plate.

(5) Sample delivery pressure level, duration, frequency and effect of filter screen material. Samples are delivered into the retainer plate by pressurization of the solvent used for membrane dissolution (see Figure 7.6L). The method is very effective for releasing inverted samples as well as dissolving the filter membrane, although the necessary and minimal level of pressure is unknown. Also, if a pressure pulse train is effective, the most effective combination of duration and frequency of pulses is also unknown.

The processed sample and filter membrane tend to adhere to the stainless steel filter screen after exposure to solvent, making the second half of the sample preparation process difficult and unpredictable. In the delivery step, the sample is often not released from the steel filter screen. Although this material is robust and works well in many filtration applications, it was very ineffective here.

The effect of these conditions were evaluated by visual observation of the extent of sample delivery seen through the transparent retainer plate and by direct examination of the filter/filter screen after the experiment was completed.

(6) Solvent dispensing and aspiration across the filter screen. After the delivery stage, the samples are captured in the wells of the retainer plate and trapped below the filter screen. Figures 7.6N and O show how reagents are dispensed and aspirated across the screen for sample washing and embedding. These steps

dissolve and remove the filter membrane as well as infiltrate/embed the samples in a step gradient of solvent and Epon. These steps are important and necessary for successful completion of the process. Also, due to the extensive use of solvent, they also aid release and delivery of any residual sample from the filter screen.

This was examined by manually dispensing reagents (containing blue dye) with a 1 ml syringes fitted with the same needles used on the robot and observing the passage of liquid into the transparent retainer plate section of the test device.

7.5.1 Process Screening Experimental Results

Table 7.2 lists the conditions tested in the four screening experiments. Execution and control of all experiments used the robot's pneumatic subsystem and operator interface. Except for refinement of the vacuum level for filtration, the primary objective of the screening experiments was to define the range of conditions for effective sample delivery. Therefore, the most effective delivery pressure parameter was carried to the next experiment, while the effects of the other parameters were noted, and then modified for further examination in the subsequent experiments. The sequence was followed until a set of effective conditions were attained. Although a more detailed examination is possible by direct interaction of parameters, the parameters and conditions chosen were representative of a reasonable initial effort toward process optimization. To illustrate the significance of the results of these investigations, they are presented according to their position within the sequence of events comprising the automated sample preparation protocol (rather than the sequence of experiments).

Minimization of vacuum level for filtration

Evaluation of this parameter was based upon visual observation of the filtration rate over the duration of the step (10 seconds). None of the samples filtered to dryness although the filtration rate observed in Experiments 1 and 2 (-4.9 psi vacuum level) was quick (relative to observations of sample filtration using the manual sample preparation device (see Figures 2.11 and 2.13)). The vacuum level parameter was adjusted only once (to -2.9 psi) in the subsequent experiments. This produced a slower rate of filtration that stopped naturally before 10 seconds.

Effect of reagent dispensing and aspiration velocities

All reagent handling was done manually using 1ml syringes fitted with the same needles used on the robot. Throughout the four experiments, reagent dispensing and aspiration was executed slowly and all samples remained intact; emphasizing the requirement for gentle reagent handling by the robot.

Effect of reagent dispensing and aspiration velocities on inverted samples.

All reagent handling was done manually using 1ml syringes fitted with the same needles used on the robot. Transfer of reagents across the filter screen and inverted, membrane-bound samples to the retainer plate was not observed in any experiment. The inverted, membrane-bound samples successfully acted as a barrier against the passage of liquid, further narrowing the range of prospective problems in automated sample processing.

Table 7.2: Tested conditions for sample filtration and delivery in the four successive process screening experiments. The progression of experiments culminated in Experiment 4, where a composite of successful conditions, determined from the previous experiments, were tested to determine a basis for automated sample preparation process optimization. The most effective delivery pressure from each experiment is indicated in bold type.

Experiment 1	**Experiment 2**	**Experiment 3**	**Experiment 4**
Filtration vacuum: -4.4 psi	**Filtration vacuum:** -4.4 psi	**Filtration vacuum:** -2.9 psi	**Filtration vacuum:** -2.9 psi
Pre-delivery solvent incubation: 15 min.	**Pre-delivery solvent incubation:** 15 min.	**Pre-delivery solvent incubation:** 15 min.	**Pre-delivery solvent incubation:** 15 sec. (1 & 4) 1 min. (2 & 4) 5 min. (3 & 6) 0 min. (7)
Filter screen: Perforated stainless steel	**Filter screen:** Perforated stainless steel	**Filter screen:** Perforated stainless steel (1-2) PTFE mesh (3-7)	**Filter screen:** PTFE mesh
Delivery pulses x duration: 1 x 3sec.	**Delivery pulses x duration:** 3 x 1sec.	**Delivery pulses x duration:** 5 x 2sec.	**Delivery pulses x duration:** 1 x 1sec. (1-3) 3 x 2sec. (4-7)

Case	**Delivery pressure** (psi)	**Delivery pressure** (psi)	**Delivery pressure** (psi)	**Delivery pressure** (psi)
1	0.0	12.5	12.5	25.0
2	4.0	**18.8**	18.8	25.0
3	8.8	25.0	**25.0**	**25.0**
4	12.5	37.5	31.3	25.0
5	**18.8**	43.8	37.5	25.0
6	25.0	50.0	43.8	25.0
7	25.0	62.5	50.0	25.0

Pre-delivery solvent incubation

To avoid blocking the filter screen with undissolved filter membrane, the pre-delivery solvent incubation was kept short (15 minutes) in the first three experiments while all other parameters were examined. Sample delivery performed well through these experiments. Therefore, to determine the shortest incubation time, in the final

experiment a range was examined (with the other parameters) below the previous 15 minute incubation time. This test determined that a shorter incubation time of 5 minutes was effective.

Sample delivery pressure level, duration, frequency and effect of filter screen material

Delivery pressure

A range of pressure levels for sample delivery was examined in each experiment. The filter screens and corresponding delivered samples (for each case in the range of pressures applied) were examined after each experiment. Evaluation of the delivery pressure performance was based upon the lowest pressure that produced the most sample release from the filter screen (determined by comparing the filter/filter screen and quantity of sample delivered to the Epon-loaded tube). The best delivery pressures in each experiment are indicated in bold type in Table 7.2. Although the delivery pressure was lower in experiments 1 and 2, much of the sample was not delivered but remained on the stainless steel filter screens.

Sample delivery pressure pulses and duration

Sample delivery was viewed through the transparent (acrylic) retainer plate and microfuge tube. The filter screen and delivered sample were also examined after each experiment. Based upon these observations made throughout the four experiments, it became apparent that, regardless of the duration or the delivery pressure used, the first pulse delivered the bulk of the sample and all others disrupted the released sample

fragments. This was verified in the final experiment where sample delivery using a single pulse with one second duration was determined to be most effective.

Filter screen

Figure 7.7A shows sample and undissolved filter membrane artifacts on a stainless steel filter screen used in the screening experiments. The filter membrane and much of the sample adhered to the screen, making delivery incomplete. Alternative materials capable of providing more effective sample delivery were investigated and Teflon mesh was selected as the optimal choice. Figure 7.7B shows the improvement in sample release during the delivery step obtained with a Teflon mesh. Very little sample remained undelivered and the filter membrane did not adhere to the Teflon.

In addition to its low coefficient of friction and high chemical resistance, the

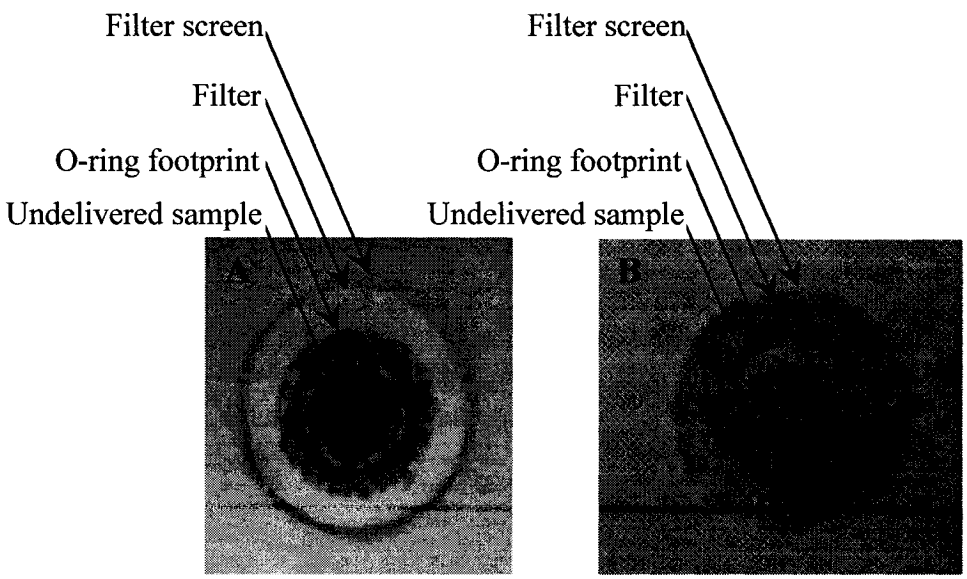

Figure 7.7: Photographs of filters, filter screens and artifacts from process screening experiments illustrating (A) ineffective release of processing sample with a stained and (B) successful release of processing sample from a Teflon filter screen.

greater flexibility of the Teflon mesh also improved sample delivery. Application of an air pulse causes the Teflon filter screen to deflect, producing better sample release as illustrated in Figures 7.8 and 7.9.

Solvent dispensing and aspiration across the filter screen.

Liquid handling for these test was done manually using 1ml syringes fitted with the same needles used on the robot. These steps were also documented as being very effective. The solvent (containing blue dye) was free to pass across the filter screen in all experiments, although the performance was enhanced by the use of a Teflon mesh filter screen.

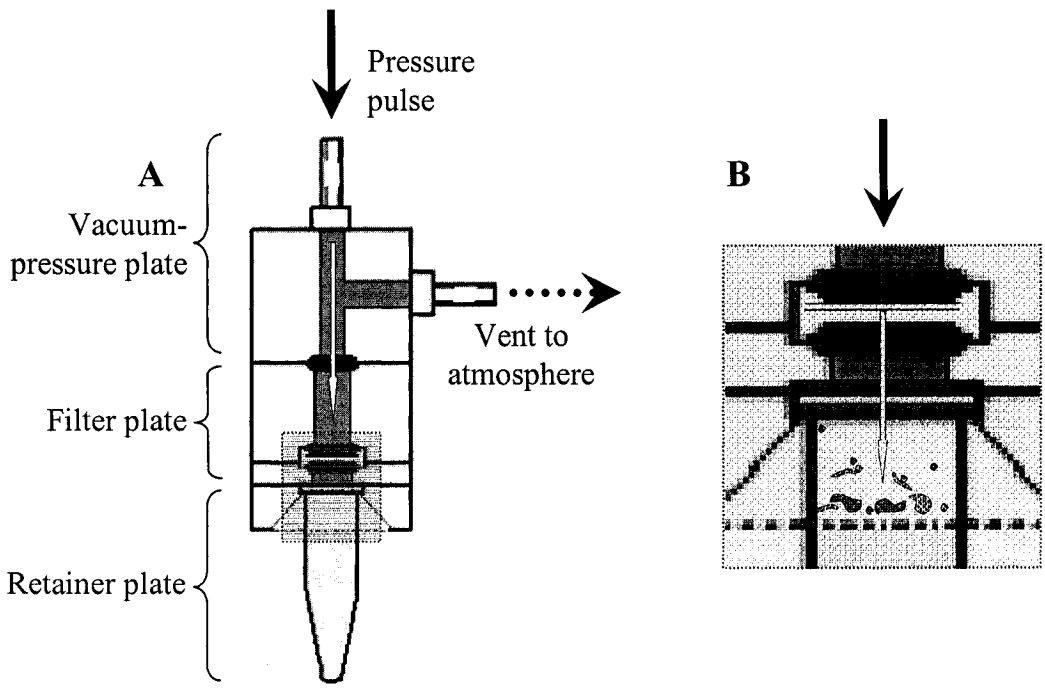

Figure 7.8: Cross-sectional schematics of (A) the delivery configuration of a single processing channel arrangement used in process screening experiments showing the flow paths (indicated with arrows) and region examined to illustrate Teflon filter screen deflection (gray shaded box), and (B) an enlarged view of the region examined illustrating the path of sample delivery.

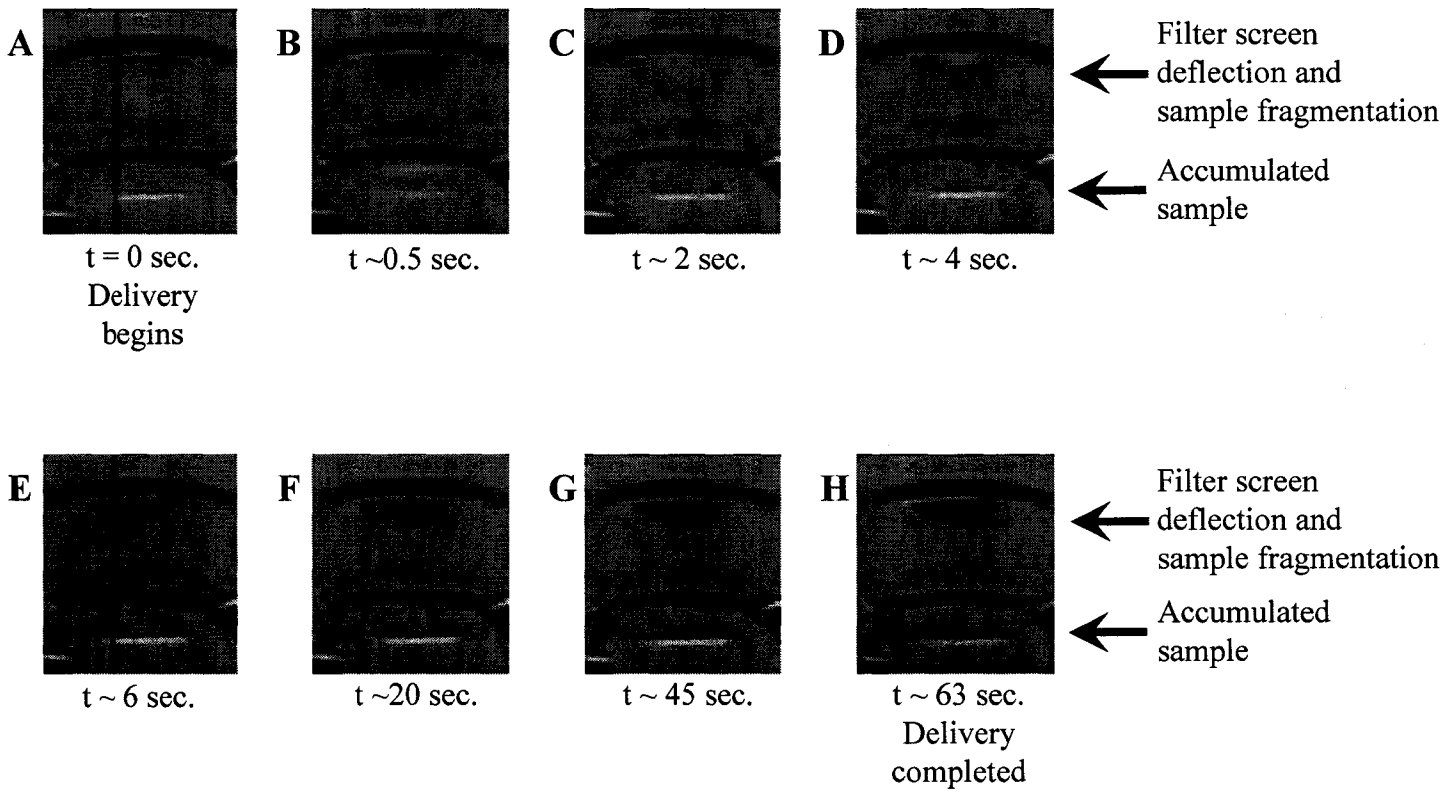

Figure 7.9: A time-course illustration of Teflon filter screen deflection during the sample delivery step of a single processing channel, process screening experiment. To illustrate the filter screen deflection, the images were captured from a digital video record of a high pressure (43.8 psi) sample delivery.

Deflection of the filter screen can be seen in the progression of Figures A to D. The pressure pulse forces the down into the retainer plate, where maximum deflection is shown in Figure C. As the pressure applied to the test device is vented to atmosphere, the screen begins to relax to its original form (see Figure D). Sample delivery is shown throughout the series of photographs, where sample fragments progressively accumulate on the surface of the polymerized Epon in the tube of the retainer plate.

7.5.2 Summary

Based upon the results of screening experiments, the following conditions were found to be most effective for automated sample preparation on the EMPOP robot:

(1) -2.9 psi vacuum level for sample filtration,

(2) 5 minute pre-delivery solvent incubation,

(3) A Teflon mesh filter screen,

(4) A single, one second delivery pressure pulse, and

(5) 25 psi delivery pressure.

The information gathered in these experiments was implemented in subsequent experiments with the EMPOP robot.

7.6 Experiment III: Optimization of Robotic Processing

The results of Experiment II provided the starting point for experiments aimed at optimizing the performance of the EMPOP robot. Consequently, we carried out a series of sample preparation experiments with the robot determine whether modifications to sealing, the preparation protocol, and fluids control could improve system performance. Four of these experiments are described below that demonstrate how the performance of the robot has improved progressively with these optimizations.

All experiments used the standard processing reagents given in Table 7.1; Table 7.3 lists the conditions, parameters, and materials used in each experiment.

Table 7.3: Conditions, parameters and materials used for the automated process development experiments.

	Experiment IIIa	**Experiment IIIb**	**Experiment IIIc**	**Experiment IIId**
Sample (μg) (glutaraldehyde-fixed, rat hepatocyte plasma membrane)	25	25	19	25
Sample location	A8 – H8	A8 – H8	A8 – D8	A8 – H8
Filtration vacuum (psi)	-4.4	-4.4	-2.9	-2.9
Reagent dispensing velocity (processing manifold, % max. velocity)	-	50	25	25
Continuous aspiration needles manifold residence time (sec./channel)	-	-	-	5
Reagent dispensing velocity (embedding manifold, % max. velocity)	-	70	70	70
Pre-delivery diluted Epon incubation (min.)	-	-	15	15
Pre-delivery solvent incubation (min.)	5	90	1	2
Delivery pressure (psi) x pulses x duration	25 x 1 x 2	25 x 1 x 2	12.5 x 1 x 1	12.5 x 1 x 1
Solvent	Propylene oxide	Propylene oxide	Acetone	Acetone
Post-delivery solvent incubation x repeated incubations	60 x 1	30 x 1	30 x 2	60 x 1

7.6.1 Experiment IIIa: Filter Screen Sealing

Although feasibility experiments (see Section 7.2) were a simple assessment of the potential of the process, they generated promising results for successful sample preparation from vacuum filtration through sample delivery steps. The results of initial process validation experiments, illustrated in Figure 7.3, showed that automated preparation of 96 samples in parallel is more complex. Thus in the feasibility experiments there was a large accumulation of processed sample delivered into the retainer plate; in contrast, in validation experiments very little sample was delivered.

Based on these results we concluded that the problem was with the inadequate sealing of the filter plate resulting in low sample retention and dispersion of processing reagents. To address this we added seals to the filter screen. Two seals having the same geometry as the Teflon mesh filter screen were fabricated from adhesive backed, ultra-high molecular weight polyethylene. An array of 4 mm diameter holes was punched out in the 96 well plate format to provide surface area for filter plate internal O-ring sealing and clearance for fluid passage through the filter screen. The adhesive surfaces of the seals were then fixed to each side of the filter screen and pressed between two flat surfaces under 30 kg of weight for 24 hours. Figure 7.10 shows the resulting sealed filter screen, the filter membrane, and the delivered samples.

Figure 7.11 shows the samples produced in an experiment using this improved filter seal. There are few artifacts outside of the area where samples were processed. Therefore, the Figure 7.11 focuses only on the section of the Epon-loaded 96 well plate showing the delivered samples and the corresponding regions of the filter membrane,

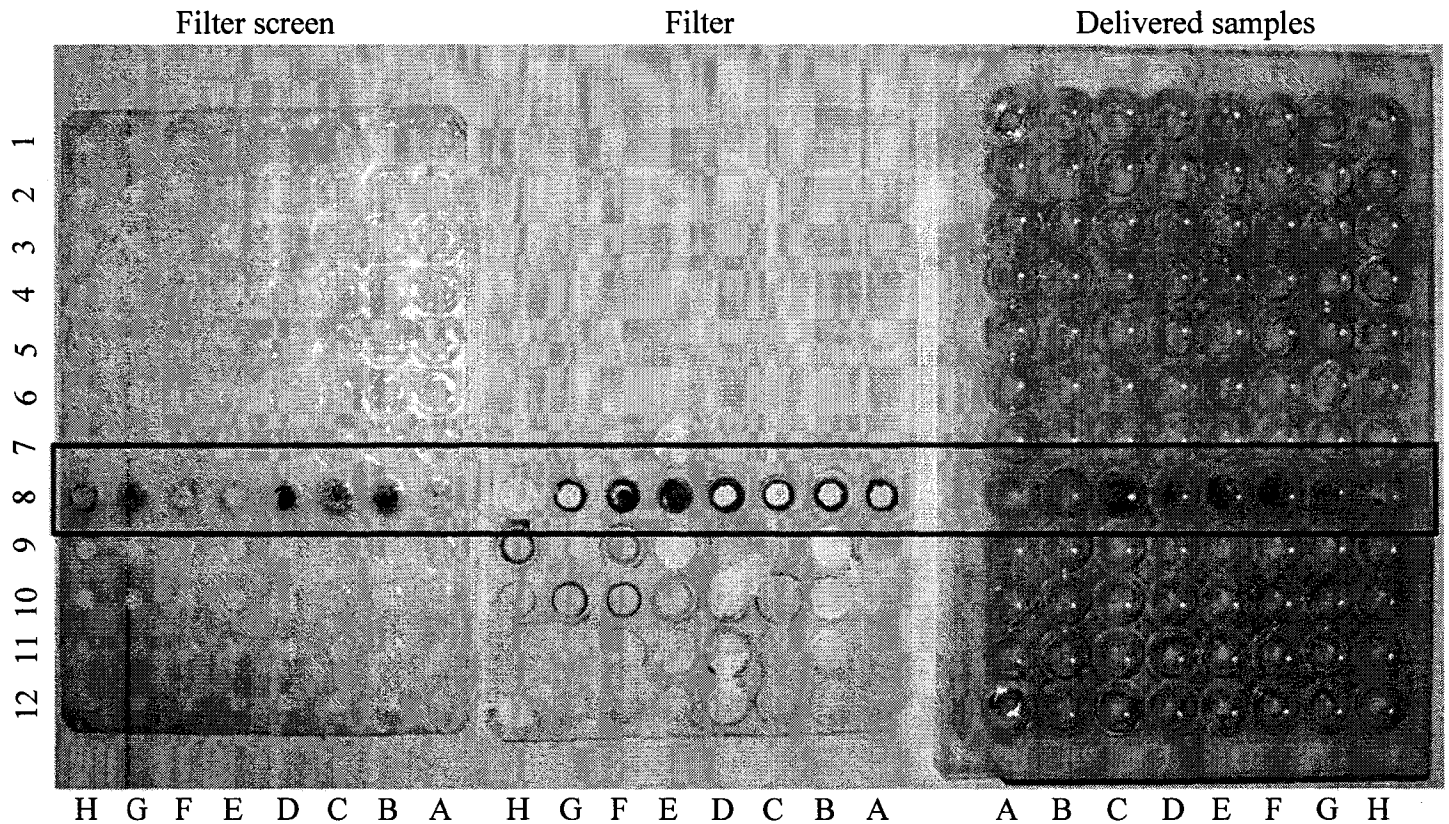

Figure 7.10: Photograph of the filter screen, filter and the Epon-loaded 96 well plate holding the delivered samples from the sample preparation experiment completed to examine the process impact of the sealed filter screen. Eight 25 µg samples of glutaraldehyde-fixed, rat hepatocyte plasma membrane suspension were processed according to the standard protocol for in locations A8 to H8 (indicated by box). The damage to the filter membrane occurred when it was removed from the filter cap after the experiment was complete.

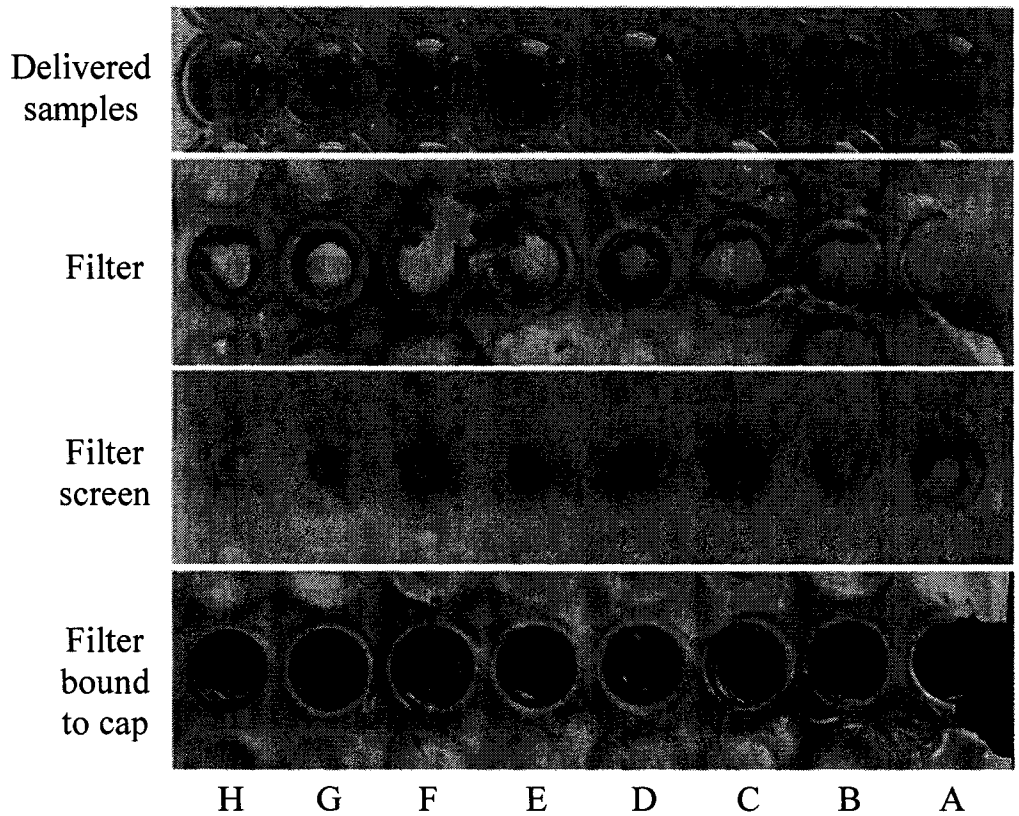

Figure 7.11: Photographs of results from the automated sample preparation experiment completed to examine the process impact of the sealed filter screen. Illustrated from top to bottom are the delivered samples in the Epon-loaded 96 well plate followed by corresponding sections of the filter, filter screen and the filter as it was bound to the filter cap immediately after the experiment was completed. Eight 25 μg samples of glutaraldehyde-fixed, rat hepatocyte plasma membrane suspension were filtered with -4.4 psi vacuum and processed in locations A8 to H8 with the chemical protocol for TEM morphometric analysis [91]. The filter-bound samples were incubated for 5 minutes with propylene oxide and delivered to the retainer plate with a 2 second pulse of 25 psi air. The damage to the filter membrane occurred when it was removed from the filter cap. After delivery, the samples were washed in the processing channels with propylene oxide for 60 minutes.

filter screen, and filter as it was bound to the filter cap at the end of the experiment (the results of following experiments are presented similarly).

Using the initial validation experiment result as a reference (see Figure 7.3), a comparison is made to illustrate that the filter screen seal dramatically improved the process performance. Although very little sample was delivered to the 96 well plate in either experiment, there were notable differences between the filters of the two experiments. There were fewer artifacts from dispersion of processing reagents using the sealed filter screen. In the initial validation experiment, reagents were dispersed across the filter screen, causing the filter to be dark with stain as well as completely dissolved in the area where samples were processed. As the photograph of the filter in Figure 7.10 shows, there was little dispersion of stain and the filter was not dissolved by solvent outside of the area sealed by the O-rings. The areas on the filter damaged in Figure 7.10 result from the removal from the filter cap when the experiment was completed. This fact is illustrated in the bottom photograph of Figure 7.11, where the same filter, bound to the cap, is intact.

7.6.2 Experiment IIIb: Adjustable Reagent Dispensing Velocity

Having resolved problems with sealing the filter screen, the next problem to be addressed was the loss of samples due to mechanical perturbations during reagent handing. Our analysis of the process suggested that liquid shear forces during reagent dispensing caused the all or part of the samples to detach from the filter membrane and so become lost to waste during subsequent aspiration steps.

The first change made to address this issue was to modify robot's control-tier programming to allow the velocity, with which reagents were dispersed, to be controlled; previously the pumping velocity was fixed. The reagent dispensing control code was altered to permit the operator to set the pumping velocity as a percent of maximum pumping velocity (see Figure 7.12).

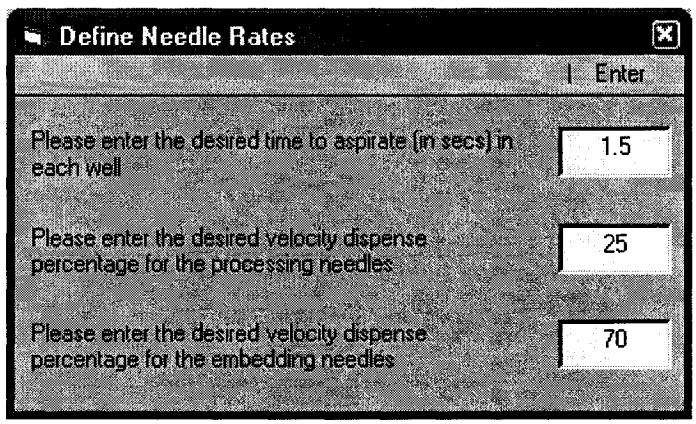

Figure 7.12: Modification to the operator interface of the EMPOP robot implementing adjustments to the control-tier programming, which allow use of an adjustable aspiration needle manifold residence time and adjustment of reagent dispensing velocities (according to the percent maximum pumping velocity (1000 µl/sec)) for the two reagent dispensing needle manifolds.

Figure 7.13 shows the results of an experiment carried out in which this new code was used to set the dispensing velocity to 50% of maximum. Although a very long pre-delivery solvent incubation hampered sample delivery in this experiment (see Section 7.5, *Pre-delivery solvent incubation*), the impact on sample retention on the filter was very apparent. Although much of the sample remained on the filter membrane, the high quantity of sample retained throughout the process resulted in more sample delivery than

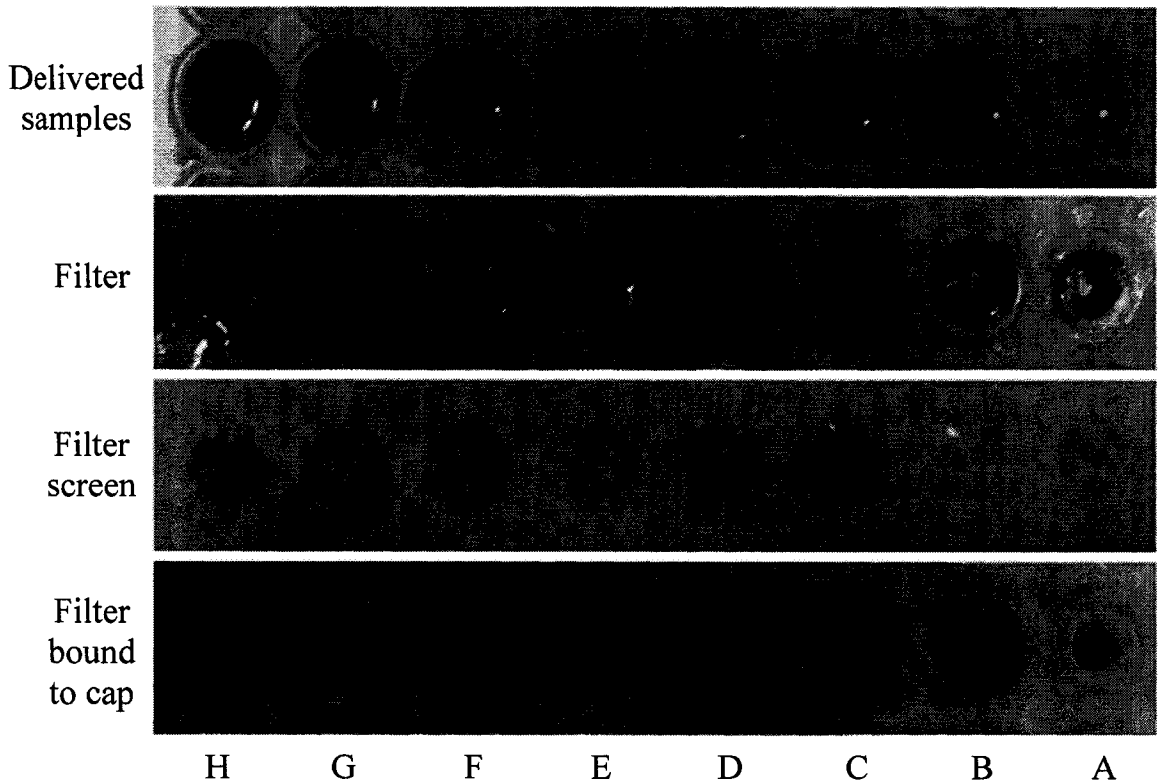

Figure 7.13: Photographs of results from the automated sample preparation experiment completed to examine the process impact of adjustable reagent dispensing. Illustrated from top to bottom are the delivered samples in the Epon-loaded 96 well plate followed by corresponding sections of the filter, filter screen and the filter as it was bound to the filter cap immediately after the experiment was completed. Eight 25 μg samples of glutaraldehyde-fixed, rat hepatocyte plasma membrane suspension were filtered with -4.4 psi vacuum and processed in locations A8 to H8 with the chemical protocol (50% processing reagent dispensing velocity) for TEM morphometric analysis [91]. The filter-bound samples were incubated for 90 minutes with propylene oxide (70% embedding reagent dispensing velocity) and delivered to the retainer plate with a 2 second pulse of 25 psi air. After delivery, the samples were washed in the processing channels with propylene oxide for 30 minutes.

in previous experiments. For example, the initial validation and filter seal experiments (see Figures 7.3 and 7.11, respectively) show comparative results for sample delivery. There is very little of the darkly stained sample delivered to the 96 well plate for either experiment.

7.6.3 Experiment IIIc: Pre-delivery Epon Incubation

Next, we attempted to reduce sample disruption during the sample delivery step. A new step was added to the sample preparation protocol after the sample dehydration ethanol step gradient (see Table 7.1, steps 10-14). In this new step, the samples were briefly incubated with a 3:1 dilution of ethanol and Epon, an epoxy resin, to try to hold the samples together more effectively. Because Epon is also introduced to the processing samples with solvent in the subsequent infiltration step gradient that leads to sample embedding (and Epon is dissolved by the solvent), its brief use at this stage is not a large deviation from the standard preparation protocol.

Figure 7.14 shows the results of adding a pre-delivery incubation with the diluted Epon to the protocol. The samples delivered are much less dispersed and many more large fragments can be seen in the 96 well plate in comparison to the results obtained in the three previous experiments illustrated in Figures 7.3, 7.11 and 7.13.

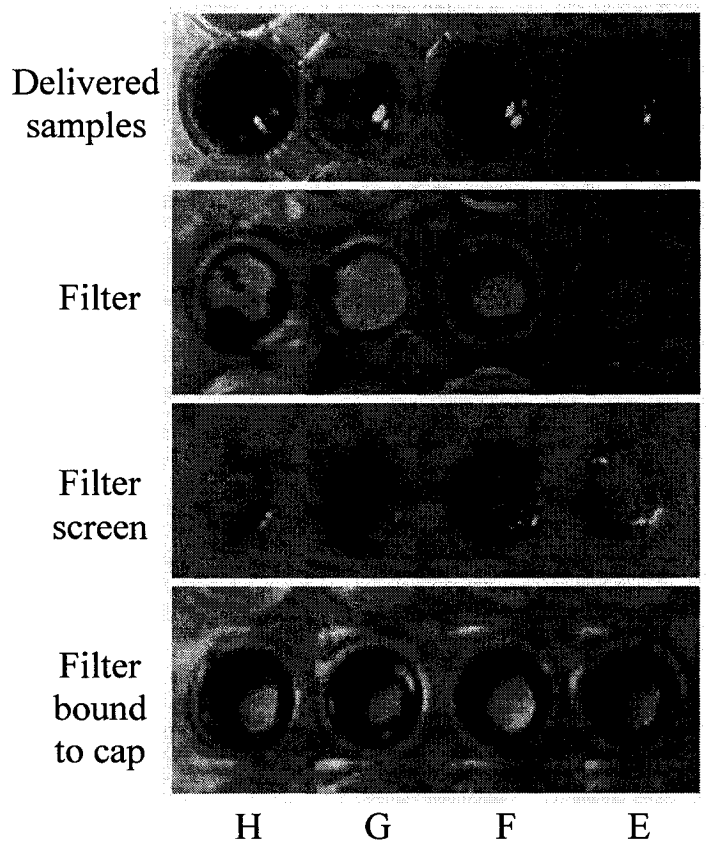

Figure 7.14: Photographs of results from the automated sample preparation experiment completed to examine the process impact of pre-delivery incubation in a 3:1 diluted solution of ethanol and Epon. Illustrated from top to bottom are the delivered samples in the Epon-loaded 96 well plate followed by corresponding sections of the filter, filter screen and the filter as it was bound to the filter cap immediately after the experiment was completed. Four 19 μg samples of glutaraldehyde-fixed, rat hepatocyte plasma membrane suspension were filtered with -2.9 psi vacuum and processed in locations A8 to H8 with the chemical protocol (25% processing reagent dispensing velocity) for TEM morphometric analysis [91] modified with the ethanol:Epon pre-delivery incubation. The filter-bound samples were incubated for 1 minute with acetone (70% embedding reagent dispensing velocity) and delivered to the retainer plate with a 1 second pulse of 12.5 psi air. After delivery, the samples were washed twice in the processing channels with acetone for 30 minutes per wash and incubated for 60 minutes in a 1:1 Epon:acetone solution.

7.6.4 Experiment IIId: Continuous Reagent Aspiration

The issue of sample disruption was further addressed by modifying the method used for reagent aspiration. In the initial design, a solenoid valve, in-line with the vacuum reservoir, was actuated to aspirate spent reagents from individual processing channels. The sudden opening of the fluid line to the vacuum source produced an abrupt acceleration of liquid above the processing sample. We felt that this resulted in mechanical perturbations to the samples that removed some or all of the sample from the filter membrane. Moreover, reagent aspiration was unreliable; channel-to-channel reagent aspiration (with a fixed aspiration needle residence time) was inconsistent because the vacuum reservoir was progressively depleted. This resulted in the dilution of reagents that were subsequently dispensed and/or flooding of the core mechanism due to the accumulation of liquid.

Consequently, we modified the control routine for vacuum aspiration to permit continuous charging of the vacuum reservoir and continuous actuation of the solenoid valve connected to the aspiration needles. In this case, the compressor rapidly evacuates the vacuum reservoir and a needle valve restricts the flow rate from the aspiration needles; to maintain the vacuum level is at its maximum. Furthermore, reagent aspiration begins as soon as the needle penetrates the filled processing channel, and removes most of the liquid as the needle approaches the operator defined penetration depth. To permit use of very slow aspiration rates, an operator-defined needle residence time was also implemented.

Figure 7.15 shows the result of these changes. Compared to previous results (see Figures 7.3, 7.11, 7.13 and 7.14), the density of the stained sample in the 96 well plate

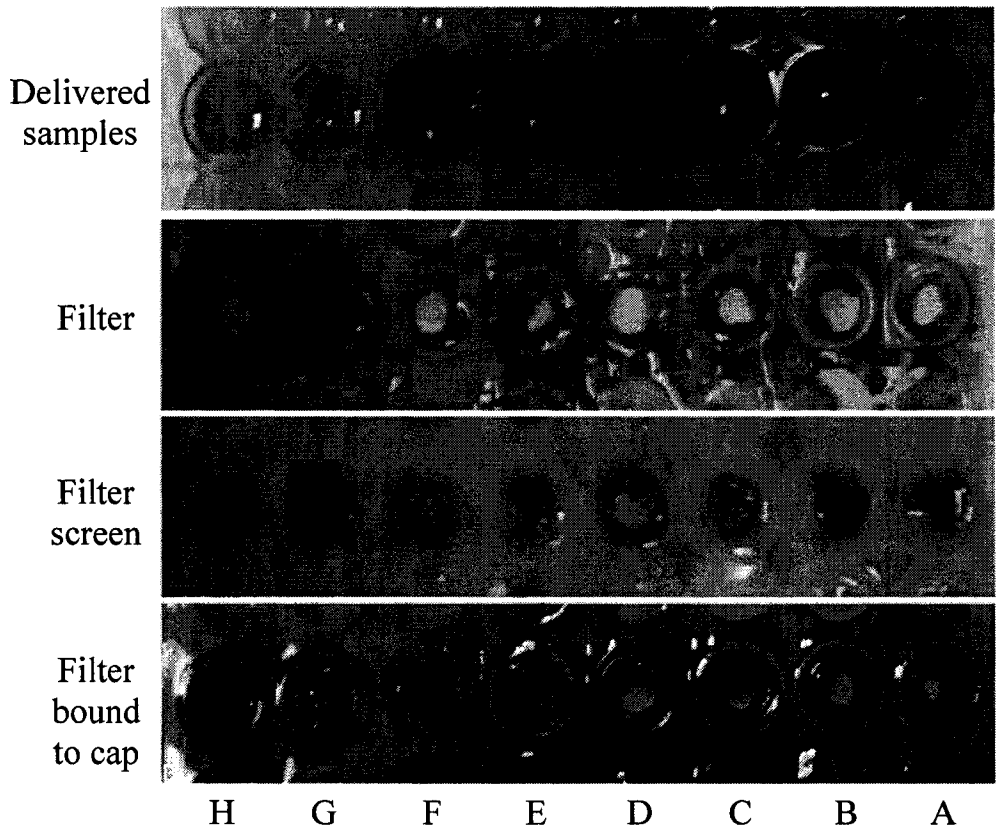

Figure 7.15: Photograph of results from the automated sample preparation experiment completed to examine the process impact of continuous aspiration of spent reagents with an adjustable aspiration needle residence time. Illustrated from top to bottom are the delivered samples in the Epon-loaded 96 well plate followed by corresponding sections of the filter, filter screen and the filter as it was bound to the filter cap immediately after the experiment was completed. Eight 25 μg samples of glutaraldehyde-fixed, rat hepatocyte plasma membrane suspension were filtered with -2.9 psi vacuum and processed in locations A8 to H8 with the chemical protocol (25% processing reagent dispensing velocity and continuous aspiration) for TEM morphometric analysis [91] modified with the ethanol:Epon pre-delivery incubation. The filter-bound samples were incubated for 1 minute with acetone (70% embedding reagent dispensing velocity) and delivered to the retainer plate with a 1 second pulse of 12.5 psi air. After delivery, the samples were washed in the processing channels with acetone for 60 minutes and incubated for 60 minutes in a 1:1 Epon:acetone solution.

was very high and very little sample was retained on the filter membrane and filter screen.

7.6.5 Summary

The results of optimization experiments demonstrated that the following modifications improved automated sample preparation on the EMPOP robot:

(1) Inclusion of a filter screen seal to isolate all processing channels within the filter plate and limit dispersion of reagents over the filter.
(2) Reduction of the reagent dispensing velocity to minimize liquid perturbations and resultant in sample disruption.
(3) Pre-delivery Epon incubation to maintain the structural integrity of samples during the delivery step [Note that this also illustrates the feasibility of potential modifications to the processing protocol].
(4) Elimination of reagent aspiration velocity changes by a continuous and adjustable vacuum level to minimize perturbations resulting in sample disruption.

Subsequent experiments using these improvements demonstrated the capabilities of the EMPOP robot.

7.7 Experiment IV: Full Sample Preparation Capacity

The results of Experiment III provided a basis for testing the complete automated process. Therefore, we carried out a set of sample preparation experiments aimed at examining the parallel preparation of 96 samples with the EMPOP robot.

All experiments used standard processing reagents given in Table 7.1; Table 7.4 lists all other conditions, parameters, and materials used in each experiment.

7.7.1 Experiment IVa: Implementation of Process Improvements

This experiment implemented the process improvements determined in Experiment III except for pre-delivery Epon incubation. Due to the increased level of sample recovery, the quantity of sample loaded to each processing channel was reduced from 25 to 20 μg. In addition, the filtration vacuum level was increased by -1 psi to accommodate parallel filtration of all 96 samples. Otherwise, the sample preparation run was executed according to the protocol in Table 7.1.

Figures 7.16 show the results of the experiment. Sample retention was very good but sample delivery was incomplete. As Figure 7.16 shows, most samples remained bound to the filter membrane and only a small percentage were delivered to the 96 well plate. Regardless, those samples in the 96 well plate were processed for embedding. The samples were placed under vacuum for several minutes to remove residual solvent from the 1:1 acetone:Epon infiltration solution. Next, a layer of Epon was applied and the samples were incubated under vacuum for an additional 24 hours to completely infiltrate the samples and remove all solvent. Afterward, the Epon was polymerized at 65°C for 24 hours to complete the embedding process (see Figures 7.17).

Table 7.4: Conditions, parameters and materials used for the full sample preparation capacity experiments.

	Experiment IV a	Experiment IV b
Sample (μg) (glutaraldehyde-fixed, rat hepatocyte plasma membrane)	20	20
Filtration vacuum (psi)	-3.9	-2.4
Reagent dispensing velocity (processing needle manifold, % max. velocity)	40	40
Continuous aspiration needles manifold residence time (sec./channel)	3	3
Reagent dispensing velocity (embedding needle manifold, % max. velocity)	70	100
Fluid transfer plate dispensing needle penetration depth (mm)	17	19
Fluid transfer plate aspiration needle penetration depth (mm)	17	20
Filter plate dispensing needle penetration depth (mm)	16	17
Filter plate aspiration needle penetration depth (mm)	16	17
Pre-delivery solvent incubation (min.)	15	15
Delivery pressure (psi) x pulses x duration (sec.)	12.5 x 1 x 1	12.5 x 1 x 1
Post-delivery solvent incubation (min.) x repeated incubations	60 x 1	15 x 4
Infiltration gradient 1:3 Acetone:Epon incubation (min.) x repeated incubations	60 x 1	30 x 2
Infiltration gradient 1:1 Acetone:Epon incubation (min.) x repeated incubations	60 x 1	60 x 1
Preloaded Epon volume (μl)	450	200

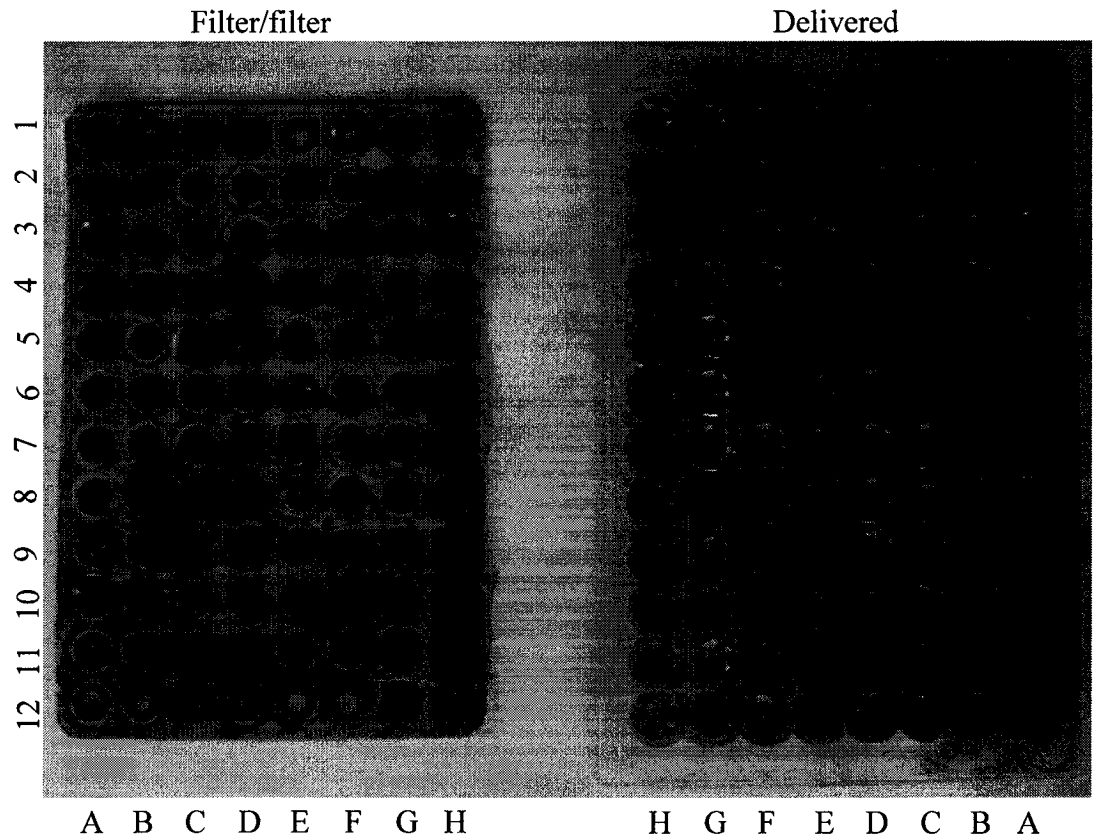

Figure 7.16: Photograph of the filter screen, filter and the Epon-loaded 96 well plate holding the delivered samples from the first experiment completed to examine the full sample preparation capacity of the EMPOP robot (Experiment IVa). Ninety six 20 μg samples of glutaraldehyde-fixed, rat hepatocyte plasma membrane suspension were filtered with -3.9 psi vacuum and processed according to the standard protocol for TEM morphometric analysis [91]. Chemical processing was completed with a 40% processing reagent dispensing velocity and an aspiration needle time of 3 sec./channel. The filter-bound samples were incubated for 15 minutes in acetone (70% embedding reagent dispensing velocity) and delivered by a 1 second pulse of 12.5 psi air to the retainer plate with 450 μl pre-loaded, polymerized Epon/well. After delivery, the samples were processed through an infiltration step-gradient by successive 60 minute incubations in solutions of acetone, 1:3 acetone:Epon, and 1:1 acetone:Epon.

The time required to complete all steps of the experiment, from setup to examination of the delivery result, was approximately 15 hours. Also, because sample delivery was incomplete, the filter and filter screen were not separated to illustrate the locations of undelivered samples.

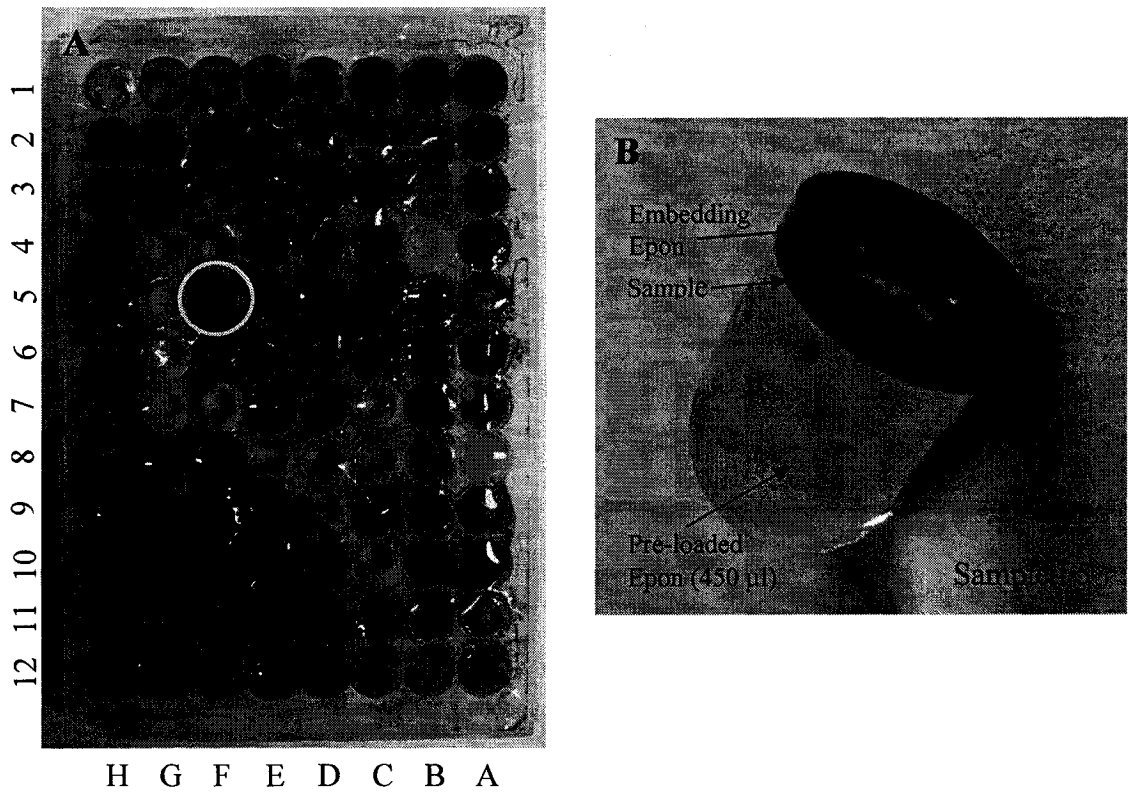

Figures 7.17: Photographs of the embedded samples recovered from the first experiment to examine the full sample preparation capacity of the EMPOP robot (Experiment IVa). (A) All delivered samples embedded in 100% Epon. (B) A representative embedded sample (indicated by the circle in Figure A) showing the layers of Epon around the delivered sample. After the preparation run was complete, the plate of delivered samples was placed under vacuum for several minutes to remove residual solvent from the 1:1 acetone:Epon infiltration solution. A layer of Epon was applied on the samples for embedding and vacuum incubation continued for an additional 24 hours. Afterward, the Epon was polymerized at 65°C for 24 hours to complete embedding.

Although the Epon layers were sufficiently hard, the delivered samples were soft due to incomplete infiltration of the Epon and/or incomplete removal of residual solvent. This resulted in separation of the delivered sample and Epon layers when they were cut into blocks for sectioning by an ultramicrotome. Therefore, these samples could not be prepared as specimens for the transmission electron microscope.

7.7.2 Experiment IVb: Sample Delivery Improvements

The experiment was repeated after adjusting the process parameters to improve sample delivery (see Table 7.4). In addition to small parameter changes to improve filtration and chemical processing, the following changes were applied:

(1) The reagent dispense velocity was increased to 100% of the maximum pumping rate to aid solvent penetration of the filter screen and sample release.

(2) The filter plate dispensing and aspiration needle penetration depths were increased to aid solvent penetration and removal of dissolved filter membrane across the filter screen (see Figures 7.6N and O).

(3) The number of incubations for the two steps of the infiltration stage were increased to aid delivery by washing the samples to the 96 well plate by repeated application of the solutions.

(4) The volume of pre-loaded Epon was reduced to create a wider gap between the delivered samples and the filter screen; aiding sample capture and limiting loss due to the high reagent dispense velocity and the proximity of the aspiration needle (see Figures 7.6L, N and O).

Figure 7.18 shows the results of the experiment, processed samples were delivered into all locations of the 96 well plate. Additionally, the filter dissolved in all processing channels and only a small fraction of the samples remained on the filter screen; indicating that the added infiltration steps aided sample delivery.

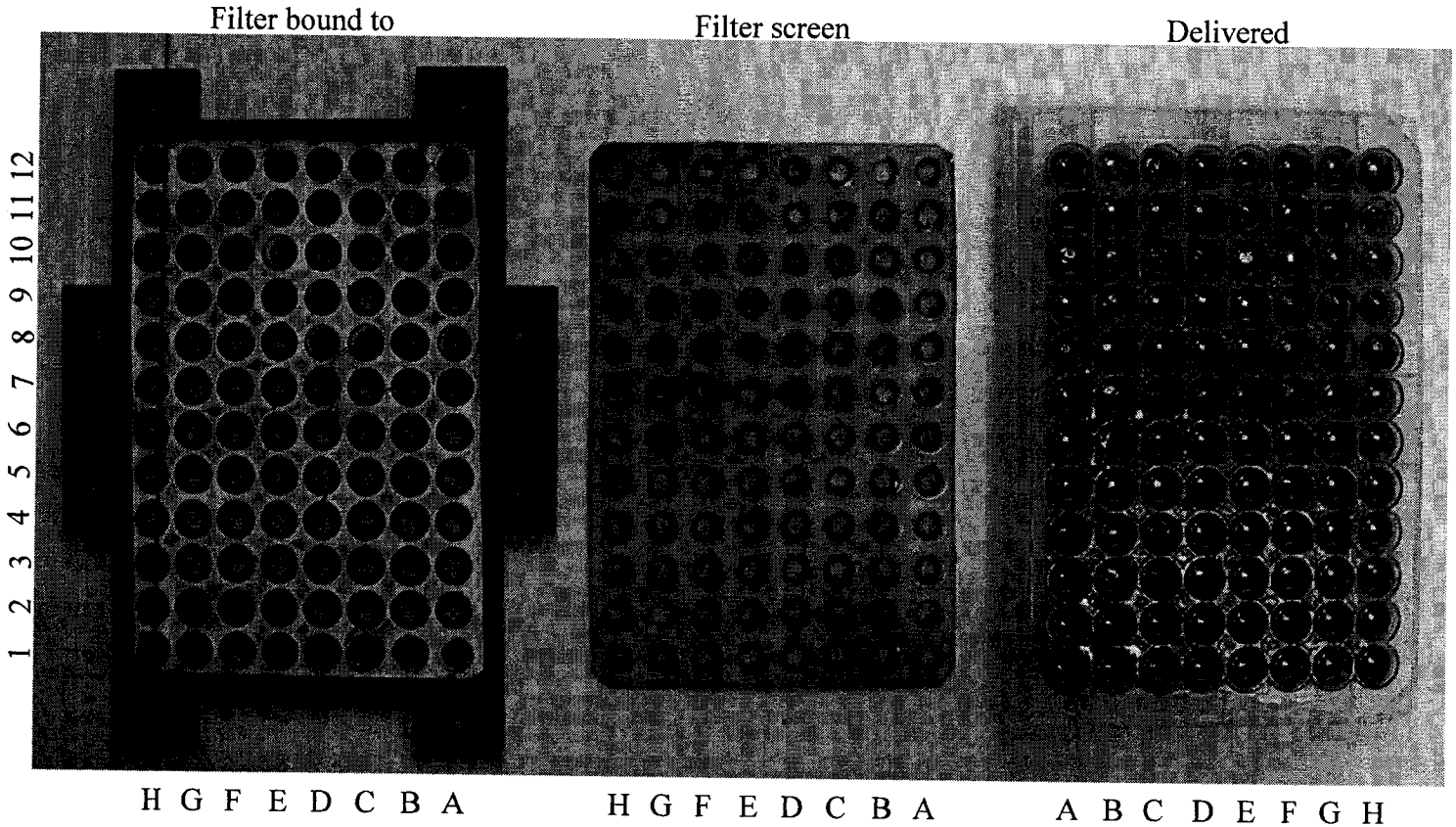

Figure 7.18: Photograph of the filter screen, filter and the Epon-loaded 96 well plate holding the delivered samples from the second experiment completed to examine the full sample preparation capacity of the EMPOP robot (Experiment IVb). Ninety six 20 μg samples of glutaraldehyde-fixed, rat hepatocyte plasma membrane suspension were filtered with -2.4 psi vacuum and processed according to the standard protocol for TEM morphometric analysis [91] with an additional wash in cacodylate buffer after treatment with OsO_4 solution. Chemical processing was completed with a 40% processing reagent dispensing velocity and an aspiration needle time of 3 sec./channel. The filter-bound samples were incubated for 15 minutes in acetone (100% embedding reagent dispensing velocity) and delivered by a 1 second pulse of 12.5 psi air to the retainer plate with 200 μl pre-loaded, polymerized Epon/well. After delivery, the samples were processed through an infiltration step-gradient comprised of four successive 15 minute incubations in acetone, two 30 minute incubations in 1:3 acetone:Epon, and one 60 minute incubation in 1:1 acetone:Epon. The time required to complete all steps of the experiment, from setup to examination of the delivery result, was approximately 16 hours.

The delivered samples were embedded with the method used in the previous experiment (see Figures 7.19). However, due to inadequate removal of the residual 1:1 acetone:Epon infiltration solution, polymerization of the embedding Epon was inhibited. Therefore, the embedded samples were rendered too soft for cutting; making it impossible to prepare them as specimens for the transmission electron microscope.

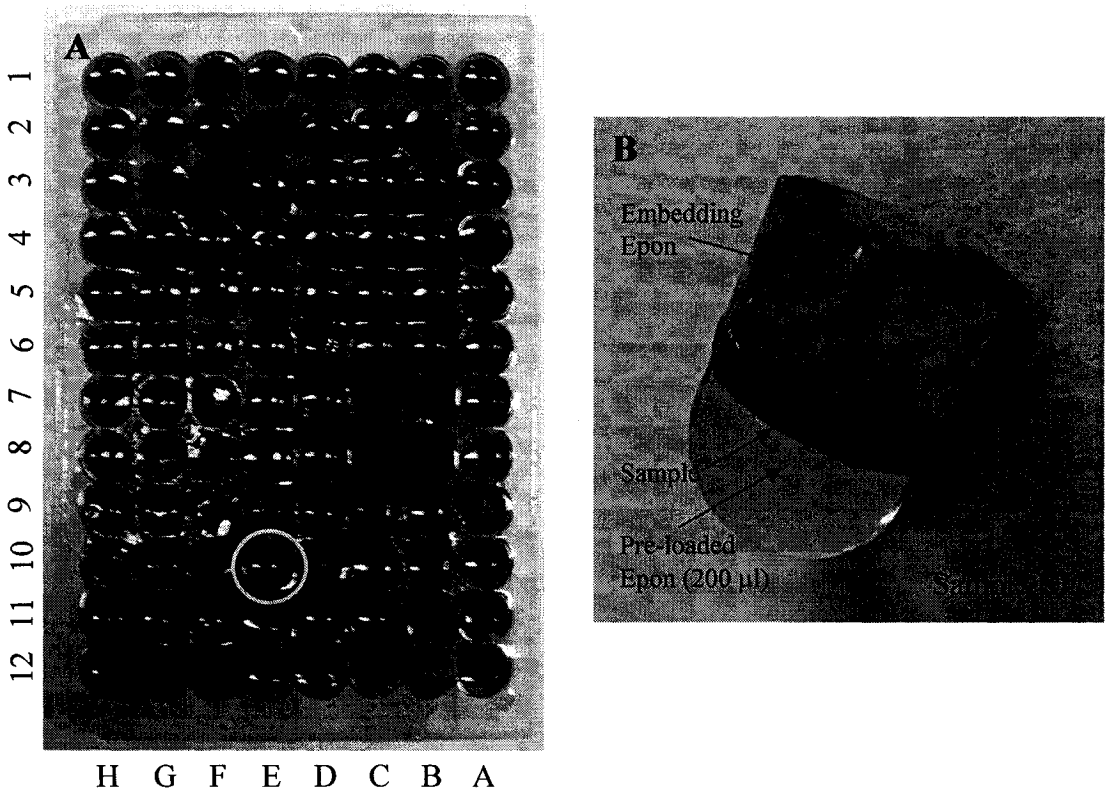

Figures 7.19: Photographs of the embedded samples recovered from the second experiment to examine the full sample preparation capacity of the EMPOP robot (Experiment IVb). (A) All delivered samples embedded in 100% Epon. (B) A representative embedded sample (indicated by the circle in Figure A) showing the layers of Epon around the delivered sample. After the preparation run was complete, Epon was layered on the samples for embedding and incubated under vacuum for 48 hours. Afterward, the Epon was polymerized at 65°C for 24 hours to complete embedding.

7.8 Summary

At the time of this thesis writing, the robot was not fully automated. Although all electrical and mechanical aspects were complete, programming for the transfer platform had yet to be finished. Therefore, all core mechanism inversions in the robotic experiments were done manually. Otherwise, sample processing was automatic.

Regardless, after conducting two sets of experiments for process screening and optimization, the yield of useful subcellular fraction samples prepared by the EMPOP robot increased significantly. Initially, less than 5 to 10% of the delivered samples from process validation experiments were useful. The methods determined from optimization experiments to increase the level of sample preservation produced yields of useful samples ranging from 75 to 100%, which appeared as much larger fragments that were suitable for TEM analysis. Finally, the results of the full sample preparation capacity experiments demonstrated the ability of the EMPOP robot to successfully prepare 96 samples and established a basic level of optimization for the process.

A more rigorous approach toward optimization of sample preparation (as well as the post-preparation steps) is now possible to establish an automated protocol that provides standardized and reproducible samples for direct comparison and quantitative analyses.

8 Discussion

In this thesis, we have developed a tool for the organellar approach to proteomics; an autonomous robotic system for the automated, standardized preparation of up to 96 parallel subcellular fraction samples as specimens for transmission electron microscopy. The system was designed as a single unit that operates to minimize mechanical stress on the samples by integrating support subsystems for cooling, fluids handling and positioning around a core mechanism, where all sample preparation processing occurs.

8.1 Sample Preparation

All mechanical and electrical aspects of the robot are complete, and only operation of the transfer platform subsystem has to be included in the control programming. Because of this, the inversion step is performed manually. Otherwise, the robot functions automatically and it has been shown to generate 96 processed samples with an efficiency of 100%.

Several operational parameters require attention for optimization of the automatic process and a higher level of system performance. Many of these are noted in Chapter 7 and should be approach in a structured series of experiments. In approaching these remaining issues, the level of processed sample quality should increase.

Due to time limitations for thesis research, we could not approach the full range of sample preparation steps, and lacking from the experimental results are electron micrographs. We made efforts to subject embedded samples to electron microscopic

analysis, but none could be prepared as specimens with an ultramicrotome. These attempts illustrated the requirement for refinement of the vacuum incubation post-processing step; to dissipate all residual solvent that left over from the infiltration step-gradient.

After these issues are approached the robot could be utilized for massive, parallel, reproducible preparation of subcellular fraction samples for electron microscopic screening and quantitative analysis of subcellular and protein targets necessary for high-throughput proteomics.

8.2 Original Contributions

The development of the EMPOP robot provided five original contributions applicable to the fields of electron microscopy, proteomics and laboratory automation:

(1) The automated method. The EMPOP robot is the first automated device designed for EM subcellular fraction sample preparation.

(2) The integrated, autonomous system design. Subcellular fraction samples are immobilized within the core mechanism that is supported by a modular, integrated robot which performs all mechanical manipulations.

(3) The high-throughput process for EM subcellular fraction sample preparation. The process provides random sampling filtration, chemical processing, delivery and embedding of up to 96 subcellular fraction samples in parallel within the period of a day; effectively reducing the time and labor requirement for sample preparation by up to 1,000 fold.

(4) The standardized method for subcellular fraction sample processing. The extensive use of closed-loop control provided by the robot's hardware sensor systems and control software support standardized subcellular fraction sample processing *via* precise execution of all automated events as well as re-execution of the automated process from a record of the operational parameters.

(5) The core mechanism. The set of multifunctional, stacking plates that automatically couple and interchange for parallel reconfiguration of processing channels, is new to the field of laboratory automation. The principle of magnetic coupling/decoupling has applications for similar devices and permits extension of the automated capabilities of a robot directly to modular sub-devices that hold or process biological or chemical samples.

A United States Patent Application was filed for the EMPOP robot [277] to support these original contributions.

8.3 Future Work

Optimization of the automated sample preparation process is the primary concern for future work. Improvements to the robot hardware and software, that may improve process performance, are also possible. Successful application warrants the next logical step, development of a second generation robot.

8.3.1: Process Optimization and Application

The process screening and optimization experiments completed in this thesis were basic and primarily intended for a proof-of-principle illustration of the device. However, many controlled methods have yet to be implemented with the functioning robot. With additional experimentation to develop the automated process, it will be possible to attain a much higher degree of optimization. Furthermore, a rigorous and structured approach toward process optimization leading to standardized reproducibility would suitably compose a project for a Master's thesis student.

Although optimization of this process would be a considerable achievement, most motivation for further development comes from the intended application in proteomics research. No analytical device compares to the combined resolution of TEM for protein detection and detailed morphological information for subcellular substructure. Use of the EMPOP robot in organellar proteomics research would permit use of TEM for quantitative screening and analysis of organelles and proteins.

8.3.2: Improvements to the Current Prototype

The core mechanism and subsystems of the EMPOP robot are complex, but are composed of many simple subcomponents that function individually and together under simple principles. Furthermore, to aid development toward a working prototype, the subsystems were designed as large subsections to permit direct examination of individual and integrated processes or problems that may occur. In this regard, all aspects of the EMPOP robot received careful consideration and operate very well to successfully execute all of the steps of the automated sample preparation protocol.

However, throughout the course of development and testing, we identified six aspects of hardware and software that could be modified to improve the function and capabilities of the robot.

(1) We have developed technology for capacitive liquid level sensing for the EMPOP robot [278, 279], but it is currently not part of the system. Although inter- and intra-plate sealing of the core mechanism is robust and operates well without liquid level sensors, their inclusion would protect the processing samples by permitting closed-loop control. In the event of a liquid handling or sealing failure, where a processing channel may have too much or too little reagent, level sensors would allow the system to detect and correct these irregularities.

(2) Miniature O-rings provide inter and intra-plate fluid sealing for the array of 96 processing channels. There are individually installed with an adhesive and must be regularly inspected and periodically replaced to avoid surface irregularities that hamper sealing performance. Custom-made, molded seals that cover the entire array of 96 processing channels would simplify maintenance of the core mechanism sealing surfaces.

(3) Although the sealed Teflon filter screen, introduced in the process optimization experiments, functions well to isolate processing reagents and release samples during the delivery step, it could be modified to improve both aspects of performance. Using the same geometry, a custom-designed filter screen with embedded, integrated seals can be deigned. Other filter screen materials (Teflon

or otherwise) may offer better performance during sample delivery and seals could be specifically designed for the internal environment of the filter plate.

(4) Reagent mixing is inefficient at high mixing ratios. To feed reagents into the mixer simultaneously, the pumping velocities adjust in direct proportion to the mixing ratio. The low-velocity pumping becomes rate-limiting, rendering high ratio mixing to slow for the timing of the process. An intermediate mixing reservoir, installed between the stepper pumps and the mixer, would eliminate the problem and improve the performance of reagent mixing.

(5) The control software supports two protocol for sample preparation and it is not possible deviate from the preparation sequence in a continuous sample preparation run. Currently, the operator can only change the order of events by executing them on a semi-automatic, step-by-step basis. Although the modifications to the control programming would likely be extensive, automatic execution of an altered processing sequence would provide a higher degree of process flexibility.

(6) A uniform preparation protocol is applied to all samples treated in a processing run. Although, modifications to the control programming would also be extensive here, automatic execution of an altered protocol for adjustable chemical processing from sample to sample would also provide a higher degree of process flexibility.

8.3.3 The Application to Cells in Culture

The automated concept is applicable to preparation of other biological samples such as bacteria, yeast, animal cells and viruses as samples for EM.

8.3.4 Second Generation EMPOP Robot

Improvements in the next generation of the EMPOP robot will stem from characterization of an optimized process as well as characterization of the integrated mechanical and electrical structure, function and performance of the current prototype. Significant enhancement in performance and efficiency for the process and automation could result while maintaining the core mechanism design concept of multifunctional, reconfigurable, stacking plates as well as the sample preparation process it supports; filtration, processing, transfer, capture, isolation and embedding.

The current prototype was developed in large subsections for direct examination of processes or problems that may occur. A much more consolidated design is feasible with all automation located within a small enclosure. This step has a tremendous and cumulative impact on successive subsystems, components and design concepts. Furthermore, it is possible to maximize the efficiency and performance of sample processing through restructuring and further integration of the core mechanism.

Bibliography

[1] Venter, J.C. *et al.* The sequence of the human genome. *Science* 291:1304-1351, 2001.

[2] Lander, E.S. *et al.* Initial sequencing and analysis of the human genome. *Nature* 409:860-921, 2001.

[3] Walsh, C.T. *Posttranslational modifications of proteins: expanding nature's inventory.* Roberts and Co. Publishers, Englewood, CO, 2006.

[4] Ideker, T., Galitski, T., and Hood, L. A new approach to decoding life: systems biology. *Annual Review of Genomics and Human Genetics* 2:343-372, 2001.

[5] Hood, L. Systems biology: integrating technology, biology, and computation. *Mechanisms of Ageing and Development* 124:9-16, 2003.

[6] Kitano, H. Systems biology: a brief overview. *Science* 295:1662-1664, 2002.

[7] Wilkins, M.R., Sanchez, J.C., Gooley, A.A., Appel, R.D., Humphery-Smith, I., Hochstrasser, D.F., and Williams, K.L. Why all proteins expressed by a genome should be identified and how to do it. *Biotechnology and Genetic Engineering Review* 13:19-50, 1996.

[8] Anderson, N.L. and Anderson, N.G. Proteome and proteomics: new technologies, new concepts and new words. *Electrophoresis* 19:1853-1861, 1998.

[9] Blackstock, W.P. and Wier, M.P. Proteomics: quantitative and physical mapping of cellular Proteins. *Trends in Biotechnology* 17:121-127, 1999.

[10] De Hoog, C.L. and Mann, M. Proteomics, *Annual Review of Human Genetics.* 5:267-293, 2004.

[11] Liebler, D.C. *Introduction to proteomics: tools for the new biology.* Humana Press, Totowa, New Jersey 2002.

[12] Lopez, M.F. Proteome analysis I: gene products are where the biological action is. *Journal of Chromatography B* 772:191-202, 1999.

[13] McDonald, W.H. and Yates, J.R. III. Proteomic tools for cell biology. *Traffic* 1:747-754, 2000.

[14] Patterson, S.D. Proteomics: the industrialization of protein chemistry. *Current Opinion in Biotechnology*. 11:413-418, 2000.

[15] Patterson, S.D. and Abersold, R.H. Proteomics: the first decade and beyond. *Nature Genetics* Supplement 33:311-323, 2003.

[16] Phizicky, E., Bastiaens, P.I.H., Zhu, H., Snyder, M. and Fields, S. Protein analysis on a proteomic scale. *Nature* 422:208-215, 2003.

[17] Tyers, M. and Mann, M. From genomics to proteomics. *Nature* 422:193-197, 2003.

[18] Zhu, H., Bilgin, M. and Snyder, M. Proteomics. *Annual Review of Biochemistry*. 72:783-812, 2003.

[19] Yarmush, M.L. and Jayaraman, A. Advances in proteomics technologies. *Annual Review of Biomedical Engineering* 4:349-373, 2002.

[20] Abersold, R. and Mann, M. Mass spectrometry-based proteomics. *Nature* 422:198-207, 2003.

[21] Mann, M. and Jensen, O.N. Proteomic analysis of post-translational modifications. *Nature Biotechnology* 21:255-261, 2003.

[22] Zaia, J. Mass spectrometry of oligosaccharides. *Mass Spectrometry Reviews* 23: 161-227, 2004.

[23] Zhang, H., Li, X. J., Martin, D. B., Aebersold, R. Identification and quantification of N-linked glycoproteins using hydrazide chemistry, stable isotope labeling and mass spectrometry. *Nature Biotechnology* 21: 660-666, 2003.

[24] Zhou, H., Watts, J. D., Aebersold, R. A systematic approach to the analysis of protein phosphorylation. *Nature Biotechnology* 19: 375-378, 2001.

[25] Oda, Y., Nagasu, T., Chait, B. T. Enrichment analysis of phosphorylated proteins as a tool for probing the phosphoproteome. *Nature Biotechnology* 19: 379-382, 2001.

[26] Nikov, G., Bhat, V., Wishnok, J. S., Tannenbaum, S. R. Analysis of nitrated proteins by nitrotyrosine-specific affinity probes and mass spectrometry. *Analytical Biochemistry* 320: 214-222, 2003.

[27] Jensen, O. N. Modification-specific proteomics: characterization of post-translational modifications by mass spectrometry. *Current Opinion in Chemical Biology* 8: 33-41, 2004.

[28] Ficarro, S. B., McCleland, M. L., Stukenberg, P. T., Burke, D. J., Ross, M. M., Shabanowitz, J., Hunt, D. F., White, F. M. Phosphoproteome analysis by mass spectrometry and its application to Saccharomyces cerevisiae. *Nature Biotechnology* 20:301-305, 2002.

[29] Conrads, T. P., Issaq, H. J., Veenstra, T. D. New tools for quantitative phosphoproteome analysis. *Biochemical and Biophysical Research Communications* 290: 885-890, 2002.

[30] Gerber, S. A., Rush, J., Stemman, O., Kirschner, M. W., Gygi, S. P. Absolute quantification of proteins and phosphoproteins from cell lysates by tandem MS. *Proceedings of the National Academy of Sciences USA* 100: 6940-6945, 2003.

[31] Gronborg, M., Kristiansen, T. Z., Stensballe, A., Andersen, J. S., Ohara, O., Mann, M., Jensen, O. N., Pandey, A. A mass spectrometry-based proteomic approach for identification of serine/threonine-phosphorylated proteins by enrichment with phospho-specific antibodies: identification of a novel protein, Frigg, as a protein kinase A substrate. *Molecular and Cellular Proteomics* 1: 517-527, 2002.

[32] Lambert, J., Either, M., Smith, J.C., and Figeys, D. Proteomics: from gel based to gel free. *Analytical Chemistry* 77:3771-3788, 2005.

[33] Monti, M., Orru, S., Pagnozzi, D. and Pucci, P. Interaction proteomics. *Bioscience Reports* 25:45-56, 2005.

[34] Huber, L.A. Is proteomics heading in the wrong direction? *Nature* 4:74-80, 2003.

[35] Stasyk, T. and Huber, L.A. Zooming in: fractionation strategies in proteomics. *Proteomics* 4:3704-3716, 2004.

[36] Issaq, H.J., Chan, K.C., Janini, G.M., Conrads, T.P. and Veenstra, T.D. Multidimensional separation of peptides for effective proteomic analysis. *Journal of Chromatography B* 817, 35-47, 2005.

[37] Brunet, S., Thibault, P., Gagnon, E., Kearney, P., Bergeron, J.J.M and Desjardins, M. Organelle proteomics: looking at less to see more. *Trends in Cell Biology* 13:629-638, 2003.

[38] Dreger, M. Proteome analysis at the level of subcellular structures. *European Journal of Biochemistry* 270:589-599, 2003.

[39] Dreger, M. Subcellular proteomics. *Mass Spectrometry Reviews* 22:27-56, 2003.

[40] Jung, E., Heller, M., Sanchez, J., and Hochstrasser, D. F. Proteomics meets cell biology: the establishment of subcellular proteomes. *Electrophoresis* 21:3369-3377, 2000.

[41] Huber, L.A. Pfaller, K. and Vietor, I. Organelle proteomics: implications for subcellular fractionation in proteomics. *Circulation Research* 92:962-968, 2003.

[42] Mann, M. Organellar proteomics. *The Scientist* 18:32, 2004.

[43] Pasquali, C., Fialka, I. and Huber, L.A. Subcellular fractionation, electromigration analysis and mapping of organelles. *Journal of Chromatography B* 722:89-102, 1999.

[44] Schirmer, E.C. and Gerace, L. Organellar proteomics: the prizes and the pitfalls of opening the nuclear envelope. *Genome Biology* 3:1-4, 2002.

[45] Taylor, S.W., Fahy, E. and Ghosh, S.S. Global organellar proteomics. *Trends in Biotechnology* 21:82-88, 2003.

[46] Yates, J.R. III, Gilchrist, A., Howell, K.E., Bergeron, J.J.M. Proteomics of organelles and large subcellular structures. *Nature Reviews in Molecular Cell Biology* 6:702-714, 2005.

[47] De Duve, C. and Beaufay, H. A short history of tissue fractionation. *Journal of Cell Biology* 91:293s- 299s, 1981.

[48] Howell, K.E., Devaney, E. and Gruenberg, J. Subcellular fractionation of tissue culture cells. *Trends in Biochemical Sciences* 14: 44-47, 1989.

[49] Storrie, B. and Madden, E.A. Isolation of subcellular organelles. *Methods in Enzymology* 182:203-225, 1990.

[50] Warnock, D.E., Fahy, E., and Taylor, S.W. Identification of protein associations in organelles using mass spectrometry-based proteomics. *Mass Spectrometry Reviews* 23:259-280, 2004.

[51] Dykstra, M.J. and Reuss, L.E. *Biological electron microscopy: theory techniques and troubleshooting, 2nd ed.* Kluwer Academic/Plenum Publishers, New York, 2003.

[52] Alberts, B., Johnson, A., Lewis, J., Raff, M., Roberts, K., and Walter, P. *Molecular biology of the cell, 4th ed.,* Garland Publishing, Inc., New York 2002.

[53] Geuze, H.J. A future for electron microscopy in cell biology. *Trends in Cell Biology* 9:92-93, 1999.

[54] Griffiths, G. Bringing electron microscopy back into focus for cell biology. *Trends in Cell Biology* 11(4):153-154, 2001.

[55] Hainfeld J.F. and Powell R.D. New frontiers in gold labeling. *Journal of Histochemistry and Cytochemistry* 48(4):471-80, 2000.

[56] Koster, A. and Klumperman, J. Electron microscopy in cell biology: integrating structure and function. *Nature Reviews in Molecular Cell Biology* 4(9)(suppl):SS6-SS10, 2003.

[57] McIntosh, J.R. Electron microscopy of cells: a new beginning for a new century. *The Journal of Cell Biology* 153(6):F25-F32, 2001.

[58] Robinson J.M., Takizawa T., Pombo A., and Cook P.R. Correlative fluorescence and electron microscopy on ultrathin cryosections: bridging the resolution gap. *Journal of Histochemistry and Cytochemistry* 49(7):803-8, 2001.

[59] Baudhuin, P.; Evrard, P.; Berthet, J. Electron microscopic examination of subcellular fractions. *Journal of Cell Biology* 1967, 32, 181-191.

[60] Waterbury, R.G., Bergeron, J.J.M. and Kearney, R.E. Electron microscopy cell fraction preparation robot. *Proceedings of the IEEE EMBS-BMES Second Joint Conference* 3:1817-1818, 2002.

[61] Waterbury, R.G., Punwani, K., Bergeron, J.J.M. and Kearney, R.E. Electron microscopy cell fraction preparation robot. *Molecular and Cellular Proteomics* 2(9):997, 2003.

[62] Waterbury, R., Punwani, K., Bergeron, J.J.M. and Kearney, R.E. Design and automated control of the electron microscopy proteomic organellar preparation robot. *Journal of the Association for Laboratory Automation* 10(4):246-253, 2005.

[63] Blonder, J. et al. Enrichment of integral membrane proteins for proteomic analysis using liquid chromatography-tandem mass spectrometry. *Journal of Proteome Research* 1:351-360, 2002.

[64] Washburn, M.P. Wolters, D. and Yates, J.R. III. Large-scale analysis of the yeast proteome by multidimensional protein identification technology. *Nature Biotechnology* 19:242-247, 2001.

[65] Wu, C.C., MacCross, M.J., Howell, K.E. and Yates, J.R. III. A method for the comprehensive proteomic analysis of membrane proteins. *Nature Biotechnology* 21:532-538, 2003.

[66] Gorg, A., Weiss, W. and Dunn, M.J. Current two-dimensional electrophoresis technology for proteomics. *Proteomics* 4:3665-3685, 2004.

[67] Lodish, H., Berk, A., Zipursky, L.S., Matsudaira, P., Baltimore, D., and Darnell, J. *Molecular Cell Biology, 5th ed.*, W. H. Freeman & Company, New York, 2003.

[68] Rabilloud, T. Two-dimensional gel electrophoresis in proteomics: old, old fashioned, but it still climbs up the mountains. *Proteomics* 2:3-10, 2002.

[69] Righetti, P.G., Castagna, A., Herbert, B. and Candiano, G. How to bring the "unseen" proteome to the limelight *via* electrophoretic pre-fractionation techniques. *Bioscience Reports* 25:3-17, 2005.

[70] Righetti, P.G., Castagna, A., Antonioli, P. and Boschetti, E. Prefractionation techniques in proteome analysis: the mining tools of the third millennium. *Electrophoresis* 26:297-319, 2005.

[71] Westermeier, R. and Marouga, R. Protein detection methods in proteomics research. *Bioscience Reports* 25:19-32, 2005.

[72] Hillencamp, F., Karas, M., Beavis, R.C. and Chait, B. Matrix-assisted laser desorption/ionization mass spectrometry of biopolymers. *Analytical Chemistry* 63:1193A-1202A, 1991.

[73] Abersold, R. and Goodlett, D.R. Mass spectrometry in proteomics. *Chemistry Reviews* 101:269-295, 2001.

[74] Liebler, D.C. *Introduction to proteomics: tools for the new biology.* Humana Press Inc., New Jersey, 2002.

[75] Guerrera, I.C. and Kleiner, O. Applications of mass spectrometry in proteomics. *Bioscience Reports* 25:71-93, 2005.

[76] Mann, M., Hendrickson, R. C. and Pandey, A. Analysis of proteins and proteomes by mass spectrometry. *Annual Review of Biochemistry* 70:437-473, 2001.

[77] Rowley, A., Choudhary, J.S., Marzioch, M., Ward, M.A., Weir, M., Solari, R.C.E. and Blackstock, W.P. Applications of protein mass spectrometry in cell biology. *Methods* 20:383-397, 2000.

[78] Wysocki, V.H., Resing, K.A., Zhang, Q. and Cheng, G. Mass spectrometry of peptides and proteins. *Methods* 35:211-222, 2005.

[79] Yates, J.R. III. Mass spectrometry and the age of the proteome. *Journal of Mass Spectrometry* 33:1-19, 1998.

[80] Clauser, K.R., Baker, P. and Burlingame, A.L. Role of accurate mass measurement (±10 ppm) in protein identification strategies employing MS or MS/MS and database searching. *Analytical Chemistry* 71:2871-2882, 1999.

[81] Henzel, W. J. *et al.* Identifying proteins from two-dimensional gels by molecular mass searching of peptide fragments in protein sequence databases. *Proceedings of the National Academy of Sciences USA* 90:5011–5015, 1993.

[82] Fenyö, D. Identifying the proteome: software tools. *Current Opinion in Biotechnology* 11:391-395, 2000.

[83] Lin, D., Tabb, D. L. and Yates, J.R. III. Large-scale protein identification using mass spectrometry. *Biochimica et Biophysica Acta* 1646:1–10, 2003.

[84] Mann, M., Hojrup, P. and Roepstorff, P. Use of mass spectrometric molecular weight information to identify proteins in sequence databases. *Biological Mass Spectrometry* 22:338–345, 1993.

[85] Thiede, B., Hohenwarter, W., Krah, A., Mattow, J., Schmid, M., Schmidt,F. and Jungblut, P.R. Peptide mass fingerprinting. *Methods* 35:237-247, 2005.

[86] Jensen, O.N., Podtelejnikov, A.V. and Mann, M. Identification of the components of simple protein mixtures by high-accuracy peptide mass mapping and database searching. *Analytical Chemistry* 69:4741-4750 (1997).

[87] Yates, J.R. III. Mass spectral analysis in proteomics. *Annual Review of Biophysics and Biomolecular Structures* 33:297–316, 2004.

[88] Yates, J.R. III, Speicher, S., Griffin, P. R. and Hunkapiller, T. Peptide mass maps: a highly informative approach to protein identification. *Analytical Biochemistry* 214:397–408, 1993.

[89] Romjin, E.P, Krijgsveld, J. and Heck, A.J.R. Recent liquid chromatographic-(tandem) mass spectrometric applications in proteomics. *Journal of Chromatography A* 1000:589-608, 2003.

[90] Steen, H. and Mann, M. The ABC's (and XYZ's) of peptide sequencing. *Nature Reviews in Molecular Cell Biology* 5:699-711, 2004.

[91] Perkins, D.N., Pappin, D.J.C., Creasy, D.M., and Cottrell, J.S. Probability-based protein identification by searching sequence databases using mass spectrometry data. *Electrophoresis* 20:3551-3567, 1999.

[92] Yates, J.R. III, Eng, J.K., McCormack, A.L. and Schietz, D. Method to correlate tandem mass spectra of modified peptides to amino acid sequences in the protein database. *Analytical Chemistry* 67:1426-1436, 1995.

[93] Yates, J.R. III, Eng, J.K. and McCormack, A.L. Mining genomes: correlating tandem mass spectra of modified and unmodified peptides to sequences in nucleotide databases. *Analytical Chemistry* 67:3202-3210, 1995.

[94] Zhang, W. and Chait, B.T. ProFound: an expert system for protein identification using mass spectrometric peptide mapping information. *Analytical Chemistry* 72:2482-2489, 2000.

[95] Uhlén, M. et al. A human protein atlas for normal and cancer tissues based on antibody proteomics. *Molecular and Cellular Proteomics* 4:1920-1932, 2005.

[96] Ghaennaghami, S., Huh, W., Bower, K., Howson, R.W., Belle, A., Dephoure, N., O'Shea, E.K. and Weissman, J.S. Global analysis of protein expression in yeast. *Nature* 425:737-741, 2003.

[97] Bastiaens, P.I.H. and Pepperkok, R. Observing proteins in their natural habitat: the living cell. *Trends in Biochemical Sciences* 25:631-637, 2000.

[98] Hu, Y. and Murphy, R.F. Automated interpretation of subcellular patterns from immunofluorescence microscopy. *Journal of Immunological Methods* 290:93-105, 2004.

[99] Murphy, R.F. Cytomics and location proteomics: automated interpretation of subcellular patterns in fluorescence microscope images. *Cytometry Part A* 67A:1-3, 2005.

[100] Murphy, R.F. Location proteomics: a systems approach to subcellular location. *Biochemical Society Transactions* 33:535-538, 2005.

[101] Simpson, J.C. and Pepperkok, R. Localizing the proteome. *Genome Biology* 4:240-243, 2003.

[102] Wouters, F.S., Verveer, P.J. and Bastiaens, P.I.H. Imaging biochemistry inside cells. *Trends in Cell Biology* 11:203-211, 2001.

[103] Dahan, S., Ahluwalia, J.P., Posner, B.I. Bergeron, J.J.M. Concentration of intracellular hepatic apolipoprotein E in Golgi apparatus saccular distensions and endosomes. *The Journal of Cell Biology* 127:1859-1869, 1994.

[104] De Graef, M. *Introduction to Conventional Transmission Electron Microscopy.* Cambridge University Press, New York, 2003.

[105] Pease, D.C. and Porter, K.R. Electron Microscopy and Ultramicrotomy. *Journal of Cell Biology* 91:287s-292s, 1981.

[106] De Duve, C. Exploring Cells with a Centrifuge. *Science* 189:186-19, 1975.

[107] Baudhuin, P., Morphometry of subcellular fractions. *Methods in Enzymology* 32:3-20, 1974.

[108] Baudhuin, P. and Berthet, J. Electron microscopic examination of subcellular fractions II: quantitative analysis of the mitochondrial population isolated from rat liver. *Journal of Cell Biology* 35:631-648, 1967.

[109] GE. Palade. Fine Structure of Mitochondria. *Anat. Rec.* 114:427-451, 1952.

[110] MG. Farquhar and GE. Palade. Golgi apparatus (complex) - (1954-1981) - from artifact to center stage. *Journal of Cell Biology* 91:77s-103s, 1981.

[111] Palade, G.E. The endoplasmic reticulum. *Journal of Cell Biology* 2:85-97, 1956.

[112] Bainton, D.F. The discovery of lysosomes. *Journal of Cell Biology* 91: 66s-76s, 1981.

[113] De Duve, C. and Baudhuin, P. Peroxisomes (microbodies and related particles). *Physiological Reviews* 46:323-357, 1966.

[114] Afzelius, B.A. and Maunsbach, A.B. Biological ultrastructure research; the first 50 years. *Tissue & Cell* 36:83-94, 2004.

[115] Porter, K.R., Claude, A. and Fullam, E.F. A study of tissue culture cells by electron microscopy. *Journal of Experimental Medicine* 81:233-246, 1945.

[116] Bagshaw, R.D., Mahuran, D.J. and Callahan, J.W. A Proteomic analysis of lysosomal integral membrane proteins reveals the diverse composition of the organelle. *Molecular & Cellular Proteomics* 4:133-143, 2005.

[117] Bell, A.W., Ward, M.A., Blackstock, W.P., Freeman, H.M.N., Choudhary, J.S., Lewis, A.P., Chotai, D., Fazel, A., Gushue, J.N., Paiement, J., Palcy, S., Chevet, E., Lafrenière-Roula, M., Solari, R., Thomas, D.Y., Rowley, A., Bergeron, J.J.M. Proteomics characterization of abundant golgi membrane proteins. *The Journal of Biological Chemistry* 276:5152-5165, 2001.

[118] Coughenour, H.D., Spaulding, R.S. and Thompson, C.M. The synaptic vesicle proteome: a comparative study in membrane protein identification. *Proteomics* 4:3141-3155, 2004.

[119] Kikuchi, M., Hatano, N., Yokota, S., Shimozawa, N., Imanaka, T. and Taniguchi, H. Proteomic analysis of rat liver peroxisome. *The Journal of Biological Chemistry* 279:421-428, 2004.

[120] Mears, R., Craven, R.A., Hanrahan, S., Totty, N., Upton, C., Young, S.L., Patel, P., Selby, P.J. and Banks, R.E. Proteomic analysis of melanoma-derived exosomes by two-dimensional polyacrylamide gel electrophoresis and mass spectrometry. *Proteomics* 4:4019-4031, 2004.

[121] Nebl, T., Pestonjamasp, K.N., Laeszyk, J.D., Crowley, J.L., Oh, S.W. and Luna, E.J. Proteomic analysis of detergent-resistant membrane skeleton from neutrophil plasma membranes. *The Journal of Biological Chemistry* 277:43399-43409, 2002.

[122] Ritter, B., Blondeau, F., Denisov, A.Y, Gehring, K., and McPherson, P.S. Molecular mechanisms in clathrin-mediated membrane budding revealed through subcellular proteomics. *Biochemical Society Transactions* 32:769-773, 2004.

[123] Rout, M.P. and Field, M.C. Isolations and characterization of subnuclear compartments from trypanosoma brucei. *The Journal of Biological Chemistry* 276:38261-38271, 2001.

[124] Stevens, S.M., Zharikova, A.D. and Prokai, L. Proteomic analysis of the synaptic plasma membrane fraction isolated from rat forebrain. *Molecular Brain Research* 117:116-128, 2003.

[125] Tribl, F., Gerlach, M., Marcus, K., Asan, E., Tatschner, T., Arzberger, T., Meyer, H.E., Bringmann, G. and Riederer, P. "Subcellular proteomics" of neuromelanin granules isolated from the human brain. *Molecular & Cellular Proteomics* 4:945-957, 2005.

[126] Wu, C.C., Howell, K.E., Neville, M.C., Yates, J.R. III and McManaman, J.L.. Proteomics reveal a link between the endoplasmic reticulum and lipid secretor mechanisms in mammary epithelial cells. *Electrophoresis* 21:3470-3482, 2000.

[127] Wu, C.C., Taylor, R.S., Lane, D.R., Landinsky, M.S., Weisz, J.A and Howell, K.E. GMx33: a novel family of trans-Golgi proteins identified by proteomics. *Traffic* 1:963-975, 2000.

[128] Wu, C.C., Yates, J.R. III, Neville, M.C. and Howell, K.E. Proteomic analysis of two functional states of the Golgi complex in mammary epithelial cells. *Traffic* 1:769-782, 2000.

[129] Weibel, E.R. *Stereological methods I: practical methods for biological morphometry.* Academic Press, Inc. New York, 1979.

[130] Hayat, M.A. *Principles and techniques of electron microscopy: biological applications, Vol. 3.* VanNostrand Reinhold Company, New York, 1973.

[131] Dawes, C.J. *Biological techniques in electron microscopy.* Barnes & Noble, Inc., New York, 1971.

[132] Dykstra, M.J. and Reuss, L.E. *Biological electron microscopy: theory, techniques and troubleshooting, 2nd ed.* Kluwer Acedemic/Plenum Publishers, New York, 2003.

[133] Glauert, A.M. and Lewis, P.R. *Biological speciemen preparation for transmission electron microscopy.* Princton University Press, Princton, New Jersey, 1998.

[134] Robinson, D.G. *Methods of preparation for electron microscopy: an introduction for the biomedical sciences.* Springer-Verlag, New York, 1987.

[135] Lavoie, C.; Lanoix, J.; Kan, F. W. K.; Paiement, J. Cell-free assembly of rough and smooth endoplasmic reticulum. *Journal of Cell Science* 109:1415-1425, 1996.

[136] Boyd J. *Robotic Laboratory Automation.* Science 295:517-8, 2002.

[137] Branca, M.A. Attack of the lab-bots. *Bio-IT World*, May 19, 2004.

[138] Gecks, W. and Pedersen, S.T. Robotics – an efficient tool for laboratory automation. *IEEE Transactions on Industry Applications* 28(4):938-944, 1992.

[139] Hollen, R.M. Laboratory robotics: getting machines to do the hazardous work. *IEEE Potentials* December, pp6-7, 1991.

[140] Lane, L. Sourcebook: speed it up. *Bio-IT World*, January 21, 2005.

[141] Borman, S. Combinatorial chemists focus on small molecules, molecular recognition, and automation. *Chemical & Engineering News*, February 12, 1996.

[142] Cargill, J.F. and Lebl, M. New methods in combinatorial chemistry – robotics and parallel synthesis. *Current Opinion in Chemical Biology* 1:67-71, 1997.

[143] Czarnick, A.W. and Wilson, S.R. *Combinatorial chemistry: synthesis and applications.* Wiley, New York, 1997.

[144] Hardin, J.H. and Smietana, F.R. Automating combinatorial chemistry: a primer on benchtop robotic systems. *Molecular Diversity* 1:270-274, 1996.

[145] Houston, J.G. and Banks, M. The chemical – biological interface: developments in automated and miniaturized screening technology. *Current Opinion in Chemical Biology* 8:734-740, 1997.

[146] Hughes, I. and Hunter, D. Techniques for analysis and purification in high-throughput chemistry. *Current Opinion in Chemical Biology* 5:243-247, 2001.

[147] Van Hijfte, L., Marciniak, G., and Froloff, N. Combinatorial chemistry, automation and molecular diversity: new trends in the pharmaceutical industry. *Journal of Chromatography B* 725:3-15, 1999.

[148] Beggs, M., Blok, H. and Diels, A. The high throughput screening infrastructure: the right tools for the task. *Journal of Biomolecular Screening* 4:143-149, 1999.

[149] Chapman, T. Lab automation and robotics: automation on the move. *Nature* 421:661-666, 2003.

[150] Cleaves, K.S. Automating R&D. *Modern Drug Discovery* 7:37-39, 2004.

[151] Delorme, D.S. Automation of high throughput screening. *Industrial Robot* 25:16-19, 1998.

[152] Hamilton, S.D., Armstrong, J.W., Gerren, R.A., Jassen, A.M. Peterson, V., and Stanton, R.A. An overview of biotechnology screening. *Laboratory Robotics and Automation* 8:287-294, 1996.

[153] Janzen, W.P., Ed. *High throughput screening: methods and protocols*. Humana PressTotowa, New Jersey, 2002.

[154] Nettekoven, M. and Thomas, A.W. Accelerating drug discovery by integrative implementation of laboratory automation in the work flow. *Current Medicinal Chemistry* 9:2179-2190, 2002.

[155] Reichman, M. Marples, E. and Lenz, S. Approaches to automation for high-throughput screening. *Laboratory Robotics and Automation* 8:267-276, 1996.

[156] Rutherford, M.L. and Stinger, T. Recent trends in laboratory automation in the pharmaceutical industry. *Current Opinion in Drug Discovery and Development* 4:343-346, 2001.

[157] Smith, A. Screening for drug discovery: the leading question. *Nature* 418:453-459, 2002.

[158] Hodgson, J. Gene Sequencing's Industrial Revolution: How automation made deciphering the human genome possible. *IEEE Spectrum*, November, pp36-42, 2000.

[159] Jaklevic, J.M., Garner, H.R. and Miller, G.A. Instrumentation for the genome project. *Annual Review of Biomedical Engineering* 1:649-678, 1999.

[160] Meldrum, D. Automating for genomics, part one: preparation for sequencing. *Genome Research* 10:1081-1092, 2000.

[161] Meldrum, D. Automating for genomics, part two: sequencers, microarrays, and future trends. *Genome Research* 10:1081-1092, 2000.

[162] Wells, D.A. and Herron, L.L. Automation of sample preparation for genomics. *LCGC North America* 20:416-428, 2002.

[163] Dongre, A.R., Opiteck, G., Cosand, W.L., and Hefta, S.A. Proteomics in the post-genome age. *Biopolymers* 60:206-211:2001.

[164] Harry, J.L., Wilkins, M.R., Herbert, B.R., Packer, N.H., Gooley, A.A., and Williams, K.L. Proteomics: capacity versus utility. *Electrophoresis* 21:1071-1081, 2000.

[165] Lopez, M.F. Better approaches to finding the needle in a haystack: optimizing proteome analysis through automation. *Electrophoresis* 21:1082-1093, 2000.

[166] Lesney, M.S. Juggling the mix. *Modern Drug Discovery* 5:26-31, 2002.

[167] Lesley, S. A. High-throughput proteomics: protein expression and purification in the postgenomic world. *Protein Expression and Purification* 22:159-164, 2001.

[168] Quadroni, M. and James, P. Proteomics and Automation. *Electrophoresis* 21:664-677, 1999.

[169] Service R. F. High-speed biologists search for gold in proteins. *Science* 294:2074-2077, 2001.

[170] Wells, D.A. and Weil, D.A. Directions in automated sample preparation of proteins. *PharmaGenomics*, November/December, 42-54, 2003.

[171] Waterbury, R. *The EMPOP robot manual.* Montreal, Canada: McGill University, 2006.

[172] Punwani, K. *Automated control of the electron microscopy cell fraction preparation robot*, Master's Thesis, McGill University, Department of Biomedical Engineering, Montreal, Canada, 2005.

[173] Lide, D.R., Ed. *CRC handbook of chemistry and physics, 73rd ed.* The Chemical Rubber Publishing company, Boca Raton, Florida 1993.

[174] McCauley, C.J., Ed. *Machinery's handbook 26th ed.* Industrial Press, Inc. New York 2000.

[175] Walsh, R.A. *Electromechanical design handbook.* McGraw-Hill, Inc., New York 1990.

[176] Edwards, J. *Coating and surface treatment systems for metals: a comprehensive guide to selection.* ASM International, Materials Park, Ohio 1997.

[177] Ross, R.B. *Handbook of metals treatments and testing.* John Wiley & sons, New York 1977.

[178] Kempner, M.E., Timoney, C.F. and Felder, R.A. Developments in microplate automation. *Journal of Laboratory Automation* 7:67, 2002.

[179] *Parker O-ring Handbook.* Parker Hannifin Corporation, Cleveland, OH 2001.

[180] Brink, R.V., Ed. *Handbook of fluid sealing.* McGraw Hill Companies, Inc., New York 1993.

[181] Brown, M. *Seals & sealing handbook 4th ed.* Elsevier Science Publishers Ltd. Kidlington, Oxford 1995.

[182] Muller, H.K. and Nau, B.S. *Fluid sealing technology: principles and applications.* Marcel Dekker, Inc., New York 1998.

[183] Kamm, L.J. Designing cost-efficient mechanisms. Society of Automotive Engineers, Inc. Salem, MA 1990.

[184] Klafter, R.D., Chmielewski, T.A. and Negin, M. Robotic engineering: an integrated approach. Prentice Hall, Inc., Englewood Cliffs, NJ 1989.

[185] Bradley, F.N. *Materials for magnetic functions.* Hayden Book Company, Inc. New York, 1971.

[186] Campbell, P. Permanent magnet materials and their applications. Cambridge University Press, New York, 1994.

[187] Du Trémolet de Lacheisserie, É., Gignoux, D. and Schlenker, M. Eds. *Magnetism I: fundamentals.* Kluwer Acedemic Publishers, Norwell, MA, 2002.

[188] Du Trémolet de Lacheisserie, É., Gignoux, D. and Schlenker, M. Eds. *Magnetism II: materials & applications.* Kluwer Acedemic Publishers, Norwell, MA, 2002.

[189] Moskowitz, L.A. *Permanent magnet design and application handbook.* Krieger Publishing Company, Malabar, FL, 1986.

[190] Parker, R.J. *Advances in permanent magnets.* John Wiley and Sons, Inc., New York, 1990.

[191] Parker, R.J. and Studders, R.J. *Permanent magnets and their applications.* John Wiley and Sons, Inc., New York, 1962.

[192] Cooper, R.K., Neil, V.K. and Woodruff, W.R. Optimum permanent-magnet dimensions for repulsion applications. *IEEE Transactions on Magnetics* 9:125-127, 1973.

[193] Delamare, J. Yonnet, J.P. and Rulliere, E. A compact magnetic suspension with only one axis control. . *IEEE Transactions on Magnetics* 30:4746-4748, 1994.

[194] Lequesne, B. Permanent magnet linear motors for short strokes. *IEEE Transactions of Industrial Applications* 32:161-168, 1996.

[195] Oshima, M., Miyazawa, S., Deido, T., Chiba, A., Nakamura, F., and Fukao, T. Characteristics of a permanent type bearingless motor. *IEEE Transactions of Industrial Applications* 32:363-370, 1996.

[196] Tsui, J.B.Y., Iden, D.J. Strnat, K.J. and Evers, A.J. The effect of intrinsic magnetic properties on permanent magnet repulsion. *IEEE Transactions on Magnetics* 8:188-194, 1972.

[197] Boldea, I. and Nasar, S.A. *Linear motion electromagnetic devices.* Sheridan Books, Ann Arbor, MI, 2001.

[198] De Wolf, D.A. Essentials of electromagnetics for engineering. Cambridge University Press, New York, 2001.

[199] Hammond, P. Electromagnetism for engineers: an introductory course. Oxford University Press, New York, 1997.

[200] Rao, N.N. Elements of Engineering Electromagnets 4th ed. Prentice Hall, Englewood cliffs, NJ, 1994.

[201] Ulaby, F.T. Fundamentals of applied electromagnetics. Prentice Hall, Upper Saddle River, NJ, 1999.

[202] Hunter, R.P. *Automated process control systems: concepts and hardware 2nd ed.* Prentice Hall, Inc. Englewood Cliffs, NJ, 1987.

[203] Johnson, C.D. *Process control instrumentation technology 6th ed.* Prentice Hall, Inc. Upper Saddle River, NJ, 2000.

[204] Lipták, B.G., Ed. *Instrument engineer's handbook 4th ed.: process measurement and analysis.* CRC Press, Boca Raton, FL, 2003.

[205] Moore, J.H., Davis, C.C. and Coplan, M.A. *Building scientific apparatus: a practical guide to design and construction, 3rd ed.* Westview Press, Boulder, CO, 2002.

[206] Nolas, G.S., sharp, J., and Goldsmid, H.J. *Thermo-electrics: basic principles and new material developments.* Spinger-Verlag, New York, 2001.

[207] Riedel, T.E., Cox, J.C. and Ellington, A.D. Low temperature microplate station. *Journal of the Association for Laboratory Automation* 10:29-34, 2005.

[208] Rowe, D.M. (Ed.) *CRC handbook of thermoelectrics.* CRC Press, Inc.: Boca Raton, FL, 1995.

[209] Steinberg, D.S., *Cooling Techniques for Electronic Equipment 2nd Ed.* John Wiley & Sons, Inc., New York, New York, 1991.

[210] Althouse, A.D., Turnquist, C.H. and Bracciano, A.F. *Modern refrigeration and air conditioning.* Gooheart-Wilcox Co., Inc.: South Holland, IL, 1982.

[211] Incropera, F.P. *Liquid cooling of electronic devices by single-phase convection.* John Wiley and Sons, Inc., New York, 1999.

[212] Janna, W.S. *Engineering heat transfer, 2nd ed.* CRC Press, Boca Raton, FL, 2000.

[213] Kakaç, S. and Liu, H. *Heat exchangers: selection, ratings and thermal design.* CRC Press, Boca Raton, FL, 1998.

[214] Kordyban, T. *Hot air rises and heat sinks: everything you know about cooling electronics is wrong.* ASME Press, New York, 1998.

[215] Kordyban, T. *More hot air.* ASME Press, New York, 2005.

[216] Mull, T.E. *HVAC principles and applications manual.* McGraw-Hill, New York 1998.

[217] Bird, R.B., Stewart, W.E. and Lightfoot, E.N. *Transport Phenomena.* John Wiley & Sons, Inc. New York, 1960.

[218] Green, D.W. *Perry's chemical engineers' handbook 7th ed.* McGraw Hill Companies, Inc., New York, 1997.

[219] McCabe, W.L., Smith, J.C. and Harriot, P. *Unit operations of chemical engineering.* McGraw Hill Companies, Inc., New York, 1993.

[220] Welty, J.R., Wicks, C.E. and Wilson, R.E. *Fundamentals of momentum, heat and mass transfer 4th ed.* John Wiley & Sons, Inc. New York, 2001.

[221] Belsterling, C.A. *Fluidic systems design.* Wiley-Interscience, New York, 1971.

[222] Buzzard, W.S. *Flow Control.* Instrument Society of America, Research Triangle Park, North Carolina, 1997.

[223] Kirshner, J.M and Katz, S. *Design theory of fluidic components.* Academic Press, New York, 1975.

[224] Schweitzer, P.A. *Handbook of valves.* Industrial Press Inc. New York, 1972.

[225] Skousen, P.L. *Valve Handbook 2nd ed.* McGraw-Hill, New York, 2004.

[226] Smith, P. and Zappe, R.W. *Valve Selection Handbook.* Elsevier, Inc., Jordon Hill, Oxford, 2004.

[227] Spellman, F.R. and Drinan, J. *Pumping.* Technomic Publishing Company, Inc. Lancaster, PA, 2001.

[228] Mackay, R. *The practical pumping handbook.* Elsevier Ltd., Kidlington, Oxford, 2004.

[229] *Variable volume pump manual.* The Lee Company, Westbrook, CT, 1999.

[230] Humphrey, E.F. and Tarumoto, D.H. *Fluidics.* Fluid Amplifier Associates, Ann Arbor, MI, 1968.

[231] Myers K.J., Bakker A., Ryan D. Static Mixer Fundamentals and Applications. *Chemical Engineering Progress* 93(6):28-38, 1997.

[232] Brown, R.N. *Compressors: selection and sizing 2nd ed.* Gulf Publishing Company, Houston, TX, 1997.

[233] O'Hanlon, J.F. *A user's guide to vacuum technology 2nd ed.* John Wiley and Sons, Inc., New York, 1989.

[234] Majumdar, S.J. *Pneumatic systems: principles and maintenance.* McGraw-Hill, Inc., New York, 1995.

[235] Mills, D. *Pneumatic conveying design guide 2nd ed.* Elsevier Butterworth-Heinemann, Jordan Hill, Oxford, 2004.

[236] Rozanov, L.N. *Vacuum technique.* Taylor & Francis, New York, 2002.

[237] *Vacuum and pressure systems handbook.* Gast Manufactring Company, Benton Harbor, MI, 1986.

[238] Edwards, K.S. Jr. and McKee, R.B. *Fundamentals of mechanical component design.* McGraw-Hill, Inc., New York, 1991.

[239] Jones, F.D., Ed. *Ingenious mechanisms for designers and inventors, vols. 1-4.* Industrial Press, Inc. New York, 1930.

[240] Kutz, M., Ed. *Mechanical Engineers' Handbook 2nd ed.* John Wiley & Sons, Inc., New York, 1998.

[241] Norton, R.L. *Design of machinery 2nd ed.* McGraw Hill, New York, 1999.

[242] Spotts, M.F. *Design of machine elements 6th ed.* Prentice Hall, Englewood Cliffs, NJ, 1985.

[243] Halliday, D. and Resnick, R. *Fundamentals of Physics, 3rd ed.* John Wiley & Sons, Inc., New York, 1988.

[244] Ceccarelli, M. *Fundamentals of mechanics of robotic manipulation.* Kluwer Academic Publishers, Boston 2004.

[245] Mason, M.T. *Mechanics of robotic manipulation.* MIT Press, Cambridge, MA 2001.

[246] Groover, M.P., Weiss, M.N, Roger, N. and Odrey, N.G. *Industrial Robotics: Technology, Programming, and Applications.* New York: McGraw-Hill Book Company, 1986.

[247] Humphrey, W.M. *Introduction to Servo Mechanism System Design.* Englewood Cliffs, N.J.: Prentice-Hall, Inc., 1973.

[248] Kiong, T.K. *Precision motion control: design and implementation.* Springer, New York 2001.

[249] Tal, J. *Step-by-step design of motion control systems.* Galil Motion Control, Inc. Mountain View, CA 1994.

[250] *Electromechanical Positioning Systems- Catalog (8000-2/USA).* Parker Hannifin Corporation: Compumotor Division.

[251] *Electromechanical Positioning Systems- Catalog (8080/USA). Parker* Hannifin Corporation: Daedal Division.

[252] *Servo motors/drives - Catalog (8000-4/USA).* Parker Hannifin Corporation: Compumotor Division.

[253] Craig, J.J. *Introduction to robotics: mechanics and control, 2nd ed.*, Addison-Wesley, 1989

[254] L'Hoter, F., Kauffmann, J., André, P. and Taillard, J. *Robot Technology, Vol. 4, Robot Components and Systems.* Englewood Cliffs, N.J.: Prentice-Hall, Inc., 1983.

[255] Auslander, D.M. and Kempf, C.J. *Mechatronics: mechanical system interfacing.* Prentice Hall, inc., Upper Sadle River, NJ 1996.

[256] Bishop, R.H. (ed.) *The mechatronics handbook.* Boca Raton, FL: CRC Press, 2002.

[257] Cetinkunt, S. *Mechatronics.* New York: John Wiley & Sons, 2007.

[258] Onwubolu, G.C. *Mechatronics: principles and applications.* Jordan Hill, Oxford: Elsevier Butterworth-Heinemann, 2005.

[259] Popovic, D. and Vlačić, L. (eds.) *Mechatronics in engineering design and product development.* New York: Marcel Dekker, Inc., 1999.

[260] Trevathan, V.L. (ed.). *A Guide to the Automation Body of Knowledge.* Instrumentation Society of America, Research triangle Park, NC 2006.

[261] *Motion Control Systems - Catalog (8000-3/USA).* Parker Hannifin Corporation: Compumotor Division.

[262] *6K Series Programmer's Guide.* 1998. Parker Hannifin Corporation: Compumotor Division.

[263] Carr, J.J., *Electronic Circuit Guidebook Volume 1: Sensors.* Prompt Publications, Indianapolis, IN 1997.

[264] Fraden, J. *Handbook of modern sensors: physics, designs and applications, 3rd ed.* Springer-Verlag, Inc., New York 2004.

[265] Sinclair, I.R. *Sensors and transducers.* Oxford University Press, Boston 2001.

[266] Lenk, R. *Practical design of power supplies.* IEEE Press, New York 1998.

[267] Bugg, D. *Electronics: circuits, amplifiers and gates.* Institute of Physics Publishing, Philadelphia, 1996.

[268] DeSa, A. *Electronics for scientists: physical principles with applications to instrumentation.* Prentice Hall Europe, Hemel Hempstead, Hertfordshire 1997.

[269] Horowitz, P. and Hill, W. *The art of electronics 2nd ed.* Cambridge University Press, New York, New York 1989.

[270] Sedra, A.S. and Smith, K.C. *Microelectronic Circuits.* Oxford University Press, New York, 1998.

[271] Valentine, R. *Motor control electronics handbook.* McGraw Hill, New York 1998.

[272] Stroo, E., Zimmerman, M.W. and Zucker, W. Eds. *Microsoft visual basic 6.0 programmer's guide.* Microsoft Press, Redmond, WA 1998.

[273] *6K Series Command Reference.* Parker Hannifin Corporation: Compumotor Division, 1998.

[274] Kozierok, C. *The TCP/IP guide.* No Starch Press, Inc., San Francisco, CA 2005.

[275] McCormick, J. *The human/machine interface. Automotive Industries* 183:39, 2003.

[276] Weigant, J. *Creating human machine interfaces using visual basic, 4th ed.* IndustrialVB.com, 2001.

[277] Waterbury, R., Kearney, R. and Bergeron, J. *Electron Microscopy Cell Fraction Sample Preparation Robot.* United States Patent Application, Filed: 16 July 2002.

[278] Seliskar, D.P., Waterbury, R.G. and Kearney, R.E. Proportional Microvolume Capacitive Liquid Level Sensor Array. *Proceedings of the 27th Annual International Conference of the IEEE EMBS.* 7258-7261, 2005.

[279] Waterbury, R., Seliskar, D., Johnstone, E. and Kearney, R. *Methods and Apparatus for Detecting Liquid Inside Individual Wells in a Multi-Well Plate.* United States Provisional Patent Application, Filed: 1 September 2005.